University of Alberta

Forebay Thermal Dynamics at Hydropower Facilities on the Columbia River System

by

Catherine Beth Robertson

A thesis submitted to the Faculty of Graduate Studies and Research
in partial fulfillment of the requirements for the degree of

Master of Science

in

Water Resources Engineering

Civil and Environmental Engineering

Fall 2012
Edmonton, Alberta

To my father, for giving me my drive and determination.

Abstract

The risk of fish entrainment is influenced by thermal dynamics within reservoir forebays. The study objective was to understand these dynamics at Kinbasket (Mica Dam), Revelstoke (Revelstoke Dam), and Arrow Lakes (Hugh Keenleyside Dam) reservoirs on the Columbia River. Temperature profiles measured in the forebay of Arrow Lake and Kinbasket portrayed two-layer and linear temperature profiles, respectively. A waveform analysis revealed most internal seiching periods were wind driven and multiple vertical modes at Kinbasket. In Kinbasket, 1 day mid-depth seiches had negative and positive correlations with low and high discharges, respectively. Calculations showed some Arrow Lake seiching was controlled by a boundary 100km upstream. Kinbasket seiching was controlled by 150km and 15km reaches. Calculations revealed selective withdrawal from the epiliminion in Arrow Lakes and withdrawal layer growth with discharge in Kinbasket. Revelstoke and Kinbasket historic temperature profiles were similar. Warmer local inflow at Revelstoke allowed development of an epiliminion layer.

Acknowledgements

I would like to thank my supervisor, Dr. David Zhu, for his guidance throughout my research and his encouragement to partake in a Master's program.

Thanks to my research partner, Mat Langford, who is focussing on the velocity measurements within the reservoirs. Thank you for collaborating in the planning and execution of field measurements, development of the model, and preparation of BC Hydro reports.

Thanks to Chris Krath, who accompanied us during our field trips. His ingenuity and tenacity were a huge help in the field. Also, thanks to Adam Marriner, Emily Chen, and Greg Courtice who also assisted in obtaining the field measurements.

Thanks to Alf Leake (and many others) from BC Hydro for facilitating the field work and research project. Thanks to David Patterson and Jayme Hill of DFO and Eduardo Martins of Carleton University for the use of their equipment and retrieving thermistor information.

I very much appreciate the financial support given to me during my studies from various institutions and individuals including NSERC, the University of Alberta, and John and Patricia Schlosser.

Finally, I would like to thank my friends and family for their patience and support throughout my academic career. A special thanks to my mother and soon-to-be husband for their generosity, love, and understanding.

Table of Contents

List of Tables

List of Figures

List of Symbols

α	albedo of the water surface
a	solar altitude
α^*	volumetric coefficient of thermal expansion
A, B	empirical constants
β	Bowen's ratio
C_D	drag coefficient
C_p	specific heat of water
δ	declination of the sun
δ_w	withdrawal layer thickness
$\delta\bar{T}/\delta z$	local temperature gradient estimated from the mean temperature profile
Δ	saturation vapour pressure gradient
Δh	magnitude of the interface oscillation
$\Delta\rho$	density difference between hypolimnion and metalimnion
ΔT_{RMS}^{x}	RMS temperature change for thermistor x
D	number of overlapping points for segments in Welch's procedure
D_t	approximate depth of wind mixing
$\frac{dh_2}{dx}$	slope of the interface
$\frac{d\rho}{dz}$	density gradient with depth

ε	emittance for non-perfect black bodies
E	evaporation rate
E_c	combined evaporation rate
e_a	actual vapour pressure
E_a	aerodynamic evaporation rate
ε_r	normalized random error
e_s	saturation vapour pressure
E_s	energy balance evaporation rate
F_c	critical Froude number
γ	psychrometric constant
g	acceleration due to gravity
g'	reduced gravity
H	depth of the basin
h_1	depth of the epilimnion
h_2	depth of the hypolimnion
h_c	distance from the centre of the outlet to the water layer interface
H_E	energy used for evaporation
H_H	sensible heat flux
H_L	net long wave radiation
H_{LA}	long wave radiation reflected back from atmosphere
H_{LS}	long wave radiation from water's surface
H_N	total heat exchange at the water's surface

H_s	net solar radiation (short wave)
i	number of vertical nodes
I_o	effective radiation intensity
j	number of horizontal nodes
k^*	von Karman constant
k	0 for fundamental frequency, 1 for first mode, and 2 for second mode
L_B	length of the basin
L_v	latent heat of vaporization
μ	reservoir depth / the reservoir length
m	time step
M	number of time series points
N	number of values for each segment in Welch's procedure
N_b	buoyancy frequency
n_d	number of overlapping segments in Welch's procedure
ω_{ij}	wave frequency
φ	local latitude
P	atmospheric pressure
Q	total discharge
Q_c	critical discharge
ρ_1	density of the epilimnion
ρ_2	density of the hypolimnion
ρ_A	density of air

ρ_o	average profile density
ρ_w	density of water
r	(actual earth – sun distance)/(mean earth – sun distance)
σ	Stefan-Boltzman constant
ζ_{RMS}^{x}	RMS seiche amplitude for thermistor x;
τ	sun's hour angle
T	water temperature
T_2	period of the interface oscillation
T_a	temperature of air near the ground
τ_o	wind shear stress
T_s	temperature at the surface
$\bar{T}(Z_x)$	mean temperature profile for thermistor x
$T(z_x, t_m)$	temperature at (depth of thermistor x, time step m)
U	wind velocity
u^*	shear velocity of the wind
W_o	solar constant/4
Z_o	roughness height
Z_{10}	height at which wind measurements are taken from

List of Acronyms

ADCP	acoustic Doppler current profiler
ALH	Arrow Lakes Hydro
BC	British Columbia
CFD	computational fluid dynamics
CTD	conductivity – temperature – depth
DFO	Department of Fisheries and Oceans
GCM	geodetic control monument
HLK	Hugh Keenleyside Dam
LLO	low level outlet
MCA	Mica Dam
REV	Revelstoke Dam
RMS	root mean square
RTK GPS	real-time kinematic global positioning system

1. Introduction

Fish entrainment occurs when resident fish of an upstream reservoir are involuntarily passed through a dam's water release structures, resulting in displacement and possibly injury or death. This has been identified as a key potential impact of hydro-facilities on the productivity and biodiversity of these aquatic species. It is anticipated that the risk of fish entrainment at a particular dam facility is correlated with the effect of hydropower operations on the flow and thermal structures of the forebay.

BC Hydro operates a number of hydroelectric facilities throughout British Columbia. There are plans in place to add additional turbines at existing facilities located on the Columbia River to increase the operational flexibility. Given this change in hydropower operations, there is an interest to address the risk of fish entrainment at these facilities. A multi-disciplinary study has been initiated by BC Hydro. The overall objective is to combine both hydraulic and biological research in order to develop general methods to assess the risk of fish entrainment and to develop strategies for operation optimization.

During summer months, reservoirs can become thermally stratified. The thermal regime of a reservoir can significantly affect fish and fish habitat in the system and the depth distribution of fish (RL&L, 2000). A risk screening exercise of the risk of fish entrainment at Kinbasket reservoir was completed involving BC Hydro and a variety of stakeholders, such as government, industry, and First Nations (BC Hydro, 2009). Kokanee were identified as one species at risk, which may even vary seasonally. Kokanee have temperature preferences that change throughout the year (Maiolie and Elam, 1994). The thermal properties in a reservoir also change throughout the year, which will affect the vertical distribution of fish in the water column. If the Kokanee seasonal temperature preference coincides with the location of intake withdrawal, it can increase their risk of entrainment. Therefore, it is important to understand the thermal properties within a reservoir, how they are changing naturally, and how hydropower operations can affect them.

Reservoir temperatures fluctuate naturally due to natural reservoir thermal dynamics from wind, meteorological, and flow conditions. Dam intake operations can also cause similar internal fluctuations of the temperature profile. This study focuses on the temperature profile fluctuations in the reservoirs of hydropower facilities, mainly in the immediate forebay, an area just upstream of

the dam face. The flow in the forebay is affected most strongly by hydropower operations and is of interest when considering the risk of fish entrainment.

The overall objective of this study was to further understand the thermal dynamics in the forebay areas of hydro-facilities. Three hydropower facilities were considered for this study: Mica Dam, Revelstoke Dam, and Hugh Keenleyside Dam. These dams and reservoirs were located in succession on the Columbia River system in southeastern British Columbia (BC), as shown in Figure 1.1. The Columbia River flowed generally northwestwardly into Kinbasket reservoir. From here, water continued flowing northwest until it made an almost 90° turn near Mica Dam. Water flowed directly from Mica Dam into the Revelstoke reservoir. This reservoir extended southwardly until it reached Revelstoke Dam. Here, water was discharged into the Columbia River. After a few kilometres, the Columbia River once again flowed into a reservoir, the Arrow Lakes. Water continued flowing in a southwardly direction until it reached the final facility of interest, Hugh Keenleyside Dam.

Each facility of interest possessed a variety of different characteristics. Mica dam (MCA) was a high head dam (244 m) about 130 km north of the town of Revelstoke, BC. This facility formed the approximately 190 km long Kinbasket reservoir on the Columbia River system. The water level fluctuated about 30 m annually. MCA generated power through the release of water from four intakes located at the base of the dam structure. Revelstoke dam (REV) was a 175 m high dam just north of the town of Revelstoke, BC. This facility formed the approximately 130 km long Revelstoke reservoir on the Columbia River system, immediately downstream of MCA dam. The reservoir was operated as run-of-the-river with maximum water level fluctuations of only 4.5 m. Hugh Keenleyside dam (HLK) was a low head (52 m), high flow, high storage system near the town of Castlegar, BC. This dam formed the 230 km long Arrow Lakes reservoir on the Columbia River system. HLK regulated the water level (no power generation) in the reservoir via four surface sluice gates and eight low level intakes. The water level fluctuated about 11 m annually.

The main focus of this study was on the HLK and MCA facilities and the thermal stratification in their reservoirs. These two facilities were favoured based on their diverse characteristics. HLK was a non-power generating facility with respectively shallower intakes and generally low flows, around 65 – 250 m^3/s. MCA was a huge generation station with very deep intakes and a variety of low and very high flows, up to 1109 m^3/s. Detailed temperature profile

measurements were collected in the forebay at these two locations. The stratification structures and periodic oscillations in the temperature profiles of each reservoir were studied, along with their possible causes. Furthermore, theoretical calculations of the motions occurring in each of the reservoirs were completed. No detailed field measurements were taken at the Revelstoke reservoir for this study. However, previous studies were carried out by BC Hydro, which included profile and inflow temperature measurements throughout both Revelstoke and Kinbasket reservoir. Therefore, a review of these previous reports was also completed for this study.

2. Reservoir Thermal Dynamics

The construction of hydropower facilities creates upstream impoundments which can develop a water temperature gradient. In the forebay area close to the dam face this temperature gradient is influenced by, but not limited to, reservoir heating and cooling processes, wind shear forces, and hydropower facility operations. The development and movement of this temperature gradient is referred to as the thermal dynamics in a reservoir. The objective of this study was to understand these dynamics in the forebay of a reservoir. These dynamics are described in more detail below.

2.1 Stratification

It is well know that deep reservoirs in mid-latitude locations, such as BC, will develop a thermal stratification. Due to the cooler climate in these locations, reservoirs will also have an annual cycle of temperature stratification (Fischer et al., 1979). Referred to as dimictic, these reservoirs will turn over twice throughout the year, the first occurring in the spring. During the warm summer months, the reservoir is heated and temperature stratification develops. In the fall, the surface layers are cooled and turnover occurs for a second time. In the winter, temperatures are cold and generally homogeneous in ice free reservoirs.

Different gradients of thermal stratification structures can develop throughout the water profile. The thickness and temperature of each water layer are related to the reservoir geometry, reservoir location, meteorological conditions, hydrology, and reservoir operations (Owens et al., 1986). Two extreme cases of different temperature profile shapes include a two-layer stratification profile and a linear (continuous) stratification profile.

A typical two-layer stratification profile is shown in Figure 2.1. This profile is defined by a warm, well-mixed epilimnion layer overtop a relatively homogeneous, cooler hypolimnion layer. Dividing these two layers is a sharp temperature transition referred to as a thermocline or metalimnion. The thickness of each layer varies, but typically the thermocline is relatively smaller than the epilimnion and hypolimnion. Temperature profiles can often be approximated by this two-layer stratification. Many reservoirs, however, do not have these characteristics and cannot be approximated by the two-layer pattern (Vidal et al., 2005). Some reservoirs will have profiles closer to a linear

(continuous) stratification profile, as shown in Figure 2.2. This profile is characterized by a very thick metalimnion layer overtop a relatively homogeneous hypolimnion layer. The thick metalimnion layer displays a linear temperature gradient from the surface down to the hypolimnion.

The classic two-layer stratification is characterized by a well-mixed epilimnion layer. If this layer is deeper, the thermocline layer is smaller, and the stratification is more easily approximated as a two-layer profile. The temperature and depth of the epilimnion layer depends on the degree of solar insolation and wind mixing (Prigo et al., 1995). With no wind mixing, the surface epilimnion layer will be small, or even non-existent. This would lead to a linear stratification profile. A stratified lake in British Columbia was studied by Wiegand and Chamberlain (1987). They observed a thick thermocline region and attributed it to light wind conditions (no withdrawal structures in the lake). However, linear stratification is still found in windy reservoirs. Several studies suggest other reasons for the development of a linear stratification. Moreno-Ostos et al. (2008) observed in a Mediterranean reservoir the deepening of the thermocline and widening of the metalimnion layer. This coincided with hypolimnetic withdrawal, which heated the reservoir with the withdrawal of cooler water (Moreno-Ostos et al., 2008). Perez-Losada et al. (2003) stated that the changes in the thermal structure of a Mediterranean reservoir depend highly on rain variability and discharge operations. Due to the discharge of hypolimnetic waters, a warm linear stratification developed. A study on several lakes and reservoirs in British Columbia was done by Stevens and Lawrence (1997). They stated that a typical two-layer temperature profile develops after late August in the Northern Hemisphere. However, a linear stratification profile with the characteristic broad thermocline was found prior to August (Stevens and Lawrence, 1997).

Reservoirs in temperate locations will develop thermal stratification in the summer months. The shape of this temperature profile depends on the reservoir geometry, meteorological conditions, hydrology, and reservoir operations. Typical two-layer stratification profiles can often be used to approximate reservoir stratification. However, linear stratification profiles can also be found, possibly due to low winds, reservoir operations, or geographic location. The spatial and temporal distribution of fish is influenced by the thermal stratification in a reservoir (RL&L, 2000). Therefore, it is important to

determine the stratification structure in a reservoir and what influences its development.

2.2 Seiching

When a reservoir exhibits a thermal gradient, periodic oscillations, or internal seiches, can develop within the water body (Fischer et al., 1979). Internal seiching is developed when an external force disturbs the internal isotherms from their position of equilibrium. The subsidence of this force creates an oscillation in the reservoir isotherms called an internal seiche. Typically, these fluctuations are wind-driven (Fischer et al., 1979).

An idealized two-layer system, where the epilimnion and hypolimnion are divided by an interface, can be used to describe the flow within the water body when an internal seiche develops. As shown in Figure 2.3, prolonged wind over a reservoir provides a stress on the water surface, promoting the flow of water toward the downwind shore (Mortimer, 1951). This additional flow of water will force the thermocline interface below its equilibrium on the downwind side (Mortimer, 1951). Furthermore, the required replacement of water on the upwind side causes the thermocline to be forced above its equilibrium, causing a tilt in the interface (Mortimer, 1951). When the wind forcing stops the thermocline will try to return to a state of equilibrium. The interface will oscillate until the energy input from the wind forcing is dissipated. This oscillation is referred to as an internal seiche and is most pronounced at the boundaries. Seiches may also be driven by changes in hydropower intake operations if the flows provided through the intakes are large enough to be considered the systems major outfall (Ji, 2008). As such, major changes in operations may result in seiches within the reservoir.

The example shown in Figure 2.3 is an idealized representation of an internal seiche. The characteristics of internal seiches (internal waves) are governed by the thermal stratification and the basin geometry (Vidal et al., 2007). Differences in these attributes lead to the development of several classifications of internal seiches. The idealized example shown in Figure 2.3 is an example of a V1H1 internal wave motion. This class of internal seiche is characterized by the oscillation through one vertical node (V1) and one horizontal (in the longitudinal direction) node (H1). Internal wave motions are classified based on the number

of vertical (*i*) and horizontal (*j*) nodes they are oscillating through, or V*i*H*j* (Vidal et al., 2007).

The V1H1 internal seiche is the most commonly observed, which results when the stratification structure is close to the idealized two-layer system (Vidal et al., 2005). This fundamental mode of oscillation is most common since it is the most energetic and therefore less susceptible to damping (Vidal et al., 2007). However, different modes of oscillation do occur. Multiple nodes of oscillation in the horizontal plane can develop from wind forcing at the fundamental period.

Multiple vertical modes of oscillation, as seen in Figure 2.4, occur as well. The temperature profiles in reservoirs are not generally described well by an idealized two-layer structure (Vidal et al., 2005). Profiles closer to a linear stratification frequently occur, which is characterized by a thick metalimnion layer. Several studies have found that the presence of a thicker metalimnion layer leads to the development of higher vertical modes (Perez-Losada et al., 2003, Vidal et al., 2005, Vidal et al., 2007, Wiegand et al., 1987). In fact, Vidal et al. (2007) found that a dense spectrum of internal oscillations developed with linearly stratified reservoirs, with observations of up to a V5H1 mode. Vidal et al. (2005) found that when the metalimnion is thick higher vertical modes of oscillation become excited by periodic winds. Vidal et al. (2007) goes on further to say that higher vertical modes become dominant due to the resonance developed by periodic winds.

The temperature distribution in a reservoir is constantly changing due to external forces such as wind or dam operations causing internal seiche motions. Since fish have certain temperature preferences, these motions could place them in a location that is more susceptible to entrainment (RL&L, 2000). Therefore, it is important to understand the causes and development of these motions, which is the objective of this study.

2.3 Selective Withdrawal

When a reservoir is thermally stratified, the vertical density gradient will limit the withdrawal of water from certain depths, a phenomenon called selective withdrawal. This occurs when the discharge is not strong enough to overcome the buoyancy forces created by the thermal gradient (Fischer et al., 1979). Only the horizontal water layer adjacent to an intake will be withdrawn. However,

when some critical discharge is reached, water will begin to withdraw from other layers (Shammaa and Zhu, 2010).

Several studies have looked at the effect of selective withdrawal on the stratification profile in a reservoir. Casajitjana et al. (2003) developed a one-dimensional numerical model to determine the effect of withdrawal from different levels. They found that the depth of the outlets coincided with, and governed, the thermocline position. Caliskan and Elci (2009) developed a three-dimensional model for a reservoir. They found that withdrawal from the thermocline and hypolimnion caused warming of these layers and reduction of the stability in the thermal profile. Anohin et al. (2006) studied the effect local flow dynamics had on the selective withdrawal layer. They found that both internal waves and selective withdrawal were responsible for the quality of extracted water. Furthermore, steady-state estimations of selective withdrawal were still applicable even with large fluctuations from internal waves.

As many ecological and biological processes of fish are influenced by water temperature, the thermal stratification can influence the location of fish within a reservoir (RL&L, 2000). If favourable conditions coincide within a selective withdrawal layer, this could increase the risk of fish entrainment. Therefore, it is important to understand selective withdrawal and how it will influence the thermal structure in the forebay of a reservoir.

2.4 Previous Studies on the Columbia River

A few studies on the thermal regimes and hydraulics in the reservoirs on the Columbia River system in Canada have been done. Studies focussing on pre- and post-impoundment temperatures of the Arrow Lakes reservoir have been conducted. A survey of temperature information in the Kinbasket and Revelstoke reservoirs had been conducted, and some of this information was used to investigate the reservoirs plunging inflows. Also, a three-dimensional model was developed to simulate the flow fields upstream of MCA and REV. These studies are discussed below.

In response to the installation of the Arrow Lakes Hydro (ALH) generating facility next to HLK, a study of the historic and contemporary changes of the thermal regime on the Columbia River due to dam construction was undertaken (McAdam, 2000). Historic temperature data was collected from Environment Canada while contemporary measurements were taken by various organizations.

McAdam (2000) found that the construction of REV led to increased inflow temperatures into Arrow Lakes reservoir in the winter and summer. Also, McAdam (2000) concluded that increased residence time could lead to greater heat absorption in the Arrow Lakes reservoir. McAdam (2000) goes on further to state that thermal measurements have not been conducted in Kinbasket and Revelstoke reservoirs, which would be useful for a more detailed understanding of their flow dynamics.

Hamblin and McAdam (2003) studied the unexpected increase in downstream temperatures after the construction of HLK on Arrow Lakes reservoir. Mathematical models were applied to test a hypothesis that a natural sill located in the reservoir was a hydraulic control only allowing warmer waters to pass (Hamblin and McAdam, 2003). Confirming with velocity and temperature measurements, it was determined that cooler water was not blocked by the sill. Instead, Hamblin and McAdam (2003) found that increased retention time in the reservoir caused the increase in outflow temperatures.

Due to a lack of biological and ecological data in the Kinbasket and Revelstoke reservoirs, BC Hydro implemented ecological productivity monitoring program that would provide long term data on reservoir limnology (Bray 2010, 2011, and 2012). The intention was to understand the reservoir limnology and how current hydroelectric operations influenced it (Bray, 2010). Water temperature information gathered for these reports is discussed in more detail in Section 4.3.6 and Section 5.3.2.

The flow fields upstream of MCA and REV were studied using a computational fluid dynamics model (Bhuiyan and Zhu, 2009). The intake structures and forebay reservoir bathymetry were modelled and different operational scenarios were simulated (Bhuiyan and Zhu, 2009). Velocity and acceleration results were used to determine a zone of potential fish entrainment (Bhuiyan and Zhu, 2009). Furthermore, it was found that the velocity regime was significantly influenced by the shape of the structure near the intakes (Bhuiyan and Zhu, 2009). However, this study did not include reservoir thermal stratification. This density gradient will influence the flow of the water and is important when considering the risk of fish entrainment.

A study by Pieters and Lawrence in 2011 looked at nutrient resupply below the photic zone through plunging inflows. A review of water quality information collected throughout Kinbasket and Revelstoke reservoirs by BC Hydro (Bray,

2010, 2011, and 2012) was undertaken. Pieters and Lawrence (2011) found that most inflows were cold and would plunge below the photic zone.

The historical studies have generally not focussed on the dynamics of the thermal regime within reservoirs on the Columbia River system. This is an important aspect in understanding the flow dynamics within a reservoir. Continuous thermal profile surveys would enhance this understanding and aid in the assessment of the risk of fish entrainment at these reservoirs.

3. Hugh Keenleyside Dam (Arrow Lakes Reservoir)

A study of the reservoir thermal dynamics was carried out at Arrow Lakes reservoir. This reservoir was formed by HLK and was downstream of both REV and MCA. Multiple studies have found that the entrainment of resident fish was a common occurrence at hydroelectric facilities on the Columbia River system downstream of HLK (RL&L, 2000). Fish entrainment could also occur at HLK, and further studies were needed to determine the risk at this facility.

Many fish use temperature as a cue for biological processes, and some fish species in Arrow Lakes reservoir are reaching their thermal tolerance limits (Hamblin and McAdam, 2003). Therefore, it is important to understand how the dam operations affect the thermal regime within this reservoir in order to be able to assess the risk of fish entrainment at this site.

Field studies on the thermal regime were conducted in the HLK forebay during 2010. The following chapter describes the site, data collected, results and observations, data analysis, theoretical calculations, and conclusions.

3.1 Site Description

Hugh Keenleyside Dam was completed in 1968. This concrete and earth filled dam was 52 m high and located about 12 km upstream of the town of Castlegar, BC (BC Hydro, 2004), as seen in Figure 3.1. The embankment dammed the Columbia River forming the Arrow Lakes reservoir. The facility maintaining the water level through intake release was located on the north side of the channel. The immediate forebay, as seen in Figure 3.2, was located just upstream of this facility. HLK was designed for the provision of flood protection and did not provide any power generation.

There were two styles of intakes at HLK, eight low level outlets (LLO's) and four sluice gate style spill ways. The LLO's and sluice gates were located at two different elevations, as seen in Figure 3.3. All of the LLO's had crest elevations of 411.48 m. Four LLO's flanked both the north and south sides of the four sluice gates, which had crest elevations of 424.89 m. As a reference, the average water level in mid-August 2010 was 435.96 m. The LLO's and sluice gates spacing was approximately 10.7 m and 18.9 m from centreline to centreline, respectively. The sluice gates were approximately 15.5 m wide and the 6.0 m square LLO's

faces were flush with the vertical dam headwall. The sluice gate intakes were named Sluice 1, Sluice 2, Sluice 3, and Sluice 4, starting from the northernmost and moving to the southernmost. LLO's intakes were named Port 1, Port 2, Port 3, Port 4, Port 5, Port 6, Port 7 and Port 8, starting from the northernmost and moving to the southernmost. A variety of combinations of LLO's and sluice gates could be operating at any time.

One important feature to note was the presence of a hydropower facility directly north of the HLK facility. This generating station was named ALH and was built in 2002 by the Columbia Power Corporation. Water flowed into a power canal inlet, which was located approximately 900 m upstream of HLK, as seen in Figure 3.2. The power canal was about 65 m wide, and travelled parallel to the Columbia River for 1400 m, until it reached the ALH facility. ALH discharged about 400 m downstream of HLK.

Another important feature to note was the presence of a ship lock on HLK. This structure was located just south of the LLO's and sluice gates, as seen in Figure 3.2. This passage way was operated daily and passed all boat traffic free of charge. There was mainly commercial traffic, transporting timber from upstream logging operations. A floating navigation guide wall extended perpendicularly out from the dam face in order to aide in the passage of boat traffic.

Arrow Lakes reservoir was about 230 km long and 2 km wide with two main reaches, as shown in Figure 3.1. The Upper Arrow Lakes Reach, which was about 130 km long and 3 km wide, began near Revelstoke, BC, immediately downstream of Revelstoke Dam. This reach extended mainly southward, with a small degree of sinuosity. Upper Arrow was generally deeper than Lower Arrow (Hamblin and McAdam, 2003). The Lower Arrow Lakes reach, which was about 100 km long and 1.6 km wide, was connected to the Upper Arrow Lakes Reach by an area called the Narrows. The Narrows area was characterized by fast flowing water (BC Hydro, 2005), significant narrowing of the channel, and two 90° bends. The Lower Arrow Lakes reach extends mainly southward. The most southern portion of the reservoir turned to flow in a west to east direction, as shown in Figure 3.1. HLK was located at the end of the Lower Arrow Lakes reach, near Castlegar, BC.

3.2 Collected Data

The first field trip of the study was performed at HLK in 2010. Temperature and velocity information was collected in the forebay area close to the dam face. Meteorological information for HLK and Castlegar, BC was gathered from Environment Canada. Dam operation information for HLK was provided by BC Hydro. A more detailed description of the collection and content of this information are described in the next two sections.

3.2.1 Field Data

Field measurements were taken in the HLK forebay during the summer of 2010. Continuous temperature profile measurements were taken during July and August. Additionally, from August 16 – 19, University of Alberta personnel were on-site performing temperature and flow field profile measurements. These were collected in the forebay of the dam as well as near the inlet of the ALH power canal.

The on-site field studies were planned and organized with BC Hydro personnel Alf Leake and Krista Watts. Furthermore, Krista Watts helped with the installation of the thermistor chain and participated in the collection of the temperature and velocity profile measurements during the on-site field studies. BC Hydro supplied a boat to use for the duration of the on-site field studies, which was driven by David Derosa of BC Hydro. Mat Langford and Beth Robertson of the University of Alberta were present for the duration of the on-site field studies, with supporting personnel swapping out (Chris Krath, Adam Marriner, Emily Chen, and Greg Courtice).

A continuous temperature profile was measured autonomously from July 16, 2010 to August 19, 2010 using a fabricated thermistor chain. The chain consisted of twenty Onset Tidbit v2 thermistors, recording at 5 min intervals, which were physically spaced in order to capture the thermocline position. The top eighteen thermistors were spaced approximately 1.0 m apart, while the bottom two thermistors were spaced 2.0 m apart. The thermistor naming convention and approximate depths are shown in Table 3.1. The thermistor chain was attached to the floating navigation guide wall, about 90 m from the dam face, as shown in Figure 3.2. The Onset Tidbit v2 thermistors had an accuracy of 0.2 °C over the range of temperatures measured in this study, and read to a resolution of 0.02 °C.

In addition to the thermistor measurements, conductivity, temperature, and depth (CTD) point measurements were taken daily during the on-site field studies. This was completed using a Schlumberger Water Services CTD-Diver datalogger. The instrument was attached to a nylon rope with a weight and lowered from either the boat, which was kept stationary, or the navigation guide wall. Measurements were taken vertically approximately every 1.0 m and the CTD was held for about 30 sec at each elevation. The CTD datalogger has an accuracy of 0.1 °C over the range of temperatures that were measured in this study and has a resolution of 0.01 °C. Two measurements were taken within the HLK forebay (one at thermistor chain location) and one was taken at the inlet of ALH power canal, as shown in Figure 3.2.

Velocity profiles were also measured during the week of on-site field studies. The Teledyne RD Instruments Workhorse Rio Grande 600kHz (Rio Grande) acoustic Doppler current profiler (ADCP) was used, utilizing the equipment's self-contained measurement feature. In terms of velocity measurement, the Rio Grande has an accuracy of 0.25 % of the water + boat velocity, or 2.5 mm/s and a resolution of 1 mm/s. Flow profiles were recorded when the dam spilling rate was held constant, with minimal variations throughout the day (about 65 m^3/s from Sluice 3).

In reservoirs, flow profiles mainly consist of very slow velocities, on the order of 0.1 m/s. In order to obtain high quality measurements, the ADCP instrument velocity had to be low, on the same order of magnitude or smaller. Therefore, measurements taken in the forebay had to be relatively stationary. For each point along the transects, the ADCP collected flow profiles for a duration of 5 min each. This allowed for time averaging during the post processing of the data. This was done in order to reduce the error inherent in measuring relatively low velocity flow fields.

Since boats were not allowed within the debris boom, due to safety concerns, a nylon rope guideline was set up across the forebay, as seen in Figure 3.4. The ADCP was tethered to this line which extended from the rip rap bank on the left bank to the navigation guide wall. Four parallel transects were measured, with multiple points taken along each transect (10 – 20 m spacing), as shown in Figure 3.5.

The physical location of each temperature and velocity profile was determined using a real-time kinematic global positioning system (RTK GPS). For

autonomous velocity measurements within the debris boom, the rover was fixed directly above the ADCP transducer head, as shown in Figure 3.4. A base station was set up on top of the dam face, using a benchmark (GCM #70C158) located near the navigation wall access, as shown in Figure 3.2. The RTK GPS unit that was used for the field study included a Trimble R8 GNSS (Model 2) GPS receiver. For kinematic surveying, this unit has a vertical accuracy of 20 mm + 1 ppm RMS and a horizontal accuracy of 20 mm + 1 ppm RMS. The second component (RMS) of the accuracy only becomes significant for projects where the survey rover is a large distance (> 8 km) away from the receiver. For this project, the rover was always within a relatively short range of the receiver (< 1.5 km).

3.2.2 Supplementary Data

Information on the meteorological conditions was collected from Environment Canada. Three meteorological stations were located in the area (Environment Canada, 2010). The closest was located at the dam site (CASTLEGAR BCHPA DAM, Climate ID: 1141457). Another station was located at the Castlegar airport (CASTLEGAR A, Climate ID: 1141455), approximately 12 km away from HLK. A third station was located in Nelson (NELSON CS, Climate ID: 1145M29), approximately 40 km away from HLK. The meteorological station at the dam only reported daily recordings of maximum, minimum and mean temperature and total precipitation. The meteorological station at the airport recorded data on temperature and wind speed from 05:00 to 20:00 daily. The station in Nelson had hourly temperature and wind speed data.

Further information collected included dam operation information. BC Hydro provided the hourly flow rates of both HLK and ALH. This included individual intake flow rates for HLK and total discharges for ALH. This information was provided for the duration of the 2010 field studies, from July 16 to August 19.

3.3 Results and Observations

The following results and observations are from the period of HLK field studies, July 16 – August 19, 2010. A total of 35 days of meteorological, temperature profile, and dam operation information was collected. Also, a few conductivity, temperature, and depth profiles and velocity profiles were collected on August 16 – 19, 2010.

3.3.1 Meteorological Measurements

The daily maximum, mean, and minimum air temperatures recorded at the HLK facility are plotted in Figure 3.6. Temperatures were relatively warm during the summer months of the field studies. Daily maximum temperatures varied from 23.4 – 37.0 °C, and on average was 30 °C. Daily mean temperatures varied from 18.5 – 26.3 C, and on average was 22.5 °C. Daily minimum temperatures varied from 13.0 – 18.5 °C, and on average was 14.9 °C.

Additionally, hourly air temperatures recorded at the Castlegar airport are also plotted in Figure 3.6. Air temperatures from Nelson were compared to Castlegar airport air temperatures. It was found that they were relatively similar during simultaneously recorded intervals (i.e. 05:00 to 20:00). Therefore, the Castlegar Airport data was supplemented with the Nelson data for the hours from 21:00 to 04:00, which is plotted in Figure 3.6. This data shows the diurnal variation of the air temperature. The values ranged from 10.3 – 35.6 °C, and on average was 21.1 °C. The HLK Dam measurements and Castlegar airport measurements were fairly similar. The largest difference in maximum values was 4.5 °C on August 2, 2010. In general, HLK Dam maximum temperatures were hotter than the Castlegar airport. The largest difference in minimum values was 3.8 °C on August 15, 2010. In general, HLK Dam minimum temperatures were hotter than the Castlegar airport.

The daily total precipitation at the HLK facility is plotted in Figure 3.7. There were two significant precipitation events in the field study period, 13.8 mm on July 27, 2010 and 11.2 mm on August 5, 2010. The remaining days had relatively little precipitation. On days that did include precipitation, it was, on average, little more than 1.0 mm total.

The hourly wind speed from 05:00 – 20:00 at the Castlegar airport during the field study period is presented in Figure 3.8. The wind speed was fairly periodic daily, and ranged from 0 – 28.0 km/h. On average, the wind speed was 7.4 km/h. Wind was present on a daily basis. Ignoring the 0 km/h measurements, wind speed ranged from 6.0 – 28.0 km/h and averaged 11.9 km/h.

3.3.2 Dam Operations

Both HLK and ALH were operating during the time of the field studies. These daily discharges are shown in Figure 3.9. Note that ALH flows were much higher than HLK flows, and were represented on the secondary axis of the figure.

Furthermore, HLK discharges fluctuated almost daily, while ALH discharges remained relatively constant throughout the entire field study period.

At HLK, only the sluice gates were in operation during the field studies as seen in Figure 3.9. Sluice 3 discharges were the highest from July 16 – July 29, with an average flow of 231 m^3/s. Sluice 4 was operated for a short period (July 28 – August 4), with an average flow of 207 m^3/s. Sluice 1 and 2 were operated in conjunction at lower flows (103 and 84 m m^3/s, respectively) for a few days at the beginning of August. Afterwards, Sluice 3 was operating again on August 6 at 205 m^3/s, then dropped down to an average discharge of 65 m^3/s from August 8 – 19.

ALH operations were significantly higher than HLK operations, and fairly consistent, as seen in Figure 3.9. On average, from July 16 – August 19, ALH discharges were 1096 m^3/s. This discharge was more than quadruple of HLK's highest average flow. This situation was to be expected, since ALH provided power generation while HLK was intended only for water level regulation.

3.3.3 CTD Measurements

CTD measurements were used to compare different locations in the forebay area to the thermistor chain located off the navigation guide wall. This was done to determine if the forebay had a consistent temperature profile throughout. The CTD measurements were collected at three different locations in the forebay: the ALH power canal inlet, the HLK debris boom, and the HLK navigation guide wall (see Figure 3.2). The results of the CTD measurements were plotted with the recorded thermistor chain measurements and are shown in Figure 3.10. The thermistor chain measurements collected at the same time as the CTD measurements were averaged and presented in these figures. The CTD measurements generally matched the thermistor chain measurements at all three locations. All CTD measurements were within 1.54 °C of the thermistor chain measurements, and on average within 0.29 °C.

One noticeable deviation was observed at the ALH power canal inlet, as seen in Figure 3.10a. The deepest CTD values (17 and 18 m) were cooler than the thermistor chain values and differed by 0.76 and 0.81 °C, respectively. Since this CTD measurement was the furthest from the thermistor chain location, some variation could have been expected. As well, the large volumetric withdrawal from the ALH facility could have affected the flow and thermal dynamics in the ALH power canal. This change could have resulted in the deviation observed.

Other deviations were found at all three CTD measurement locations. These differences were not noticeable graphically since they occurred within the thermocline, an area of rapid temperature transition. Therefore, these measurement points were giving a triangle symbol. Deviations of 1.00 °C and 0.75 °C were observed at the ALH power canal inlet (Figure 3.10a), 1.54 °C at the HLK debris boom (Figure 3.10b), and 1.11 °C and 1.20 °C at the HLK navigation wall (Figure 3.10c). Since the water temperature changed so drastically over a short distance at the thermocline elevation it was difficult to thoroughly define it with the discrete point measurements taken.

From these results, it was determined that the forebay area had similar thermal characteristics. Deviations at the ALH power canal inlet near the bed were thought to be due to the effects of the ALH discharges on the flow. The main differences were found in all three CTD measurements at the elevation of the thermocline. Since this was an area of such significant temperature change, it was difficult to define with limited measurements. It should be noted that when excluding all the deviations mentioned, the remaining CTD measurements had, on average, only a difference of 0.17 °C from the thermistor chain.

3.3.4 Thermistor Chain Measurements

The thermistor chain measured the top 24 m of the forebay temperature profile every 5 min for a total of 35 days in the summer of 2010. The recorded profiles mostly exuded a classic two-layer temperature profile, with a well-mixed epilimnion and a cooler hypolimnion. These layers were separated by a relatively sharp thermocline. The maximum water temperature during this time period was 23.14 °C, occurring at the highest thermistor, approximately 1.2 m below the surface. The minimum water temperature was 7.77 °C, occurring at the lowest thermistor, approximately 23.8 m below the surface.

A contour plot of the mean daily temperature variations with depth from July 16, 2010 (day 197) to August 19, 2010 (day 231) is shown in Figure 3.11. The water temperature was relatively stable near the surface (on average 20.15 °C) and near the bed (on average 9.00 °C). The most significant variations were mainly within the middle layers (10 – 17 m). The top nine thermistors (1.20 – 9.89 m) remained mostly within the 17 - 22 °C temperature range, while the bottom five thermistors (17.5 – 23.8 m) remained mostly within the 8 – 12 °C range. There were two occasions where the top and bottom thermistors did not remain in these ranges, as discussed below.

During the period of July 29 – 31, 2010 (days 210 – 212) the upper water temperatures decreased significantly, and the entire profile dropped below 18 °C. The overall stratification structure could no longer be defined as a two-layer temperature profile, as seen in Figure 3.12. The thermal profile was more like a continuous temperature profile. On July 29 and 30, the thermocline position was not well defined, and the temperature decreased almost linearly from the surface to an approximately 15 m depth. On July 31, a well-mixed epilimnion layer was forming once again.

There are many factors that could have caused the drop in water temperature, including meteorological conditions and dam operations. The air temperature at the dam on July 29 and July 30 was actually quite high, 32.5 °C and 33.8 °C, respectively (see Figure 3.6). The air temperature did drop on July 31 (26.5 °C). However, the water temperatures were already beginning to recover on this day, so it was unlikely that the air temperature caused this fluctuation. Furthermore, there was minimal precipitation and fairly average wind periods (see Figure 3.7 and Figure 3.8). The only significant observable change was in the HLK dam operations (see Figure 3.9). Sluice 3 was turned off from 281 m^3/s on July 28 – July 30. Sluice 4 was turned on to 280 m^3/s on July 29 – July 30. However, during this transition, the total discharge remained at 280 m^3/s. It is unlikely that the gradual transition in operating sluice gates at the same discharge would cause such a significant decrease in water temperatures. The rapid change in temperature is more likely a result of internal seiching in the reservoir, which will be discussed further in Section 3.4.

On August 14 (day 226), the lower thermistor layer temperatures increased significantly, as seen in the mean daily water temperature contours in Figure 3.11. The water at depths 17.5 m and 18.5 m increased by about 5 °C from the previous day. The middle layers followed suit with this trend, but the top layers remained relatively constant. Furthermore, the thermocline depth dropped significantly, as seen in the water temperature profile in Figure 3.13. The thermocline position was at about an 18 m depth on August 14, while the average thermocline depth was about 14 m during the field studies.

Again, many factors could have been responsible for this dramatic increase in water temperature. The air temperature did increase from previous days, from 26.6 °C on August 12 to 31 °C on August 14 (see Figure 3.6). However, the deepening of the thermocline would not be due to only air temperature increase, but would require wind mixing as well. As seen in Figure 3.8, wind

speed was actually quite low on August 14, on average 2.5 km/h. There was no precipitation during August 14 (see Figure 3.7) and HLK operations were constant at 65 m^3/s (see Figure 3.9). Again, the explanation for the rapid temperature change seems to be reservoir internal seiching. Further analysis and discussion will follow in Section 3.4.

Another regular water temperature fluctuation can be seen in Figure 3.11. It appears as though the water temperature near the thermocline depth (about 11 m) has a peak about every three days. This three day oscillation period indicates the presence of an internal seiche within the reservoir. Further analysis will follow in Section 3.4.

Diurnal or daily fluctuations were also present in the thermal profile in the HLK forebay. For example, Figure 3.14 shows some instantaneous thermal profiles measured by the thermistor chain during July 16, 2010. It can be noted that the depth of the thermocline fluctuated approximately 2.5 m over the course of the day. In general the thermocline was at its shallowest mid-morning (10:00) and at its deepest mid-afternoon (14:00 – 16:00), indicating a diurnal fluctuation. It is logical to assume that the changes in thermal profile over the course of the day are due to daily changes in air temperatures. On July 16, air temperature peaked at 15:00 (see Figure 3.6), when the thermocline was the deepest. Also, there was no wind in the morning whereas the afternoon had speeds up to 15 km/h (see Figure 3.8). The wind further deepened the thermocline position in the afternoon through mixing of the epilimnion.

HLK thermal profiles were generally classified as a two-layer profile, with a well-mixed epilimnion and a cooler hypolimnion separated by a sharp thermocline. There were also some reservoir fluctuations apparent in the thermistor time series. Rapid temperature fluctuations (warming and cooling) with no apparent meteorological or dam changes led to the conclusion that internal seiching was occurring in the reservoir. In fact, an approximately three day oscillation period was observed in the temperature contours. An analysis and discussion of the internal seiching present in Arrow Lakes reservoir will follow in Section 3.4. Diurnal fluctuations were also present, and thermocline depth changes due to daily variations in air temperature and wind could be seen in the profiles.

3.3.5 ADCP Measurements

A total of four transects were collected from August 16 – 19 in the immediate forebay of HLK, as seen in Figure 3.5. A total of 62 point profiles were collected in this area. An example of a velocity profile plot along Transect 1 is seen in Figure 3.15. The 5 min time averaged velocities in Transects 1 – 4 ranged from - 59 mm/s to 69 mm/s, with positive flows going downstream towards the dam face. The average velocity was 8.8, 9.8, 11.3, and 12.3 mm/s for Transects 1, 2, 3, and 4, respectively.

The presentation of further results and observations of the collected water velocity profiles was not included in this study. The reason the measurements were mentioned was because these collected water velocity profiles were used to develop a three-dimensional computational fluid dynamics (CFD) model of the temperature and flow in the HLK forebay. The CFD model was used for further analysis of thermal dynamics in the reservoir. If further information is required on the ADCP velocity measurements, readers are referred to Langford et al. (2011).

3.4 Analysis

It was apparent from the temperature time series data from HLK that oscillations (or internal seiches) were taking place within the reservoir. In order to quantify these observations, a spectral analysis (or waveform analysis) of the temperature time series was performed. Spectral analysis uses the Fourier transform in order to convert data from the time domain to the frequency domain (Weimer, 2012). The Fourier transform splits up the waveform in the time domain into multiple, unique sinusoidal waves (Weimer, 2012). When added together, these sinusoidal waves reproduce the original waveform (Weimer, 2012). A spectrum is created by plotting the sinusoidal wave amplitudes versus frequencies, which is a representation of the waveform in the frequency domain (Weimer, 2012). This transformation will determine the dominant frequencies (and periods) of oscillations within a signal. This analysis will determine the periods of the internal seiches travelling through the reservoir.

The spectral analysis was completed using Welch's method, which reduced the noise in the estimated power spectra (Welch, 1967). The first step was preliminary processing, where the mean and any trends were removed from each time series. Next, the time series was divided into n_d segments which each

consisting of N values (various N values used for each analysis), overlapping by D points. The overlapping segments then had a window applied to them in the time domain (Blackman window used for this analysis). Finally, the modified series was converted to the frequency domain by taking the Fourier transform and calculating the squared magnitude of the result. The resulting periodogram (estimate of the spectral density) was a plot of power magnitude vs. frequency. This procedure was performed on the HLK thermistor chain measurements, as discussed below.

3.4.1 HLK Spectral (Waveform) Analysis

During the summer at HLK, reservoir stratification led to the development of not only surface seiches, but also internal seiches. It can be seen in the mean daily temperature contours in Figure 3.11 that the most frequent temperature fluctuations occurred at the thermocline position, from about 9 – 18 m. These fluctuations were due to internal seiching occurring at the thermocline. Also, large temperature fluctuations did occur at the surface and near the bed, as discussed in Section 3.3.4, which were most likely caused by internal seiching.

The raw data set of thermistor measurements included a total of 9965 temperature profiles. A spectral analysis was conducted on each thermistor time series in order to determine the frequencies of the most dominant oscillations. Welch's analysis was done twice using two different segment lengths (N # of measurements). This helped determine oscillations in the order of days and in the order of hours.

For the first analysis, the time series was divided into segments with N = 4982 values. With an overlap of 99% (i.e. D = 4981), this allowed for n_d = 4983 segments. These values were chosen in order to reduce the normalized random error, which is given by the equation:

$$\varepsilon_r = \frac{1}{\sqrt{n_d}} \qquad [1]$$

where:

ε_r = normalized random error; and
n_d = number of overlapping segments.

With the chosen values, ε_r of the resulting spectra was only 1.4%. Also, large segment lengths are good for a waveform that is low in variations since a lot of data averaging is done (Physics Forums, 2010). If looking at the time series on an

order of days there is not a lot of small variations, or jitter, in the signal (for example, see the mean daily averaged contours in Figure 3.11). Therefore, a long segment length was appropriate for determining oscillation periods in the order of days.

For the second Welch's analysis, each time series was high-pass filtered. All frequencies in the waveforms less than 24 hrs were removed (i.e. periods greater than a day). The signal was divided into segments with N = 500 values. An overlap of 75% was used (i.e. D = 375), which allowed for n_d = 75 and a normalized random error of 11.5%. Smaller segment lengths are good for when the signal is highly variable, since it results in less smearing and finer spectral resolution (Physics Forum, 2010). If looking at the time series on an order of hours, as seen in Figure 3.16, the signal was measured every 5 min and was quite variable, or jittery. A shorter segment length was beneficial to determine oscillation periods in the order of hours.

An example of the dominant oscillation frequencies found in the periodogram from the thermistor 10 time series is shown in Figure 3.17. For a clearer picture of the dominant oscillations, only the power magnitudes of the peaks in the periodogram were plotted with the corresponding period (i.e. in terms of days rather than Hz). Results of the spectral analysis are included in Figure 3.18 and Figure 3.19. The X-axis represented the period of the signal oscillation (either in days or hours) and the Y-axis represented the power magnitude of the spectral analysis.

The magnitude of the Fourier transform results was directly proportional to the length of segments (N) used in the analysis (Lyons, 2010). Since equal N values were used for all the frequency analysis, we could compare the relative magnitudes between the results.

There were three dominant periods of oscillation found in the thermistor chains in the order of days. These were 1.0 day, 3.5 days, and 11.6 days, as seen in Figure 3.18. The 1.0 day period was most dominant in the mid-depth thermistors, from about 7.7 – 13.2 m. This oscillation was partially due to diurnal fluctuations in the daily air temperatures causing the thermocline to deepen and rise. The 3.5 day period also had the highest powers in the mid-depth thermistors, but ranging from 11.0 – 16.4 m. The power magnitude of the 3.5 day period was also substantially higher than the 1.0 day period. It was understandable that these two dominant periods occurred at the mid-depth

thermistors. This was where the thermocline was located, which oscillated most frequently over time. The well-mixed epilimnion and hypolimnion layers remained relatively constant, as is typical of two-layer temperature profiles. However, the final period of 11.6 days was dominant in the upper and lower layers. These fluctuations were seen as the significant drop and rise in the mean daily water temperatures discussed earlier. This indicated an upwelling event in the reservoir.

Upwelling occurs in a stratified reservoir when the horizontal pressure gradient is balanced by the wind stress at the water surface (Schladow et al., 2004). This causes the thermal layers to rise at the upwind end, bringing the cooler water in the metalimnion (intermediate upwelling) or hypolimnion (total upwelling) to the surface (Schladow et al., 2004). Intermediate upwelling was the event seen on July 30, 2010. The event on August 14, 2010 could have been the reflection of the internal wave, warming the thermocline layer almost as substantially as it had been cooled.

There was no significant wind event on or around July 30, 2010 in the Castlegar airport wind speed data (see Figure 3.8). It was thought that the upwelling event could have been due to an internal seiche already travelling through the reservoir. Therefore, a spectral analysis of the hourly wind speed time series was completed in order to determine the dominant periods. The Castlegar airport wind speed data from July 1 – August 31, 2010 was analysed, as well as Nakusp wind speed data during the same time frame. While not directly on the water, the Nakusp meteorological station was located at the airport, less than one kilometre from the reservoir. It was thought that this would complement the information provided from the Castlegar airport station.

The dominant periods found in the wind speed time series are shown in Figure 3.20. The most dominant period in both sets of data was 1.0 day. These diurnal wind fluctuations were partially responsible for the 1.0 day oscillation found in the thermistor chain data. The diurnal air temperature change was also responsible for the 1.0 day internal seiche that formed in the reservoir. A period of 1.5 days was found in the Castlegar airport data, while periods of 1.7 days and 2.8 days were found in the Nakusp data. These wind fluctuations were all related to the internal seiche period of 3.5 days found in the thermistor data. It appears as though this internal wave period was created by regularly occurring wind forcing events.

Periods of 7.7 days (Castlegar airport) and 8.9 days (Nakusp) were also found in the frequency analysis of the wind speed data. Furthermore, the power magnitudes associated with this oscillation were significantly higher than other periods found (excluding the 1.0 day period) meaning they were more dominant. This means they were associated with the higher wind speed events occurring over the time frame of the data sets. It was thought that these regular high wind events led to internal seiching in the reservoir that caused an upwelling on July 30. The fact that the period determined from the thermistor chain data (11.6 days) was higher than the period determined from the wind data (average of 8.3 days) was thought to be due to the length of the thermistor time series used. The thermistor chain data set was about half as long as the wind speed data set. Only one cycle of the internal seiche was detected in the thermistor time series. Perhaps if the temperature time series was one month longer, the internal seiche period would have been averaged closer to an 8 day period.

There were three dominant oscillation periods found in the thermistor time series in the order of hours, two of which were expressed in ranges. As seen in Figure 3.19, the periods found were 6.8 – 7.2 hours, 12 hours, and 13.6 – 16.0 hours. The 12 hour period was due to the diurnal fluctuations in the air temperatures heating and cooling the water surface. This period was only found in the thermistor nearest the surface, at a 1.2 m depth. The 6.8 – 7.2 hour period found was also close to the surface, from 3.4 – 5.4 m. However, these two period ranges were miniscule compared to the 13.6 – 16.0 hour period range that was found. The power magnitudes in this range were smaller near the surface (starting at 3.4 m), about the same as the 12 hour and 6.8 – 7.2 hour ranges. The power magnitudes grew larger with depth, until they reached a maximum near the middle of the thermistor chain (13.2 m). The values were about 30 times larger than the maximum values of the 12 and 6.8 – 7.2 hour periods. The 13.6 – 16.0 hour ranges power magnitudes tapered off again with depth, until the second last thermistor, at a depth of 21.7 m.

The fluctuations from 6.8 – 7.2 hours and 13.6 – 16.0 hours can be explained by wind forced internal seiching. The spectral analysis of the wind speed data from Castlegar airport and Nakusp had periods in the range of 14.3 – 17.5 hours as well as 6.6 – 7.4 hours, as seen in Figure 3.20. Also, the 6.6 – 7.4 hour range had substantially lower power magnitudes than the 14.3 – 17.5 hour range. This was the same result found in the thermistor time series.

A spectral analysis was completed using Welch's method on each thermistor time series. This was done in order to determine the dominant periods of oscillation (internal seiche) within the reservoir. Periods in the order of days and in the order of hours were found. The 1.0 day period was thought to be caused by both diurnal air temperature heating and cooling and regular fluctuations in the wind speed. In fact, a spectral analysis was also completed on the wind speed data in the surrounding area. The results were similar to all of the periods present in the thermistor chain data. It was thought that all internal seiching apparent in the reservoir during the field study was a result of recurring wind forcing. There were no significant regular oscillations in either the HLK or ALH dam operations during the field studies, so it appears that they were not a seiche forcing mechanism.

3.5 Theoretical Calculations

Many processes affect the thermal dynamics of a reservoir. Wind can cause mixing at the surface, as well as induce internal seiching in a reservoir. Internal wave periods and amplitudes will be governed by the size and shape of the reservoir in which they are traveling. The wave will dissipate and/or reflect off these boundaries, influencing the thermal stratification in the reservoir. Significant changes in dam operations may also induce internal seiching. Furthermore, the magnitude of discharges will influence the location of withdrawal from the thermal profile. Operating below the critical discharge can result in a selective withdrawal scenario from a temperature layer adjacent to the intake. Operating above the critical discharge will result in withdrawal from more layers. These two operating scenarios will influence the thermal profile.

The thermal dynamics of the reservoir at HLK are trying to be understood due to the aforementioned processes. It is valuable to use equations that theoretically describe these processes, in order to gain a better understanding of the reservoir dynamics. Therefore, the depth of wind mixing, internal seiche oscillation period, and critical discharge were calculated for the Arrow Lakes reservoir.

HLK temperatures typically displayed a well-mixed epilimnion layer, a sharp thermocline layer, and a cooler hypolimnion layer. An estimation of this type of stratification can be made with an idealized two-layer system. The temperature profile is divided into two separate layers with a thermocline layer of infinitely

small thickness separating them. This was an important assumption that was made in the theoretical calculations for HLK.

3.5.1 Depth of Wind Mixing

The depth of wind mixing can be calculated based on the wind shear stress and the net heat flux at the water surface. These parameters are calculated on the basis of numerous meteorological conditions including short wave and long wave radiation, vapour heat flux and sensible heat flux. A more detailed overview of the required calculations is found in Appendix A. Average values of the wind shear and net heat flux were determined over the course of the thermistor installation using information from the Castlegar airport meteorological station. This resulted in a mixing depth of 9.8 m. This depth coincided with the 9.4 m average depth of the transition from the epilimnion and the metalimnion for the 35 day period.

3.5.2 Thermocline Oscillations

Based on the measurements taken in July and August of 2010, Arrow Lakes reservoir near HLK can be described as a two-layer stratification structure. Wind induced oscillations in bodies of water with this type of stratification structure can be estimated using formulae developed from the Navier-Stokes equations for two-dimensional steady flows. These formulae determine the thermocline's oscillation period and magnitude due to the wind shear stress exerted on the surface. This was thought to be representative of the internal waves recorded in the reservoir because most fluctuations occurred at the middle layers, in the area of rapid temperature transition. Also, many of the observed internal seiching were thought to be wind induced, as discussed in Section 3.4.1.

The magnitude of the thermocline oscillation was defined by (Fischer et al., 1979):

$$\Delta h = \frac{dh_2}{dx} L_B \qquad [2]$$

where:

Δh = the magnitude of the interface oscillation;

$\frac{dh_2}{dx}$ = the slope of the interface; and

L_B = the length of the basin.

The magnitude of oscillation of the thermocline slope was determined using the reduced form of the two dimensional Navier-Stokes equations. The resulting equation was as follows (Fischer et al., 1979):

$$\frac{dh_2}{dx} = \frac{\tau_o}{\Delta\rho g h_1} \quad [3]$$

where:

τ_o = the wind shear stress;

$\Delta\rho$ = the density difference between hypolimnion and metalimnion;

g = the acceleration due to gravity; and

h_1 = the depth of the epilimnion.

The wind shear stress was calculated using (Fischer et al., 1979):

$$\tau_o = C_D \rho_A U^2 \quad [4]$$

where:

C_D = a drag coefficient (1.3 x 10^{-3});

ρ_A = the density of air (1.3 kg/m^3); and

U = the wind velocity at a height of 10 m (3.4 m/s).

The frequency of oscillation is a function of the features of the upper and lower longitudinal boundaries in a reservoir. A closed boundary will allow reflection of waves and oscillations may also develop at one of numerous horizontal modes (along the reservoir). The fundamental, first, and second horizontal modes were calculated. The period of oscillation of the interface was calculated using the following equation:

$$T_2 = \frac{2L_B}{(k+1)\sqrt{g' \frac{h_1 h_2}{H}}} \quad [5]$$

where:

T_2 = the period of the interface (thermocline) oscillation;

k = 0 for fundamental frequency, 1 for first mode, and 2 for second mode;

g' = the reduced gravity;

h_2 = the depth of the hypolimnion; and

H = the depth of the basin (epilimnion and hypolimnion).

The reduced gravity term was defined as follows:

$$g' = g\ \frac{\rho_2 - \rho_1}{0.5(\rho_1 + \rho_2)} \quad [6]$$

where:

ρ_1 = the density of the epilimnion; and

ρ_2 = the density of the hypolimnion.

This approach required numerous assumptions and idealizations to be made. One assumption was the reservoir being represented as a channel with a rectangular cross section having two, discrete layers of different temperatures. The surface, epilimnion layer was assumed to be 13.7 m in depth and the lower, hypolimnion layer was assumed to be 10.2 m in depth. These values were based on the average depth of the thermocline over the course of the 35 day measurement period. During this time, the thermocline depth ranged from 9.4 – 18.0 m. Therefore, average temperatures of the epilimnion and hypolimnion layers were taken from the measurements above and below this range, respectively. The average temperature of the epilimnion was 19.7 °C, corresponding to a density of 996.87 kg/m^3. The average hypolimnion temperature was 10.0 °C, corresponding to a density of 998.80 kg/m^3. The density of water at each of these depths was assumed to change due to temperature only, and a salinity gradient was not included in these calculations. This was due to the fact that the salinity measured by the CTD instrument was generally constant and extremely small (average of 0.10 mS/cm). For this analysis, the thermocline area was assumed to be a single plane of infinitely small thickness. The wind speed (which provides surface shear stress), was assumed to be 11.9 km/hr.

The length of the reservoir, L_B, corresponded to the horizontal length between the upstream and downstream boundaries, which would affect the development of the seiche. The downstream boundary was considered to be the dam face, a closed boundary which reflects oscillations. The Burton boundary, a location about 100 km upstream, was assumed as a closed boundary because according to Hamblin and McAdam (2003), there was no backflow from Lower Arrow basin

to Upper Arrow basin. This location was also previously referred to as the Narrows in Section 3.1.

The results of the calculated magnitude and period of the thermocline oscillations for various horizontal modes are given in Table 3.2. The lowest frequency mode (longest period) found at the Burton boundary was a calculated wave period of 7.0 days. This was associated with the observed period of 11.6 days. As was discussed in Section 3.4.1, the period of record for the thermistor chain was relatively short. If the thermistor measurement period were longer, perhaps an oscillation closer to 7 – 8 days would emerge. This internal wave travelling through the reservoir from HLK to the Burton boundary would be sustained by the oscillatory wind speed patterns of approximately 8 days. Also, using an average wind speed of 11.9 km/h resulted in an average thermocline oscillation magnitude of 7.0 m. This would nearly cause upwelling of the metalimnion, as was seen on July 30. An increase to constant 18 km/h winds would result in a 15.1 m oscillation magnitude, which would result in upwelling of the metalimnion. This suggested that the temperature rise and drop were most likely controlled by the Burton boundary.

A second mode oscillation was also found relevant at the Burton boundary, resulting in a period of 3.5 days. As discussed earlier in Section 3.4.1, this period was observed in the thermistor temperature measurements. This suggested that a second mode internal wave with the period of 3.5 days was travelling through the reservoir and reflecting off the Burton boundary.

It should be noted that these calculations were very approximate. A number of assumptions were made in the calculations, including an ideal two-layer system and a rectangular cross section. Furthermore, other influencing factors were not considered, including reservoir inflow quantity and quality, bathymetry, and meteorological effects. The calculated periods give a rough estimate of what boundaries were influencing the internal wave motions.

3.5.3 Selective Withdrawal: Critical Discharge

Although the dam operations seen during the field studies did not seem to force the internal seiching within the reservoir, this does not mean that they had no effect on the thermal structure. Water temperatures near the dam face will be affected by the operations through the process of selective withdrawal. If the withdrawal operations are too small to overcome the buoyancy forces due to the temperature stratification, selective withdrawal will occur (Fischer et al., 1979).

This will prohibit vertical motions in the water column and only the horizontal water layer adjacent to an intake will flow (Fischer et al., 1979). However, when some critical discharge is reached, water will begin to withdraw from other layers (Shammaa and Zhu, 2010).

The thermal regime of HLK was idealized as a two-layer stratification structure in order to complete the analysis to estimate the critical discharge in the HLK forebay. Following Craya's (1949) solution for a point sink, the following equation was used:

$$Q_c = F_c\sqrt{g' h_c^{\,5}} \qquad [7]$$

where:

Q_c = the critical discharge;

F_c = the critical Froude number;

h_c = the distance from the centre of the outlet to the water layer interface.

The selective withdrawal will be influenced by the effects of boundaries close to the intakes. Boundaries such as the channel bed and water surface will decrease the value of the critical Froude number. This value was calculated for a point sink by Islam and Zhu (2012). Using theoretical development and confirming with CFD model simulations, a critical Froude number of 1.26 was obtained for a point sink withdrawal near a boundary (Islam and Zhu, 2012).

This calculation employed the same conditions that were used for the thermocline depth oscillations analysis discussed previously (*i.e.* epilimnion: 13.7 m, 996.87kg/m^3 and hypolimnion: 10.2 m, 998.80 kg/m^3). The critical discharge for a sluice gate, an intake located on the surface, was calculated to be 122 m^3/s. For an idealized two-layer stratification, this means for discharges below 122 m^3/s, water would only be withdrawn from the upper epilimnion layer. Buoyancy forces would prevent vertical motions across the sharp density gradient of the thermocline. Theoretically, when the discharge exceeded 122 m^3/s, the buoyancy forces will be overcome and water will begin to withdraw from the lower hypolimnion layer.

For most of the field season, from July 16 – August 10, the sluice gates were operating at an average discharge of 240 m^3/s. This implies that discharges were

above the critical discharge and selective withdrawal was not occurring during this period. However, from August 7 – August 10, Sluice 3 was operating, on average, at 65 m^3/s. This suggested that during these dates, selective withdrawal was most likely occurring at HLK.

3.5.4 Computational Fluid Dynamics Modelling

A three-dimensional CFD model was developed for HLK using the ANSYS CFX 12.1 program. The model extents covered the forebay area extending from the dam face to approximately 1.0 km upstream. The model boundaries were constructed using unstructured tetrahedral mesh which was created using topographic information provided by BC Hydro. The spacing of the mesh used ranged from 3.4 m (closer to the intakes) to 67 m (near the upstream boundary). A free-slip wall boundary was used at the reservoir's free surface, while other walls were modelled using no-slip conditions. At the ALH intake canal and at the LLOs and spill ways, mass-flow rate boundary conditions were provided. At the upstream boundary, an 'opening' boundary was provided. This allows both inflow and outflow across the boundary. The CFD solver uses the three dimensional Reynolds averaged Navier-Stokes equations, with the $k-\varepsilon$ turbulence model to assess eddy viscosity. The average temperature profile over the course of the field measurements was fit to an empirical equation to use in the model. To compute temperature transport, a full buoyancy model was chosen.

The flow field upstream of the dam was simulated under the conditions during field studies. Such conditions included discharge, temperature profile, and water level. Results were then compared to the velocity measurements taken during the field studies that were collected using an ADCP. Generally the simulations done using ANSYS CFX 12.1 matched the field measured results well. Details regarding the models governing equations, boundary conditions, and mesh can be found in a report prepared for BC Hydro (Langford et al., 2011).

The model was used to evaluate the reservoirs flow field during different operational scenarios. The average temperature stratification and ALH discharge conditions for the field season were input into the CFD model. As mentioned before, the critical discharge of a HLK sluice gate was calculated to be 122 m^3/s. HLK discharge scenarios above and below the calculated critical discharge were run for the sluice gate. This was done in order to determine if the CFD results agreed with the theoretical critical discharge calculated, as discussed below.

During the week of on-site field studies, Sluice 3 was operating at about 65 m^3/s, which was well below the calculated critical discharge. Inputting this discharge for the sluice gate into the CFD model resulted in a selective withdrawal scenario. The streamlines on a plane perpendicular to the dam face in Figure 3.21 showed water being withdrawn from only the top epilimnion layer. The middle metalimnion layer is acting as a barrier and no water from the deeper hypolimnion layer is being withdrawn.

A higher discharge from the HLK sluice gate was also analysed using the CFD model. As shown in Figure 3.22, for a discharge of 200 m^3/s, the sluice gate was withdrawing from below the thermocline and the critical discharge was overcome. The streamlines on a plane perpendicular to the dam face showed water being withdrawn from the epilimnion and hypolimnion layer. These results agreed well with the prediction of the theoretical critical discharge of 122 m^3/s for a sluice gate at HLK.

3.5.5 Conclusions of HLK Theoretical Calculations

All of the theoretical calculations for HLK were completed assuming an idealized two-layer temperature with an infinitely small thermocline between. The depth of wind mixing was theoretically calculated for the meteorological conditions at HLK. A mixing depth of 9.8 m resulted, very close to the observed average mixing depth of 9.4 m.

Theoretical calculations were undertaken to determine which boundaries in the reservoir controlled certain oscillatory periods. The Navier-Stokes two dimensional equations of flow were used with many idealizations, including a two-layer stratification structure. The Burton boundary, which separates the Upper Arrow Lakes and Lower Arrow Lakes, was chosen. Periods of 7.0 days (fundamental mode) and 3.5 days (second mode) were attributed to reflecting off the closed Burton boundary, which was ~100 km upstream of HLK. These calculated periods were generally close to the periods observed in the reservoir.

An estimation of the critical discharge in the reservoir was completed. This theoretical calculation required numerous assumptions, including an idealized two-layer stratification profile. A resulting value of 122 m^3/s was determined for a spill way located at the surface. Further investigation of the critical discharge was done by utilizing a CFD model that was developed for the site. A value of 200 m^3/s showed that withdrawal was not selective and water was being pulled from layers below the thermocline. For a discharge of 65 m^3/s, what Sluice 3 was

operating at for part of the field studies, selective withdrawal was occurring and the critical discharge had not been surpassed. The theoretical calculations corresponded well with the CFD predictions of the critical discharge.

Overall, the theoretical calculations were representative of the processes occurring within the reservoir. Therefore, it was thought that the HLK reservoir could be idealized as a two-layer stratification system. This would be valid for the period of field measurements, from July 16 – August 10.

4. Mica Dam (Kinbasket Reservoir)

A study of the reservoir thermal dynamics was carried out at Kinbasket reservoir. This reservoir was formed by MCA and located upstream of REV on the Columbia River system. This reservoir and facility possessed a lot of features that could increase the risk of fish entrainment. Discharge is one of the most important features affecting fish entrainment (RL&L, 2000). Discharges at MCA were very large, which could mean an increased risk of fish entrainment. Furthermore, larger discharges mean shorter retention times than natural lake systems. Shorter retention times lead to higher flushing rates and water velocities in a reservoir, which can guide fish downstream and possibly increase their risk of entrainment (RL&L, 2000). Also, extensive drawdown of water levels, such as in Kinbasket, can further decrease retention times and increase the risk of fish entrainment (RL&L, 2000). Therefore, a potential for the risk of fish entrainment at MCA exists.

A combined biological and hydraulic study is being undertaken for Kinbasket reservoir to estimate the risk of fish entrainment. Since fish entrainment is partially a function of the thermal regime within the reservoir, it is important to understand these dynamics within the forebay area. This study will be used in conjunction with other hydraulic and biologic measurements towards the goal of estimating the risk of fish entrainment at this site.

Field studies on the thermal regime were conducted in the MCA forebay during 2011. The following chapter describes the site, data collected, results and observations, waveform analysis, theoretical calculations, and conclusions.

4.1 Site Description

MCA was constructed on the Columbia River in 1973. The facility was situated about 130 km north of Revelstoke, BC, as seen in Figure 4.1. The 244 m high concrete and earth filled dam accounted for about 15% of BC's energy production (Caulfield, 2012). Photos of this dam and dam forebay are shown in Figure 4.2.

This hydropower facility included four operational Francis turbines, with an intention of expanding to two more. The intakes were located on the west side of the structure, near the base of the dam, as seen in Figure 4.3. The middle of

the intake structures was at an elevation of 689.8 m. The spacing of the intakes was approximately 21.5 m from centreline to centreline. The 12.7 m wide by 13.6 m tall rectangular intake faces were flush with the inclined dam headwall, which had a slope of 1:1.75 (Horizontal:Vertical). The intakes tapered to 5.4 m wide by 6.7 m tall rectangular shape within the dam structure. The intakes were named Intake 1, Intake 2, Intake 3, Intake 4, Intake 5 (future intake), and Intake 6 (future intake) starting from the easternmost and moving to the westernmost.

Many different operational scenarios were employed at MCA. The maximum discharge of any given intake was approximately 300 m^3/s. Operational scenarios varied from month to month. Total intake operations were, on average, at an annual minimum in May. Total discharges were generally less than 100 m^3/s. This trend continued until early July, when intake operations increased throughout the month. Total discharge was generally at a maximum in August, with total flows of 1000 m^3/s, on average. Intake operations also varied on a daily basis. In general, low flow occurred during the evening and early morning hours, while higher flows occurred throughout the day.

Kinbasket reservoir water levels varied substantially on an annual basis, as seen in Figure 4.4. This plot shows the water levels in 2011, which were historically similar. At the beginning of the year, from January – April, the reservoir level was dropping. Reservoir attenuation began in the beginning of May, when the water level was at a minimum elevation of about 725.0 m. The reservoir filled until it reached a maximum elevation of about 754.2 m in September. This level was held relatively constant until the end of October, when the water elevation dropped again. It was not uncommon for the Kinbasket reservoir level to differ by 30 m annually, as seen in 2011.

Kinbasket reservoir was about 190 km long with two main arms, as shown in Figure 4.1. The Canoe Reach, which was 90 km long and about 1.4 km wide, began near Valemount, BC and extended to the southeast. The Columbia Reach, which was 100 km long and about 1.4 km wide, began at the mouth of the Columbia River and extended to the northwest. MCA was located near where these two arms met, at the end of a 15 km long and about 1.2 km wide local reach, which extended perpendicularly out to the southwest.

There were three main categories of inflow sources for Kinbasket reservoir, the Columbia River, the Canoe River, and local flow. The Columbia River accounted for about 31% of inflow, while Canoe River accounted for only 3% (Bray, 2012).

The majority of flow came from local flow, accounting for about 66% (Bray, 2012). This included several streams flowing into the reservoir along the major arms. On the Columbia Reach, some stream inflows included Beaver River, Gold River, Bush River, Windy Creek, Sullivan River, Kinbasket Creek, Cummins River, and Wood Creek. On the Canoe Reach, some stream inflows include Dave Henry Creek, Ptarmigan Creek, Hugh Allan Creek, Foster Creek, and Molson Creek.

4.2 Collected Data

The main focus of this study was the MCA and Kinbasket reservoir. Extended field measurements were collected at this location and two field trips were taken in 2011. Temperature and velocity information was collected for the MCA forebay. Meteorological and dam operation information for MCA was provided by BC Hydro. Studies from 2008 – 2010 including water temperature information were also provided by BC Hydro. More detailed descriptions of the collection and content of this information are described below.

4.2.1 Field Data

Field measurements in the MCA forebay were collected during the spring, summer, and fall of 2011. Continuous temperature measurements were taken from May through November. As well, on July 11 – 13 and August 8 – 10, University of Alberta personnel were on-site performing temperature and flow field measurements which were collected within and near the debris boom as well as in the forebay of the dam.

The on-site field studies were planned and organized with BC Hydro personnel Alf Leake, Giles Shearing, and Morgan McLennan. Furthermore, Giles Shearing assisted in the installation of the thermistor chain. David Patterson and Jayme Hills of Department of Fisheries and Oceans (DFO) also helped with the collaboration and installation of the thermistor chain. BC Hydro supplied a boat to use for the duration of the on-site field studies, which was operated by Pierre Bourget and Beth Manson of BC Hydro. Chris Krath, Mat Langford, and Beth Robertson of the University of Alberta collected the temperature and velocity measurement data during the on-site field studies.

Continuous temperature profiles were measured autonomously from May 13, 2011 to November 3, 2011 using a fabricated thermistor chain. The thermistor chain was installed in two sections on two separate occasions. The upper portion of the chain, provided by DFO, consisted of eleven Onset Tidbit v2

thermistors attached to a nylon rope. This section was installed on May 13, 2011 by securing it to the floating debris boom, at the location shown in Figure 4.5. The lower portion of the chain, provided by University of Alberta, consisted of twenty Onset Tidbit v2 thermistors attached to a nylon rope. This section was installed on July 5, 2011 by attaching it to the end of the upper portion of the thermistor chain. All thermistors were recording at 5 min intervals and were physically spaced at approximately 2 m intervals. The thermistor naming convention and approximate depths are shown in Table 4.1.

In addition to the thermistor chain measurements, during the final week of on-site field studies, four CTD measurements were taken using a SWS CTD-Diver datalogger. The instrument was attached to the boats hydraulic winch line and weighted. Point measurements were taken for 30 sec, with combination of 1, 2, and 5 m intervals used for each CTD cast. These measurements were taken in the MCA forebay approximately 740 m and 560 m upstream of the debris boom, on the west side of the debris boom, and on the east side of the debris boom where the thermistor chain was located, as shown in Figure 4.5. Measurements taken near the debris boom had minimal drift, as the boat was anchored to it. During the two CTD measurements taken further upstream, the boat was not anchored and did drift throughout the measurement period. However, this drift was considered acceptable, as the entire forebay area showed similar temperature profile characteristics.

Velocity profiles were measured during the two weeks of on-site field studies from July 11 – 13, 2011 and August 8 – 10, 2011. The Teledyne RD Instruments Workhorse Sentinel 600 kHz (Sentinel) ADCP was used in conjunction with the boats hydraulic winch system. Flow profiles were recorded when the dam discharge rates were held relatively constant. Several different discharges (63 m^3/s – 274 m^3/s) and two different operational scenarios (one intake vs. all four intakes) occurred during the field data collection periods. In terms of velocity measurement, the Sentinel has an accuracy of 0.3 % of the water velocity relative to the instruments, or 3.0 mm/s and a resolution of 1 mm/s.

Velocity measurement sets included either one (July measurements) or four transects (August measurements), approximately perpendicular to each operating intake on the dam face. The Kinbasket forebay was approximately 61 m and 67 m deep during the 2011 July and August on-site field studies, respectively. Since the intakes were located at the very base of the dam face, it was concluded that velocities in the upper portion of the flow profile were of

little significance. Therefore, in order to collect a more detailed view of the area of interest, the Sentinel was placed in a mooring cage and submerged between 20 – 35 m using the boats hydraulic winch system, as shown in Figure 4.6. This allowed the instrument to record velocities down to the bottom of the reservoir.

As before in the HLK forebay, in order to obtain high quality measurements the ADCP instrument velocity (and therefore boat velocity) had to be minimal, on the same order of the flow field within the reservoir or smaller. In order to collect relatively stationary measurements, nylon rope guidelines were used to anchor the boat, as shown in Figure 4.6c. During the first 2011 on-site field trip in July, two guidelines were used, tied on either side of the boat and attached to the debris boom. Since there was noticeable drift occurring while using this method, alterations were made for the second 2011 on-site field trip in August. During that field trip, a three point anchoring system was used; two guidelines were attached to the debris boom as before, and one extra guideline was attached to the dam face.

Velocity profile measurements were collected for a duration of about 5 min at each point of interest. This allowed for time averaging during the post processing of the data in order to reduce the error inherent to measuring relatively low velocity flow fields. Multiple points along each velocity transect were measured with a 10, 20, and 50 m spacing (approximately). The approximate locations of the ADCP measurements are shown in Figure 4.5.

The physical location of each measurement was again determined using a real-RTK GPS. For ADCP measurements, the rover was fixed on a tri-maran boat which was floating directly above the submerged ADCP transducer head, as shown in Figure 4.6. A base station was set up on top of the left bank, using a self-established benchmark, shown in Figure 4.5. The location of this benchmark was checked against several bench marks that were located on the dam structure (GCM #73C091, BM2500 – 2503, BM2248 - 2251). The RTK GPS unit used for the field study was a Trimble R8 GNSS (Model 2) GPS receiver.

4.2.2 Supplementary Data

Information on the meteorological conditions was provided by BC Hydro. A meteorological station was located near the middle of the dam crest. This included hourly measurements of temperature and wind speed for all of 2011. Additionally, rainfall accumulation was also recorded at the toe of the dam, near the downstream tailrace.

Dam operation information was also provided by BC Hydro. This included individual intake flow rates on an hourly basis. This information was provided for almost the duration of the 2011 field studies, from May 1 to October 25.

Furthermore, a monitoring program of the Kinbasket reservoirs ecological productivity has been ongoing since 2008. Three years of preliminary data collected by BC Hydro have been reported and made publically available (Bray, 2010 – 2012). Some of the information of interest to this study included temperature profiles collected throughout the reservoir, reservoir characteristics, and tributary flow and temperature characteristics.

4.3 Results and Observations

The following results and observations are from the period of MCA field studies, May 13 – November 3, 2011, a total of 175 days. General trends in the meteorological data and dam operations at MCA were discussed. Observations in the general monthly water temperature stratification were made. Seasonal water temperature fluctuations and possible causes were also discussed. Furthermore, water temperature information from 2008 – 2010 BC Hydro studies were presented and compared to the 2011 field measurements.

4.3.1 Meteorological Measurements

The hourly air temperatures recorded at the MCA facility are plotted in Figure 4.7 (a – f). Average temperatures changed throughout the seasons. In May, air temperatures were cool (on average 7.9 °C), and ranged from -1.4 °C to 19.6 °C. June air temperatures were warmer, on average 12.7 °C, and ranged from 5.1 °C to 24.6 °C. Warming continued into July, with average air temperatures of 13.6 °C and ranges of 5.9 °C to 27.2 °C. The warmest month on average was August, at 14.5 °C. The temperature range was slightly cooler than July, from 4.1 °C to 26.6 °C. Cooling was apparent in September, with an average of 11.3 °C and a range of 0.9 °C to 21.9 °C. Cooling continued into October, with an average of 4.4 °C and a range of -0.8 °C to 12.7 °C.

During July and August MCA temperatures were relatively cooler than at HLK. It should be noted that these measurements were taken in different years, and the intent was not to describe the climate of these two areas with this comparison. The intent of this comparison was to see what the climate was like during the field measurement periods. MCA maximum daily temperatures were, on

average, 10 °C cooler than HLK. MCA minimum daily temperatures were, on average, 5 °C cooler than HLK.

The daily total precipitation at the MCA facility is plotted in Figure 4.8 (a-f). Total precipitation was relatively low. The largest daily total measurement was 2.1 mm on July 7, 2011. May, June, and September had few precipitation events, with monthly totals of 5.0 mm, 6.0 mm, and 7.3 mm, respectively. July and October were the wettest months, with 11.1 mm and 16.1 mm, respectively. August was the driest month with only 2.5 mm of precipitation. MCA precipitation during the field studies was somewhat of a contrast to HLK, where one event in July had more precipitation than that entire month at MCA.

The hourly wind speed at the crest of MCA during the field study period is presented in Figure 4.9 (a-f). Some wind was consistently measured at MCA and the reading rarely went to 0.0 km/h. There were monthly trends in the average wind speeds. May had the highest average, at 11.2 km/h. May also had the highest recorded wind speed, and ranged from values of 0.2 – 64.7 km/h. June was slightly lower, with an average wind speed of 10.6 km/h and ranging from 0.3 – 44.8 km/h. July was similar to June, with an average wind speed of 10.7 km/h and a range of 0.0 – 57.4 km/h. August had slightly lower values, with an average wind speed of 8.0 km/h and a range of only 0.0 – 31.9 km/h. September and October wind speeds were similar to August, with averages of 9.4 km/h and 9.2 km/h, respectively, and ranges from 0.1 – 36.1 km/h and 0.0 – 41.6 km/h, respectively.

It appears that the wind speed at MCA was somewhat higher than HLK during their respective field study periods. The averages in July at MCA and HLK were 10.7 km/h and 7.4 km/h, respectively. Also, the individual wind events at MCA were significantly higher than HLK. In July and August, MCA wind speed maximums were 57.4 and 31.9 km/h, respectively, whereas at HLK, wind speed maximums in July and August were both only 28.0 km/h. The location the meteorological stations should be noted. MCA wind speeds were measured on top of the dam crest, next to open water. HLK wind speeds were measured at the Castlegar airport, about 12 km from the reservoir. Wind speeds over land are generally less than wind speeds over water (Hamblin and McAdam, 2003).

4.3.2 Dam Operations

The total hourly discharge at MCA during the field study period is shown in Figure 4.10 (a-f). One general trend noted in May and June was semi-diurnal

withdrawal; the intakes would operate for a few hours in the morning (around 08:00) and a few hours in the evening (around 20:00). By contrast, the general trend in July, August, September, and October was diurnal withdrawal; the discharges would begin in the morning (around 07:00) and last throughout the day until the late evening (around 00:00). These trends were just on average, and flows did start and stop at different times.

During the first week of May, discharges were relatively high, as seen in Figure 4.10a. During operating hours, on average, the discharge was 510 m^3/s. Intakes 1, 2, and 3 were operating during this period. For the remainder of May and the month of June (Figure 4.10b), the discharges were relatively low. During operating hours, the discharge was 69 m^3/s, on average. Different combinations of intakes were operating during this period, including Intakes 1, 2, and 3 (May 7 – 13 and June 24 – 25), Intakes 1 and 2 (May 14 – June 10, June 12 – June 17, and June 20 – 23), Intakes 1, 2, and 4 (June 10 – June 11), Intake 1 (June 17 – June 20), Intakes 2 and 3 (June 25 – 26), and Intakes 1 and 3 (June 27 – 30). It can be seen in Figure 4.11 (a-d) that multiple intakes are employed in discharge operations with many different combinations that change every few days. This was true for every month.

In July, discharge operations were ramped up, as seen in Figure 4.10c. The average total discharge (excluding the first few days of low discharges) was around 400 m^3/s during operating hours. In August, discharges were the largest, with a maximum value of 1109 m^3/s, as shown in Figure 4.10d, when all four intakes were operating. Discharges were higher in the first two-thirds of the month, with an average of 898 m^3/s during operating hours. Mostly all four intakes were operating during this period. In the last third of the month, average operating total discharge was 608 m^3/s. September discharges were still fairly high, as seen in Figure 4.10e. The average total discharge during operating hours in September was 650 m^3/s. This included several day long periods of constant discharges, where the intakes were not turned off in the evening hours. Average operations in October (see Figure 4.10f) were still quite high, 608 m^3/s during operating hours. There were several day long periods of constant discharges, similar to September.

Mica dam operations were generally low in May and June. In July, discharges were increased until a maximum was reached in August. September and October discharges were slightly lower than August, but still higher than July. Discharges mainly followed a semi-daily (May and June) or daily (July – October)

cyclical pattern, with intakes discharging throughout the day and turned off in the evening. Furthermore, many different combinations of the four operational intakes were used. These combinations were also changed frequently, normally every few days.

4.3.3 CTD Measurements

CTD measurements were completed in order to determine if the entire forebay area had similar temperature stratification structure as compared to the location where the thermistor chain was installed. The results of the CTD measurements were plotted with corresponding recorded thermistor chain measurements and are shown in Figure 4.12. The thermistor chain measurements were recorded during the same time period CTD measurements were taken, with one exception. When the thermistor chain was out of the water and downloading, a CTD measurement took place at the same location. For this plot, thermistor chain measurements taken 10 min prior to the CTD measurement were used for comparison. The CTD measurements were collected at four different locations: ~560 m upstream of dam face, west MCA debris boom, thermistor chain location, and ~740m upstream of dam face, as shown on Figure 4.5.

The CTD measurements matched closely with the thermistor chain measurements at all four locations. All CTD measurements were within 0.72 °C of the thermistor chain measurements and on average within 0.21 °C. The largest observable deviation from the thermistor chain temperature was the CTD measurement below 50 m depth, taken approximately 740m upstream of the dam face (see Figure 4.12c). This was the location furthest away from the thermistor chain and would be expected to be the most different from the temperature stratification near the dam.

From these results, it was determined that the forebay area had similar thermal characteristics. The largest deviations from the thermistor chain were at the ~740 m upstream position and were thought to be due to the far distance from the other measurements. Even when including these deviations, the measurements were still within an average of 0.21 °C. This was comparable to the results seen at HLK, which had an average deviation of 0.29 °C.

4.3.4 Thermistor Chain Measurements

The thermistor chain at MCA measured only the top 20 m of the water column temperature for a total of 53 days in the spring of 2011. After an extension was installed on July 5, 2011, the top 63 m of the water column temperature was

measured for 122 days. There was a total of 175 days of temperature measurements collected after two data recovery trips, once during field studies in mid-August, 2011 and once in early November, 2011.

It should be noted that there were a few problems with some of the thermistors. Thermistor 10, at a depth of ~18.2 m, consistently recorded at an interval slightly greater than 5 min. Due to this inconsistency, it was not used in any of the results or analyses. Also, after the August data download, thermistors 1, 7, 16, 20, and 21 at depths of approximately 0.20 m, 12.20 m, 32.65 m, 40.65 m, and 42.65 m, respectively, no longer were recording data.

Contour plots of the mean hourly temperature variations with depth in May (starts on day 133) and June (starts on day 152), July (starts on day 182) and August (starts on day 213), and September (starts on day 244) and October (starts on day 274) are shown in Figure 4.13(a – c). In spring, the water column temperature was homogeneous. Around May 30 (day 150), the top layers of water were warming up and the thermal regime started to become stratified. In mid-summer, around July 29 (day 210), the reservoir was fully stratified. As the summer progressed, warmer water was continuously getting deeper. For example, the 11 °C isotherm was at a depth of ~20 m on July 29 and at a ~35 m depth on September 11 (day 254). After September 11, the top layers began to cool off and the reservoir was once again transforming into a homogeneous state.

Regular periods of oscillation were seen in the contour plots. Looking at the 4 °C isotherm in Figure 4.13a, it reached the surface on May 27 (day 147), June 4 (day 155), June 14 (day 165), and June 24 (day 175). This was evidence of an internal seiche with an approximately 10 day period travelling throughout the reservoir. The oscillation magnitude of this seiche was larger than 20 m. During July and August the multi-day period of oscillation changed. As seen Figure 4.13b, the 8 °C isotherm has peaks on July 9 (day 190), July 15 (day 196), July 21 (day 202), July 27 (day 208), August 14 (day 226), August 18 (day 230), August 23 (day 235), and August 29 (day 241). These regular fluctuations were evidence of a shorter internal wave period of approximately 5 days travelling throughout the reservoir. The oscillation magnitude in July was an average of about 18 m. In August, the oscillation magnitude was smaller, with an average of about 10 m. The stratification was changing from a homogeneous profile in May to a well-defined, linear profile in July and August. This change in stratification was partially responsible for the change in fluctuations (from a 10 day to a 5 day

internal seiche period). As well, wind speeds were generally smaller in July and August, leading to smaller periods of fluctuation. An approximately 3 day period was observed during July and August in depths from about 30 – 50 m. This period was most clear in the 6 °C isotherm. The magnitude of the oscillation during this time frame was about 5 m. September and October had regular diurnal periods of oscillation, as seen in Figure 4.13c in the deeper layers from about 40 – 60 m. As well, an approximately 20 day period can be seen looking at the 12 °C isotherm. A peak in the isotherm occurs on September 3 (day 246), a trough on September 11 (day 254), another peak on September 26 (day 265), and another trough on October 2 (day 275).

Substantial deepening of the warmer surface waters occurred on a few occasions, including August 7 (day 219) and September 11 (day 254). On both days large wind speeds were occurring, up to a maximum 32 km/h for both days. This caused mixing at the surface layer, deepening the warmer water temperatures.

The following sub-sections will describe and discuss the general shape of the temperature profile in Kinbasket reservoir, which will also be compared to the HLK profile. As well, temperature changes from month to month will be discussed. Representative profiles for each month will be presented. Finally, an extensive review of day to day fluctuations will be analysed. An attempt to explain these fluctuations will be done by looking at meteorological conditions, frequency of occurrence, and discharge operations.

4.3.4.1 Linear (Continuous) Temperature Profile

The water temperature ranged from a maximum value of 20.44 °C near the surface to a minimum of 3.72 °C at a ~63 m depth throughout the field measurement period. In general, the summer temperature stratification was close to linear, meaning the temperature gradient was almost linear from the surface down to a hypolimnion layer. This shape is shown in the typical hourly profiles from July 11 in Figure 4.14a. This was in contrast to the well-defined, two-layered structure that was found in HLK. MCA did not have an obvious sharp thermocline separating an epilimnion and hypolimnion. This could be due to differences in meteorological conditions, dam operations, and/or water withdrawal locations.

As mentioned before, HLK air temperatures were generally warmer than MCA in July and August. This could have resulted in a higher net heat influx and warmer

surface water temperatures at HLK. However, wind causes mixing in the top layers, creating a homogeneous, well-mixed epilimnion. Wind was present at both dams during July and August. Even though HLK wind speeds were lower, it should be noted that those measurements were taken over land. Open water measurements would have been higher, and more comparable to MCA. Although wind was constantly present, MCA still did not have a well-mixed epilimnion layer (at least not for a long period of time) in July and August.

Other factors were affecting the temperature stratification. Average discharges at MCA (737 m^3/s) were much higher than HLK (174 m^3/s) in July and August. Also, the intakes were located much deeper in MCA, at an average depth of 62 m. The HLK sluice gates were discharging water from the surface.

It has been found that deep reservoirs with deep intakes display the characteristics of a thick metalimnion layer with linear or continuous stratification (Vidal et al., 2007). Also, the linear stratification observed at MCA was typical of northern lakes. Stevens and Lawrence (1997) state that the two-layer idealization of a Northern Hemisphere reservoir is usually appropriate only after late August, when the autumn cooling deepens the top mixed layer to a sharp thermocline. Before this time, Stevens and Lawrence (1997) describe the thermal regime as having a shallow epilimnion (a few metres) overtop a thick metalimnion layer, similar to the observed MCA profile. A well-mixed epilimnion during this time will only be present following significant wind events or cooling processes (Stevens and Lawrence, 1997). In the study of Casamitjan et al. (2003), observed temperature profiles from a reservoir containing relatively deep withdrawal structures were compared with simulated temperature profiles from a calibrated one-dimensional simulation model. In the model simulation, no withdrawal or inflow was taking place, and the results represented traditional lake profiles, where the epilimnion was growing with time. By contrast, the observed profiles showed a linear stratification pattern down to the intake elevation, with the thermocline occurring at this level. It was obvious from this comparison that the thermocline position and the whole thermal profile were greatly affected by the intake withdrawal.

During summer stratification at MCA it was observed that the temperature profile could be described as linear. Several factors could have caused this shape, including the generally lower air temperatures and high discharge from deep intakes. Several studies found that thermal profiles are affected by intake

withdrawal. As well, this shape was described as typical of lakes in the Northern Hemisphere during July and August.

4.3.4.2 Typical Monthly Temperature Profiles

Although the profile was generally linear in the summer, there were significant differences in the typical temperature profiles at MCA from month to month. Typical hourly temperature profile plots for each month are shown in Figure 4.14 (a-h).

Temperature profiles from May 13 – May 30 showed similar characteristics. As shown in Figure 4.14b (May 23), the profile was rather homogeneous, with the most variation occurring at the surface. During hours 00:00 – 12:00, the surface was relatively constant at about 5.0 °C. Then, during hours 13:00 – 16:00, the surface warmed to a maximum of 7.9 °C. After this, the surface layers cooled, and return to about 5.0 °C the following morning. This trend was generally followed throughout the month of May.

The water temperatures in the month of June were warming up overall, and the profiles began to show a more linearly stratified trend. As seen in Figure 4.14c (June 27), the surface layers were warmer (~11.0 – 15.0 °C) compared to the May profile, along with the 20 m depth temperature (~7.5 °C in June compared to ~4.5 °C in May). Figure 4.14c also shows the general daily warming and cooling trend, mainly in the surface layers. It should be noted that the temperature profiles throughout the month fluctuated immensely, up to 9 °C at one location over the course of the day. Figure 4.14c was only a general profile of the stratification structure for the month of June.

The month of July had water temperature profiles similar to June, but an extra 40 m of the water column temperature was recorded when the thermistor chain extension was added on July 5, 2011. As seen previously, Figure 4.14a (July 11) shows a typical profile shape from the month of July. The temperature was linearly stratified from top to bottom with no well-defined thermocline structure. During July 11, the top layer was on average 15.3 °C, whereas the monthly average was 12.6 °C and ranged from 18.8 – 7.1 °C. The bottom layer varied significantly less. On July 11 the bottom layer was, on average, 4.6 °C, whereas the monthly average was 4.4 °C and ranged from 6.2 – 3.7 °C.

Water temperature profiles in the month of August were fairly consistent. A typical profile is shown in Figure 4.14d (August 28). The average surface and bottom temperature on August 28 was 17.0 °C and 4.7 °C, respectively. The

monthly average water temperature for the surface was 16.3 °C and ranged from 19.6 – 12.9 °C, warmer than July. The monthly average water temperature for the bottom thermistors was 4.6 °C and ranged from 6.3 – 3.9 °C, which was almost identical to July.

The beginning of September, from September 1 – 11, had similar profiles to August except with lower surface water temperatures. As seen in Figure 4.14e (September 4), the average for this day was 15.4 °C at the surface and 4.9 °C at the bottom layer. The average water temperature during September 1 – 11 at the surface was 15.8 °C and ranged from 17.4 – 13.8 °C, cooler than August. The average water temperature during September 1 - 11 at the bottom was 4.8 °C and ranged from 5.7 – 4.2 °C, similar to August. After September 11, the profile began to change. The top layers quickly became homogeneous. On September 12 – 14, the first ~10 m of the water column was ~17 °C. The top layers cooled over the next two days until the well-mixed epilimnion was at ~13 °C for the top ~15 m of the water column. The top layers remained at ~13 °C for the remainder of the month, with the depth of mixing fluctuating, up to a maximum of ~30 m deep, as shown in Figure 4.14f (September 19). Air temperature was generally decreasing after September 11, as seen in Figure 4.7e. Concurrently, the wind speed increased dramatically for a few days following September 11, up to 36 km/h (see Figure 4.9e). These two meteorological changes were the reason for the well-mixed epilimnion with increasing depth.

Water temperature profiles in October were similar to the end of September profiles. The top layers were very well-mixed and remained nearly the same temperature throughout the day, as seen in Figure 4.14g (October 8). At the beginning of October the top layer was at a temperature of ~13 °C, which slowly cooled throughout the month, with a few fluctuations, to a temperature of ~10 °C. The depth of mixing fluctuated between ~15 – 40 m, but on average was at ~30 m, as seen in Figure 4.14h (October 30). It seems this cooling and deepening trend would continue until the profile became homogeneous, as was expected in the winter months.

There were general profiles that were typical of each month. In May, the profile was cool and generally homogeneous. Warming of the surface occurred in June, and a more stratified profile was seen. July also had a linearly stratified profile, with overall warmer temperatures than June. This trend continued into August, with still warmer temperatures and a consistently linear temperature gradient. In September, surface temperatures began to cool and the temperature profile

shape changed. The surface was a homogeneous layer over top of a linear temperature gradient. October had the same profile shape as September, but the layers were generally cooler.

4.3.4.3 Temperature Profile Changes

As mentioned in the previous sub-section, the temperature profiles did deviate substantially from their typical monthly profiles. These fluctuations in the temperature profile provided evidence of some of the warming processes due to air temperature and also mixing processes due to wind, internal seiching effects, and dam operations. These fluctuations are discussed in more detail below.

Some dramatic differences can be seen when looking at the temperature profiles from May 17 to May 18 in Figure 4.15. The top 2.5 m of the water column increased substantially from about 4.5 °C up to almost 10 °C in only the span of one day. These characteristics can be attributed to the trends in the meteorological data during this time frame. As seen in Figure 4.16a (a detailed plot of air temperature and wind speed), the air temperature was higher during May 18 than previously, reaching a maximum of 14 °C. Concurrently, the wind speed was relatively low, remaining below 10 km/h for most of the day. Concurrently, the dam operations were relatively low (<300 m^3/s), as shown in Figure 4.16b, and were unlikely to have significantly affected the thermal profile. This trend was also observed in the temperature profiles on June 22, as seen in Figure 4.17. Air temperatures were relatively high on June 22 (up to 24.6 °C), as seen in Figure 4.18a. This period was also characterized by low winds (on average 6.9 km/h). This leads to the conclusion that a combination of slow winds and high temperatures will lead to steep temperature gradients near the surface, when the radiant heat energy can be absorbed at the top of the water column. It should be noted that during this time period, the dam operations were also relatively low (<100 m^3/s), as shown in Figure 4.18b, and unlikely to significantly affect the thermal profile.

Wind had the opposite effect on the water temperature gradient as the high temperatures discussed above. Wind caused mixing at the surface and flattened out the temperature gradient to a more homogeneous profile. This can be seen in the June 8 water temperature profiles in Figure 4.19. During the first half of the day wind speeds were consistently high, on average 22 km/h, as seen in Figure 4.20a. This caused the water temperature profile to flatten out and become homogeneous. This transition can be seen from 00:00 to 02:00 in Figure 4.19a. The profile remained relatively consistent until 12:00. After this time, the

wind speed dropped (below 15 km/h) and air temperature increased to 15 °C. This again led to the steepening of the temperature gradient in the water profiles, as seen at 15:00 to 23:00 in Figure 4.19b. Again, it should be noted that the dam operations were relatively low (<100 m^3/s), as shown in Figure 4.20b.

An extremely high wind even occurred on July 8 as seen in Figure 4.21a. The maximum wind speed was 57 km/h and the average wind speed was above 30 km/h for most of the day. This day was also characterized by low air temperatures, on average about 10 °C throughout the day. Also, the discharge was relatively low, about 200 m^3/s for only an hour (see Figure 4.21b). The water profiles on July 8 are shown in Figure 4.22. It can be seen that the temperature profiles cooled while becoming homogeneous near the surface throughout the day. For example, at 00:00, there was a small mixed layer at the surface (about 2.5 m deep) at a temperature of about 16 °C. At 10:00, the mixed layer was about 5 m deep and cooled to 13 °C. By the end of the day, at 22:00, the surface mixed layer had grown to about 7 m deep and cooled to a temperature of 9 °C.

Another example of reservoir mixing can be seen in Figure 4.23 (July 26, July 28, and July 30). The top layers of the profile began to cool in the early morning of July 26. This trend created a somewhat more defined thermocline shape, as seen in Figure 4.23b (July 28). The top ~35 m could have been characterized as a well-mixed epilimnion while the bottom ~5 m was the cooler hypolimnion. The transition from ~35 – 55 m could have been characterized as the thermocline.

This deepening of the well-mixed upper layer can be explained by a penetrative convection process. On July 28 the air temperature was cooler, reaching a peak of only 15 °C, as seen in Figure 4.24. When the air temperature cools, the thermal exchange of heat at the water surface begins to decline (Fischer et al., 1979). This loss of heat induces convective motions within the surface layers which results in mixing (Fisher et al., 1979). The mixing can progress further and further down the water column until it reaches a stable thermocline structure or the air temperature warms and radiative heating begins to warm the surface layers again (Fisher et al., 1979).

This “two-layer profile” in July was not sustained, which can be seen on July 30 in Figure 4.23c. The top layers of water began to warm, creating the typical linear stratification profile again. This leads to the belief that the penetrative

convection process was not stopped by a stable thermocline structure, but more due to the addition of radiant heat energy to the surface water layers.

Penetrative convection was also seen during reservoir cooling periods in late September and October (Figure 4.14f and Figure 4.14g). Air temperatures were generally cooler, causing the water surface to lose heat. This, in turn, induced the convective motions which thoroughly mixed the surface layers. As the air temperatures were remaining cool, the linear profile was not regenerated as it had been in July. This caused the formation of the well-mixed epilimnion layer found in late September. As the air temperature became cooler, this well-mixed layer became deeper, as found in October.

An interesting phenomenon to note was the bottom thermistor temperature increase on July 7, at 08:00 (Figure 4.25a). At a depth of 55 m, the temperature increased from about 4.5 °C at 06:00 to about 7.5 °C at 08:00. During this time period the wind speed was relatively low and only increased slightly (3.9 – 5.4 km/h), as seen in Figure 4.21a. Also, the air temperature was relatively consistent (11.9 – 13.6 °C). The intake discharge did increase over this period by 109 m^3/s (see Figure 4.21b), which is relatively low compared to the previous days 600 m^3/s discharge. Also note that on July 6 there were similar air temperatures and wind speeds to July 7, and the profiles were generally consistent throughout the whole day, as seen in Figure 4.25b. This leads to the belief that meteorological conditions and dam discharge operations were not responsible for the temperature increase seen on July 7. A possible explanation for this rapid temperature change could be the internal seiching effects. If an internal wave(s) were moving through the reservoir, it could push warmer water to a deeper position in a short amount of time.

A similar phenomenon was noted on June 26 (Figure 4.26a). From 06:00 to 22:00, the entire 20 m water profile consistently increased about 1 °C every four hours. The wind speed during the day was relatively low, on average 8 km/h (Figure 4.27a). The air temperature did increase substantially from 8 °C in the morning to about 20.5 °C in the evening. As discussed earlier, low winds and high temperatures should lead to a steep temperature gradient as the surface warms. However, in this instance, the entire top 20 m of the water column warmed uniformly. This trend could also be explained by the effects of internal seiching. As the surface was heating, warmer water could have been pushed down to a 20 m depth, creating a homogeneous profile. Near the end of the day, at 22:00, the top 2.5 m of the profile began to steepen. This was consistent with

the low wind (7.1 km/h) and high air temperature (17.8 °C) occurring at the time. This could indicate that the internal wave had passed, and the temperature profile was responding to the meteorological data as it previously had been. It is interesting to note that a high wind event occurred on June 24, two days prior to the internal wave arrival (see Figure 4.27a). Average wind speeds were quite high, with an average of 20 km/h sustained throughout the day. This wind event could have perturbed the isotherms from equilibrium, setting up an internal seiche.

This same trend was also noted on June 5 and June 16, as seen in Figure 4.26b and Figure 4.26c, respectively. The air temperature on June 5 was quite high, up to 22.1 °C as seen in Figure 4.27b. The wind speed was relatively low (average of 5.6 km/h). This combination should have resulted in a steep temperature gradient on the surface. The June 5 profile did exude a steep temperature gradient, however it is uniformly increased through the entire 20 m profile. Previously, the increased water temperature only occurred close to the surface, no more than 5 m deep. On June 5, at a depth of 10 m the water temperature increased from about 4.0 °C to about 8.0 °C over the course of only 14 hrs. A similar trend occurred on the morning of June 16. The profile warmed uniformly over the entire 20 m profile, from about 5 °C at 05:00 to about 10 °C at 21:00. The wind speed was relatively low on this day, about 6.8 km/h, on average (see Figure 4.27c). The air temperature was diurnal, increasing from about 9 °C in the morning to about 15 °C in the mid-afternoon then decreasing again in the evening. Therefore, it was unlikely that the day's meteorological effects caused the increase in water profile temperatures. However, on June 3 and June 14 the wind speed was relatively high, with averages of 15.0 km/h and 19.4 km/h, respectively, for most of the day. These events could have set up an internal seiche in the reservoir and the rapid temperature fluctuations could be explained by the effects of internal seiching. The surface water was warmed by radiant heat energy which was pushed to deeper thermistors by the internal wave motions, which increased the entire profile temperature. Surface heating was stronger on June 5 (22.1 °C) compared to June 16 (15.1 °C), so the June 5 thermal gradient also steepened closer to the surface. The June 5, June 16, June 26, and July 7 phenomenon occurred 11, 10, and 11 days, respectively, apart from one another. This period agreed well with the observations from the average hourly contours and could have been the period of an internal seiche wave travelling through the reservoir.

This trend of rapid temperature change continued into July and part of August. However, the temperature change occurred deeper in the profile, was less substantial (see Figure 4.28a), and more frequent. Rapid temperature fluctuations were found on July 12, July 17, July 23, July 27, August 1, and August 6. The mid-depth thermistors, located around 25 – 55 m, seemed to be affected by internal seiching about every 5 days, which was also observed in the mean hourly temperature contours. These water temperatures changed by about 2 °C over the period of a day. For example, on July 17, at a depth of 50 m the temperature increased from 4.6 °C at 12:00 to 6.6 °C at 22:00 (see Figure 4.28a). Wind was relatively low during this time frame (average of 8.2 km/h), as seen in Figure 4.29a. The air temperature was peaking at 20.4 °C in the afternoon and then falling to 15.6 °C in the evening. Therefore, it is unlikely that the day's meteorological effects caused the fluctuation. The dam operations were being turned off during this period, as seen in Figure 4.29b. The total discharge decreased from 457 m^3/s at 17:00 to 2 m^3/s at 19:00. The sudden change in operations could have created a response in the thermal profile. However, during the previous day the dam operations dropped from 413 m^3/s at 23:00 to 0 m^3/s at 01:00. During this time period, the bottom temperature remained relatively consistent as seen in Figure 4.28b. It appeared as though the sudden dam operation change did not noticeably affect the temperature profiles. Therefore, the temperature raise in bottom thermistors observed on July 17 most likely was due to an internal wave travelling through the reservoir. Again, a somewhat significant wind event was seen prior to the seiche phenomenon (see Figure 4.29a). On July 15, the wind was sustained throughout the day at about 18.3 km/h. This event could have forced the internal seiche seen on July 17.

For most of remainder of August temperature fluctuations were small, and remained within 2 °C each day. This period was characterized by fairly high air temperatures (Figure 4.7) and relatively low wind speeds, which were mostly below 15 km/h (Figure 4.9). These conditions could have decreased the amount of mixing in the water column. The low wind speeds would lessen the mixing on the surface, as well as excite smaller internal seiches within the reservoir.

Dam operations were largest during the month of August. There was some evidence during August of dam operations affecting the thermal regime. In general, when dam operations were ramped up, thermistors nearest the intakes decreased in temperature. Some examples of this trend were seen on August 11 and August 23. Four of the bottom thermistors and the total intake discharges

are plotted on these days in Figure 4.30a and Figure 4.30b. On August 11, the discharge increased from 488 m^3/s to 1104 m^3/s over the course of three hours (06:00 to 09:00). Thermistors located at 50.7 m, 54.7 m, 58.7 m, and 62.7 m each decreased in temperature by 0.771 °C, 0.517 °C, 0.518 °C, and 0.26 °C, respectively. Similarly, on August 23, the total intake discharge changed from 6 m^3/s at 06:00 to 755 m^3/s at 14:00. Thermistors located at the bottom decreased in temperature during this time period by 1.287 °C (at 50.7 m), 1.197 °C (at 54.7 m), 1.335 °C (at 58.7 m), and 1.031 °C (at 62.7 m). These observations suggest that high discharge dam operations do cause a fluctuating response in the temperature profile of the reservoir.

In the month of September, most daily temperature fluctuations were small and remained within 2 °C. A few exceptions to this did occur, such as on September 5, September 12, September 17, and September 27. Due to this trend, it appears as though an internal seiche with a 5 or 10 day period was still present in the reservoir. Since the top layers were mostly homogeneous, most of the fluctuations occurred in the bottom layers, as seen on September 17 in Figure 4.31a. Increases and decreases in the water temperatures were seen in the profile from ~35 – 60 m throughout the day.

In the month of October, daily temperature fluctuations below 30 m were generally larger than in September. However, most changes were within 3 °C throughout the day. Again, exceptions to this were found occurring at a frequency about every 5 days. A clear example of the motion of an internal wave in a short period of time was found on October 15, as seen in Figure 4.31b. Focussing on a depth of 50 m, the water temperature gradually fell from 9.7 °C at 02:00 to 4.9 °C at 14:00. The water temperature then began to rise gradually, up to a temperature of 9.4 °C at 22:00. This example illustrates the rising and falling of an internal wave.

Dam operations were also found to affect the lower thermistor water temperatures in October. A good example of this can be seen in the thermistor temperature plots with time on October 15 – October 18, as shown in Figure 4.32. Each day, the thermistor temperatures from 38.7 m to 60.7 m decreased when the intake discharges were increased. The dam operations were fairly oscillatory during this time frame. Discharges were ramped up in the early morning, around 05:00. Discharge magnitudes were fairly consistent each day, with a peak of about 700 m^3/s. Discharges were then decreased around 00:00 each day. This cyclical pattern in the dam operations could have caused the

oscillations present in the thermistor chain. In fact, resonance may occur if the discharge frequency was the same as the natural frequency within the reservoir (Vidal et al., 2007), resulting in oscillations of greater amplitude.

Several reservoir processes that cause temperature fluctuations in the profile were discussed. When the air temperature was high and the wind speed was low, the surface layers absorbed the radiant heat energy. This caused warming and a steep thermal gradient occurred at the surface. However, when the wind speed was high, mixing occurred at the surface. This caused a flat thermal gradient and the top layers were homogeneous. A similar flattening of the surface thermal gradient occurred during the evenings, when the air temperature was quite cool. This process, called penetrative convection, resulted from net heat loss at the surface. This caused convective motions at the surface which leads to mixing. The process was ceased when water temperatures began to warm again from increased air temperatures.

Large water temperature fluctuations in relatively short periods of time were discussed. Earlier in the year (May and June) they were seen near the surface. For the remainder of the year, large fluctuations were seen at the mid-depth (July and August) and deep (September and October) thermistors. Due to the periodic nature of these disturbances and the absence of extreme meteorological or withdrawal influences during the same day, the temperature fluctuations were attributed to internal seiching. Furthermore, significant wind events were typically seen two days prior to the internal seiche, which were probably driving the motions. Finally, correlations between withdrawal operations and thermistor temperatures were observed. As seen in August, when intake discharges were increased, the thermistors near the bottom (>50 m) decreased in temperature. In October, the consistent increasing and decreasing of intake discharges may have resonated with a natural frequency in the reservoir and increased the amplitude of temperature changes seen in the profile. Internal seiching in the reservoir will be discussed further in Section 4.4.1.

4.3.5 ADCP Measurements

A total of ten transects perpendicular to the dam face were collected from July 11 – 12, 2011 and August 8 – 9, 2011 in the immediate forebay of MCA, as seen in Figure 4.5. A total of 64 point profiles were collected in this area.

The presentation of further results and observations of the collected water velocity profiles was not included in this study. The reason the measurements were mentioned was because these collected water velocity profiles were used to develop a three-dimensional computational fluid dynamics (CFD) model of the temperature and flow in the MCA forebay. The CFD model was used for further analysis of thermal dynamics in the reservoir. If further information is required on the ADCP velocity measurements, readers are referred to Langford et al. (2012).

4.3.6 Historical Temperature Measurements in Kinbasket Reservoir

A monitoring program was implemented by BC Hydro to provide information on the ecological productivity of Kinbasket and Revelstoke reservoirs and how they are affected by reservoir operations. This long term study, beginning in 2008, is scheduled to continue for a total of twelve years. Currently, three years of data is available to the public from the years 2008 – 2010 (Bray, 2010 - 2012).

Many water quality parameters were collected for these reports. However, only information of interest to this study will be discussed. This includes inflow temperatures for tributaries entering each reservoir. Also, instantaneous temperature profiles taken at different areas throughout the Kinbasket and Revelstoke reservoirs at different times of the year will be presented. The intent of discussing this information is twofold. Firstly, to compare previously recorded temperature profile measurements at MCA with the information collected in 2011, which is discussed in the sub-section below. Secondly, to compare and contrast the thermal characteristics at MCA and REV in order to better understand the thermal regimes at each. This will be discussed later, in Section 5.3.2.2.

4.3.6.1. Temperature of Inflows

A number of local tributaries (excluding the Columbia River) flow into Kinbasket reservoir. These local inflows account for 66% of the total inflow. Columbia River and Canoe River account for 31% and 3% of the total inflow, respectively. The temperature of these inflows will greatly influence and somewhat determine the temperature characteristics of Kinbasket reservoir.

Tributary temperatures were measured in 2008, 2009, and 2010 and were published in the BC Hydro ecological monitoring reports (Bray, 2010, Bray, 2011, and Bray, 2012). Temperature measurements for Kinbasket reservoir local tributaries were taken at the mouth of each stream using a handheld thermometer. Temperature measurements for the Columbia River were taken at Donald Station, about 20 km upstream of the mouth, using a handheld thermometer.

Tributary temperatures were measured throughout the year from 2008 – 2010, as seen in Figure 4.33. In 2008, Columbia River was sampled on June 25 and fourteen local tributaries were sampled on August 5. The temperature at Columbia River was measured at a temperature of 11.5 °C, while local inflow temperatures ranged from 7.5 °C to 11.0 °C, with an average temperature of 9.7 °C. In 2009, eighteen local tributaries were sampled on July 8. Local inflow temperatures ranged from 6.0 °C to 8.0 °C, with an average temperature of 6.8 °C. Furthermore, the Columbia River and one local inflow source (Gold River) were each measured on ten occasions from May – November (within one day of each other). The Columbia River temperature ranged from 3 °C (November) to 17.5 °C (July), with an average value of 11.4 °C. The Gold River temperature ranged from 4 °C (May) to 10.5 °C (October), with an average value of 7.7 °C. Columbia River had higher temperatures than Gold River from May to September, on average 5.5 °C warmer. In October and November Gold River had higher temperatures, on average 3.5 °C warmer. In 2010, one local inflow temperature of 7.0 °C was measured on May 31. Also, Columbia River temperature was measured on June 1, at a value of 9.0 °C.

There were a few generalities to note about the water temperatures measured at the MCA tributaries. Inflow temperatures warmed from May until August. After this time they began cooling until November. Also, the Columbia River inflow was warmer than all local inflows from May – September. However, in October and November, local inflow was warmer than the Columbia River.

The density of water in Kinbasket and these tributaries was mainly due to the temperature (Pieters and Lawrence, 2011). Local inflows were relatively cold compared to the surface temperature, as seen in Figure 4.33. The surface temperatures were averages from instantaneous profiles collected throughout the reservoir in 2008, 2009, and 2010. Colder inflows would result in the tributary flow plunging below the surface waters (Pieters and Lawrence, 2011). This could help explain the linear temperature profile found in the reservoir. In

June, July, and August, when the tributary flows were highest, the average local inflow temperature was 8.2 °C. Based on general temperature profiles during these months (see Figure 4.14a and Figure 4.14d) flows would plunge to depths around 20 – 40 m. This constant input of cooler water below the surface, could have prohibited the development of a well-mixed, warm epiliminion layer. In late September and October, tributary flows were significantly less, which could have allowed the development of a well-mixed epiliminion layer.

4.3.6.2. Instantaneous Temperature Profiles

Water temperature profiles were measured in 2008 (Bray, 2010), 2009 (Bray, 2011), and 2010 (Bray, 2012) throughout the Kinbasket reservoir. There were five general locations where temperature profiles were measured: in the forebay near the dam (FB), in the middle (MI) where the Columbia Reach and Canoe Reach meet, in the Columbia Reach (CO), in the Canoe Reach (CA), and in the Wood Arm (reach near Wood Creek, WO). These general locations are outlined in Figure 4.34. The temperature measurements were collected using a Sea-Bird Electronics SBE 19plus V2 profiler. It should be noted that problems with the Sea-Bird profiler pump were identified and some profiles were measured inaccurately in 2009 and 2010. These profiles are noted with an asterisk and will not be discussed.

2008 Instantaneous Profile Measurements

In 2008, twenty-five instantaneous profile measurements were conducted from July – October. Each month, measurements were taken within one or two days of each other. In general, the shape of the temperature stratification was similar to general profiles measured using a thermistor chain in 2011.

In July 2008, the thermal gradient was somewhat linear from the surface to about a 55 m depth, as seen in Figure 4.35a. This was the depth where the intakes were located (indicated as “Outlet” on the figure). After this depth, the profile was somewhat homogeneous at a temperature of about 4 °C. This shape was similar to the profiles measured in July 2011. The July profiles varied somewhat at different locations throughout the reservoir, as much as 5 °C at certain depths. The profile taken in the forebay was the warmest. Note that corresponding REV instantaneous temperature profiles are plotted alongside all of the MCA instantaneous temperature profiles and will be discussed further in Section 5.3.2.2.

The August 2008 instantaneous temperature profiles are seen in Figure 4.36a. The profiles were generally linear from the surface to about a 60 m depth, where the intakes were located. This shape of profile was similar to what was measured using a thermistor chain in 2011. The 2008 profiles were nearly identical throughout the reservoir, within 2 °C for most of the water column. However, the forebay profile had a cooler, well-mixed layer at the surface of approximately 10 m deep. The main difference with the forebay profile occurred at the surface, well away from the intake location. This could indicate that high discharges in August were not affecting the stratification profile significantly, since no significant difference was seen between the forebay and the rest of the reservoir at a depth of 60 m. Effects of intake operations could occur on a smaller scale.

In September 2008, approximately the top 20 m of the profile was becoming a homogeneous, well-mixed layer, as shown in Figure 4.37a. Below this the linear stratification extended from ~20m to the depth where the intakes were located (62 m). Below this the profile was approximately 4 °C. The profiles taken throughout the reservoir were very similar to each other. These 2008 profiles also generally matched the shape of profiles measured with the thermistor chain in September of 2011.

Instantaneous profile from October 2008 were similar throughout the reservoir, as seen in Figure 4.38a. The top ~20 m was well-mixed throughout the reservoir, with a linear profile extending from ~20 m to the intake depth of 62 m. After this, the profile was homogeneous at 4 °C. This was similar to what was seen in thermistor chain profiles in October 2011.

2009 Instantaneous Profile Measurements

In 2009, forty-four profile measurements were conducted from June – October. Six of these profiles were affected by the pump malfunction and are indicated with an asterisk. Each month, profiles throughout the forebay were taken within one or two days of each other. The 2009 profiles also exhibited similar characteristics to the 2011 thermistor chain measurements in the forebay area.

In June 2009, the profiles were linear from the surface to about a depth of 30 m. Below this, the temperature was a relatively constant 4 °C. The profiles were very similar throughout the reservoir, within a few degrees of each other, as shown in Figure 4.39. This general shape of the top 20 m was also observed in the 2011 thermistor chain measurements.

In July 2009, the linear stratification profile was deeper, extending from ~10 – 50 m depth, as shown in Figure 4.40a. Below this, the temperature was relatively constant at 4 °C. The profiles also had a well-mixed layer on the surface, about 10 m deep. This could be an indication of significant wind events occurring throughout the reservoir. The measured profiles were similar at the different locations, varying by only a few degrees. Furthermore, the profiles were generally similar to the July profiles measured after a wind event in 2011 (see Figure 4.22).

August 2009 profiles were more uniform throughout the reservoir than July 2009 profiles, as seen in Figure 4.41a. However, the Columbia Arm was somewhat warmer at depths below 20 m. Again, a well-mixed layer occupied about 10 m of the surface, as was synonymous with high wind events in the 2011 thermistor measurements. The profiles were linear from ~10 m to about a depth of 55 m, below which the temperature remained at about 4 °C. In later August and early September, the profiles were still very similar throughout the reservoir, as seen in Figure 4.42a. The linear stratification from the surface to about a depth of 60 m, was also seen in the August 2011 thermistor profiles. Below a depth of 60 m the profile was around 4 °C.

In mid-September 2009, profiles were generally cooler than August 2009. The surface layers were becoming homogeneous, but the overall profile was still mostly linear to a depth of 60 m, as seen in Figure 4.43a. Below this, the temperature was consistent at a temperature of 4 °C. These measurements were similar throughout the reservoir and agree well with the general September 2011 thermistor chain measurements.

In October 2009, the surface of the profile had cooled and mixed to a depth of about 40 m (see Figure 4.44a). From about 40 – 70 m the profile was nearly linear. Below this the profile was fixed at about 4 °C. Throughout the reservoir, the profile shape was very similar. Furthermore, these profile shapes had the same patterns as the October 2011 temperature measurements.

2010 Instantaneous Profile Measurements

In 2010, fifty-one instantaneous profile measurements were recorded from May – October. Eight profiles were affected by a pump malfunction (profiles with asterisk). Monthly profiles taken throughout the forebay were measured within one or two days of each other. The profiles again exhibit similar characteristics to the thermistor chain measurements in 2011.

In May 2010, temperature profiles were fairly similar, except in the forebay, as shown in Figure 4.45a. Generally, the reservoir temperatures had a steep temperature gradient from the surface to about a 15 m depth. Below 15 m the temperature was close to 4 °C. In the forebay, the profile was somewhat homogeneous. This difference could be due to the time of day profiles were taken. The rapid change from steep temperature gradient at the surface to homogeneous profile was seen during one day for 2011 thermistor measurements in May (see Figure 4.14b).

In June 2010, a linear profile shape was seen from the surface to about a 40 m depth in the forebay and Wood Arm, as shown in Figure 4.46a. In the middle of the reservoir, however, the top 20 m of the water profile was homogeneous overtop a linear profile to about 40 m. This area is open and very susceptible to wind events, and this profile shape could indicate wind induced surface mixing. Below 40 m, the profiles remained generally consistent at around 4 °C. These two general shapes were seen in the top 20 m of the thermal profile for June 2011 measurements collected by the thermistor chain (see Figure 4.19a and Figure 4.19b).

In July 2010, the profiles were mostly linear to a depth of about 65 m, as shown in Figure 4.47a. However, profiles in the middle, Canoe Reach and Columbia Reach did have a well-mixed surface layer to about a 15 m depth. These areas were more susceptible to northwesterly and southeasterly winds, whereas the Wood Arm and forebay were more sheltered. This could have caused the well-mixed layer seen in only some locations. Below 65 m, the profiles generally were at 4 °C. Throughout the reservoir, the profile shapes were similar, but did vary by a difference of about 4 °C. This general shape was similar to profiles measured in July 2011 by the thermistor chain.

In August 2010, the profiles were very similar to one another (within about 2 °C) with the typical linear stratification from the surface to about a 60 m depth, as seen in Figure 4.48a. Below 60 m, the profiles were generally at 4 °C. These measurements were comparable to the August 2011 thermistor chain measurements.

In September 2010, the profiles were very similar to one another, as seen in Figure 4.49a. Furthermore, they portrayed a well-mixed surface layer to about a 20 m depth, which was similar to the September 2011 temperature

measurements. From ~20 – 70 m the profiles were linear. Below 70 m, the profiles were homogeneous at a temperature of about 4 °C.

In early October 2010, the profiles had a well-mixed surface layer to about a depth of 30 m, as seen in Figure 4.50a. From ~30 – 80 m, the profiles were somewhat linear. There was some variation in temperature below 30 m. A couple of profiles located in the shallower Columbia Reach were warmer by about 2 °C. In mid-October 2010, the profiles had the same characteristics as the early October profiles, as seen in Figure 4.51a. In general, the October 2011 thermistor profiles matched these October profiles well.

There were some generally similar characteristics of the temperature profiles collected from 2008 – 2010. The seasonal changes were very similar from year to year, and also similar to measurements collected in 2011. In May, the profile changed from homogeneous to a steep temperature gradient at the surface within the span of a day. In June, the temperature profile became somewhat linear from the surface to about a 30 m depth. In July and August, the stratification remained linear, but deepened to about a 50 – 60 m depth. Also, well-mixed surface layers were sometimes seen in a few wind susceptible areas. In September and October, the surface layer was becoming cooler and homogeneous. This well-mixed layer was about 20 – 30 m deep. Another similar characteristic from year to year was the monthly temperature variation throughout the reservoir. In May, June and July, the profiles were similar in shape, but varied in temperature throughout the reservoir. In August, the profiles were all very similar, usually within 2.0 °C. This trend continued in September and October.

4.4 Analysis

It was apparent from the temperature time series data from MCA that periodic oscillations (or internal seiches) were taking place within the reservoir. Therefore, a spectral analysis of the temperature time series was performed in order to quantify these observations. This analysis determines the dominant periods of the internal seiches travelling through the reservoirs. Similar to the analysis for HLK discussed in Section 3.4, the spectral analysis was completed on the MCA thermistor chain time series using Welch's method.

4.4.1 MCA Waveform Analysis

The reservoir stratification at MCA led to the development of surface and internal seiches. In this reservoir, the stratification was linear, in that there was no clearly defined thermocline. The temperature decreased linearly, either from the surface (in July and August) or from the bottom of a well-mixed layer (in September and October), to a depth around 60 m. In a reservoir with a linear stratification, wind forcing can result in internal waves of higher vertical modes (Vidal et al., 2007). This leads to the spectrum of internal oscillations being dense, where any sort of forcing frequency will cause resonance (Vidal et al., 2007). In a study by Perez-Losada et al. (2003), the thermal regime was linearly stratified. This characteristic of a thick metalimnion was shown to enhance the development of second vertical modes. An example of higher vertical modes observed in the thermistor data in September is shown in Figure 4.52. On the dashed lines it can be seen that the oscillations of the upper thermistors are out of phase with the bottom thermistors, indicating multiple vertical modes of oscillation.

The thermistor chain raw data set included a total of 50137 temperature profiles. In order to determine the frequency of the most substantial temperature oscillations, a spectral analysis was conducted on each thermistor time series. This analysis was completed in a similar manner to the HLK spectral analysis. The first step was, again, to remove the mean and any trends from each time series. Welch's method divided the time series into n_d segments which each consisted of N values (various N values used for this analysis), overlapping by D points. The overlapping segments then had a Blackman window applied to them in the time domain, and the Fourier transform was taken to convert it to the frequency domain.

Like HLK temperature data, there was a wide range of periods apparent in the thermistor time series (i.e. from the order of a few hours to several days). Therefore, two sets of spectral analyses were conducted. First, each thermistor signal was band pass filtered using a band of 20 hours up to 14 days, which was then padded with zeros in order to reach a consistent length of 9665 measurements. An N value of 9465 was used with 99% overlap to determine the lower frequencies in the signals (i.e. order of days). The averaging of data reduces the random error in the results, which was ε_r = 7.1 %. A spectral analysis was completed on these modified time series to determine low frequencies, with periods in the order of days. Secondly, each original

thermistor signal was high pass filtered at 1 day. An N value of 1200 was used with 75% overlap in Welch's procedure, resulting in a ε_r = 32%. This spectral analysis was completed in order to determine higher frequencies, with periods in the order of hours.

There were a few differences from the HLK spectral analysis since the MCA time series was longer. The overall temperature profile was changing monthly, meaning that different internal seiching periods would occur seasonally. Therefore, the spectral analysis was repeated on each MCA thermistor time series over different periods of time. The time frames chosen were overlapping, approximately 30 day segments. Spectral analysis was done on each thermistor time series ranging from May 13 – June 15, June 1 – 30, June 15 – July 15, July 1 – July 31, and so on.

Another difference from the HLK oscillations was that the MCA surface layers and deeper layers appeared to oscillate at different periods. There was a need to separate the thermistor time series into groups that were similar to each other. The coherence of two time series measures how linearly related they are at different frequencies. Also, a high measure of coherence is a good indication that internal seiching is causing the resulting frequency (Vidal et al., 2007). Therefore, coherence between thermistors was determined. Thermistor time series with high coherence values (higher than 50%) and low random error values (lower than 20%) were grouped together. All coherence results were large for lower frequencies (periods greater than one day). For higher frequencies (on the order of hours) thermistors in groups of three cohered well and were plotted together, in about 5 m intervals. This excluded the first three thermistors, which did not cohere well at higher frequencies, and were plotted individually.

An example of the dominant oscillation frequencies found in the periodogram from the thermistor 3 time series during the time frame from June 1 - 30 is shown in Figure 4.53. For a clearer picture of the dominant oscillations, only the power magnitudes of the peaks in the periodogram were plotted with the corresponding period (i.e. in terms of days rather than Hz).

4.4.1.1 Low Frequency Results

The low frequency spectral analysis results of each thermistor group are plotted per month in Figure 4.54 (a-e). Since equal segment lengths of N = 9465 were used for all the low frequency analysis, we can compare the relative magnitudes

between the resulting spectra. It should be noted that not all of the y-axes are the same length.

One general trend in the results was the significant decrease in power magnitude from the top thermistors to the bottom thermistors. This was due to the fact that temperature fluctuation magnitudes were greatest near the top, resulting in a larger power magnitude. Also, all of the periods observed in the mean daily average temperature plots (3 days) and temperature profiles plots (5 days and 10 days) were consistent with the results of the spectral analysis, as discussed below.

The most dominant oscillatory period that was present in the thermistor series was 6.7 days. It was the most dominant signal found in the upper ~ 27m of the profile (down to thermistor 13), but was also found in the rest of the thermistors, as seen in Figure 4.54a. When comparing the magnitudes of the power spectra, it was apparent that the 6.7 period was more dominant in the top layers than the bottom layers. For example, in the month of July, the power at 0.2 m had a magnitude of 940 and decreased to a magnitude of 0.5 at 62.7 m. The time periods with the highest power magnitudes at this frequency were May 13 – June 15, June 16 – July 15, and July 1 – July 31. There was significantly less dominance in the later months, which was probably due to the more stable thermal structure in August – October and the smaller temperature fluctuations.

A considered explanation of the 6.7 day period was the change of dam operations on a weekly basis. Due to higher demands during week-days as opposed to week-ends, dam operations are typically higher during the week. This would result in a 7 day oscillatory period that could induce internal seiching of the same period. To investigate this possibility, a spectral analysis of the hourly dam operations time series for MCA was performed. The time series used was an hourly signal of total discharge from all four intakes. This signal was divided up into approximately the same 30 day time frames as the thermistor time series. However, total discharges from May 13 – July 5 were low and semi-diurnal, as seen in Figure 4.55a. Discharges from July 6 – October 23 were much higher and diurnal, as seen in Figure 4.55b. Therefore, the signal was divided into smaller time frames based on this division. A spectral analysis was done on the following time frames: May 13 – June 15, June 1 – 30, June 16 – July 5, July6 – 31, July 16 – August 15, August 1 – 31, August 16 – September 15, September 1 – 30, September 16 – October 15, and October 1 – 23.

The dominant resulting periods of the total discharge spectral analysis from May 13 – July 5 are shown in Figure 4.56a. The main dominant periods were 12 hours and 1 day. A period of 6.7 days was present, but it was not the most dominant period of fluctuation. The total discharge spectral analysis from July 6 – October 23 is seen in Figure 4.56b. A period of 1 day was much more dominant than any other period from July – September. However, in the time frame September 16 – October 15, a 6.7 day period was most dominant. This dominant period may have caused some resonant seiching, but the resulting 6.7 day power magnitudes during this time frame were relatively small, as seen in Figure 4.54a.

Although a weak period of about 7 days was found in the dam operations, it was not dominant enough to have caused the substantial fluctuations seen in the thermistor data. Furthermore, this fluctuation of approximately 7 days was seen throughout the year, from May – October, whereas breaks in this trend are seen in the thermistor data. For example, no 6.7 day period was found in the temperature fluctuations during June 1 - 30. Finally, it was apparent that the most dominant fluctuations in the thermistor series took place in the layers closest to the surface. If dam operations were driving the internal seiche movements, it would be thought that more dominant fluctuations would be seen in the lower layers closest to the intakes. Therefore, it was thought that total discharge fluctuations were not the cause of the 6.7 day internal seiche apparent in the reservoir.

Since the 6.7 day period was most dominant in the thermistors near the surface, wind induced seiching was the next consideration as the driving force. A spectral analysis of the hourly wind time series was conducted. The results of the spectral analysis are seen in Figure 4.57. A dominant period of 6.7 days did emerge from the wind data. The first three time frames matched the most dominant time frames of the 6.7 day internal seiche results from the thermistor series (during May 13 – June 15, June 16 – July 15, and July 1 – July 31). The July 16 – August 15 period found in the internal seiche results could have been a boundary reflection of the internal seiche that had not yet dissipated after the regular 6.7 day periodic winds had ceased. This would explain the much lower power magnitude found during July 16 – August 15 and the fact that only the middle thermistors were affected. The power magnitude of the 6.7 day period found in the wind speed time series spectral analysis during October 1 – 31 was relatively large. However, since the thermal profile was homogeneous at the top

in October, significant fluctuations in the upper layers could not occur. Therefore, smaller power magnitudes were seen in the thermistor time series in most of the layers from September 16 – October 15, and a few of the layers from October 1 – 31. It was thought that the 6.7 day period found in the thermistor chain time series was primarily a result of wind induced internal seiching.

Other oscillatory periods present in the thermistor measurements during various time frames were 11.3 and 5.6 days, as seen in Figure 4.54b and Figure 4.54c, respectively. The results display the same trend as seen in the 6.7 day results, with the highest power coming from the top layers and progressively getting smaller with deeper thermistors. June 1 – June 30 had the highest power magnitudes of these periods in the upper layers (only T1 – T11 installed during this time). An approximate 10 day period was observed in the mean daily average temperature plots during June, as described above in Section 4.3.4. July 1 – 31, July 16 – August 15, August 1 – 31, and August 16 – September 15 displayed both of these periods. September 1 – 30, September 16 – October 15, and October 1 – 31 displayed the 5.6 day period, mostly in the lower layers. It should be noted that in general, the 5.6 day period had a higher power magnitude in July, August, September, and October. This was the trend discussed earlier, with an approximately 10 day internal seiche period seen in June in the upper layers and an approximately 5 day internal seiche period seen from July – October, but mainly in the lower layers.

The spectral analysis of the wind speed data also revealed periods similar to 5 and 10 days, as seen in Figure 4.57. In June, periods of 11.3 days and about 5 days were found. Periods of 11.3 days were also found in July, August, and September. As well, approximately 5 day periods were found in July, August, September, and October. As the periods and time frames match well with the periods and time frames resulting from the thermistor spectral analysis, it was thought that the 5.6 day and 11.3 day periods were driven by wind induced internal seiching.

Periods from 2.4 days to 3.7 days were grouped together to represent an average oscillatory period of 3.0 days. This period was found in every season at most of the thermistors, as seen in Figure 4.54d. The power magnitude generally decreased with depth, except in mid-September and October. The bottom thermistors had a higher power magnitude in October, mainly because the surface was homogeneous with little fluctuation. Furthermore, power magnitudes were highest during May 13 – June 15, June 1 – 30, and June 16 –

July 15 (maximum). This was consistent with the 3 day period that was observed in the mean daily temperature plots during the month of July, as described in Section 4.3.4. There was an approximately 3.0 day period found in the wind speed data during every month, as seen in Figure 4.57. Therefore it was thought that the driving force for the 3.0 day thermistor oscillation period was wind induced.

Periods from 1.0 day to 1.3 days were grouped together to represent an average oscillatory period of 1.0 day. This period was found in every season as seen in Figure 4.54e. The power magnitude was generally highest in thermistor T1 during May and June and decreased with depth. However, in July – October, the mid-depth thermistors had significantly higher power magnitudes. In July, thermistors T14 – T19 had peak magnitudes. In August – October, thermistors T20 – T28 had peak magnitudes. A fairly consistent approximately 1.0 day period was found throughout the seasons in the wind speed data. This was thought to be the driving force for the oscillations seen in the thermistor information in May and June. However, the higher power magnitudes in the deeper thermistors only in July – October suggested that wind was not the dominant driving force of these oscillations.

Another driving force to be considered was the fluctuations in the MCA operations. As discussed earlier, a spectral analysis of the MCA discharges was done using the modified 30 day time frames (June 16 – July 5 and July 6 – 31). The most dominant periods were 24 hours and 12 hours, as seen in Figure 4.55b and Figure 4.55a, respectively. Furthermore, the discharge was much smaller in May and June (<100 m^3/s) than in July (~400 m^3/s), August (~900 m^3/s), September (~650 m^3/s), and October (~610 m^3/s). The discharge magnitude trend from July – October was the same trend as seen in the resulting 1.0 day power magnitudes for the spectral analysis of the bottom thermistors. This leads to the belief that dam operation fluctuations were the driving force for the approximately 1.0 day internal wave found in the reservoir during July – October. Further investigation on the degree of correlation between the dam discharge operations and thermistor temperatures will be shown in Section 4.4.2.

A low frequency spectral analysis of the time series at each MCA thermistor revealed several internal seiche periods in the order of days. 6.7 days was the most dominant period found in the months of May, June, and July. Due to similar periods found in the spectral analysis of the wind speed data at MCA, it was concluded that the 6.7 day internal wave was wind induced. Periods of 5.6

days and 11.3 days were also found in the spectral analysis. The 11.3 day period was dominant during June, although the harmonic frequency resulting in 5.6 day periods was also found. This period coincides with the approximately 10 day period that was observed in the temperature contours recorded in June. In July - October, the 5.6 day period was more dominant, which coincides with the approximately 5 day period that was observed in the thermal profiles during these months. These motions were thought to be wind induced, as both 11.3 days and 5.6 days were found as periods in the wind speed spectral analysis. 3.0 days was found as an internal wave period in every month, as was observed in the temperature contours. As a wind speed period of 3.0 days was also found in each month, it was though that this motion was wind induced. Generally, all of these periods had their maximum power magnitudes at the surface in May and June, when the most temperature fluctuation occurred. July and August had substantially less power, which was spread across the upper and middle thermistors. This spread of power into the other layers was most likely a result of the formation of the linear stratification. September and October had even lower power magnitudes, which was shifted to the lower thermistors. This shift was due to the homogeneous surface layer that had little temperature fluctuation during this time. An approximately 1.0 day period was also found. In May and June, the highest power magnitudes were found in the upper thermistors and thought to be wind induced. However, in July – October, fluctuations shifted to the lower layers, and it was thought that these oscillations were induced by the daily cycle in dam operations.

4.4.1.2 High Frequency Results

The high frequency results of each thermistor are plotted per month in Figure 4.58. A N value of 1200 was used for all the high frequency analyses, and we can therefore compare the relative magnitudes between these resulting spectra. However, it should be noted that the high frequency results cannot be compared to the previous lower frequency spectra. Only the spectra's peak power magnitudes were plotted for each thermistor during different time frames. High frequency results were grouped into ranges, since one single period was not dominant.

The most significant oscillation occurring in the thermistor chain was in the range of 18 – 22 hours. This period range was found during every month, as seen in Figure 4.58a. In May and June, the top thermistors had the highest power magnitude. During July – October, the bottom thermistors had the highest

power magnitudes. From May until October, the top and middle (T1 – T19; 0.2 – 38.7 m) thermistors power magnitudes generally decreased with depth while the bottom (T20 – T31; 40.7 – 62.7 m) thermistors power magnitudes generally increased with depth. The change in power magnitude for the thermistor spectral results throughout the seasons was due to the change in the thermal profile. In May and June, the profile was not stratified, so wind induced seiches occurred at the surface. In July and August, the profile was linearly stratified. This transferred wind energy from the surface to the internal layers, resulting in multiple vertical modes of oscillation throughout the reservoir. In September and October, the top layers were homogeneous, inhibiting substantial oscillations in these temperatures. Therefore the power magnitude shifted to the lowest layers, below about 30 m.

A wind speed spectral analysis for higher frequencies is shown in Figure 4.59. The highest power magnitude range was from 16.4 – 19.2 hours, which was found in every month. It was thought that the 18 – 22 hour period range found in the thermistor chain measurements was due to wind induced seiching.

Another dominant period range included 11 – 14 hours, as seen in Figure 4.58b. The general power magnitude of the 11 – 14 hour range was about one third of the 18 – 22 hour range. In May, the 11 – 14 hour period range was dominant in the upper layers, but from July – October the period range was dominant in the lower layers, T20 – T31 (40.7 m – 62.7 m) in particular. The power magnitude of this range peaked in August. Also, September and October had generally higher power magnitudes than July and August.

The high frequency spectral analysis of the wind speed data at MCA did reveal an approximately 12 hour oscillatory period (11.3 – 13.9 hour), as seen in Figure 4.59b. This period range had lower power magnitudes than the 16.4 – 19.2 hour range. Furthermore, the 11.3 – 13.9 hour power magnitude was highest in May, and then decreased for the remainder of the months. Also, during July 16 – August 15 and September 16 – October 15 this period range was not found, unlike the thermistor spectral analysis. August 1 – 31 had the lowest power magnitude in the wind speed spectral analysis whereas this was one of the most dominant time frames in the thermistor spectral analysis. This led to the belief that wind forcing was not the dominant force inducing the internal wave with the approximately 12 hour period.

Another driving force that was considered earlier was the fluctuations in the MCA operations. The spectral analysis of the MCA discharges revealed dominant periods were 24 hours and 12 hours, as seen in Figure 4.55b and Figure 4.55a, respectively. Furthermore, the discharge was much smaller in May and June (<100 m^3/s) than in July (~400 m^3/s), August (~900 m^3/s), September (~650 m^3/s), and October (~610 m^3/s). This trend was also seen in the bottom thermistors power magnitudes results for the 11 – 14 hour period range, much like the approximately 1.0 day results. This led to the belief that dam operation fluctuations were also the driving force for the approximately 12 hour internal wave found in the reservoir.

The final high frequency period range found in the thermistor data was 6 – 10 hours, as seen in Figure 4.59c. Power magnitudes from this range were slightly lower than the 11 – 14 hour range. From May – August, the 6 – 10 hour range had the highest power magnitudes in both the upper and lower layers. This separation of internal waves in the profile could have resulted from the development of multiple vertical modes in the profile. From August – October, the power magnitudes were spread throughout the profile and generally tapering off.

The most likely cause of the 6 – 10 hour internal seiche was wind effects. A 6 – 10 hour period was found in the high frequency spectral analysis of the wind speed data, as seen in Figure 4.59. Furthermore, the power magnitude was generally higher from May – August, and then tapered off until October. This leads to the conclusion that the 6 – 10 hour range was caused by wind induced internal seiching.

There were three high frequency internal wave periods (expressed in ranges) found in the thermistor time series data. An 18 – 22 hour period range was the most dominant and determined to be wind induced. It was most dominant on the surface in May and June, and then became more dominant in the middle and lower layers from July – October. This change in power magnitude was attributed to the monthly changes in the thermal profile. An 11 – 14 hour period range was also found. This range was considerably more dominant in July – October, particularly in the bottom thermistors. It was concluded that this internal seiche period range was due to influence from dam operation fluctuations. Finally, a 6 – 10 hour period range was also found, which was considered to be wind induced. Also, the power magnitudes were split between the top and bottom, possibly indicating multiple vertical modes.

4.4.2 Covariance of Thermistor Temperatures and MCA Operations

The discharges of the MCA intakes were consistently oscillatory on a daily period. As discussed before, and seen in Figure 4.55a, the general trend in operations during May and June was two periods of discharge throughout the day. Low discharges (<100 m^3/s) occurred in the morning (around 08:00) and in the evening (around 20:00), for a few hours each. The general trend during July – October was higher discharges and withdrawal beginning in the morning (around 07:00) and continuing throughout the day until the late evening (around 24:00), as seen in Figure 4.55b.

Spectral analyses of the thermistor temperature data and the total discharge time series both revealed dominant periods of approximately 1.0 day and 12 hours. These periods were most dominant in the deeper thermistors, especially during the months of higher discharge operations (July – October). It was concluded that the dam operations were influencing the thermistor temperatures to oscillate at these periods.

A cross spectral density analysis was completed on the dam operation time series and each thermistor temperature time series. The cross spectral density function represents the covariance (degree of correlation) of two time series as a function of frequency (Bendat and Piersol, 1980). When one time series increases as the other increases, the resulting cross spectrum is large and positive at that frequency. Conversely, when one time series decreases as the other increases, then the resulting cross spectrum is large and negative at that frequency.

The results of the cross spectral density analysis between the operations and thermistor data are seen in Figure 4.60. Again, the data was divided into overlapping monthly segments (May 13 – June 15, June 1 – 30, and so on) in order to capture the change in covariance throughout the seasons. Each thermistors peak power magnitudes near the frequency of 0.042 Hz (1.0 day) were plotted together. This was done for each time frame.

There are three general notes about the cross spectral power magnitudes plotted in Figure 4.60. First, in every month the upper two thermistors have a positive covariance at a period of 1.0 day. This was most likely due to daily warming of the surface water due to diurnal air temperatures, and not the change in discharge operations. Secondly, in every time frame except September 16 – October 15 the bottom five thermistors have a negative

correlation with the dam operations. This means that when the intakes were turned on, the thermistor temperature decreased. These thermistors were located closest to the intakes, and the thermal structure here would be most substantially influenced. The third general note about the cross spectral power magnitudes was that the remaining thermistors had an array of positive, negative, and no correlation with the dam operations, which changed over each time frame.

For the time frames of May 13 – June 15, June 1 – 30, June 16 – July 15, and September 16 – October 15 there was little to no correlation between thermistor temperature and dam operations. This was expected, since it was during time frames when the total discharge was low and did not have a strong 1.0 day oscillation period (see Figure 4.56).

For the time frames of July 1 – 31 and July 16 – August 15, the correlation was negative for thermistors below 16.2 m. This was during a period of medium discharge (~500 m^3/s). A possible explanation for the decrease in thermistor temperature with the increase in dam operations could be the location of water withdrawal. The intakes were located at the bottom of the dam face (sill at 686.4 m), but not the bottom of the reservoir. In front of the intakes, an apron at an elevation of about 686 m extended upstream for about 90 m, which can be seen in the contours in Figure 4.5. Upstream of the apron, the reservoir deepened substantially. The thermistor chain was located about 220 m upstream of the intakes, with a bed elevation of 637 m. If the medium discharge could not overcome the buoyancy forces of the reservoir stratification, water could have been withdrawn from the deeper, hypolimnetic areas upstream of the apron. Hypolimnetic temperatures were historically around 4 °C and similar to the temperature found in front of the intakes, as seen in the instantaneous temperature profiles measured in 2008 – 2010 (Section 4.3.6.2). When the intakes were operating, it could have pulled in hypolimnetic water with similar densities and resulted in cooler thermistor temperatures.

For the time frames of August 1 – 31 and August 16 – September 15, the thermistors between depths of 20.2 – 54.7 m generally had a positive correlation with the dam operations. This was during a period of high discharge (1000 m^3/s). This increase in discharge could have overcome the buoyancy forces and forced water withdrawal from the entire profile. Perhaps water was being withdrawn from the warmer upper layers, pulling warmer water down (increasing thermistor temperatures) as discharges increased. The negative correlation of

the bottom thermistors indicates that water was being withdrawn from the lower layers as well.

During the remaining time frames, September 1 – 30 and October 1 – 31, the top thermistors (0.2 – 34.7 m) had generally no correlation with the dam operations. This was understandable, as these layers were homogeneous with little fluctuation. Thermistors below 34.7 m had a negative correlation with the dam operations, which was most notable during October 1 – 31. These results were during a period of medium discharge. Water may have been withdrawn from deeper areas in the reservoir again.

It was apparent from the cross spectral density analysis of the thermistor time series and the total dam discharge that MCA operations affected the thermal profile within the reservoir. Both positive and negative correlations existed between them, which changes throughout the seasons. It appears a critical discharge existed that decided the location of the water withdrawal. Discharges below this, as seen in July, September, and October, resulted in withdrawal from cooler, deeper waters within the reservoir. Discharges above the critical discharge resulted in withdrawal from all layers of the thermal profile, as seen in August.

4.4.3 Covariance Between Thermistors

It was mentioned in Section 4.4.1 that MCA displayed evidence of multiple vertical modes of oscillation. This phenomenon is common in linearly stratified reservoirs and is characterized by several levels of internal waves travelling in the reservoir simultaneously. For a second vertical mode, internal waves are oscillating through two vertical nodes. The two layers would be oscillating out of phase. Furthermore, for a third vertical mode, internal waves are oscillating through three vertical nodes. The top and bottom layers would be oscillating in phase, while the middle layer would be oscillating out of phase.

To further understand this feature of the reservoir dynamics in MCA, a cross spectral density analysis was completed between thermistor time series. If the results were positive, it would mean the time series have a positive linear relationship and were oscillating in phase with one another. By contrast, negative results would mean the time series were oscillating out of phase with one another. These results could be used to determine the number of vertical modes of oscillation.

Two thermistors were compared to the rest of the water column to determine which layers were oscillating in phase and out of phase. Both thermistors T2 (2.2 m depth) and T11 (20.2 m) time series were compared to every other thermistor time series. Between these two thermistors, their previous spectral analyses displayed every dominant period in the order of days that was reported. The thermistor time series were broken up into smaller, overlapping ~30 day time frames for the analysis. Thermistor results were grouped together in approximately 5 m intervals, as was done for the spectral analysis results.

For a period of 6.7 days, the results of thermistor T2 and T11 cross spectral density analysis with every other thermistor are shown in Figure 4.61 and Figure 4.62. The T2 and T11 covariance results were somewhat similar. May 13 – Jun 15 and June 16 – July 15 had a very high, positive correlation from thermistors T1 – T13 with both T2 (Figure 4.61a) and T11 (Figure 4.61b), indicating that oscillations in the top 20 m were in phase. During July 1 – 31, evidence of a third vertical mode was seen. Thermistors T1 – T16 were positively correlated, thermistors T18 – T21 were negatively correlated, and thermistors T28 – T31 were positively correlated to both T2 and T11. During July 16 – August 15, evidence of a third vertical mode was found in the T11 cross spectral density analysis, as seen in Figure 4.62b. Thermistors T1 – T14 and T29 – T31 were positively correlated with T11 while T18 – T26 were negatively correlated. September 1 – 30 showed evidence of a second vertical mode in the T11 cross spectral density analysis. Thermistors T8 – T15 were oscillating in phase with T11, while thermistors T22 – T21 were oscillating out of phase. September 16 – October 15 showed evidence of second vertical mode of seiching in both T2 (Figure 4.62a) and T11 CSD analyses. In general, T3 – T19 were oscillating in phase with T2 and T11, while T25 – T31 were oscillating out of phase. Finally, in October 1 – 31, there was no evidence of higher vertical modes, and most layers were oscillating in phase. These time frames and vertical modes applied to a period of 6.7 days. Different modes of oscillation occurred for different internal seiche periods.

For an internal seiche period of approximately 5 days, some of the T2 and T11 thermistor cross spectral density analysis matched, while some did not, as seen in Figure 4.63a (T2) and Figure 4.63b (T11). During June 1 – 30 and June 16 – July 15, thermistors T1 – T11 were oscillating in phase with a 5 day period. During July 16 – August 15, only T2 displayed a 5 day period. The results of the cross spectral analysis revealed up to six vertical modes. The results of T2 and T11

during August 1 – 31 and August 16 – September 15 did not match well. T2 results showed that most layers were oscillating in phase with each other, while T11 results revealed the top and bottom layers oscillating out of phase with each other.

The 11.3 day seiche period was dominant in June 1 – 30. T2 and T11 cross spectral analyses both revealed that all of the recorded layers (T1 – T11) were oscillating in phase. These results are shown in Figure 4.64a and Figure 4.64b.

For an internal seiche period of approximately 3 days, multiple vertical modes of oscillation were found. The cross spectral density analysis results for the 3 day seiche period are found in Figure 4.65 and Figure 4.66. Both T2 and T11 results were fairly similar for the first five ~30 day time frame periods. As seen in Figure 4.65a and Figure 4.65b, all of the recording thermistors (T1 – T11) were oscillating in phase during May 13 – June 15, June 1 – 30, and June 16 – July 15. In July 1 – 31 and July 16 – August 15 a second vertical mode of seiching becomes apparent at the 3 day period. Approximately the top 12 to 19 thermistors were oscillating in phase, while the bottom 10 to 13 thermistors were oscillating out of phase with the top thermistors. T2 and T11 cross spectral density analysis results from August 1 – 31 and August 16 – September 15 did not agree well with one another, as seen in Figure 4.66a and Figure 4.66b. T2 results suggested a fourth vertical mode of oscillation in August 1 – 31 and a third vertical mode in August 16 – September 15 while T11 results suggested a third vertical mode and second vertical mode during the corresponding time frames. The remaining results were more similar to one another. A second vertical mode was found for both T2 and T11 analysis during September 1 – 30 and September 16 – October 15. October 1 – 31 showed a third vertical mode of oscillation for both T2 and T11 results, which were actually oscillating out of phase with one another.

The oscillations in the reservoir were extremely complex. Multiple periods of seiching were travelling simultaneously through the reservoir. Furthermore, these periods were changing from season to season. The cross spectral density analysis of T2 and T11 did not correspond perfectly well with one another, but some similarities were seen. All of the periods detected in T1 – T11 during May and June (when the thermistor chain was shorter) were oscillating in phase with each other. Furthermore, second and third vertical modes were seen frequently during July, August, September, and October.

4.5 Theoretical Calculations

As mentioned before, the thermal dynamics in the forebay area of the reservoirs are trying to be understood due heating and mixing processes. It is valuable to calculate the parameters that theoretically describe these processes, in order to gain a better understanding of the reservoir dynamics. Therefore, the internal seiche oscillation period, critical discharge, and seiche amplitude were calculated for the Kinbasket reservoir.

The water temperatures in MCA typically displayed a linear stratification profile. The profile was generally linear from near the surface to a depth of about 60 m. This meant that an idealized two-layer system could not be assumed, as in HLK. Different sets theoretical equations had to be used in order to accommodate the temperature profile differences.

4.5.1 Multiple Vertical Mode Oscillations

It was apparent from the observed temperature oscillations and the resulting cross spectral density analysis that several layers were oscillating out of phase. Internal waves can have multiple nodal points, in both the horizontal and vertical directions. They are classified using the nomenclature ViHj, where i = # vertical nodes and j = # horizontal nodes. These classifications are called modes, the most common being V1H1 (Vidal et al., 2007). Since measured temperature profiles were oscillating at numerous vertical modes, a theoretical calculation of internal waves oscillating at different vertical modes was undertaken using the Kinbasket reservoir geometry.

Wave like solutions can be achieved from the component equations of two dimensional motions (Turner, 1973). If one assumes an exponential density distribution, a solution for the frequencies associated with different modes was given by Fricker and Nepf (2000):

$$\omega_{ji} = N_b \left(\left(\frac{j^2}{j + \mu^{-2} i^2 + \frac{N^4 {L_b}^2}{4\pi^2 g^2}} \right)^{1/2} \right) \qquad [8]$$

where:

ω_{ij} = wave frequency;

N_b = the buoyancy frequency;

j = the number of horizontal nodes;

i = the number of vertical nodes; and

μ = the reservoir depth / the reservoir length.

The buoyancy frequency was given by the equation:

$$N_b = \sqrt{-\frac{g}{\rho_o}\frac{d\rho}{dz}} \quad [9]$$

where:

ρ_o = the average profile density; and

$\frac{d\rho}{dz}$ = the density gradient with depth.

This analytical solution was applicable for a rectangular basin with a constant buoyancy frequency and small wave amplitudes.

Oscillation frequencies (and periods) were calculated using average buoyancy frequencies over ~30 day periods (e.g. May 13 – June 15, June 1 – June 30, June 16 – July 15, and so on). Two reservoir lengths were used for the analysis. The main reservoir was a 150 km reach extending from the southeast near the Columbia River mouth to the northwest at the Canoe River mouth. As mentioned before, in the middle of the reservoir a 14.6 km arm extended perpendicular to the southwest of the main reach. The dam structure was located at the end of this shorter arm. Therefore, a main reservoir length of 150 km was used in the analysis as well as a local reservoir length of 14.6 km.

The reservoir depths used were determined depending on the reservoir elevation and which reservoir length was being considered (main reach or local reach). For the main reach, the average depth was determined from published elevation, storage, and surface area values (Pieters et al., 2010). A normal maximum reservoir elevation of 754.4 m was associated with a depth of 57.5 m. This value was adjusted for each 30 day period by subtracting the difference between the recorded average 30 day reservoir elevations and normal maximum reservoir elevations. For the local reach, a bottom elevation of 686.4 m was assumed, which corresponds to the intake apron elevation. The bottom elevation was subtracted from the recorded average 30 day reservoir elevations to determine the reservoir depth (subtracted bottom elevation from average reservoir elevation). In general, the local reach depths were larger. This is most

likely due to the fact that the reservoir generally has a lower elevation closer to the dam face and areas closer to this location will, on average, be deeper than further away from the structure (*i.e.* the reservoir is sloping toward the dam).

The calculated frequencies and corresponding periods are shown in Table 4.2. It can be seen that the main reach produces oscillation periods in the order of days while the local reach produces smaller oscillation periods, in the order of hours. This alludes to what was causing the internal oscillations that were being observed at the thermistor chain. The longer periods were most likely controlled by the reservoir dynamics from the main reach while the smaller periods were most likely controlled by the local reach dynamics.

The calculated main reach periods were not exactly the same as the observed periods. They were in the appropriate range of about 2.5 days to about 10.2 days in vertical modes 1, 2, and 3. They also had somewhat similar dominant periods in certain time periods. For example, the calculated periods 7.6, 7.4, and 6.8 day periods occurred during May 13 – June 15, June 16 – July 15, and July 1 – July 31, respectively. This was similar to the 6.7 day period observed during the same time periods. On average, 3.7 day periods were calculated for the V1H1 mode, 7.4 day periods were measured for the V2H1 mode, and 11.1 day periods were measured for the V3H1 mode.

If the local reach results are averaged (excluding May, since the density profile is not quite exponential) periods of 6.4, 12.8, and 19.1 hours are achieved. This was also what was observed in the spectral analysis results of the thermistor time series. This leads to the conclusion that multiple vertical modes are occurring in the local reach of the reservoir. Mode V1H1, V2H1, and V3H1 have approximate periods of 6.4, 12.8, and 19.1 hours, respectively.

4.5.2 Seiche Amplitude

An estimate of the internal seiches amplitude was calculated from the thermistor chain data, following methods from Fricker and Nepf (2000). The data was split up into smaller time frames and a mean temperature profile was calculated for each period. For this analysis, time frames with similar temperature profiles were chosen (approximately 5 day periods). Next, a root mean square (RMS) temperature change was computed using:

$$\Delta T_{RMS}^{x} = \sqrt{\frac{2}{M}\sum_{m=1}^{M}[T(z_x, t_m) - \bar{T}(z_x)]^2} \quad [10]$$

where:

ΔT_{RMS}^{x} = the RMS temperature change for thermistor x;

M = the number of time series points;

m = time step;

$T(z_x, t_m)$ = temperature at (depth of thermistor x, time step m); and

$\bar{T}(Z_x)$ = the mean temperature profile for thermistor x.

The mean temperature profile for each thermistor was given by:

$$\bar{T}(z_x) = \frac{1}{M}\sum_{m=1}^{M} T(z_x, t_m). \quad [11]$$

Finally, the RMS seiche amplitude was computed using:

$$\zeta_{RMS}^{x} = \frac{\Delta T_{RMS}^{x}}{\delta\bar{T}/\delta z} \quad [12]$$

where:

ζ_{RMS}^{x} = the RMS seiche amplitude for thermistor x; and

$\delta\bar{T}/\delta z$ = the local temperature gradient estimated from the mean temperature profile.

The resulting RMS seiche amplitude values represent the absolute value of the wave envelope (Fricker and Nepf, 2000).

The resulting seiche amplitudes are displayed in Figure 4.67 (a-d). Only seiche amplitudes in July – October were calculated because May and June had less data (only ~20 m of thermistor data) and somewhat isothermal profiles. Seiche amplitude magnitudes ranged from 22.9 – 1.1 m, and were on average 6.4 m. It

should be noted that isothermal portions of the profile (i.e. slopes greater than 0.02) were excluded from the calculations, as extremely large amplitudes resulted.

As seen in Figure 4.67a, the greatest range of seiche amplitudes were found in July, ranging from 1.1 – 22.9 m. On average, the calculated seiche amplitude was 7.4 m. July 7 – 8 had the largest seiche amplitudes, which were above 10 m throughout the water column. These days were corresponding with an internal seiche (July 7) and a large wind event (July 8), as discussed in Section 4.3.4.3. If this time period were removed from the average, July's seiche amplitude would be around 6.4 m This is close to the 5 m magnitude of the approximately 3 day period seen in the mean daily contours discussed in Section 4.3.4.

The calculated seiche amplitudes in August were significantly less than July, as seen in Figure 4.67b. This was most likely due to the fact that the stratification was more developed and stable in August, enabling less fluctuation. The calculated amplitudes ranged from 2.3 – 14.0 m, with an average of 5.3 m. This agreed well with the oscillations seen in the mean daily contours in Figure 4.13c, with average magnitudes being larger in the deeper layers, around 6 m. The calculated fluctuations were most severe during August 21 – 25. This period corresponds with a time of cooler air temperatures and faster wind speeds (see Figure 4.7d and Figure 4.9d). Disregarding this time period, the average calculated fluctuations in August were slightly greater in the deeper layers (~30 – 60 m). Average seiche amplitudes here were 5.7 m, while the layers ~0.2 – 30 m had amplitudes of only 4.4 m (disregarding August 21 – 25). This agreed well with the phenomenon discussed in Section 4.3.4.3, where seiching was observed mainly in the deeper layers.

September calculated seiche amplitudes ranged from 1.8 – 18.9 m, with an average of 5.5 m, as seen in Figure 4.67c. The most substantial fluctuations occurred in the top ~20 m during the beginning of September. This was during a reservoir cooling period, when penetrative convection was developing the well-mixed epilimnion layer. This was close to the observed oscillation magnitude of about 3 m in the bottom isotherms of the mean daily water temperature contours (see Figure 4.13c).

In October, only the bottom ~35 m of seiche amplitudes was calculated, as seen in Figure 4.67d. This was due to the fact that the upper layers were isothermal in October. Seiche amplitudes ranged from 2.9 – 13.0 m, with an average of 6.1 m.

Again, these estimations were on the same order of magnitude as the observed oscillation magnitudes (about 3 m) seen in the mean daily temperature contours in Figure 4.13a.

4.5.3 Selective Withdrawal: Withdrawal Layer Thickness

In Section 3.5.3, the selective withdrawal from a two-layer stratification structure was discussed. Selective withdrawal of water also occurs in linearly stratified fluids. Instead of determining a critical discharge, which overcomes the buoyancy forces from the thermocline, selective withdrawal in linearly stratified fluids is described in terms of withdrawal layer thickness. During operations, water will be withdrawn from an adjacent layer of some thickness. This thickness is determined both by the magnitude of the discharge and the buoyancy forces.

The daily withdrawal layer thickness was calculated for MCA over the course of the field work. The operating intakes were estimated as a point sink and discharges were averaged daily. The withdrawal layer thickness was calculated daily with the following equations from Lawrence and Imberger (1979) and Ivey and Blake (1985):

$$\delta_w = 1.42\ (Q/N_b)^{1/3} \qquad [13]$$

where:

δ_w = the withdrawal layer thickness;

Q = the total discharge; and

The calculated thickness of the withdrawal layer is shown in Figure 4.68 along with the reservoir depth. In general, the withdrawal layer thickness was smallest in June, increased in July, and was largest from August – October.

These generalities excluded a short period at the beginning of May, when the withdrawal layer thickness was very large, and water was being withdrawn from the entire depth. This would be expected for two reasons. From May 13 - 19, the discharges were somewhat high with an average of 120 m^3/s, as shown in Figure 4.69. Furthermore, the buoyancy frequency was extremely small since the temperature profile was nearly homogeneous, which can also be seen in Figure 4.69. These conditions would result in withdrawal from the entire water column, as the withdrawal layer thickness calculation suggests.

From May 20 – July 3, the withdrawal layer thickness was 27 m on average. This was during a time of low discharge, about 45 m^3/s, and fluctuating buoyancy frequency, as seen in Figure 4.69. The highest buoyancy frequencies correspond to the smallest withdrawal layers in Figure 4.68 since the well-developed stratification inhibits the vertical movement of water more. The reservoir depth during this time was an average of 49 m. This suggests that water was only being withdrawn from the bottom half of the water column.

From July 4 – July 31, the reservoir was filling and discharges (average of 344 m^3/s) were increasing, as seen in Figure 4.68 and Figure 4.69. The average withdrawal layer thickness during this time was 46 m, and the average reservoir depth was 62 m. The calculated withdrawal thickness to water column depth ratio increased from half to two-thirds of the water column.

From August 1 – 22, the reservoir was operating at a maximum discharge, as seen in Figure 4.69. On average, the discharge was 890 m^3/s. Also, the calculated withdrawal layer thickness was at a maximum, as seen in Figure 4.68. The average thickness was 58 m. With an average depth of 67 m during this time period, the intakes were theoretically withdrawing from almost the entire water column.

From August 23 – October 25, discharges were slightly smaller, 621 m^3/s on average (Figure 4.69). The withdrawal layer thickness was only slightly different due to this decrease, with an average of 56 m. The average reservoir depth remained the same at 67 m, meaning that withdrawal was theoretically occurring from over 80% of the water column.

The calculation of the withdrawal layer thickness could be used to support the theory of the thermistor and dam operations correlations referred to in Section 4.4.2. As previously mentioned, the dam operations were determined to be affecting the temperatures of the thermistors. It was suggested that lower discharges, as seen in June, withdrew water from lower layers, including the deeper, hypolimnetic water beyond the intake apron. This would cause the thermistor temperatures to decrease and result in a negative correlation between the dam operations and thermistor temperatures, as was seen in Figure 4.60. This was seen in the selective withdrawal analysis; only water from the bottom half of the water column was calculated as being withdrawn with this lower discharge. Furthermore, when the discharges increased, as in August, September, and October, it was thought that the intakes were withdrawing

water from more of the water column, including the warmer upper layers. This would move warmer water down to the thermistors, creating a positive correlation relationship between the dam operations and the thermistors, which was seen in Figure 4.60. Again, the withdrawal layer thickness calculations affirmed these assumptions, as water was calculated as being withdrawn from more than 80% of the water column with these larger discharges.

A calculation of the withdrawal layer thickness was completed on a daily basis for the duration of the field season (May – October). In general, the resulting intake withdrawal layer thickness was 27 m (from 49 m depth) in June, 46 m (from 62 m depth) in July, and 57 m (from 67 m depth) in August – October. This increase in the thickness of the withdrawal layer from June – October agreed well with the theory proposed to explain the positive and negative correlations found between thermistor temperatures and dam operations (Section 4.4.2).

4.5.4 CFD Modelling

A three dimensional CFD model was also developed for MCA using the ANSYS CFX program. The model extents covered the forebay area extending from the dam face to approximately 2.5 km upstream. The model boundaries were constructed using a patch conforming tetrahedral mesh which was created using topographic information provided by BC Hydro. The horizontal and vertical spacing of the mesh generally ranged from 4 m – 20 m. Local refinement of the mesh size near the intake location ranged from 0.1 m – 2 m. A free-slip wall boundary was used at the reservoir's free surface, while other walls were modelled using no-slip conditions. At the MCA intakes, mass-flow rate boundary conditions were provided. At the upstream boundary, an 'opening' boundary was provided. This allows both inflow and outflow across the boundary. The CFD solver uses the three dimensional Reynolds averaged Navier-Stokes equations, with the $k-\varepsilon$ turbulence model to assess eddy viscosity. The average temperature profile over the course of the three days of velocity measurements (August 8 to 10, 2011) were fit to an empirical equation to use in the model. A full buoyancy model was chosen to compute temperature transport.

As with HLK, the flow field upstream of the dam was simulated under the conditions during field studies. Such conditions included discharge, temperature profile, and water level. Results were then compared to the velocity measurements taken during the field studies that were collected using an ADCP. Generally the simulations done using ANSYS CFX 12.1 matched the field measured results very well, particularly for the lateral (X and Y velocity

components). Details regarding the models governing equations, boundary conditions, and mesh can be found in a report prepared for BC Hydro (Langford et al., 2012).

The model used to evaluate the reservoir's flow field during different operational scenarios. As mentioned previously, theoretical calculations revealed different thicknesses of withdrawal layers for different discharge magnitudes. This was connected to the positive and negative correlations between the thermistor temperatures and the dam operations. In order to make a more sophisticated estimate of the selective withdrawal layer, different operational scenarios were input into the CFD model to determine the changes in the velocity profile near the thermistor chain.

Two different operational scenarios were modelled. The first scenario had a lower total discharge of 470 m^3/s; 235 m^3/s being withdrawn from Intakes 1 and 2. This scenario was similar to the discharge operations during the month of July, when negative correlations were seen between the thermistors and dam operations. The second scenario had a high total discharge of 1028 m^3/s; 257 m^3/s being withdrawn from Intakes 1, 2, 3, and 4. This scenario was similar to the discharge operations during the month of August, when positive correlations began to be seen between the mid-depth thermistors and dam operations.

For both of the scenarios the temperature distribution was as seen in Figure 4.70. These values were average field conditions from August 8 – 10. As July and August had similar temperature profiles, this approximation was considered acceptable. The water level was also the same for both model runs. It was 752.98 m, which was the average elevation from August 8 – 10. This works well for the second scenario, since the modelling is representative of condition in August. In July, which is representative of the first scenario, the water level was 5 m lower, on average. However, this difference in elevation was thought insignificant as the correlations between the thermistors and dam operations were found in the middle and lower thermistors. This suggested that the dam operations have little effect on the top thermistor temperatures.

The resulting velocity magnitudes at different elevations in the MCA dam forebay are shown in Figure 4.71. The two elevations plotted were 706 m and 740 m for both low discharge and high discharge results. These elevations were chosen based on the calculated selective withdrawal depth. Withdrawal should have been occurring for both the low and high discharges at the 706 m elevation.

However, at the 740 m elevation, withdrawal should have only been occurring for the higher discharge. The lower discharge's calculated selective withdrawal thickness would not reach this elevation.

An apparent semi-circular zone can be seen around the intakes with a radius of approximately 170 m (Figure 4.71). This was the area of local refinement in the mesh of the model, which allowed for more comprehensive modelling. The velocities in the refined area were more detailed and accurate. The velocity magnitudes had a noticeable jump outside of this area, and no longer had a distinguishable gradient. The thermistor chain was located outside of this detailed zone, which was calculated as having the same velocity magnitude for both discharges at both elevations. However, we will look at the detailed, refined zone to compare and contrast the two discharges.

At the 706 m depth, withdrawal was occurring for both the low (see Figure 4.71a) and high (see Figure 4.71b) discharges. The velocity magnitude was fairly consistent for both the low and high discharges, generally around 0.1 m/s. Closer to the intake face, the velocity increased to above 0.2 m/s. This area was larger for the higher discharge, as more intakes were operating.

At the 740 m depth, withdrawal was occurring for both the low and high discharges, but there was a noticeable difference in the velocity magnitudes. For the low discharge (see Figure 4.71c), the velocity in the refined zone was very low, in the range of 0.05 – 0.075 m/s. The velocity magnitude for the higher discharge was noticeably higher (see Figure 4.71d), in the range of 0.075 – 0.125 m/s. This indicates that more flow was being withdrawn from this layer, as compared to the lower discharge. This was what was expected from the selective withdrawal calculations.

4.5.5 Conclusions of MCA Theoretical Calculations

Theoretical calculations were undertaken to determine the oscillatory periods resulting from different boundaries in the reservoir. Wave like solutions from the component equations of two dimensional motions were used with many idealizations, including an exponential density distribution. This allowed for the calculation of seiche periods with different vertical modes. Two different reservoir lengths were chosen based configuration of the reservoir. Calculated periods were in the order of days for a 150 km main reach and in the order of hours for a 14.6 km local reach. Furthermore, the appropriate range of internal seiche periods were calculated with vertical modes of 1, 2, and 3 nodes.

The seiche amplitudes of the internal waves in the reservoir were calculated. Similar periods of stratification were grouped together and the seiche amplitudes were calculated for each time frame. July had the largest range of amplitudes, while August – October had smaller ranges. This was expected, as the stratification was more developed in these months and less fluctuating.

The selective withdrawal layer thickness was calculated for different discharges and stratification structures throughout the field season. In general, the withdrawal layer was smallest in May and June, with about half of the water column selectively withdrawn. As discharges increased in July, the thickness increased to about two-thirds of the water column. Finally, when discharges were at a peak in August, the selective withdrawal layer was about 80% of the water column, which was about the same in September and October.

The selective withdrawal was further investigated using a CFD model that was created for MCA forebay. The velocity magnitudes resulting from a 470 m^3/s discharge (similar to July) and a 1028 m^3/s discharge (similar to August) were determined. At an elevation of 706 m, about a third of the way up the water column, both discharges were withdrawing water at about the same velocity. However, at an elevation of 740 m, about three-quarters of the way up the water column, velocities from the higher discharge were noticeably larger. This agreed well with the selective withdrawal calculations.

5. Revelstoke Dam (Revelstoke Reservoir)

A study of the reservoir thermal characteristics was carried out for the Revelstoke reservoir. The REV facility impounding this reservoir was located downstream of MCA (Kinbasket reservoir) and upstream of HLK (Arrow Lakes reservoir) on the Columbia River system. The following chapter describes the site, data collected, results and observations, and conclusions.

5.1 Site Description

Revelstoke Dam was completed in 1974. This concrete gravity dam was 175 m high and was located near the city of Revelstoke, BC, as seen in Figure 5.1. The hydropower facility included five operational Francis turbines, with an intention of expanding to one more. The intakes were laterally located in the middle of the structure, at an elevation of 545.73 m, about 27 m from the water surface.

Revelstoke reservoir levels varied little throughout the year, as it was operated as a run of the river type dam. Discharges were generally low (<100 m^3/s) from January until April, when inflow from MCA was large. REV discharges usually increased from April until mid-June, during peak outflows (750 m^3/s). Afterwards, from July until November, discharges generally decreased to lower flows similar to the beginning of the year (<100 m^3/s).

Revelstoke reservoir was about 130 km long and about 0.8 km wide, as shown in Figure 5.1. The reservoir began at the MCA outlets and extended generally to the south. Revelstoke reservoir was somewhat more sinuous than Kinbasket reservoir. The end of the reservoir and the dam structure were located just outside of Revelstoke, BC.

There were two main categories of inflow sources for Revelstoke reservoir, the Columbia River at MCA and local flow. The Columbia River at MCA accounted for about 71% of inflow, while local inflows accounted for about 29% (Bray, 2012). The majority of inflow came from MCA, which was highly variable throughout the year (see Section 4.3.2). Local inflow included several streams flowing into Revelstoke reservoir, including Nagle Creek, Soards Creek, Mica Creek, Pitt Creek, Birch Creek, Bigmouth Creek, Scrip Creek, Horne Creek, Hoskins Creek, Goldstream River, Kirbyville Creek, Downie Creek, Bourne Creek, Big Eddy Creek, Carnes Creek and Martha Creek.

5.2 Collected Data

The major source of information for REV comes from the ecological productivity monitoring program reports provided by BC Hydro. Three years of data was collected for the Revelstoke reservoir. Similar measurements to Kinbasket reservoir were reported, including reservoir temperature profiles, reservoir characteristic, and tributary characteristics.

Information on the meteorological conditions was collected from Environment Canada. One meteorological station was in the area. It was located at the Revelstoke airport (REVELSTOKE A, Climate ID: 1176749), approximately 14 km downstream of REV. The meteorological station at the airport recorded hourly information, including temperature and wind speed. Information was collected from another Environment Canada meteorological station, which was located about 3 km downstream of Mica Dam at the village of Mica Creek (MICA DAM, Climate ID: 1175122). This meteorological station recorded daily average information on temperature. This will be referred to as Mica Creek, and should not be confused with the BC Hydro meteorological station located on the dam face.

5.3 Results and Observations

The following results and observations were from the ecological monitoring and productivity BC Hydro reports. Tributary inflow temperature measurements were taken along the Revelstoke and Kinbasket (previously discussed in Section 4.3.6.1) reservoirs in 2008 – 2010. These results were contrasted and compared. Furthermore, water temperature profile measurements were taken in July – October in 2008, June – October in 2009, and May – October in 2010 throughout the Revelstoke and Kinbasket (previously discussed in Section 4.3.6.2) reservoirs. Meteorological data for REV and MCA was collected for these periods as well. The meteorological information and water temperature information for REV and MCA were also contrasted and compared.

5.3.1 Meteorological Data

The hourly air temperatures recorded at the Revelstoke airport from July – October, 2008, June – October, 2009, and May – October, 2010 are plotted in Figure 5.2 (a – d), Figure 5.3 (a – e), and Figure 5.4 (a – f). Daily maximum and minimum air temperatures recorded at the Mica Creek meteorological station were also plotted for comparison.

Average temperatures at Revelstoke airport changed throughout the seasons. Air temperatures in May 2010 were on average 11.5 °C, and ranged from 0.4 °C to 26.2 °C (see Figure 5.4a). June air temperatures in 2009 (see Figure 5.3a) and 2010 (see Figure 5.4b) were warmer, on average 16.2 °C, and ranged from 4.8 °C to 31.5 °C. The warmest month on average was July (see Figure 5.2a, Figure 5.3b, and Figure 5.4c), with average air temperatures from 2008 – 2010 of 18.7 °C and ranges of 6.5 °C to 34.6 °C. August was also relatively warm (see Figure 5.2b, Figure 5.3c, and Figure 5.4d), with average air temperatures from 2008 – 2009 of 17.5 °C. The temperature range was slightly cooler than July, from 5.3 °C to 34.0 °C for all three years. Cooling was apparent in September (see Figure 5.2c, Figure 5.3d, and Figure 5.4e), with an average of 12.3 °C (from 2008 – 2010) and a range of 2.1 °C to 29.6 °C. Cooling continued into October (see Figure 5.2d, Figure 5.3e, and Figure 5.4f), with an average of 6.3 °C and a range of -6.7 °C to 19.4 °C from 2008 – 2010.

During May through October in 2008 – 2010, Revelstoke airport temperatures were slightly warmer than at Mica Creek. Revelstoke airport maximum daily temperatures were, on average, 2.6 °C warmer than Mica Creek. Revelstoke airport minimum daily temperatures were, on average, 1.8 °C warmer than Mica Creek. Revelstoke airport mean daily temperatures were 2.6 °C (on average) warmer than Mica Creek mean daily temperatures from May – October.

The hourly wind speeds at Revelstoke airport from July – October, 2008, June – October, 2009, and May – October, 2010 are presented in Figure 5.5 (a-d), Figure 5.6 (a-e), and Figure 5.7 (a-f). There were monthly trends in the average wind speeds. May had the highest average, at 8.2 km/h, and a maximum of 41.0 km/h. June was slightly lower, with an average wind speed of 7.1 km/h and a maximum of 41.0 km/h. July average wind speeds were slightly lower than June, at 6.2 km/h. However, July had the highest recorded wind speed of 54.0 km/h. August had slightly lower values, with an average wind speed of 5.5 km/h and a maximum of 46 km/h. September and October wind speeds were lower than August, with averages of 4.1 km/h and 4.4 km/h, respectively, and maximums of 33.0 km/h and 35.0 km/h, respectively.

It appears that the wind speeds at Revelstoke airport were consistently lower than BC Hydro's station at MCA dam (referred to as Mica Dam). Since wind speed data from 2008 – 2010 was not available at Mica Creek, this comparison was with the 2011 MCA wind speed data. However, it should be noted that Revelstoke airport wind speed data in 2011 was very comparable to the 2008 –

2010 averages, and the means were within less than 1 km/h of each other. Similar consistency was expected for Mica Dam. On average, the wind speed was about 4.0 km/h lower at Revelstoke airport than Mica Dam. Also, the maximum wind speed measured was about 10.0 km/h less than the Mica Dam maximum. Nevertheless, the wind speed at Revelstoke Airport was highest during May, similar to Mica Dam. Location of the meteorological station may have influenced the measurements. At Mica Dam, the station was located over open water (on top of the dam face), whereas the Revelstoke airport station was located over land. Since wind speeds over land are generally less than wind speeds over water, this could account for the consistently lower speeds measured at Revelstoke airport.

In general, the air temperature data at Revelstoke airport and Mica Creek and the wind speed data at Revelstoke airport and Mica Dam were very similar. These locations were within 120 km of each other, so this was expected. There were slight discrepancies in the air temperature. It seemed that air temperature at Revelstoke airport was slightly warmer than at Mica Creek, by about 2 °C. Also, there were some discrepancies in the wind speed data. It seemed that Revelstoke airport had slightly lower wind speeds than Mica Dam, by about 4 km/h. However, this difference may be due to the location of the measurement stations. These discrepancies were small and unlikely caused noticeable differences in the water temperature profiles at Kinbasket and Revelstoke reservoirs.

5.3.2 Historical Temperature Measurements in Revelstoke Reservoir

As mentioned previously, a monitoring program was implemented by BC Hydro to provide information on the ecological productivity of Kinbasket and Revelstoke reservoirs and how they were affected by reservoir operations. Local inflow measurements and instantaneous thermal profiles were measured throughout Revelstoke reservoir and will be contrasted and compared to the previously presented Kinbasket measurements.

5.3.2.1 Temperature Inflows

The majority of inflow into Revelstoke reservoir (71%) comes from the Columbia River at MCA (MCA discharge). Local tributaries account for 29% of the inflow. The temperatures of these water sources will partially determine the thermal characteristics of the reservoir.

Tributary temperatures were measured in 2008, 2009, and 2010 and were published in the BC Hydro ecological monitoring reports (Bray, 2010, Bray, 2011, and Bray, 2012). Temperature measurements for the Revelstoke reservoir local tributaries were either taken at the mouth (when accessed by helicopter) or at the Highway 23 crossing (when accessed by road). This highway runs along the left bank of the reservoir, and tributary crossings would be located relatively close to the mouth. The temperatures of the streams were measured using a handheld thermometer.

All of the recorded inflow temperatures for Revelstoke reservoir are shown in Figure 5.8. In 2008, MCA discharge temperature was measured to be 7 °C on June 24. Additionally, nine local tributary temperatures were measured on June 24 – 25 and eleven were measured on August 5 – 6. In June, local inflow water temperatures ranged from 6.5 °C to 9.5 °C, with an average of 8.0 °C. In August, local inflow water temperatures ranged from 9.5 °C to 14.0 °C, with an average of 12.0 °C. In 2009, sixteen local inflow tributaries temperatures were measured on July 7 – 8. These values ranged from 6.0 °C to 10.5 °C, with an average temperature of 7.5 °C. In addition, nine measurements were taken from May – November at the MCA discharge. These water temperatures ranged from 3.5 °C (May) to 9.0 °C (June), and on average were 6.5 °C. In 2010, nine local tributary water temperatures were measured on May 31. These water temperatures ranged from 4.0 °C to 7.0 °C, with an average value of 5.6 °C. Also, one water temperature measurement of 6.5 °C was taken at the MCA discharge on May 31.

A few generalities about Revelstoke inflow temperatures should be mentioned. The Columbia River at MCA temperatures were similar to local inflows for May and early June, as seen in Figure 5.8. However, in late June, July, and August, local inflow temperatures were warmer than the MCA discharge. This was due to the warming of the tributary surface waters in the summer months. The Columbia River at MCA temperature remained relatively constant since the discharge location was deep in the Kinbasket reservoir.

When comparing Columbia River temperatures upstream of Kinbasket and upstream of Revelstoke, it was apparent that the former was significantly warmer for most of the year. A plot of all the Columbia River measurements is shown in Figure 5.9. Only in October and November were the Columbia River water temperatures upstream of REV warmer than upstream of MCA. Local inflows into Kinbasket and Revelstoke reservoirs were also compared in Figure 5.10. Kinbasket local flow temperatures were quite comparable to Revelstoke

local flow temperatures in May, June, and July. However, in August, Revelstoke local inflow temperatures were generally warmer than Kinbasket local inflows. Furthermore, the Revelstoke surface water temperatures, which are plotted in Figure 5.8, were more comparable to the inflow temperatures (excluding the Columbia River inflow from MCA). As explained in Section 4.3.6.1, it was thought that the Kinbasket inflows plunged into the reservoir due to the much warmer surface waters, creating a linear temperature gradient. This may not be the case in Revelstoke reservoir with similar surface water and inflow temperatures. The discrepancies between Kinbasket and Revelstoke inflow temperatures were considered when comparing the water temperature profiles in Section 5.3.2.2.

5.3.2.2 Instantaneous Temperature Profiles

Water temperature profiles were measured in 2008 (Bray, 2010), 2009 (Bray, 2011), and 2010 (Bray, 2012) throughout the Revelstoke reservoir. There were three general locations where temperature profiles were measured: in the forebay near the dam (FB), in the middle of the reservoir (MI), and in the upper portion of the reservoir (UP), nearest the MCA outlet. These general locations are outlined in Figure 5.11.

The temperature measurements were collected using a Sea-Bird Electronics SBE 19plus V2 profiler. It should be noted that problems with the Sea-Bird profiler pump were identified and some profiles were measured inaccurately in 2009 and 2010. These profiles are noted with an asterisk. These profiles will be excluded from the discussion, which will compare the Revelstoke reservoir profiles to the Kinbasket reservoir profiles.

2008 Instantaneous Profile Measurements

In 2008, seventeen instantaneous profile measurements were conducted from July – October. Each month, measurements throughout the Revelstoke reservoir were taken within one day of each other. The results of these measurements are discussed below.

In July 2008, the thermal gradients in the middle and upper portions of the reservoir were generally linear from the surface to about a 55 m depth, as seen in Figure 4.35. After this depth, the profiles were somewhat homogeneous at a temperature of about 4 °C. It should be noted that the reservoir is much shallower in the upper portion (about 40 – 50 m) compared to the middle and forebay areas (about 80 – 120 m). These profiles were somewhat similar to the temperatures seen in Kinbasket reservoir in July 2008. However, the Revelstoke

forebay temperature profile was different, portraying a well-mixed layer at the surface which was over top a distinct thermocline layer at 25 m. Below this, the profile was linear to about a 55 m depth. The measurement was taken on July 16, during a period of high winds (see Figure 5.5a), which mixed the surface. The other measurements were taken on July 15, and a well-mixed epilimnion layer had not yet formed.

In August 2008, the profiles throughout the reservoir were somewhat similar, as seen in Figure 4.36b. In general, an approximately 10 m deep well-mixed layer was over top of a linear stratification layer down to a 60 m depth. These profiles were somewhat similar to the Kinbasket reservoir profiles in August 2008. However, only the forebay Kinbasket profile had the well-mixed layer at the surface. As discussed in Section 4.3.6.1, colder local inflows for Kinbasket plunged into the reservoir, inhibiting the development of an epiliminion layer. Inflow temperatures were generally warmer at Revelstoke during August, which would not have plunged into the reservoir. This allowed the development of a well-mixed epilimnion layer. Furthermore, local inflows only accounted for 29% of the flow and would have influenced the temperature profile less than at Kinbasket reservoir.

In August 2008, the profile in the upper portion of the Revelstoke reservoir was also cooler than the middle and forebay area profiles, by a few degrees. In contrast, all the profiles at Kinbasket were fairly similar. This was due to the cooler hypolimnion water released from MCA into the upper portion of Revelstoke reservoir. The temperature profile was warming as it travelled along the reservoir.

In September 2008, the profiles measured in Revelstoke reservoir were somewhat different from profiles measured in Kinbasket reservoir. The September Revelstoke reservoir profiles had a 'two step' shape, as shown in Figure 4.37b. The top 10 m was a well-mixed homogeneous layer. From 10 – 25 m the stratification profile was linear. Below this, the profile was homogeneous from 25 – 45 m. Finally, from 45 – 65 m, the profile was linearly stratified. Below this the temperature was constant at about 4 °C. By contrast, the Kinbasket profile had a 'one step' shape, with the linear stratification extending from ~20 – 60 m. It should be noted that the intake depths at REV (depth of 36 m) were higher than MCA (depth of 55 m). The withdrawal location can affect the location of the thermocline and the thermal profile shape

(Casamitjana et al., 2003), which may have caused these differences between the reservoirs.

It is also interesting to note the cooler profiles in the upstream portion of the Revelstoke reservoir in September 2008. These profiles gradually warmed going in the downstream direction. This was due to the colder releases from the MCA outlets into the upper portion of the Revelstoke reservoir.

In October 2008, the Revelstoke profiles were generally similar to the Kinbasket measurements. The top 20 – 30 m was homogeneous; below this the temperature profile was linear to a depth of about 60 m, as seen in Figure 4.38b. Below this the temperature was constant at about 4 °C. The only difference from Kinbasket was the change in temperature throughout the reservoir. In Revelstoke reservoir, the upper portion was generally cooler, while the middle and forebay areas were warmer. Again, this was due to the cooler MCA discharges in the upper portion of the reservoir.

2009 Instantaneous Profile Measurements

In 2009, twenty-five instantaneous profile measurements were collected from June – October in Revelstoke reservoir. However, two profiles, indicated with an asterisk, were affected by the malfunction on the Sea-Bird profiler. Monthly measurements were taken within one day of each other.

In June 2009, the forebay profile was linearly stratified from the surface to about a 35 m depth, as seen in Figure 4.39b. This was similar to Kinbasket profiles in June 2009, which had a linear stratification extending to a depth of 30 m. However, in the middle portion of Revelstoke reservoir, the linear profile was warmer and extended deeper, to about a 50 m depth. This could be due to the fact that inflow temperatures in Revelstoke reservoir during June were relatively cold. As the flow was moving from the middle portion to the forebay, cold plunging inflows could have cooled off the temperature profile and smeared it to a more linear shape. Also, the middle and forebay profiles were taken on different days, which could also been part of the reason for the discrepancy.

In July 2009, the profiles were fairly similar throughout the reservoir and had a somewhat linear profile from the surface to a depth of 50 m, as seen in Figure 4.40b. Kinbasket measurements in July 2009 were very similar to this profile. The forebay temperature profile was somewhat warmer than the other profiles in the top 20 m, creating a distinguished thermocline, which may have been due to the intake withdrawal depth. Again, the upper portion of the reservoir was a

few degrees cooler than the middle and forebay areas due to the colder inflow temperatures from the MCA discharge.

In August 2009, the Revelstoke profiles had a 'two step' shape (see Figure 4.41b) as was seen in September of 2008. The top ~10 m was homogeneous, followed by a linear stratification from ~10– 20 m. The profiles were again homogeneous from ~20 – 50 m, followed by another linear stratification portion from ~50 – 60 m. After this the profile was again homogeneous at a temperature around 4 °C. Profiles throughout the reservoir were fairly similar, although the upper portion was still cooler by a couple of degrees.

Early September 2009 profiles, seen in Figure 4.42b, were similar to the August 2009 Revelstoke profiles with a 'two step' shape. Profiles in the upper portion were generally cooler, and warmed while moving downstream. Also, the 'two step' shape became more defined in profiles closer to the forebay. September 2009 Kinbasket stratification was different and had a linear profile from the surface to a depth of about 60 m. Mid -September 2009 profiles for Revelstoke reservoir are shown in Figure 4.43b. The observations and comparisons were the same as early September profiles.

October 2009 profiles in Revelstoke reservoir had a ~40 m homogeneous surface layer, as seen in Figure 4.44b. Below this, the forebay profile had a smaller 'two step' shape. Again, this was dissimilar to Kinbasket reservoir profiles in October 2009, which had a homogeneous layer overtop a linear stratification to about 65 m. The profiles in Revelstoke reservoir were cooler in the upper portion and warmed going downstream in the reservoir.

2010 Instantaneous Profile Measurements

In 2010, thirty-one instantaneous profile measurements were collected from May – October in Revelstoke reservoir. Five profiles were affected by the Sea-Bird profiler pump malfunction, which were indicated by an asterisk. Most monthly measurements were taken within one or two days of each other. However, in May, measurements were taken on May 12, and May 25 – 26.

The profiles in May 2010 near the forebay and upper portion of the reservoir were similar, as seen in Figure 4.45b. They were relatively homogeneous, with some warming at the surface. The upper profile was warmer than those in the forebay, which was in contrast to what was seen earlier. This could be due to the fact that MCA discharges were generally low in May. Therefore, the upper

portion was not receiving a large amount of cold water, as in July – October. Therefore, the profiles along the reservoir were more comparable.

In May 2010, the Revelstoke profiles were somewhat different than the 2010 Kinbasket reservoir profiles as they did not have the steep temperature gradient at the surface. Since the profiles were not taken on the same day, it is reasonable to see such a difference from day to day. As discussed in Section 4.3.4.3, Kinbasket profiles in May changed rapidly from a steep surface temperature gradient to a homogeneous profile over short periods of time.

In June 2010, the forebay and upper profiles were nearly identical, as seen in Figure 4.46b. A linear stratification pattern developed from the surface to about a 60 m depth. These profiles were somewhat similar to the Kinbasket reservoir profiles in June 2010, except for the surface layer. In Kinbasket, a well-mixed surface layer was apparent in the top 10 – 20 m. This could be due to the difference between measurement dates. A wind event could have caused the homogeneous surface layer in Kinbasket and Revelstoke reservoirs on June 15. However, by June 22, the linear profile shape had once again returned.

In July 2010, the middle and upper profiles were similar to each other (see Figure 4.47b). A linear stratification profile reached from the surface to about a 60 m depth. This same trend was seen in the Kinbasket reservoir forebay and Wood Arm profiles in July 2010. The Canoe Reach, Columbia Reach, and middle areas of the Kinbasket reservoir were more susceptible to northwesterly and southeasterly winds and the Kinbasket forebay, Wood Arm, and Revelstoke reservoir areas were not. A northwesterly and southeasterly wind event could be why the susceptible areas showed well-mixed upper layers while the others remained linear.

August 2010 profiles were somewhat similar throughout the reservoir, but did change gradually from the upper portion of the reservoir to the downstream forebay area, as seen in Figure 4.48b. The upper portion of the reservoir was cooler and linearly stratified only to about a 20 m depth, after which it remained at about 9 °C. Going downstream in the reservoir, the profiles warmed and the linear stratification profile deepened. In the middle and near the forebay, the profile also developed about a 10 m homogeneous layer at the surface. These profile trends were somewhat different from MCA profiles in August 2010. There was no variation in temperatures throughout the Kinbasket reservoir as was apparent in the Revelstoke reservoir. This was probably due to the

extraction of the cooler hypolimnion from MCA dam creating a cooler profile in the upper portion of Revelstoke reservoir. The development of the 'classic' linear Kinbasket profile was achieved further downstream.

In September 2010, the profiles in the middle and near the forebay exhibited the 'two step' structure (see Figure 4.49b) as seen in the previous two years. This was much more defined near the forebay, where a definite thermocline was formed at about 10 m and also at 50 m. This supports the theory that the 'two-layer' structure is developed by the intake withdrawal location. These profiles were quite different from the September 2010 Kinbasket profiles, which only exhibited 'one step' from a depth of ~20 – 60 m.

The early October 2010 Revelstoke middle and forebay profiles still had the 'two step' structure somewhat, but with less defined thermocline positions. As seen in Figure 4.50b, the profiles warmed in the downstream direction. Again, these profiles were in contrast to the 'one step' profiles seen in Kinbasket reservoir. In later October 2010, the middle and forebay profiles were similar to the Kinbasket profiles. The top 20 – 30 m was a well-mixed homogeneous layer followed by linear stratification down to a depth of about 60 m, as seen in Figure 4.51b. Again, the upstream profile was cooler than the middle and forebay profiles.

The seasonal changes in the temperature profiles measured in Revelstoke reservoir were very similar from year to year. In May, a linear stratification profile was already formed from the surface to about a 40 m depth. This was similar to the forebay profile seen in Kinbasket reservoir. In June, the temperature profile remained linear, but deepened to about a 60 m depth in most locations. This was similar to most profiles found in Kinbasket reservoir. In July, the stratification remained linear, similar to the Kinbasket profiles. In August, the profiles were generally linear (similar to Kinbasket), but in some cases a 'two step' stratification had formed. This was most common in the forebay area. In September, a 'two step' structure was found in all profiles, excluding the upstream portion, as the reservoir was not deep enough for this development. Kinbasket profiles had only a 'one step' profile. The reason for this discrepancy was thought to be due to the location of the intake withdrawal. The MCA withdrawal was deep, at the bottom of the linear profile whereas the REV withdrawal was in the middle of the second homogeneous layer. This mid-depth withdrawal could have caused the development of the 'two step' profile seen in August and September. In mid-October, the surface layer was becoming cooler and homogeneous. This well-mixed layer was about 20 – 30 m deep. The

stratification below this was reverting back to a linear profile shape from ~30 – 60 m. This was similar to the profiles found in Kinbasket reservoir.

One consistent discrepancy between Revelstoke and Kinbasket reservoir profiles was the reoccurring presence of a well-mixed layer in Revelstoke reservoir from July – October. Wind speeds were fairly similar at REV and MCA, and could not account for this difference in the profiles. However, local inflow temperatures into Revelstoke reservoir were warmer than Kinbasket local inflow in July and August. This would prevent the plunging of cooler water which gave rise to a linear stratification profile. Therefore, the development of a well-mixed layer was seen consistently within the Revelstoke reservoir.

Another trend occurring from year to year was the temperature variation throughout the reservoir. In general, during July – August, the Revelstoke profiles were cooler in the upstream portion of the reservoir. The profiles generally became warmer closer to the forebay area. This was most likely due to the cooler, hypolimnetic water being released from MCA in the upstream portion of Revelstoke reservoir. As MCA flows released in May and June were much smaller, this trend was not as apparent during these months.

6. Conclusions

BC Hydro has identified the need to assess the risk of fish entrainment at their facilities on the Columbia River system. The risk of fish entrainment is related to the thermal regimes within a reservoir. For example, kokanee have been identified as a species at risk in Kinbasket reservoir. This species has annual temperature preferences which may coincide with the level of intake withdrawal, increasing their risk of entrainment. The thermal profile, which is of interest when trying to determine the risk of fish entrainment, is affected by natural fluctuations and hydro-power operations Therefore, the objective of this study was to better understand the thermal dynamics in the forebay of hydro-facilities on the Columbia River system, including natural and dam induced temperature fluctuations.

Three diverse hydro-facilities located in succession on the Columbia River were studied. Hugh Keenleyside Dam was 52 m high, non-power generating facility that regulated the water level of Arrow Lakes reservoir via four sluice gates and eight intakes. This hydro-facility was located furthest downstream. Mica Dam was a 244 m high dam generating power through the release of water from Kinbasket reservoir via four intakes located at the base of the dam structure. This hydropower facility was located furthest upstream. Revelstoke Dam was a 175 m high power generating dam that formed the Revelstoke reservoir. This hydropower facility was located downstream of MCA and upstream of HLK.

The focus of the study was on the HLK and MCA facilities. At these two facilities, thermistor chains were installed in the forebay area immediately upstream of the dam face recording temperature profile information every 5 min for 35 days in 2010 (HLK) and 175 days in 2011 (MCA). CTD profiles confirmed similar temperature stratification throughout each forebay. ADCP velocity profiles were also collected in each forebay, which were used to develop three-dimensional CFD models. Concurrent meteorological and dam operations data were also collected. Further information on Kinbasket reservoir included inflow temperature and instantaneous temperature measurements taken in 2008, 2009, and 2010 by BC Hydro. This information was also collected (by BC Hydro) for Revelstoke reservoir. Concurrent meteorological data in 2008 – 2010 was also collected.

The temperature stratification recorded at HLK could generally be classified as a two-layer profile. Mean daily contour plots revealed an approximately 3.0 day

oscillation period, one significant drop in temperature profile, and one significant rise in temperature profile. Review of the air temperature and precipitation showed they were not the cause for these changes. Dam operations were generally low (<250 m^3/s) and relatively steady (not oscillating). Therefore, it was thought that internal seiching was the cause of the regular temperature fluctuations.

In order to quantify the internal seiching in the thermal profile at HLK, a spectral analysis was carried out for each thermistor. Periods of 1.0 day and 3.5 days were found at the thermocline. A period of 11.6 days was found for the upper and lower thermistors, indicating an upwelling (large temperature rise and drop). Due to the limited length of the data set, it was thought that this period was overestimated and could be closer to 7 or 8 days. A period of 12 hours at thermistors near the surface was due to diurnal air temperature fluctuations. A period of ~7.0 hours was also found in thermistors near the surface, and a period of ~15 hours was dominant in the mid-depth thermistors. A spectral analysis conducted on the wind speed time series revealed periods similar to the internal seiche periods. Therefore it was thought that all of the internal seiche periods found in the thermistor time series were due to resonant wind forcing.

Theoretical calculations of some reservoir thermal dynamics at HLK were done in order to better understand the processes occurring. The calculated depth of wind mixing was 9.8 m which corresponded well with the observed 9.4 m average depth of the epilimnion. Thermocline oscillation periods due to wind forcing were calculated using a closed boundary 100 km upstream of HLK. Calculated internal seiche periods were similar to observed periods. A fundamental and second mode of oscillation was found at 7.0 days (related to 11.6 day period) and 3.5 days (observed), respectively. Finally, the critical discharge for a sluice gate was calculated to be 122 m^3/s. A three-dimensional CFD model of the HLK forebay was used to replicate the flow from discharges above and below critical. Results generally agreed with the theoretical calculations. Selective withdrawal from the epilimnion was occurring for discharges below the critical.

In contrast to HLK, the temperature stratification recorded at MCA could generally be classified as a linear profile. The temperature profile was generally linear from the surface to about a depth of 60 m. Although severe wind events did mix the surface for short periods, it always returned to the linear profile. Possible explanations for this were the cooler air temperatures at MCA and

higher discharges from deep intakes at MCA (as compared to HLK). Furthermore, very cold local inflow plunged into the reservoir and entrained warmer surface waters, causing the linearly shaped profile.

Mean hourly contour plots of the temperature profile showed the development of stratification at MCA. In May, the daily profile was generally homogeneous, and varied diurnally at the surface. In June, the water temperatures were warmer and began to stratify, with fluctuation magnitudes in the range of 10 – 20 m. The reservoir was fully stratified in July, with a linear profile down to about a depth of 60 m. The magnitude of fluctuations was less, with an average of 5 m. This stratification deepened in August, with warmer waters moving deeper. Oscillations were an average of 6 m near the bottom. In September the linear profile cooled. After this the surface layers cooled and became homogeneous in late September and October. The oscillation magnitudes were around 3 m near the bottom in September and October.

There were definite changes in the temperature profile at MCA, which were reviewed. Heating of the surface layers, creating a steep temperature gradient near the surface was seen during periods of low winds and high temperatures. High wind events led to the mixing of the surface layers, and the temperature gradient flattened out. Penetrative convection was also observed on a temporary basis on very cold days in July and August and also on a more permanent basis during the reservoir cooling period in September and October. Rapid temperature changes were also seen in the temperature profiles, with no apparent meteorological causes. These occurred on a periodic basis and were attributed to internal reservoir seiching. Periods of approximately 10 days were seen in June, approximately 5 days in July – October, and approximately 3 days in May - October. A negative correlation was also observed between the dam operations and bottom thermistor temperatures, meaning the temperature dropped when the intakes were operating.

In order to quantify the fluctuations in the thermistor time series at MCA, a spectral analysis was carried out. Periods of oscillation in the order of days found were 6.7 days, 11.3 days, 5.6 days, and ~3 days. All of these resulting periods had peak power magnitudes (largest fluctuations) in the upper thermistors in May and June. July and August power magnitudes were smaller, and spread across the upper and middle thermistors. In September and October, power magnitudes were still lower and concentrated mainly in the lower

thermistors. A period of ~1 day was also found. Higher power magnitudes were found in the bottom thermistors from July – October.

The MCA wind speed data spectral analysis revealed periods of 6.7 days, 11.3 days, 5.6 days, ~3 days, and ~1 day. Generally, these periods occurred during time frames that corresponded with the internal seiche periods. Therefore it was thought that most of these periods found in the thermistor data were due to wind forced internal seiching. However, the ~1 day period oscillations in July – October were near the intakes, and it was thought that this internal seiche period was influenced by the dam discharge operations.

Periods of oscillations in the order of hours were also found at MCA, including 18 – 22 hours, 11 – 14 hours, and 6 – 8 hours. The ~20 hour and ~ 7 hour periods were thought to be wind induced, as these periods were also found in the wind speed data. The ~12 hour period was considerably more dominant in July – October in the bottom thermistors. It was thought that this internal seiche period was also influenced by the dam discharge operations.

The degree of correlation between the thermistors and the dam operations was determined by calculating their covariance. Both positive and negative correlations existed, which changed over the field season. However, the bottom five thermistors were negatively correlated throughout. During medium discharges in July, the correlation between thermistor temperatures and dam operations was mainly negative. As discharge increased in August, the middle thermistors became positively correlated. This discrepancy was thought to be due to the selective withdrawal of different temperature layers. In July, it seemed that water was being withdrawn from lower, hypolimnetic layers, which caused the thermistors to cool. In August, the higher discharges seemed to overcome buoyancy forces, and warmer surface water was also being drawn down toward the intakes. In October, correlations were negative with the middle and bottom thermistors. The discharge was somewhat lower, and were withdrawing from only cooler layers once again.

Linear stratification profiles are susceptible to multiple vertical modes of oscillation. In order to find evidence of this type of fluctuation, the covariance between thermistors T2 and T11 with every other thermistor was also determined. In May and June, the fundamental mode of oscillation dominated, with the top layers being positively correlated. Evidence of second and third vertical modes were found in other months for the periods of 6.7 days, 5.6 days

and ~3.0 days. From these results, it was apparent that the Kinbasket reservoir was oscillating at multiple vertical modes.

Theoretical calculations of some reservoir thermal dynamics at MCA were calculated in order to better understand the processes occurring. Internal seiche periods with multiple vertical modes were calculated using two different boundaries. A main reach length with boundaries 150 km apart governed internal seiche periods in the order of days. A local reach length perpendicular to the main reach, with boundaries 14.6 km apart, governed internal seiche periods in the order of hours. Furthermore, the observed periods corresponded well with calculated internal seiche periods of the first, second, and third vertical modes. The seiche amplitude was calculated for July - October. Results ranged from 1.1 – 22 m and were on average about 6.4 m. These values agreed well with the observed oscillation magnitudes. The selective withdrawal thickness from the linear stratification profile was also calculated. The thickness increased with discharge, from about half (May and June) to two-thirds (July) to 80% (August) of the water column. These calculations agreed well with the flows seen in CFD model simulation. Near the intakes, the velocity magnitude was similar for both July and August average discharges. Near the surface, the velocity magnitude was moving faster for the August discharge, indicating more withdrawal from this level. These calculated selective withdrawal thicknesses agreed well with the theory presented about the positive and negative correlation of the thermistors with dam operations.

Meteorological data at REV and MCA were very comparable. Inflow into Revelstoke reservoir consisted mainly of the MCA discharge (Columbia River), which was quite cold. Columbia River inflows upstream of Kinbasket reservoir were significantly warmer. Local tributary flow into Kinbasket and Revelstoke had similar temperatures in May and June. However, during July and August, tributary temperatures were significantly colder into Kinbasket reservoir.

Instantaneous temperature profiles were collected throughout the Kinbasket and Revelstoke reservoirs in 2008 – 2010. The seasonal changes in each reservoir were similar from year to year. In May, a linear stratification profile was formed, which deepened throughout in June and July in both reservoirs. However, small layers of well-mixed epilimnion layers were also commonly found throughout the Revelstoke reservoir. This was attributed to the warmer inflow temperatures, which didn't plunge into the reservoir as at Kinbasket. In August, both reservoir profiles were generally linear, but some 'two step' profiles

were seen at Revelstoke. This 'two step' shape was also found commonly in September in Revelstoke, but not Kinbasket. This difference in shape was attributed to the mid-depth intake withdrawal at REV vs. the deep intake withdrawal at MCA. In October, both reservoirs had a ~30 m deep well-mixed layer formed over a linear profile shape to ~60 m.

The temperature profiles taken throughout the reservoir each month were very similar in Kinbasket. By contrast, Revelstoke reservoir had a profile in the upstream end that was colder, which generally warmed going downstream. This was attributed to the extremely cold discharge from MCA into the upper portion of Revelstoke reservoir.

The thermal dynamics in the forebay of three BC hydro facilities on the Columbia River system were studied. Natural reservoir dynamics were identified, as well as dam induced temperature fluctuation. This information will be used in an interdisciplinary study that will combine both biological and hydraulic research to determine a general method to determine the risk of fish entrainment.

7. Bibliography

Anderson, E.R. (1954). "Energy-budget studies." *Water loss investigations: Lake Hefner Studies, Technical Report Professional Paper* 269, Geological Survey, U.S. Department Interior, 71-119.

Anohin, V.V., Imberger, J., Romero, J.R., and Ivey, G.N. (2006). "Effect of long internal waves on the quality of water withdrawn from a stratified reservoir." *Journal of Hydraulic Engineering - ASCE*, 132(11), 1134-1145.

BC Hydro. (2004). "History and hydroelectric operation." *Hugh Keenleyside Dam,* <http://web.archive.org/web/20080221200617/http://www.bchydro.com/recreation/southern/southern1202.html> (January 10, 2012).

BC Hydro. (2005). "Boating safety." *Arrow Lakes reservoir,* <http://web.archive.org/web/20080626060749/http://www.bchydro.com/recreation/southern/southern5368.html> (January 10, 2012).

BC Hydro. (2009). "Kinbasket fish and wildlife information plan annual report: 2008." *Columbia River project water use plan*, 1-13 (accessible at: http://www.bchydro.com/etc/medialib/internet/documents/environment/pdf/wup__columbia_kin.Par.0001.File.KIN_Fish_Wildlife_2008_Annual_Report.pdf).

BC Hydro. (2009). "BC Hydro's Columbia River hydroelectric facilities." *Columbia River project water use plan – revised for acceptance by the Comptroller of Water Rights*, 1-65 (accessible at: http://www.bchydro.com/etc/medialib/internet/documents/environment/pdf/wup_columbia_water_use_plan_revised_for_acceptance_by_th.Par.0001.File.wup_columbia_water_use_plan_revised_for_acceptance_by_th.pdf).

Bendat, J.S. and Piersol, A.G. (1980). "Engineering applications of correlation and spectral analysis." *Correlations and spectral density functions*, Wiley-Interscience, New York, NY, 43-77.

Bhuiyan, F. and Zhu, D.Z. (2009). "Computational fluid dynamics modeling of flow pattern induced by hydropower intakes in Revelstoke and Mica Dams." *Interim report prepared for BC Hydro*, Department of Civil and Environmental Engineering, University of Alberta, Edmonton, AB.

Bray, K. (2010). “Kinbasket and Revelstoke Reservoirs Ecological Productivity Monitoring – Progress Report Year 1.” *Columbia River Project Water Use Plan,* BC Hydro, Revelstoke, BC, 1-140 (accessible at: http://www.bchydro.com/about/sustainability/conservation/water_use_planning/southern_interior/columbia_river/kinbasket-fish-wildlife.html).

Bray, K. (2011). “Kinbasket and Revelstoke Reservoirs Ecological Productivity Monitoring – Progress Report Year 2.” *Columbia River Project Water Use Plan,* BC Hydro, Revelstoke, BC, 1-266 (accessible at: http://www.bchydro.com/about/sustainability/conservation/water_use_planning/southern_interior/columbia_river/kinbasket-fish-wildlife.html).

Bray, K. (2012). “Kinbasket and Revelstoke Reservoirs Ecological Productivity Monitoring – Progress Report Year 3.” *Columbia River Project Water Use Plan,* BC Hydro, Revelstoke, BC, 1-274 (accessible at: http://www.bchydro.com/about/sustainability/conservation/water_use_planning/southern_interior/columbia_river/kinbasket-fish-wildlife.html).

Caliskan, A. and Elci, S. (2009). “Effects of selective withdrawal on hydrodynamics of a stratified reservoir.” *Water Resour Manage*, 23, 1257-1273.

Casamitjana, X., Serra, T., Colomer, J., Baserba, C., and Perez-Losada, J. (2003). “Effects of the water withdrawal in the stratification patterns of a reservoir.” *Hydrobiologia*, 504, 21-28.

Caulfield, P. (2012). “Mica dam getting two new generating units.” *Journal of Commerce*, < http://www.joconl.com/article/id48145> (April 4, 2012).

Craya, A. (1949). “Theoretical research on the flow of nonhomogenous fluids”, *La Houille Blanche*, 4, 44-55.

Datta, A.K. (2002). “Radiative energy transfer.” *Biological and Bioenvironmental Heat and Mass Transfer*, Marcel Dekker Inc., New York, NY, 147-171.

Environment Canada. (2010). “Canadian Climate Data Online.” *Environment Canada: National Climate Data and Information Archive*, <http://www.climate.weatheroffice.gc.ca/climateData/canada_e.html> (November 28, 2010).

Fischer, H.B., List, E.J., Koh, R.C.Y., Imberger, J., Brooks, N.H. (1979). "Mixing in reservoirs." *Mixing in Inland and Coastal Waters,* Academic Press Inc., San Diego, CA, 150-228.

Fricker, P.D., Nepf, H.M. (2000). "Bathymetry, stratification, and internal seiche structure." *Journal of Geophysical Research*, 105(C6), 14237-14251.

Gray, D.M. (1970). "Energy, evaporation, and evapotranspiration." *Handbook on the principles of hydrology: with special emphasis directed to Canadian conditions in the discussions, applications, and presentation of data*, Canadian National Committee for the International Hydrological Decade, Ottawa, ON, 3.1-3.66.

Gray, D.M. and Prowse, T.D. (1993). "Snow and floating ice." *Handbook of Hydrology*, McGraw-Hill Inc., New York, NY, 7.1-7.58.

Hamblin, P.F. and McAdam, S.O. (2003). "Impoundment effects on the thermal regimes of Kootenay Lake, the Arrow Lakes reservoir and upper Columbia River." *Hydrobiologia*, 504, 3-19.

Islam, M.R. and Zhu, D.Z. (2012). "Selective withdrawal in two-layer stratified flows", submitted to ASCE *Journal of Hydraulic Engineering*.

Ivey, G.N. and Blake, S. (1985). "Axisymmetric withdrawal and inflow in a density-stratified container." *Journal of Fluid Mechanics - ASCE*, 161, 115-137.

Ji, Z.G. (2008). "Chapter 9 – lakes and reservoirs." *Hydrodynamics and water quality: modeling rivers, lakes, and estuaries*, Wiley, Somerset, NJ, 9.2.5.

Kaczmarek, Z., Strzepek, K.M., Somlyody, L., and Priazhinskaya, V. (1996). "Impacts of climate change on water quality." *Water Resources Management in the Face of Climatic/Hydrologic Uncertainties,* Kluwer Academic Publishers, The Netherlands, 70-105.

Langford, M.T., Robertson, C.B., and Zhu, D.Z. (2011). "High Keenleyside Dam fish entrainment hydraulics: computational fluid dynamic modeling and field study." *Interim report prepared for BC Hydro*, Department of Civil and Environmental Engineering, University of Alberta, Edmonton, AB.

Langford, M.T., Robertson, C.B., and Zhu, D.Z. (2012). "Mica Dam fish entrainment hydraulics: computational fluid dynamic modeling and field

study." *Interim report prepared for BC Hydro*, Department of Civil and Environmental Engineering, University of Alberta, Edmonton, AB.

Lawrence, G.A. and Imberger, J. (1979). "Selective withdrawal through a point sink in a continuously stratified fluid with a pycnocline." *Report for Environmental Dynamics (Report No. ED-79-002)*, Department of Civil Engineering, University of Western Australia, Nedlands, WA, 1-87.

LDS Dactron. (2003). "Understanding FFT windows: application note." *LDS Dactron*, < www.ee.iitm.ac.in/~nitin/_media/ee462/fftwindows.pdf> (April 3, 2011).

Linsley, R.K., Kohler, M.A., and Paulhus, J.L.H. (1982). "Weather and hydrology: solar and earth radiation." *Hydrology for engineers*, McGraw-Hill Inc., New York, NY, 7-46.

Lyons, R.G. (2010). "Digital data formats and their effects." Understanding digital signal processing, Pearson Education Inc., Ann Arbor, MI, Chapter 12.

Maiolie, M.A. and Elam, S. (1994). "Kokanee depth distribution in Dworshak reservoir and implications toward minimizing entrainment." Dworshak Dam Impacts Assessment and Fisheries Investigation: Annual Progress Report, Idaho Department of Fish and Game, Boise, ID, 1-43.

McAdam, S. (2000). "Summary of historic and contemporary water temperatures for the Columbia River and the potential effects of impoundment." *BC Ministry of Fisheries*, Victoria, BC, 1-25.

Moreno-Ostos, E., Marce, R., Ordonez, J., Dolz, J., and Armengol, J. (2008). "Hydraulic management drives heat budgets and temperature trends in a Mediterranean reservoir." *International Review of Hydrobiology*, 93(2), 131-147.

Mortimer, C.H. (1951). "Water movements in lakes during summer stratification; evidence from the distribution of temperature in Windermere." *Philosophical Transactions of the Royal Society of London, Series B, Biological Sciences*, 236(635), 355-398.

Owens, E.M., Effler, S.W., and Trama, F. (1986). "Variability in thermal stratification in a reservoir." *Water resources bulletin, American water resources association*, 22(2), 219-227.

Perez-Losada, J., Roget, E., and Casamitjana, X. (2003). "Evidence of high vertical wave-number behavior in a continuously stratified reservoir: Boadella, Spain." *Journal of Hydraulic Engineering - ASCE*, 129(9), 734-737.

Physics Forum. (2010). "Welch's method." *Physics Forum*, <http://www.physicsforums.com/showthread.php?t=409052> (November 4, 2011).

Pieters, R., Robb, D., Akkerman, A., and Lawrence, G. (2010). "Appendix 1: Hydrology of Kinbasket and Revelstoke Reservoirs, 2008." *Columbia River Project Water Use Plan: Kinbasket and Revelstoke Reservoirs Ecological Productivity Monitoring – Progress Report Year 1*, BC Hydro, 42.

Pieters, R. and Lawrence, G. (2011). "Plunging inflows and the summer photic zone, Kinbasket and Revelstoke reservoirs." *15th Workshop on Physical Processes in Natural Waters*, Burlington, ON, 136-143.

Prigo, R.B., Manley, T.O., and Connell, B.S.H. (1995). "Linear, one-dimensional models of the surface and internal standing waves for a long and narrow lake." *American Journal of Physics*, 64(3), 288-300.

Rasmusson, E.M., Dickinson, R.E., Kutzbach, J.E., Cleaveland, M.K. (1993). "Climatology." *Handbook of Hydrology*, McGraw-Hill Inc., New York, NY, 2.1-2.44.

RL&L Environmental Services Ltd. (2000). "Resident fish entrainment information review and analysis." *Report prepared for the Canadian Columbia River Inter-tribal Fisheries Commission*, Edmonton, AB, 1-52.

Schladow, S.G., Palmarsson, S.O., Steissberg, T.E., Hook, S.J., and Prata, F.E. (2004). "An extraordinary upwelling event in a deep thermally stratified lake." *Geophysical research letters*, 31, 1-4.

Shammaa, Y. and Zhu, D.Z. (2010). "Experimental study on selective withdrawal in a two-layer reservoir using a temperature-control curtain." *Journal of Hydraulic Engineering - ASCE*, 136(4), 234-246.

Shuttleworth, W. J. (1993). "Evaporation." *Handbook of Hydrology*, McGraw-Hill Inc., New York, NY, 4.1-4.53.

Stevens, C.L. and Lawrence, G.A. (1997). “Estimation of wind-forced internal seiche amplitudes in lakes and reservoirs, with data from British Columbia, Canada.” *Aquatic Science*, 59, 115-134.

Turner, J. S. (1973). “Linear internal waves: waves in a continuously stratified fluid.” *Buoyancy Effects in Fluids*, Cambridge University Press, Cambridge, 22-23.

U.S. National Academy of Sciences (UNAS). (1975). “The globally averaged atmospheric energy balance.” *Understanding Climatic Change*, Washington, DC, 14.

Vidal, J., Casamitjana, X., Colomer, J., Serra, T. (2005). “The internal wave field in Sau reservoir: Observation and modeling of a third vertical mode.” *Limnology and Oceanography - ASLO*, 50(4), 1326-1333.

Vidal, J., Rueda, F.J., Casamitjana, X. (2007). “The seasonal evolution of high vertical-mode internal waves in a deep reservoir.” *Limnology and Oceanography - ASLO*, 52(6), 2656-2667.

Weimer, M.R. (2012). “Waveform analysis using the Fourier transform.” *DATAQ Instruments*, < http://www.dataq.com/applicat/articles/an11.htm> (September 27, 2011).

Welch, P.D. (1967). “The use of fast Fourier transform for the estimation of power spectra: a method based on time averaging over short, modified periodograms.” *IEEE Transactions on Audio and Electroacoustics*, 15(2), 70-73.

Wiegand, R.C. and Chamberlain, V. (1987). “Internal waves of the second vertical mode in a stratified lake.” *Limnology and Oceanography - ASLO*, 32(1), 29-42.

Tables

Table 3.1 HLK thermistor naming convention and depths.

Thermistor Number	Depth (m)
1	1.2
2	2.3
3	3.4
4	4.4
5	5.5
6	6.6
7	7.7
8	8.8
9	9.9
10	11.0
11	12.1
12	13.2
13	14.3
14	15.3
15	16.4
16	17.5
17	18.6
18	19.6
19	21.7
20	23.8

Table 3.2 Calculated thermocline oscillation magnitudes and periods for a closed boundary in the Arrow Lakes reservoir.

Upstream Boundary Location		Burton (closed boundary)
Description		Located at two major 90° bends where the channel narrows significantly
Distance Upstream		100 km
Average Thermocline Oscillation Magnitude		7.0 m
Thermocline Oscillation Period	Fundamental Mode	7.0 days
	Second Mode	3.5 days

Table 4.1 MCA thermistor naming convention and depths.

Thermistor Number	Depth (m)
1	0.2
2	2.2
3	4.2
4	6.2
5	8.2
6	10.2
7	12.2
8	14.2
9	16.2
10	18.2
11	20.2
12	24.7
13	26.7
14	28.7
15	30.7
16	32.7
17	34.7
18	36.7
19	38.7
20	40.7
21	42.7
22	44.7
23	46.7
24	48.7
25	50.7
26	52.7
27	54.7
28	56.7
29	58.7
30	60.7
31	62.7

Table 4.2 Calculated oscillation periods with multiple vertical modes in the Kinbasket reservoir.

L1	150000 m	Horizontal Nodes		j	1	1	1
L2	14600 m	Vertical Nodes		i	1	2	3
		Average	Average		Period		
Length	Timeframe	N^2	Depth	μ	(days)		
L1	May 13 - June 15	4.6E-05	33.62	0.00022	7.6	15.3	22.9
	Jun 1 - Jun 30	9.4E-05	39.94	0.00027	4.5	9.0	13.5
	Jun 16 - Jul 15	1.1E-04	45.81	0.00031	3.7	7.4	11.1
	Jul 1 - Jul 31	9.9E-05	51.52	0.00034	3.4	6.8	10.2
	Jul 16 - Aug 15	1.4E-04	54.74	0.00036	2.7	5.4	8.2
	Aug 1 - Aug 31	1.7E-04	56.16	0.00037	2.4	4.7	7.1
	Aug 16 - Sep 15	1.5E-04	56.50	0.00038	2.5	4.9	7.4
	Sep 1 - Sep 30	1.3E-04	55.50	0.00037	2.7	5.4	8.1
	Sep 16 - Oct 15	9.1E-05	53.50	0.00036	3.2	6.4	9.5
	Oct 1 - Oct 31	6.9E-05	49.50	0.00033	3.7	7.4	11.0
					(hours)		
L2	May 13 - June 15	4.6E-05	44.12	0.00302	13.6	27.2	40.8
	Jun 1 - Jun 30	9.4E-05	50.44	0.00345	8.3	16.6	24.9
	Jun 16 - Jul 15	1.1E-04	56.70	0.00388	6.9	13.8	20.7
	Jul 1 - Jul 31	9.9E-05	62.02	0.00425	6.6	13.2	19.8
	Jul 16 - Aug 15	1.4E-04	65.24	0.00447	5.3	10.6	15.9
	Aug 1 - Aug 31	1.7E-04	66.66	0.00457	4.7	9.3	14.0
	Aug 16 - Sep 15	1.5E-04	67.00	0.00459	4.8	9.7	14.5
	Sep 1 - Sep 30	1.0E-04	66.00	0.00452	5.9	11.8	17.6
	Sep 16 - Oct 15	9.1E-05	64.00	0.00438	6.3	12.7	19.0
	Oct 1 - Oct 31	6.9E-05	60.00	0.00411	7.3	14.7	22.0

Figures

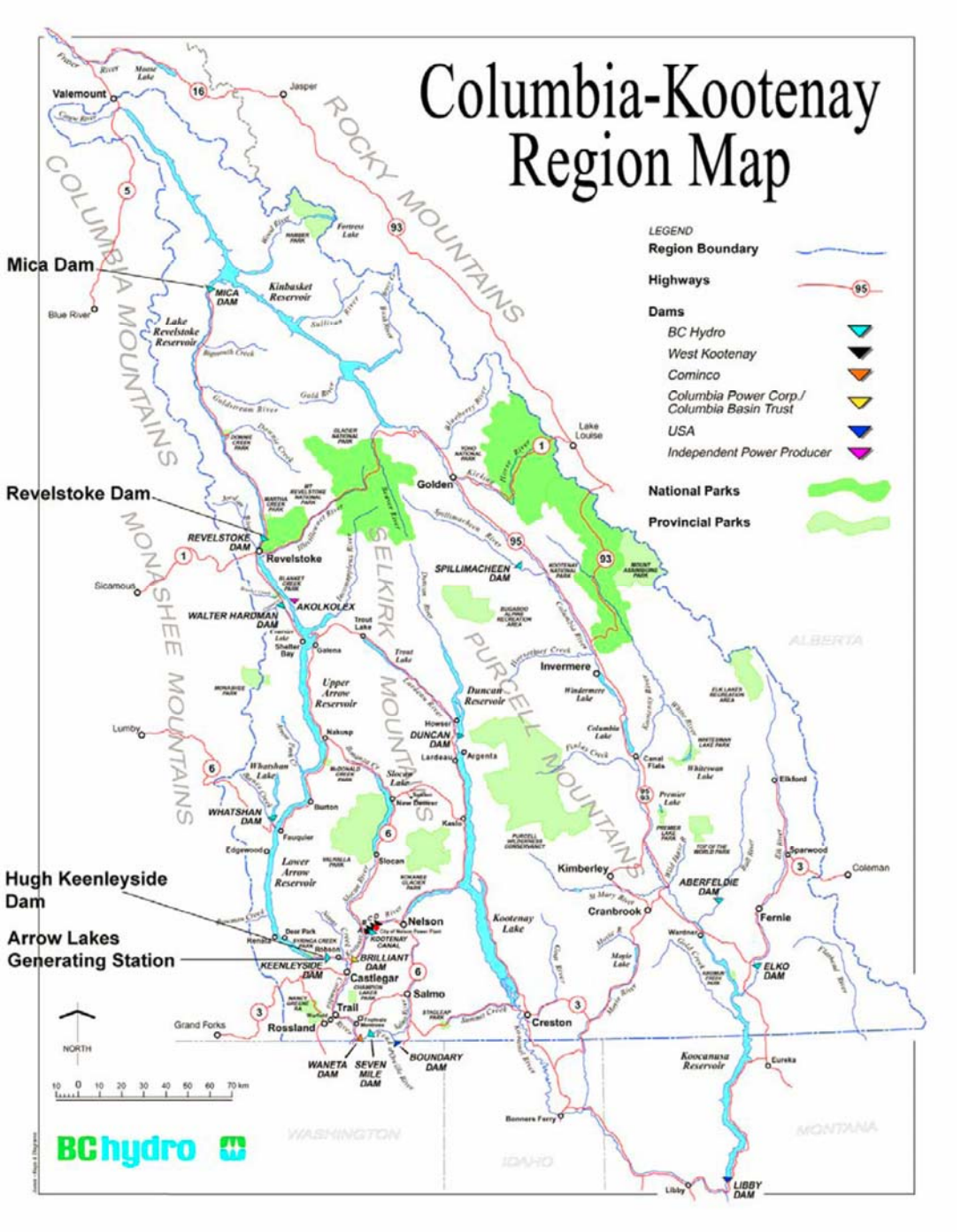

Figure 1.1 Overall site plan of the Columbia River reservoir studies (taken from BC Hydro, 2007).

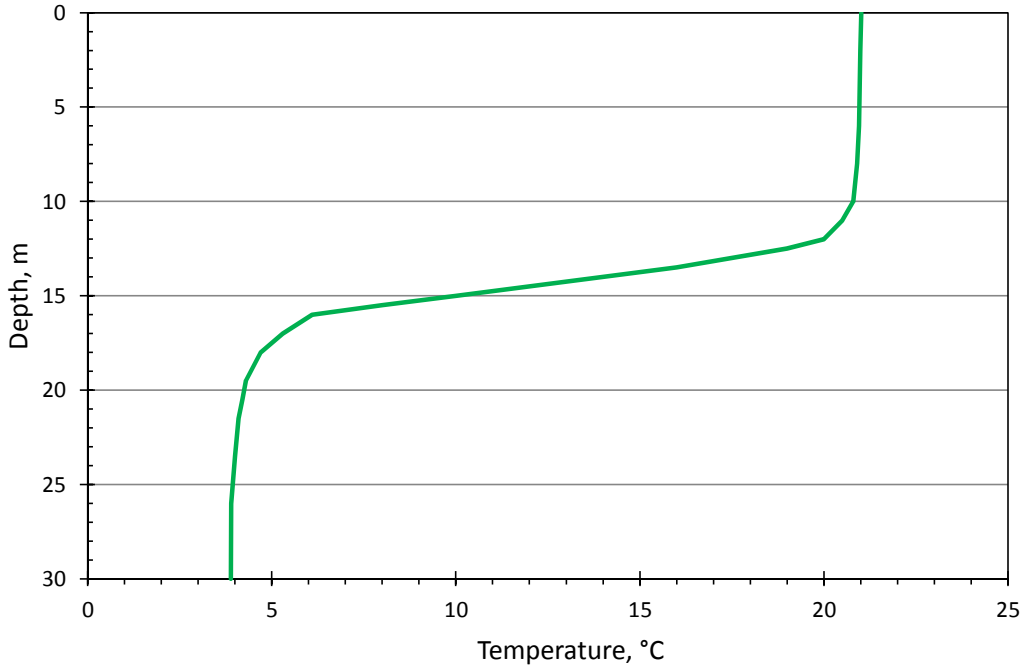

Figure 2.1 Typical shape of a two-layer temperature stratification.

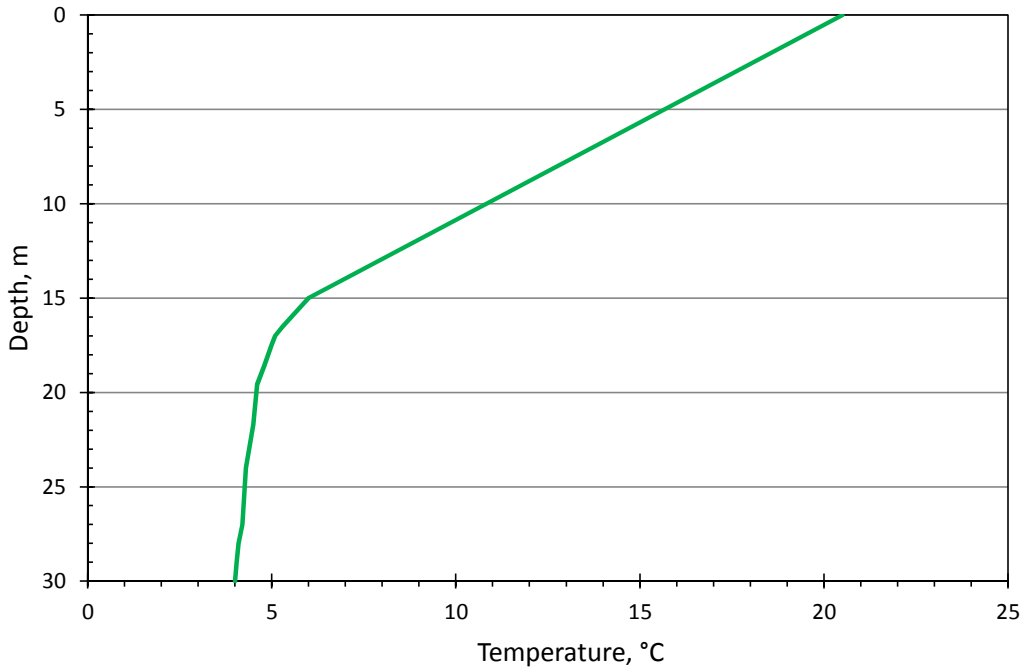

Figure 2.2 Typical shape of a continuous temperature stratification.

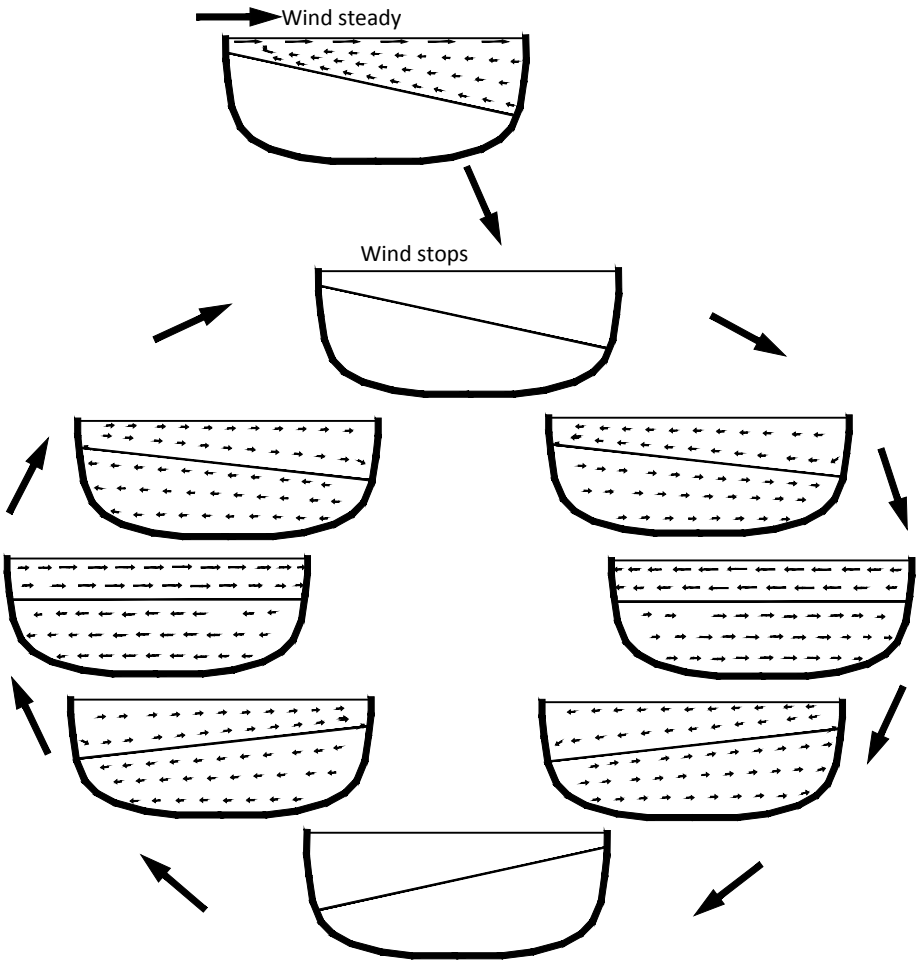

Figure 2.3 Schematic of the development of an internal seiche in an idealized two-layer reservoir (reproduced from Mortimer, 1951).

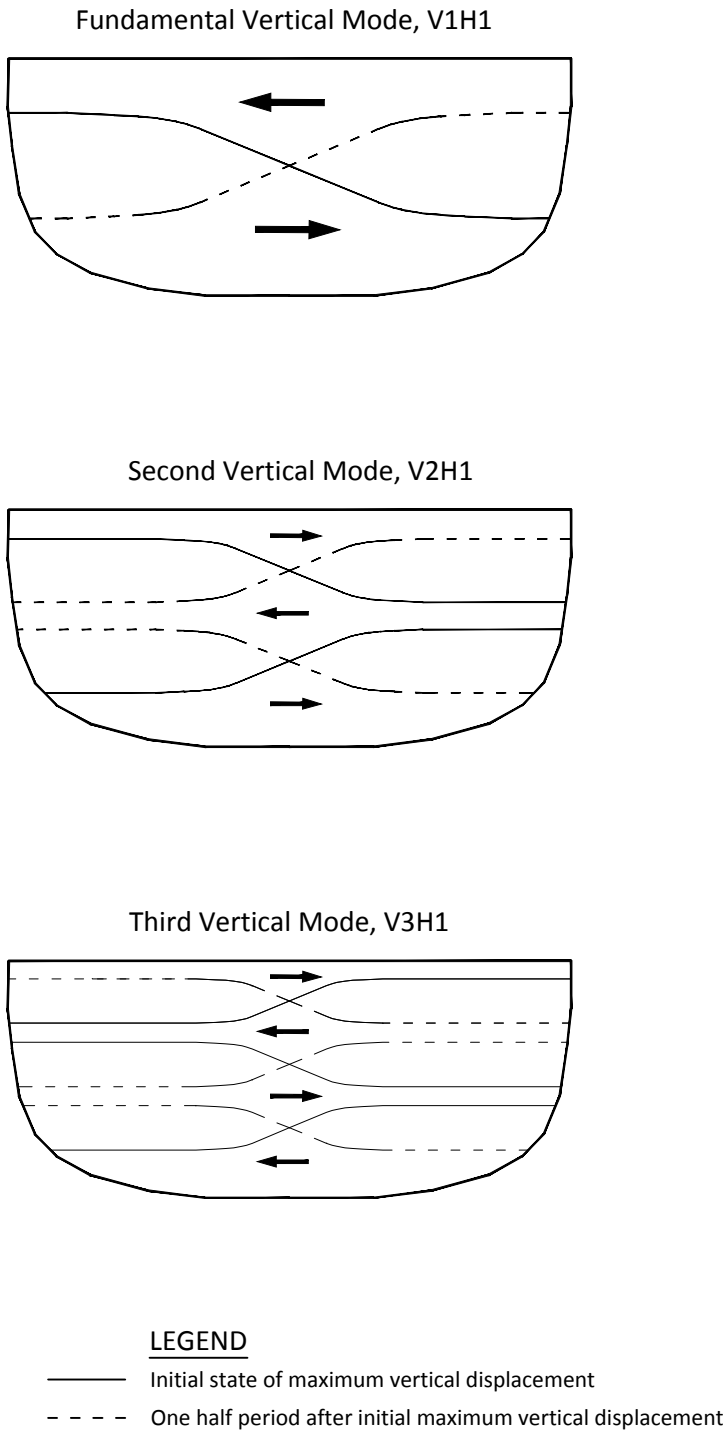

Figure 2.4 Schematic of fundamental, second, and third vertical modes of seiching (reproduced from Vidal et al., 2005).

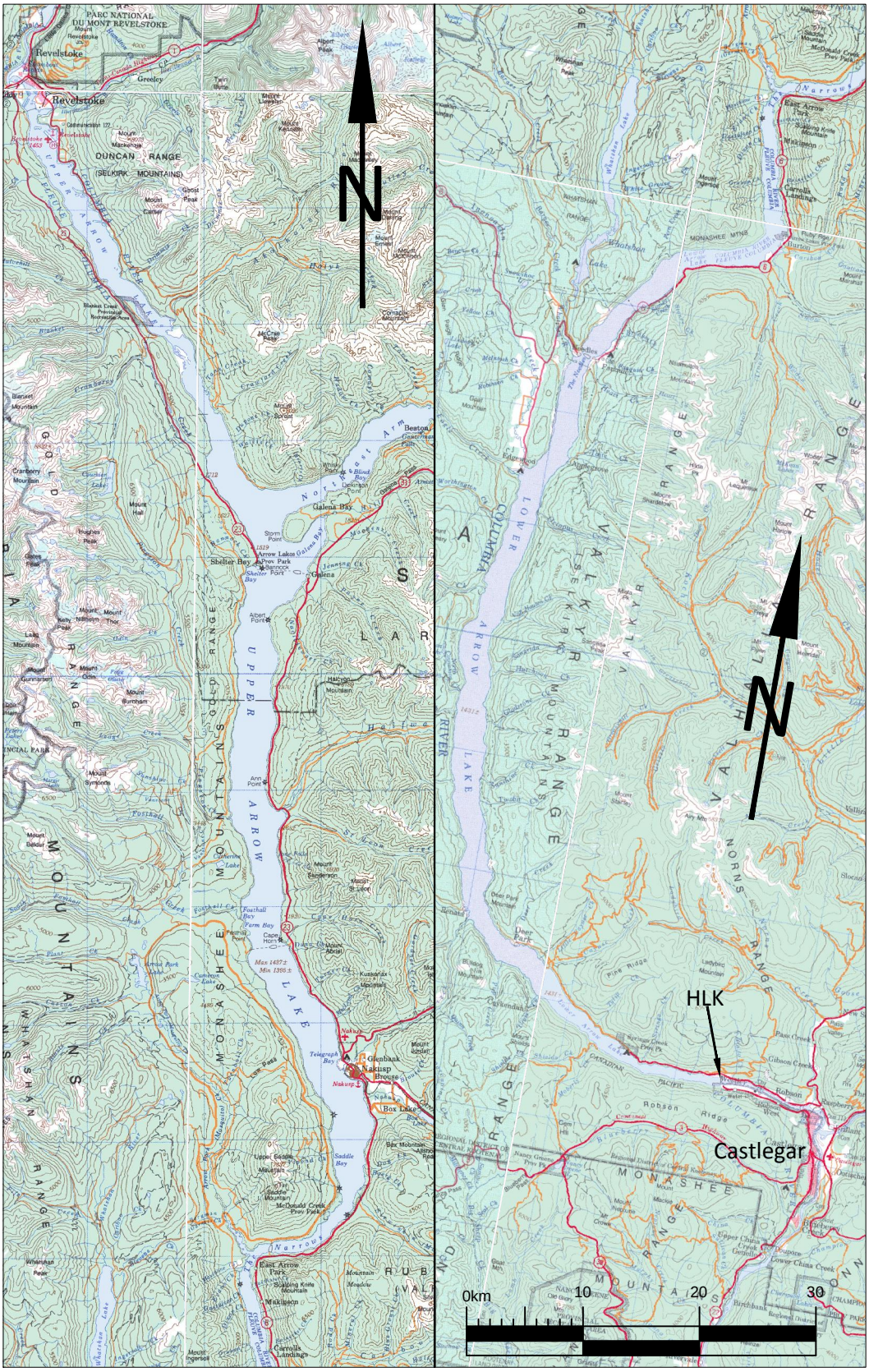

Figure 3.1 Overall site plan of Upper and Lower Arrow Lake reservoirs.

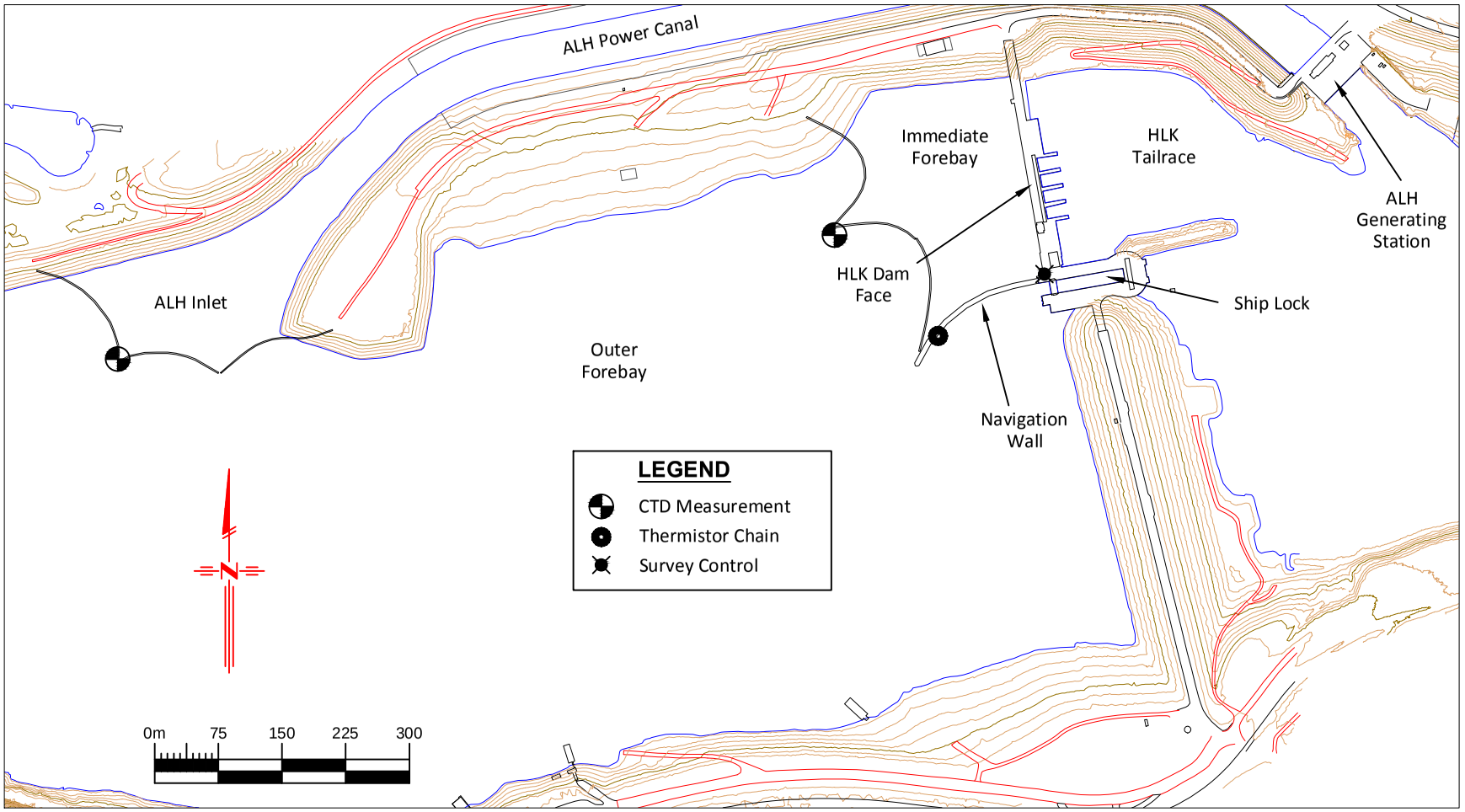

Figure 3.2 HLK forebay with CTD and thermistor chain measurement locations and survey and control point location.

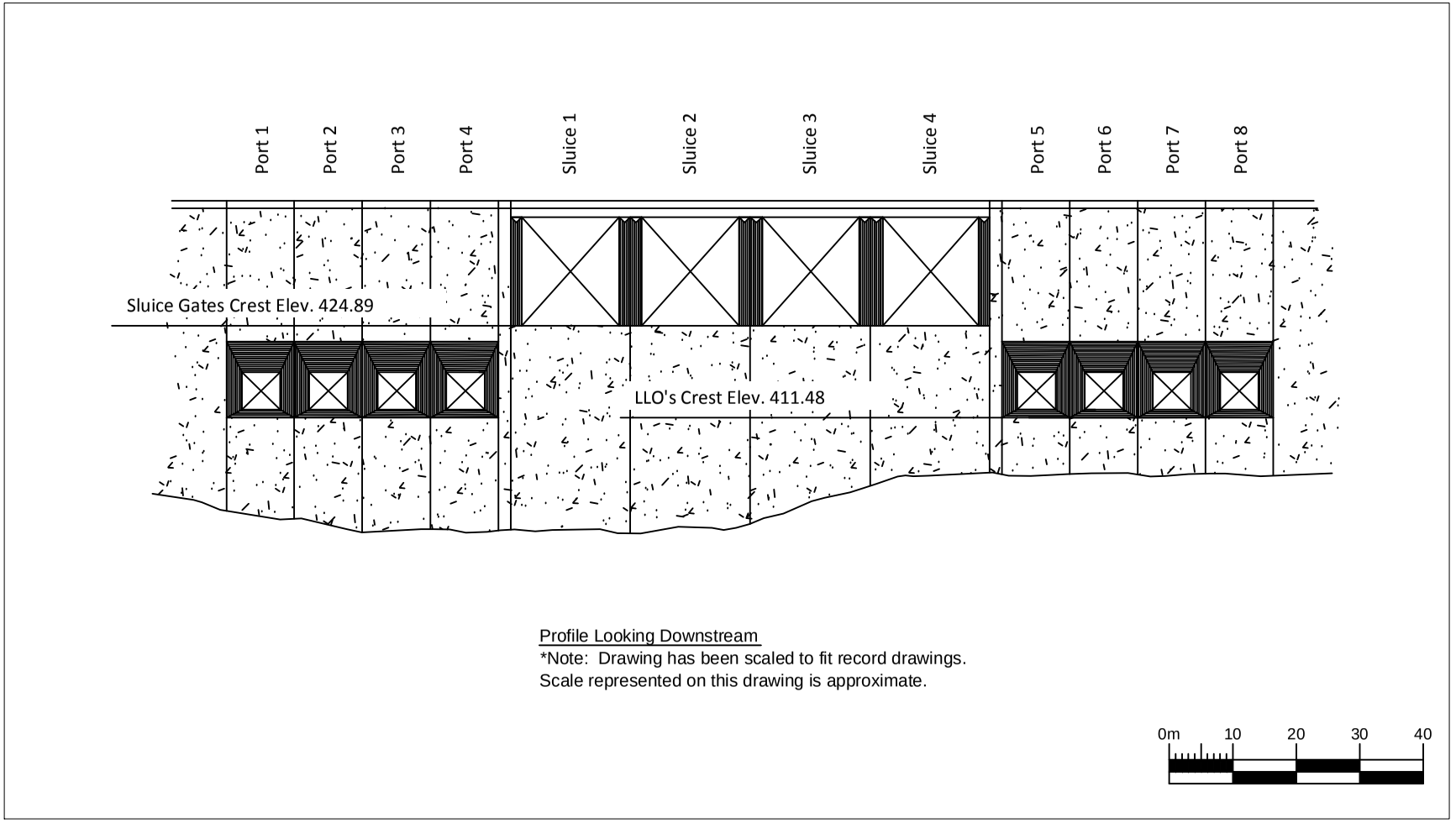

Figure 3.3 HLK LLO's and sluice gate intake configuration.

(a)

(b)

Figure 3.4 ADCP measurement set up: (a) completing a velocity transect using a guideline and (b) Rio Grande ADCP with RTK GPS set up.

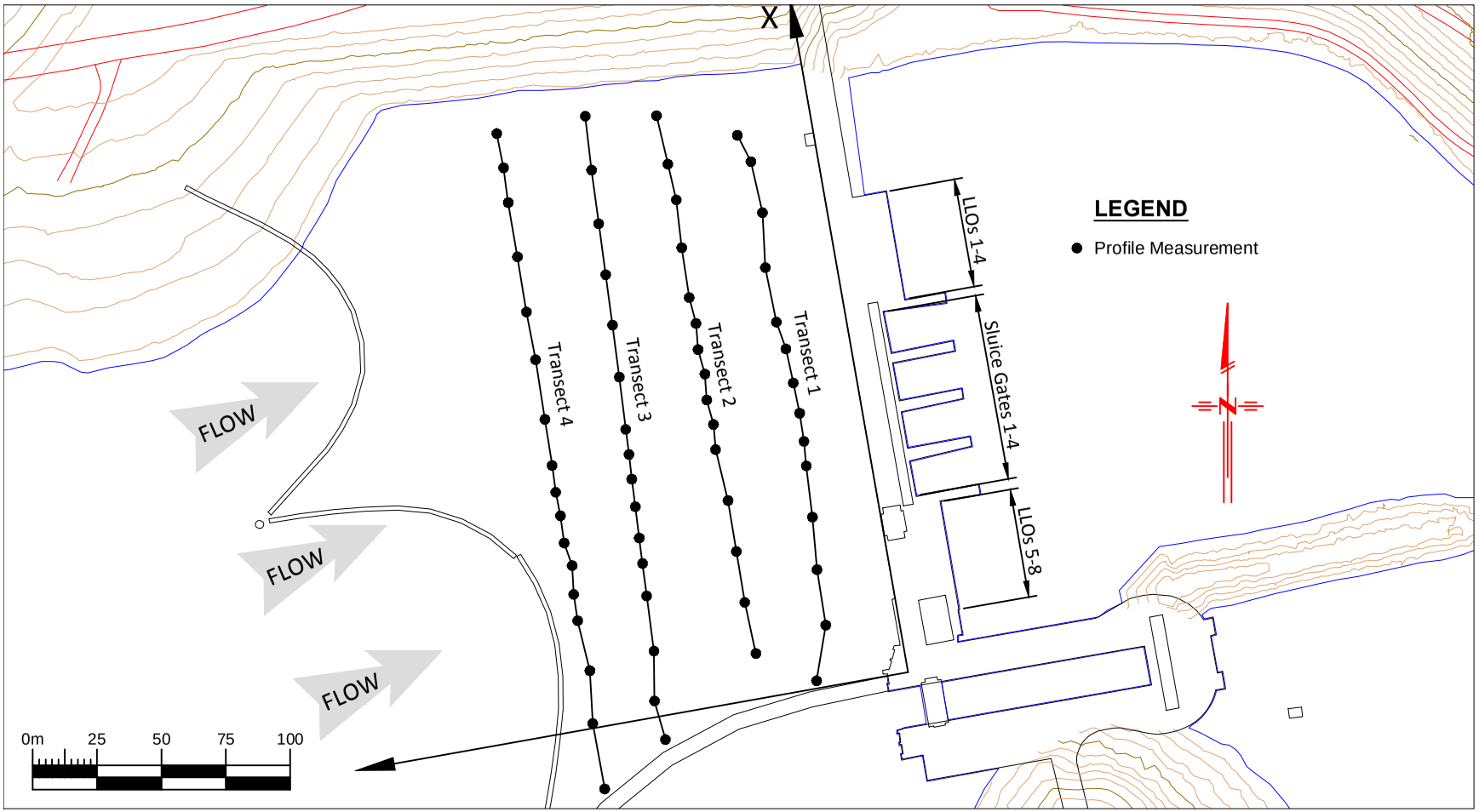

Figure 3.5 ADCP velocity profile measurement locations in the HLK forebay.

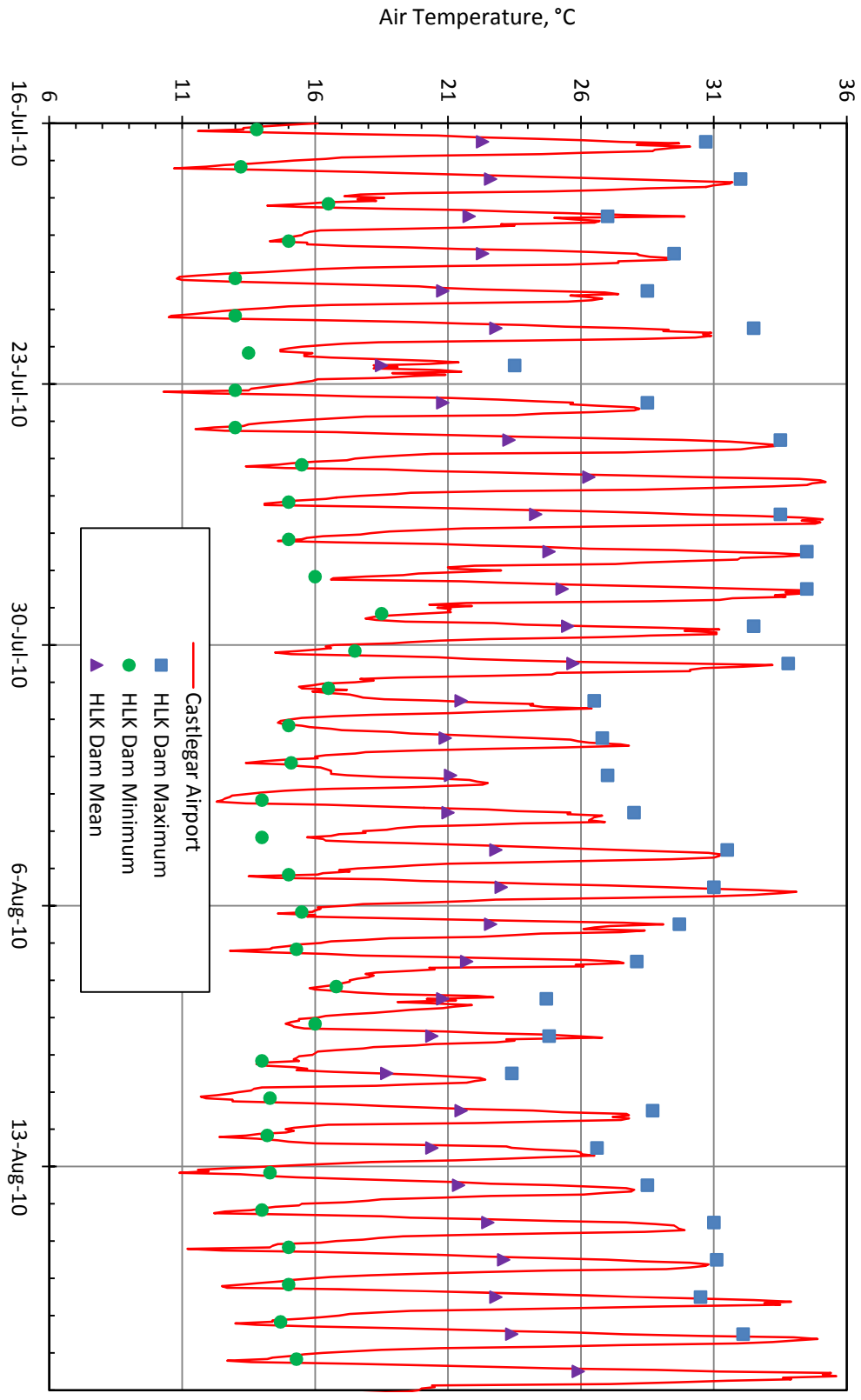

Figure 3.6 Air temperatures recorded at HLK Dam and Castlegar Airport meteorological stations.

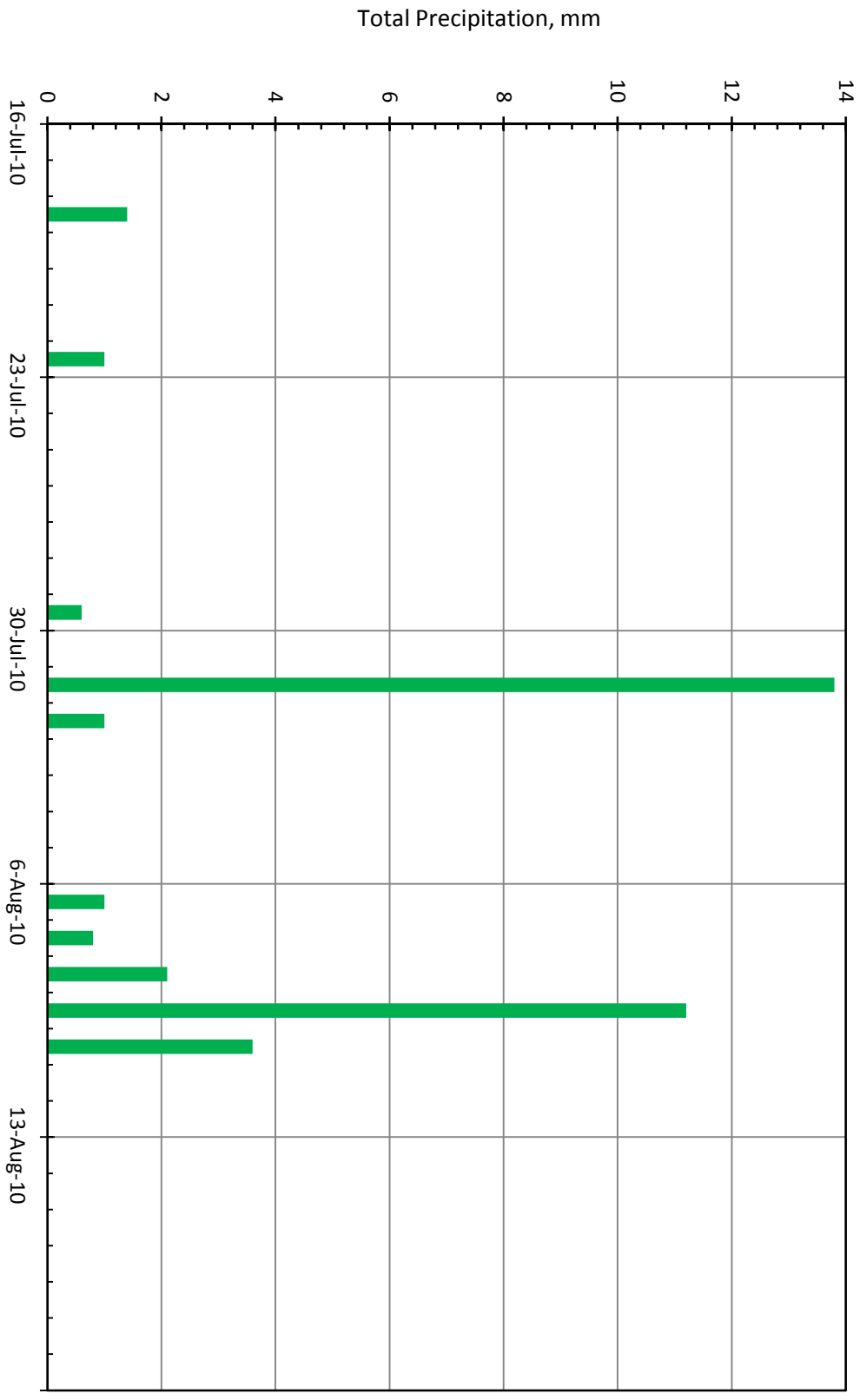

Figure 3.7 Total precipitation recorded at HLK Dam meteorological station.

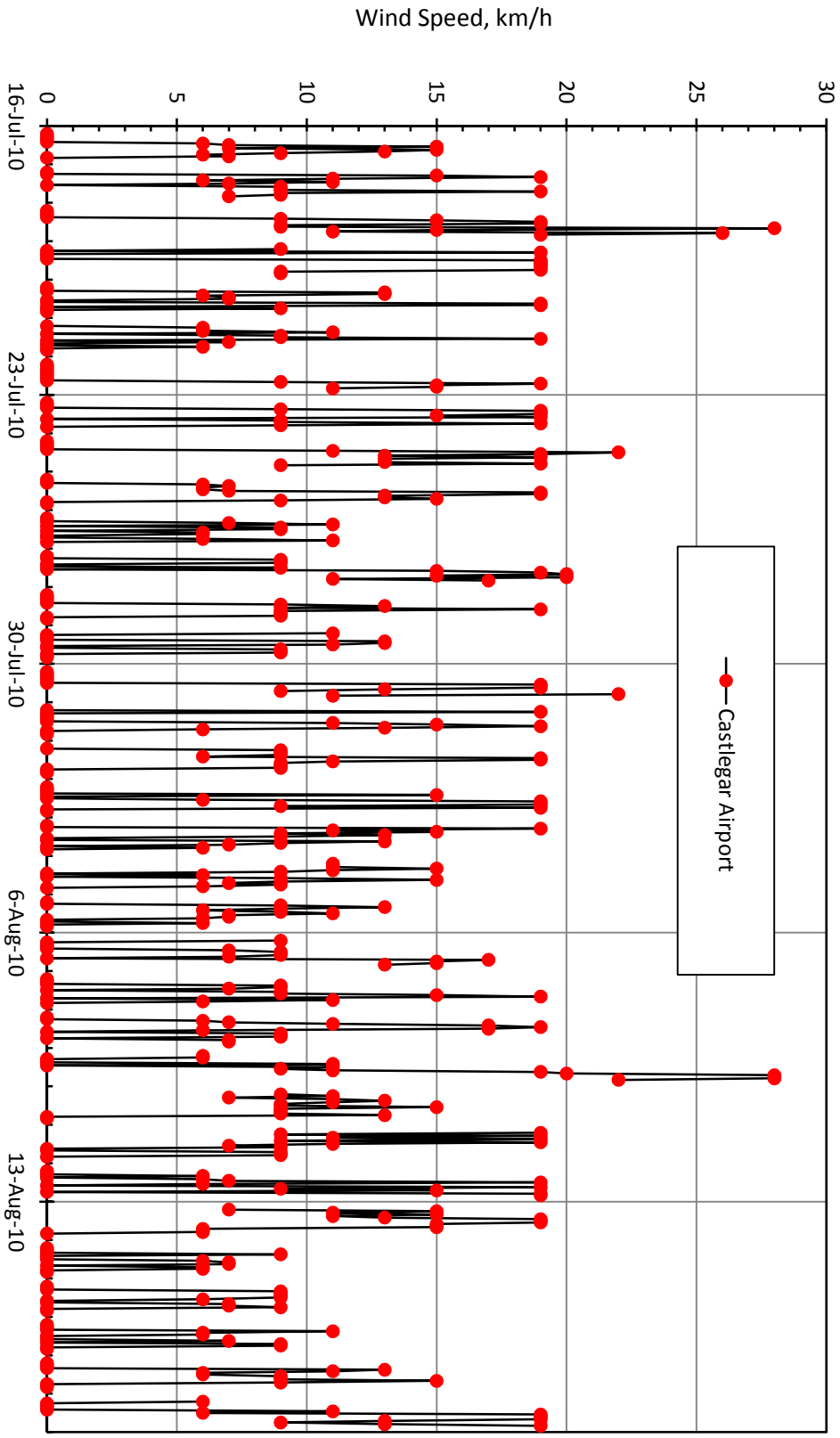

Figure 3.8 Hourly wind speed recorded at the Castlegar Airport station.

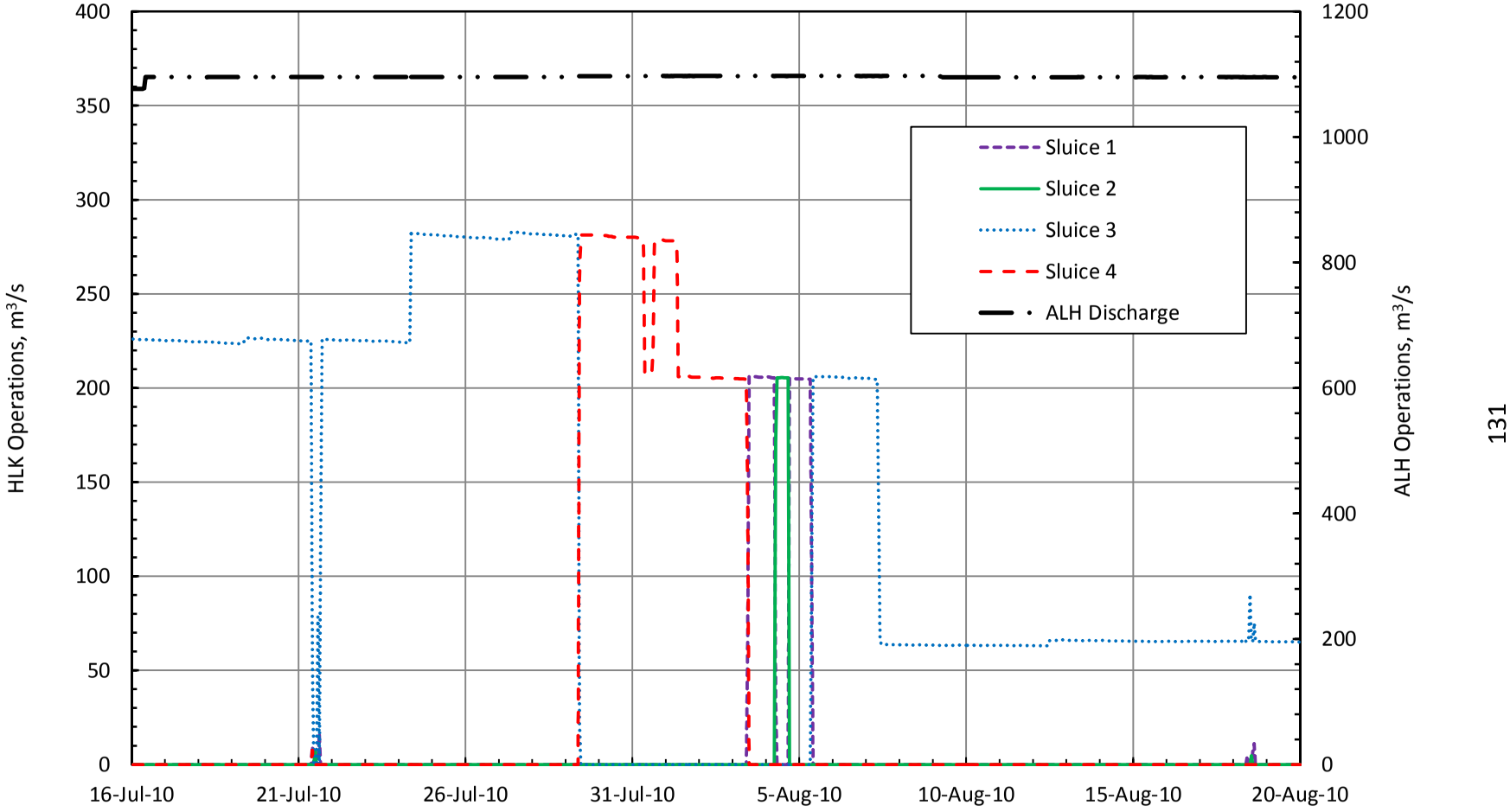

Figure 3.9 HLK sluice gates discharge and total ALH discharge.

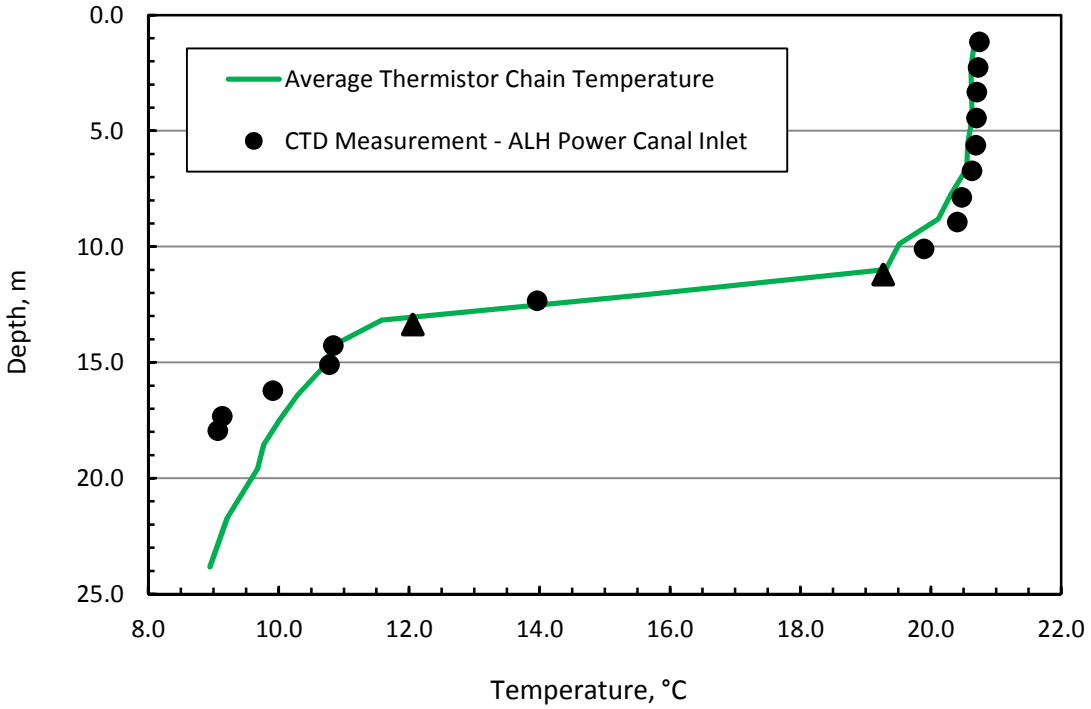

Figure 3.10a Comparison of average thermistor chain measurements and CTD measurements at the ALH power canal inlet, 09:00 August 16, 2010.

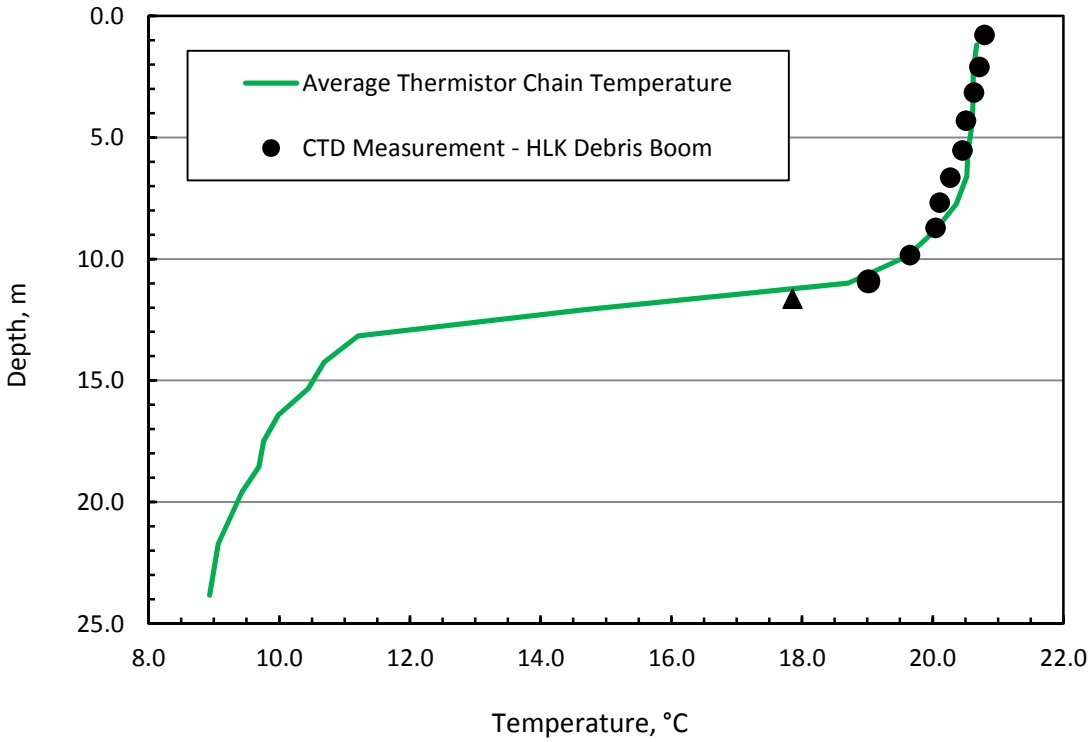

Figure 3.10b Comparison of average thermistor chain measurements and CTD measurements at the HLK debris boom, 09:20 August 16, 2010.

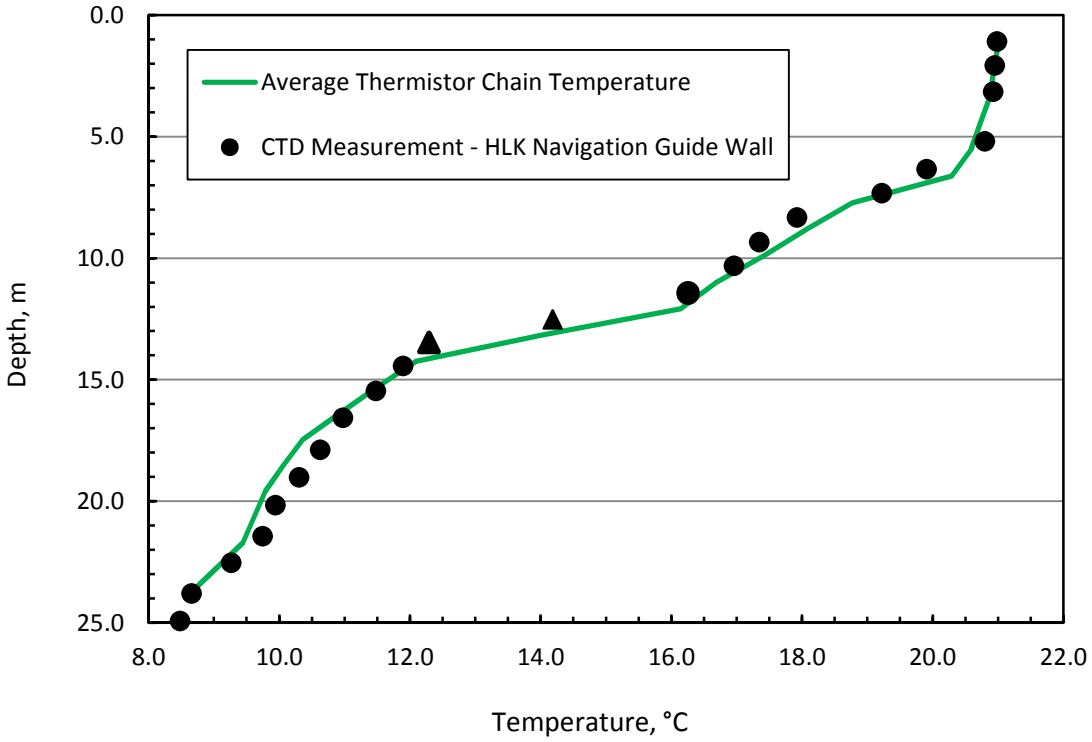

Figure 3.10c Comparison of average thermistor chain measurements and CTD measurements at the HLK navigation guide wall, 08:20 August 19, 2010.

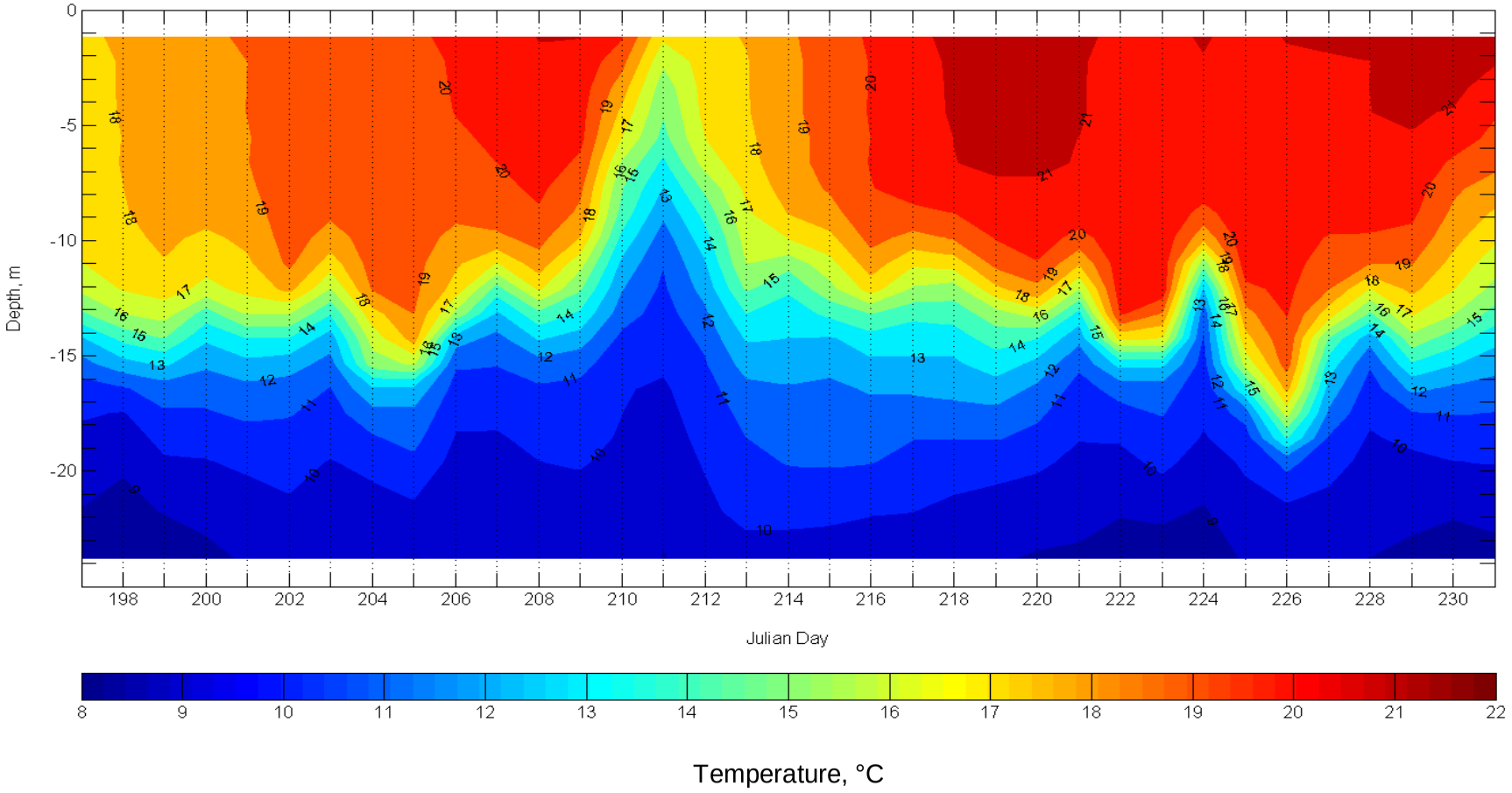

Figure 3.11 Thermistor chain mean daily water temperature contours recorded in the HLK forebay in July and August, 2010.

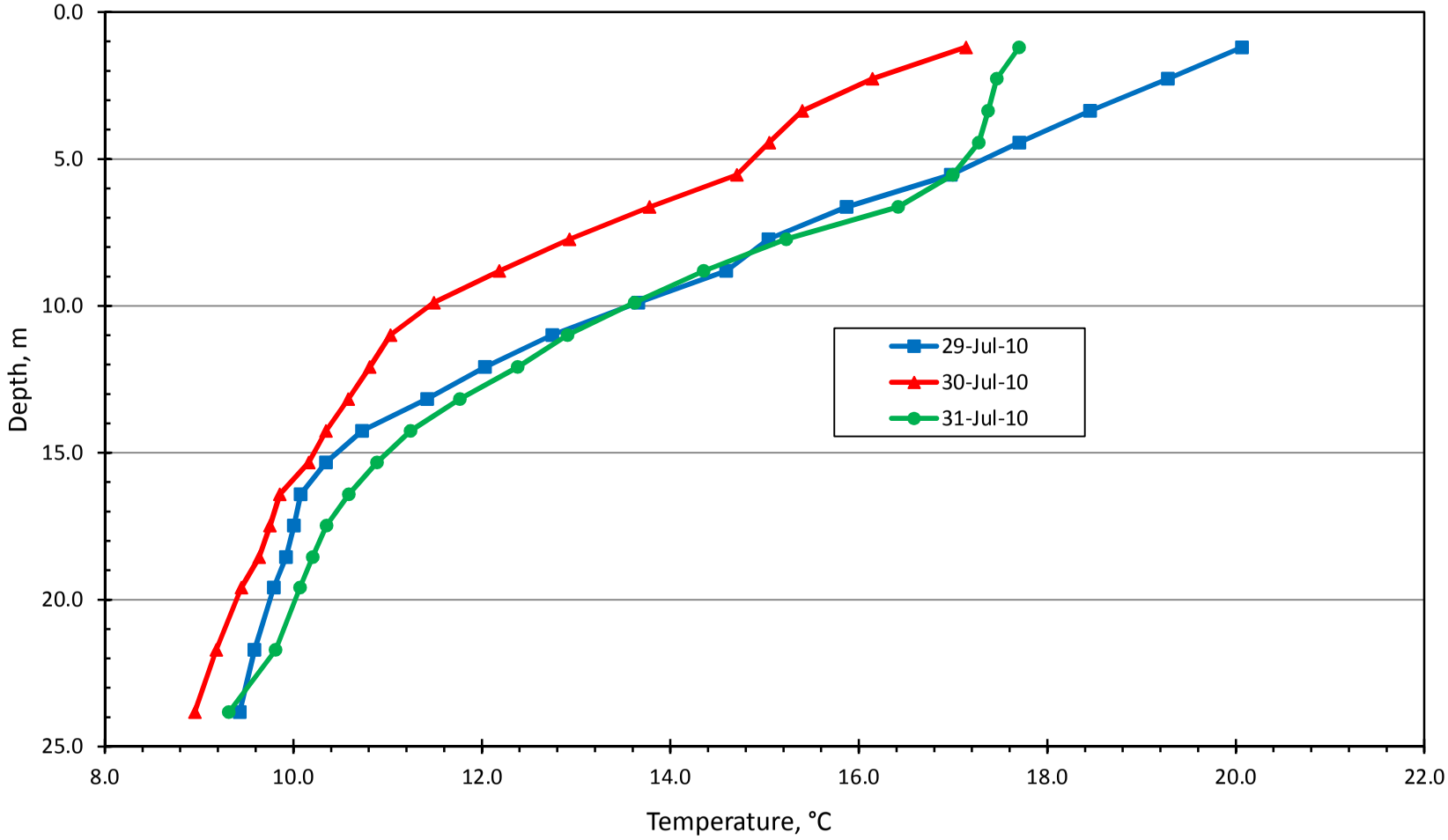

Figure 3.12 Average water temperature profiles in the HLK forebay during July 29 - July 31, 2010.

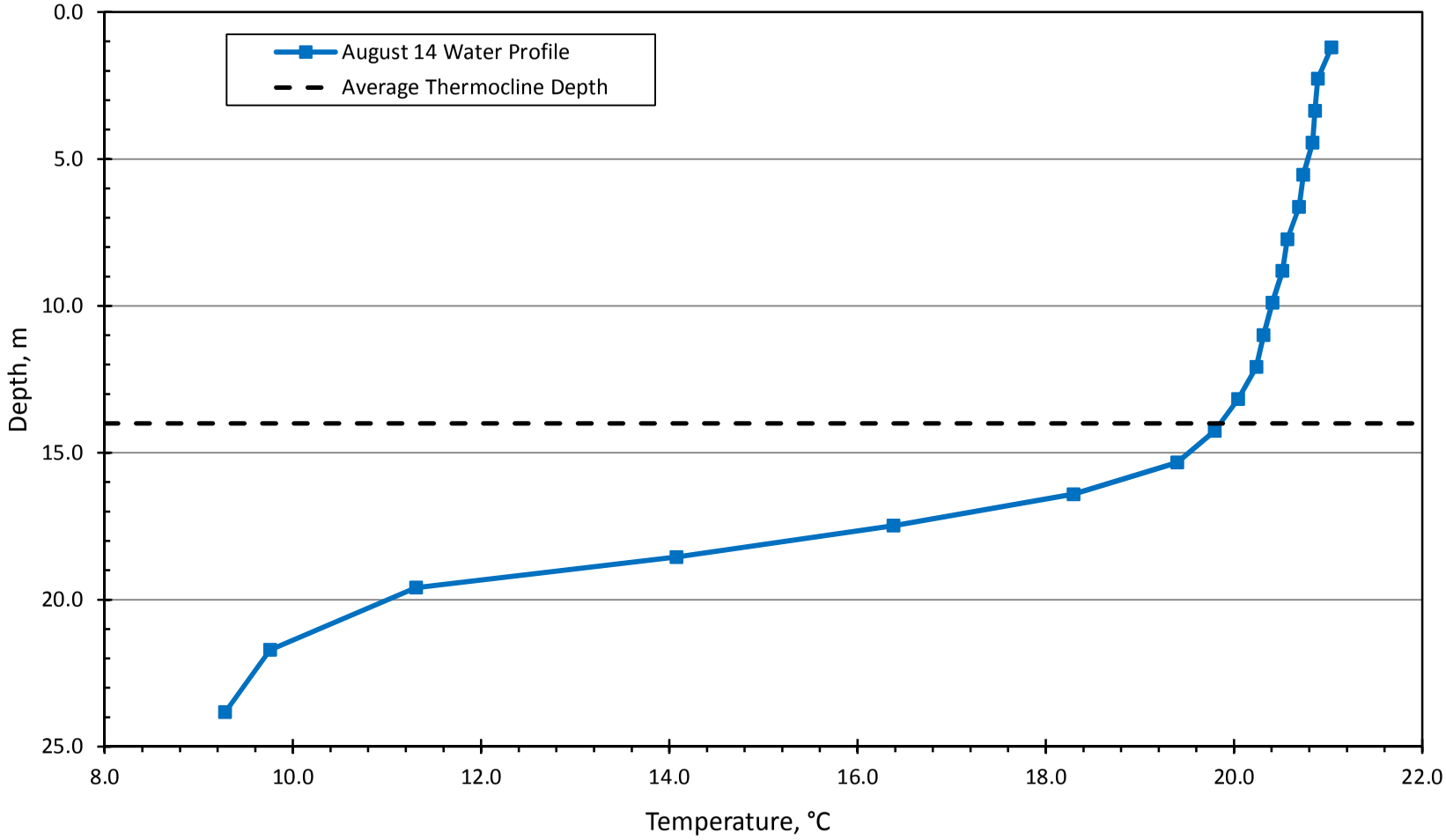

Figure 3.13 Average water temperature profile in the HLK forebay on August 14, 2010 and average thermocline depth for field studies.

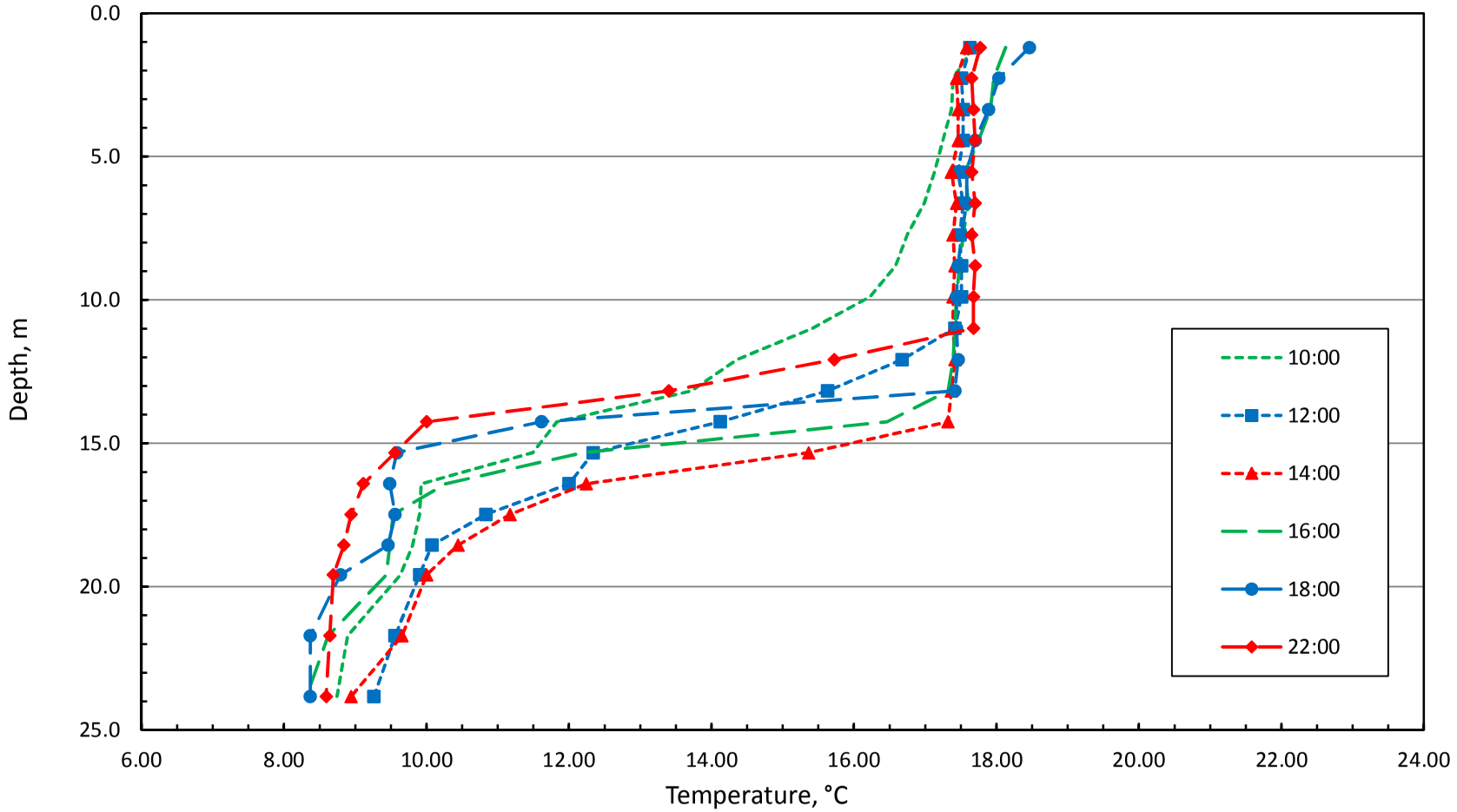

Figure 3.14 Instantaneous temperature profiles in the HLK forebay on July 16, 2010.

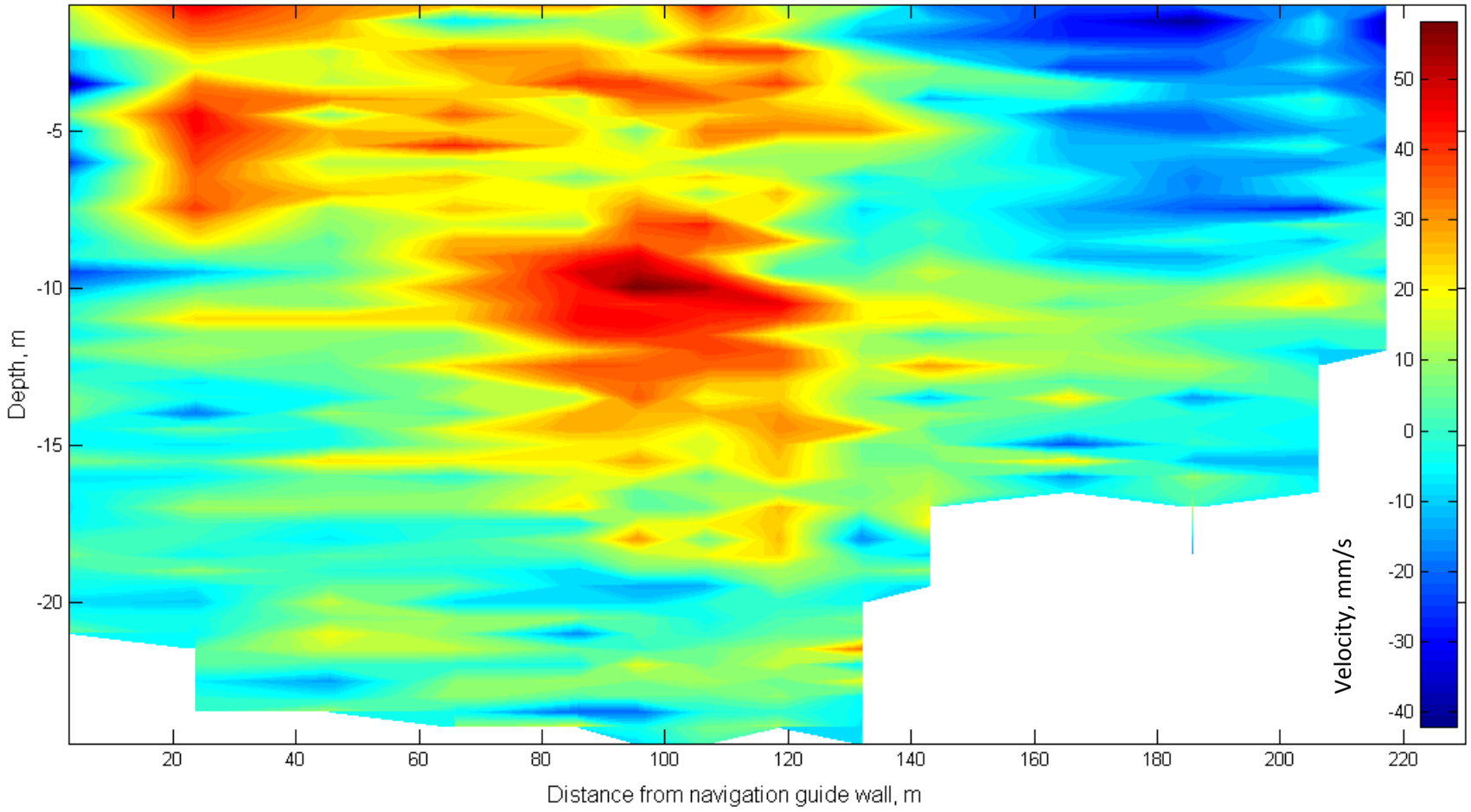

Figure 3.15 Contour plot of ADCP velocity measurement profiles taken in the HLK forebay along Transect 1.

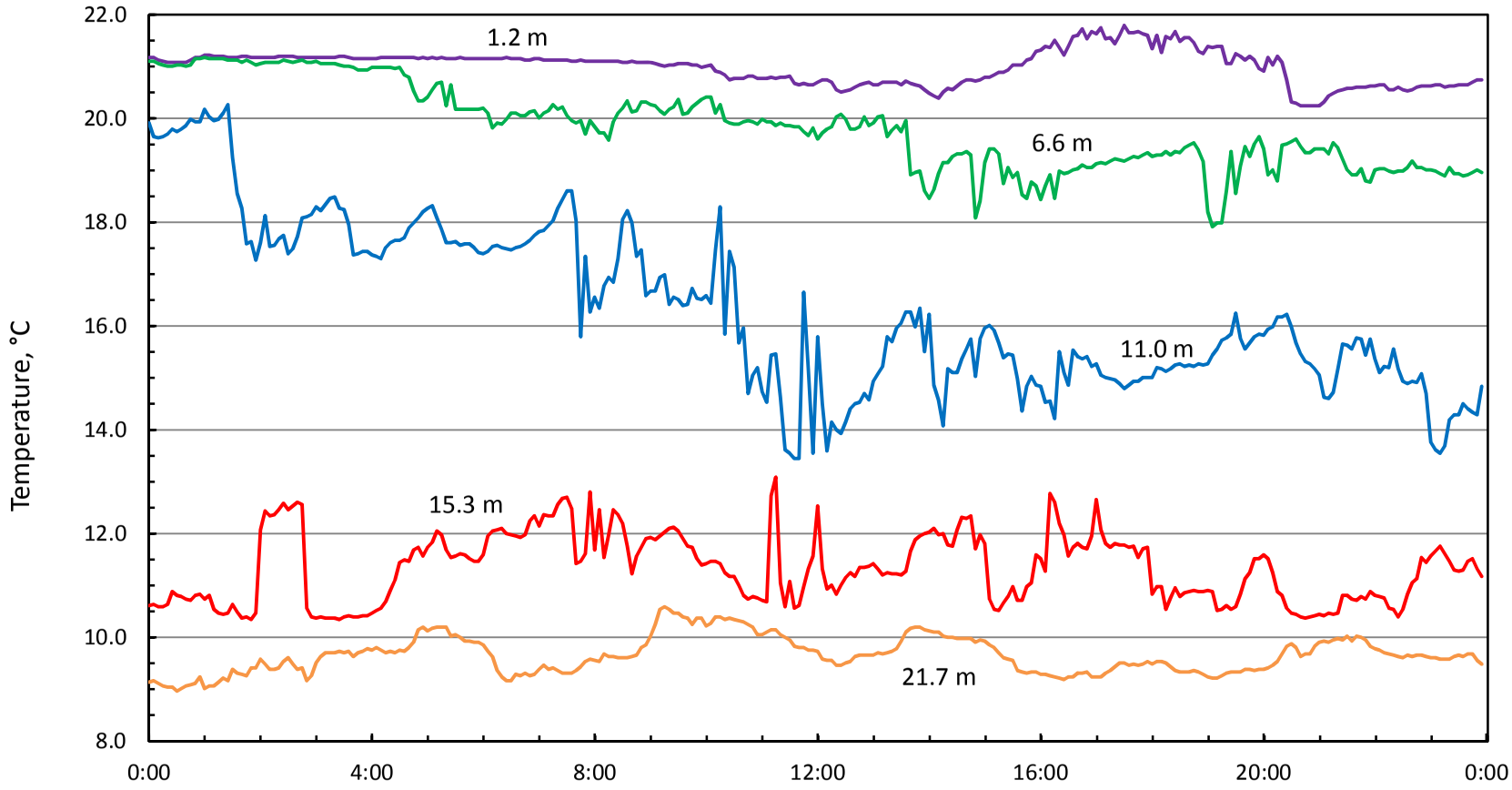

Figure 3.16 Highly variable temperature measurements in the HLK forebay at certain depths on July 28, 2010.

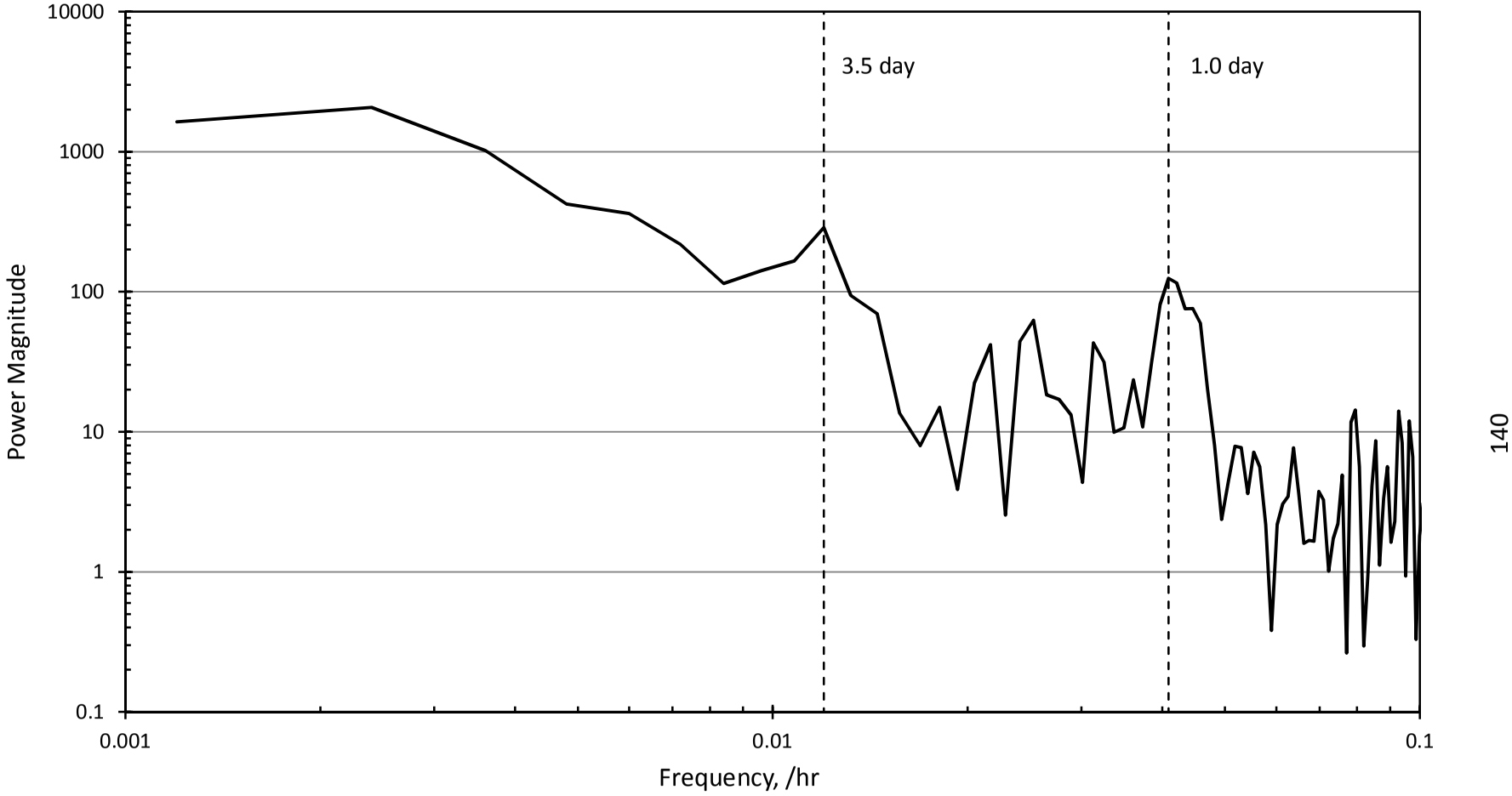

Figure 3.17 Periodogram of the HLK thermistor 10 time series from July 16 - August 19, 2010.

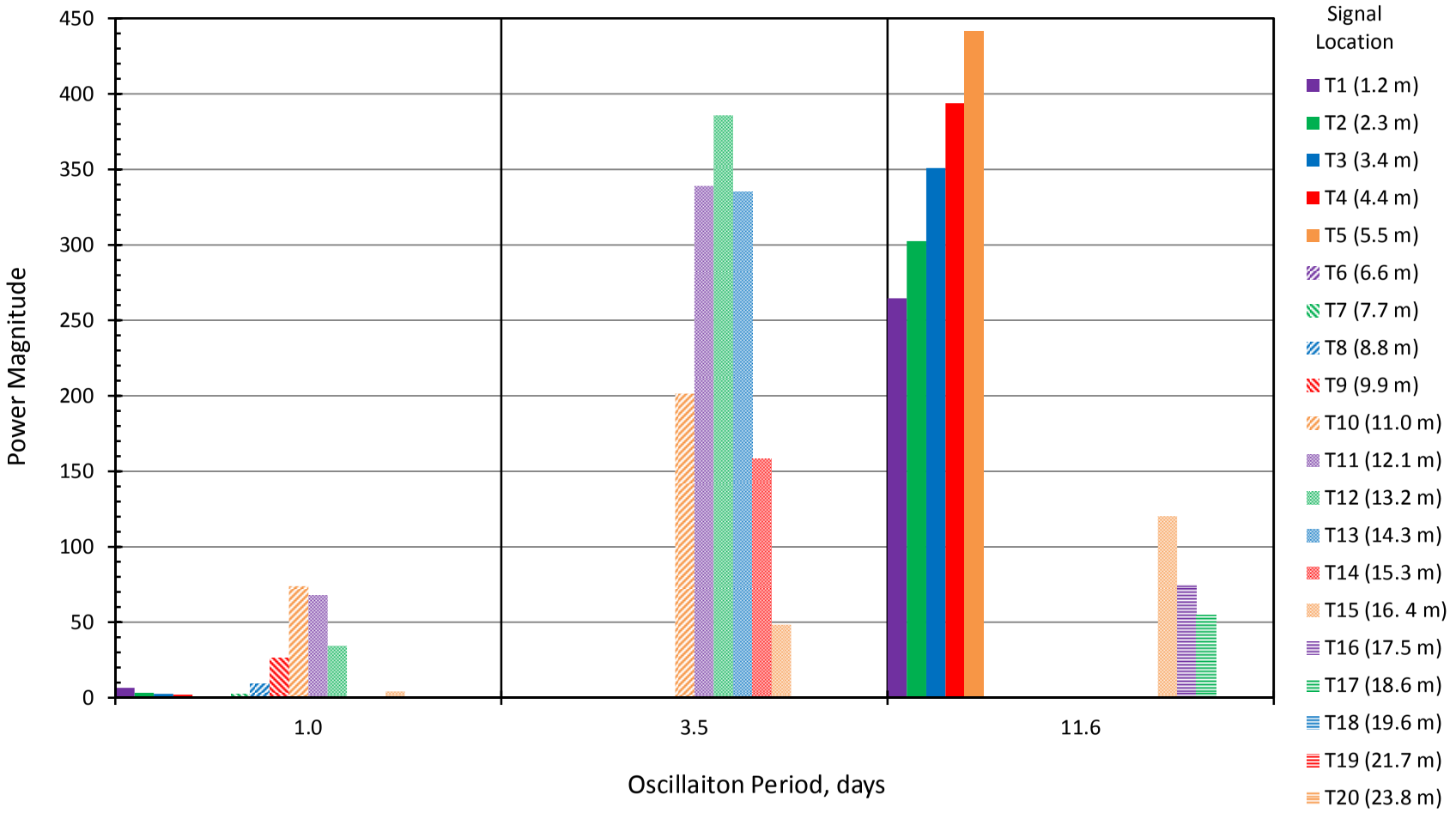

Figure 3.18 Dominant periods of oscillation, in the order of days, for different thermistor time series in the HLK forebay.

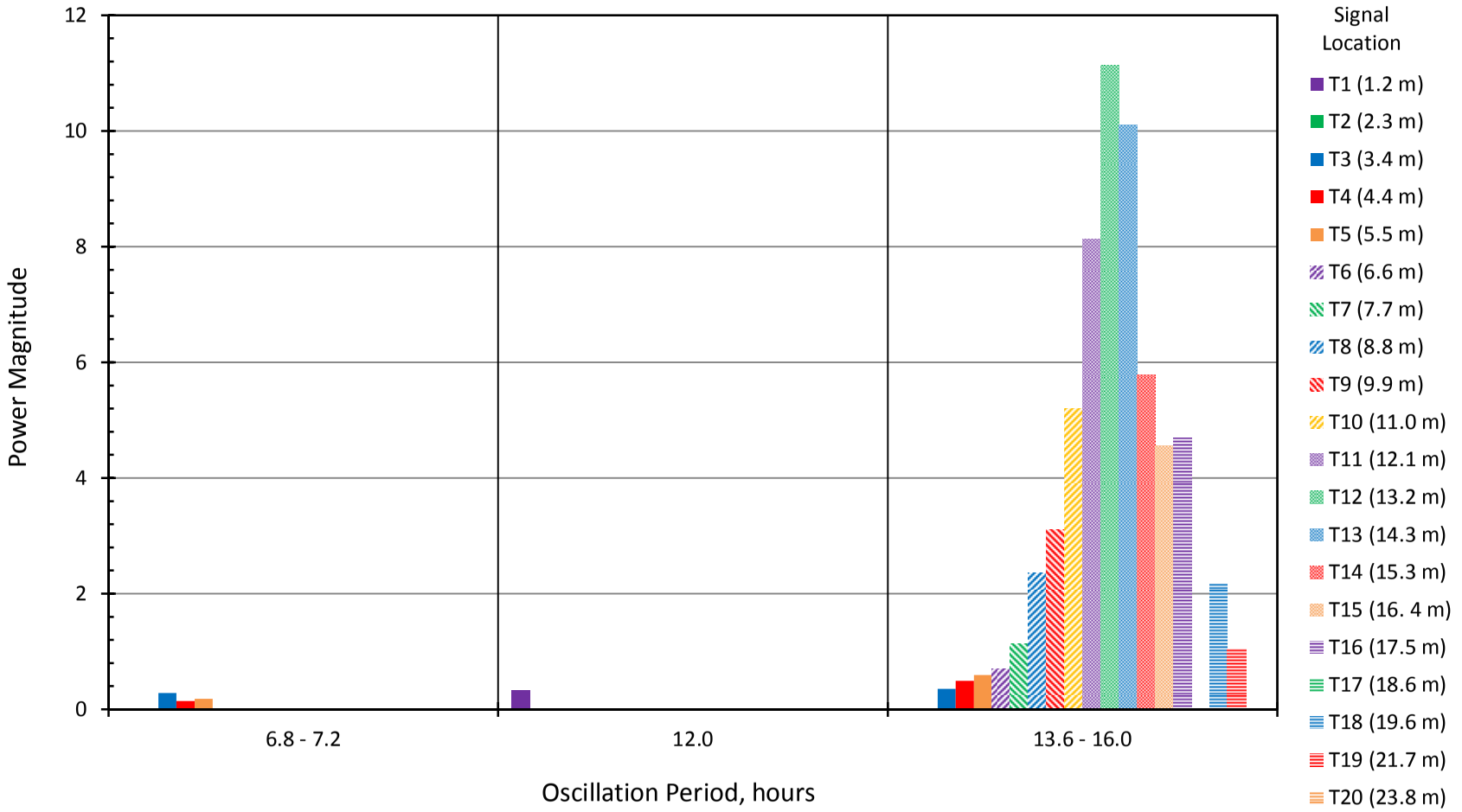

Figure 3.19 Dominant periods of oscillation, in the order of hours, for different thermistor times series in the HLK forebay.

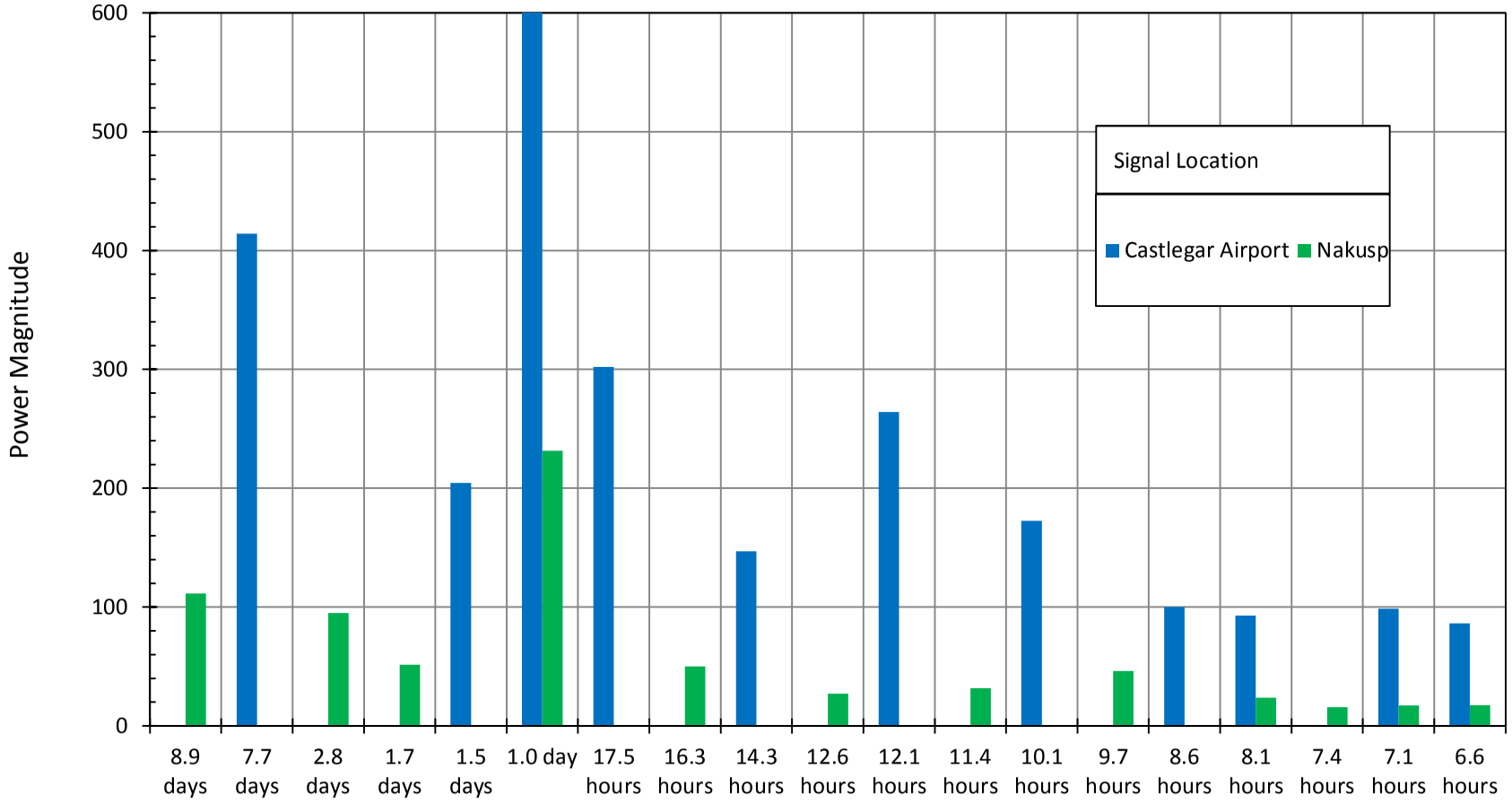

Figure 3.20 Dominant periods of oscillation for wind speed data from Castlegar Airport and Nakusp meteorological stations.

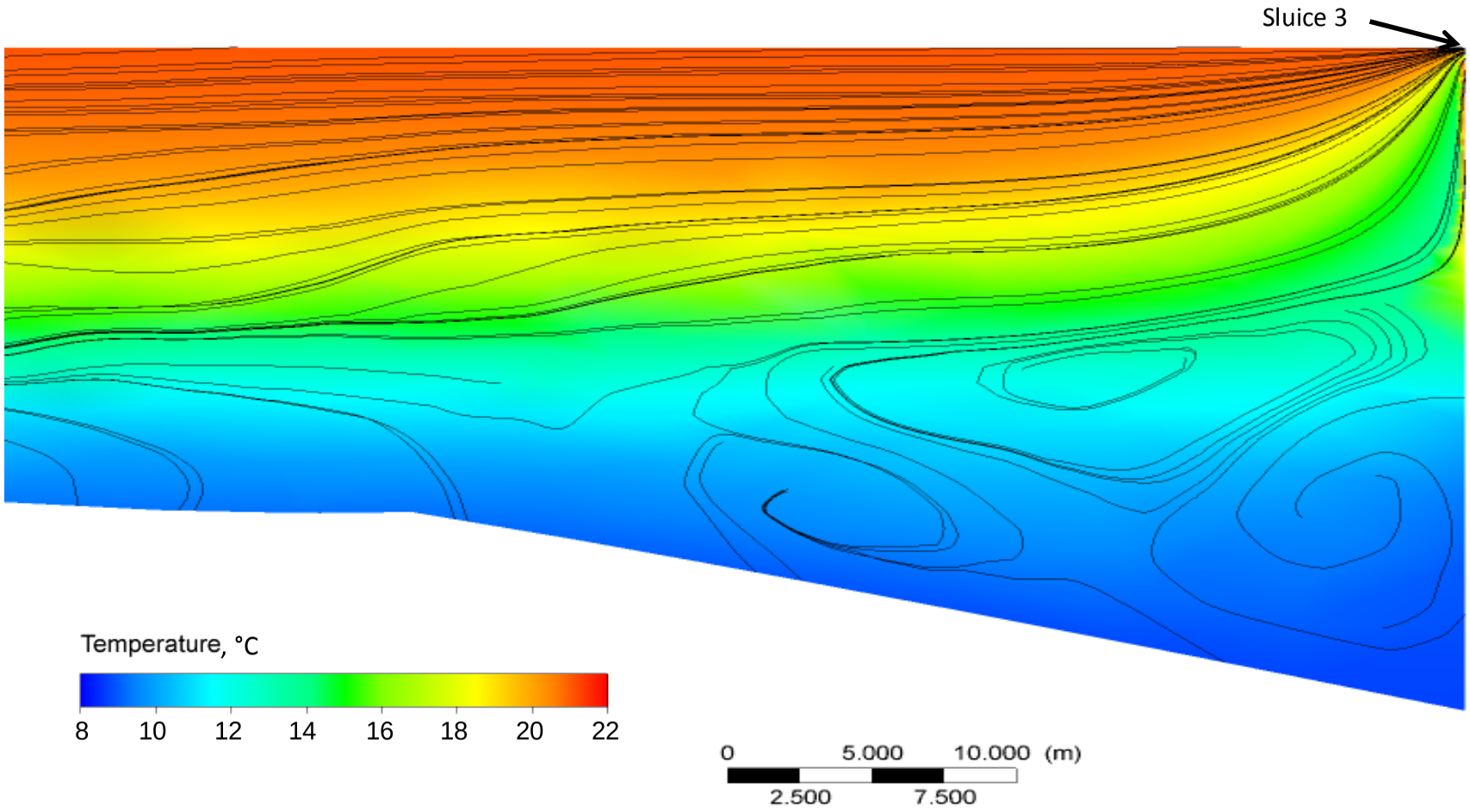

Figure 3.21 Computed temperature distribution and streamlines (black) on a plane perpendicular to Sluice 3 with a discharge of 65 m^3/s.

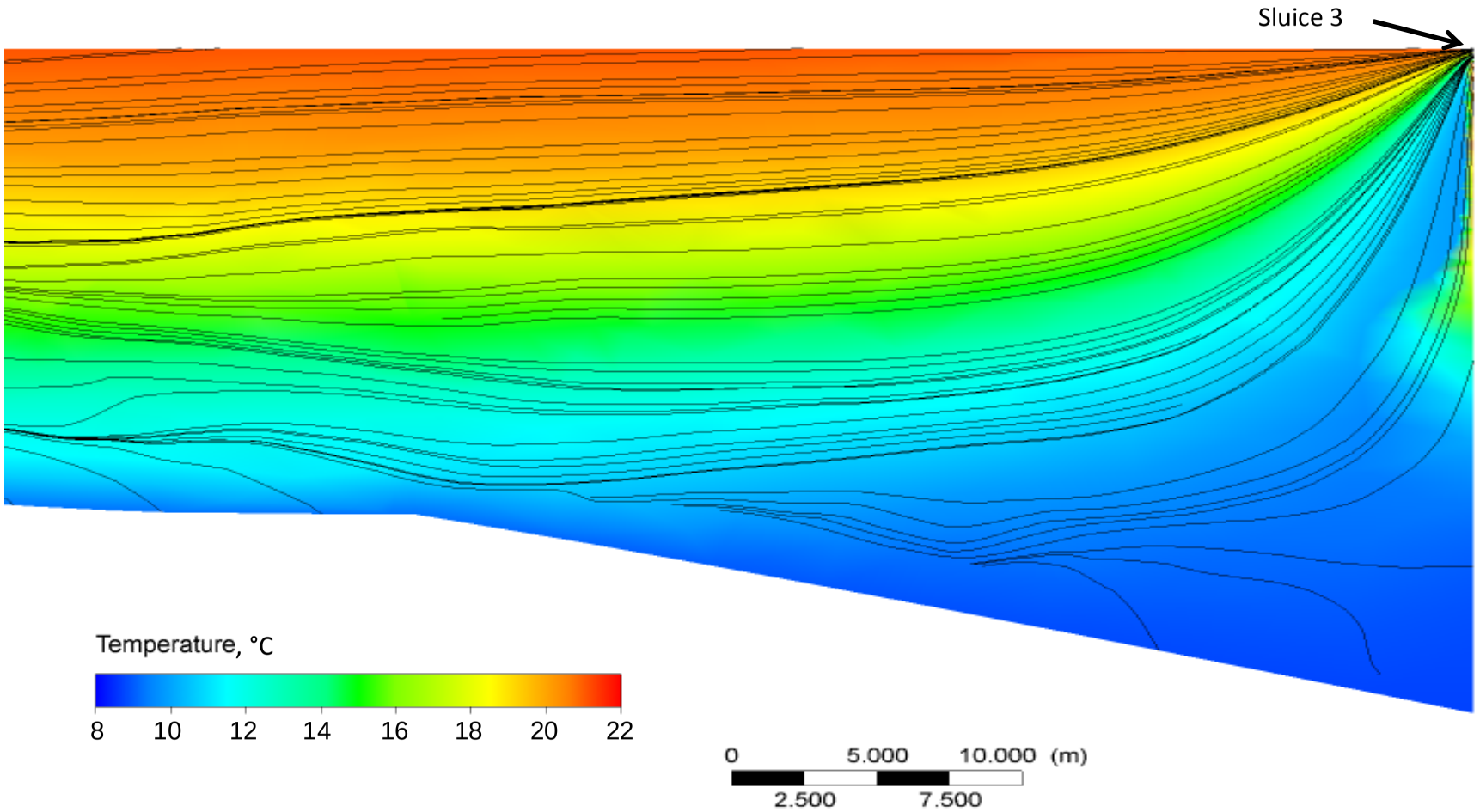

Figure 3.22 Computed temperature distribution and streamlines (black) on a plane perpendicular to Sluice 3 with a discharge of 200 m^3/s.

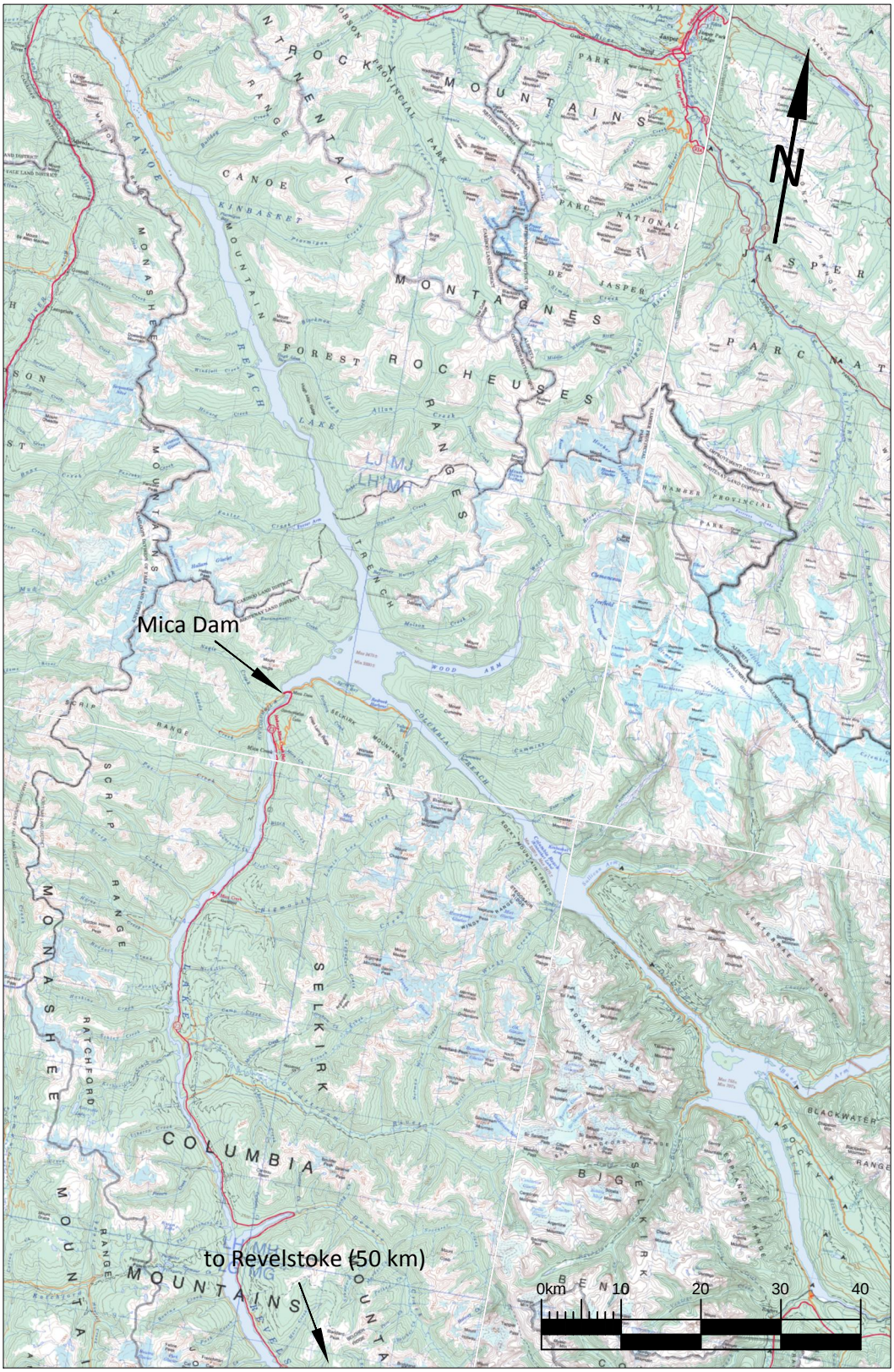

Figure 4.1 Overall site plan of Kinbasket reservoir.

(a)

(b)

Figure 4.2 MCA hydropower facility: (a) upstream side of dam from the left bank and (b) dam face (the intakes are located at the base, between the rectangular holes in the concrete).

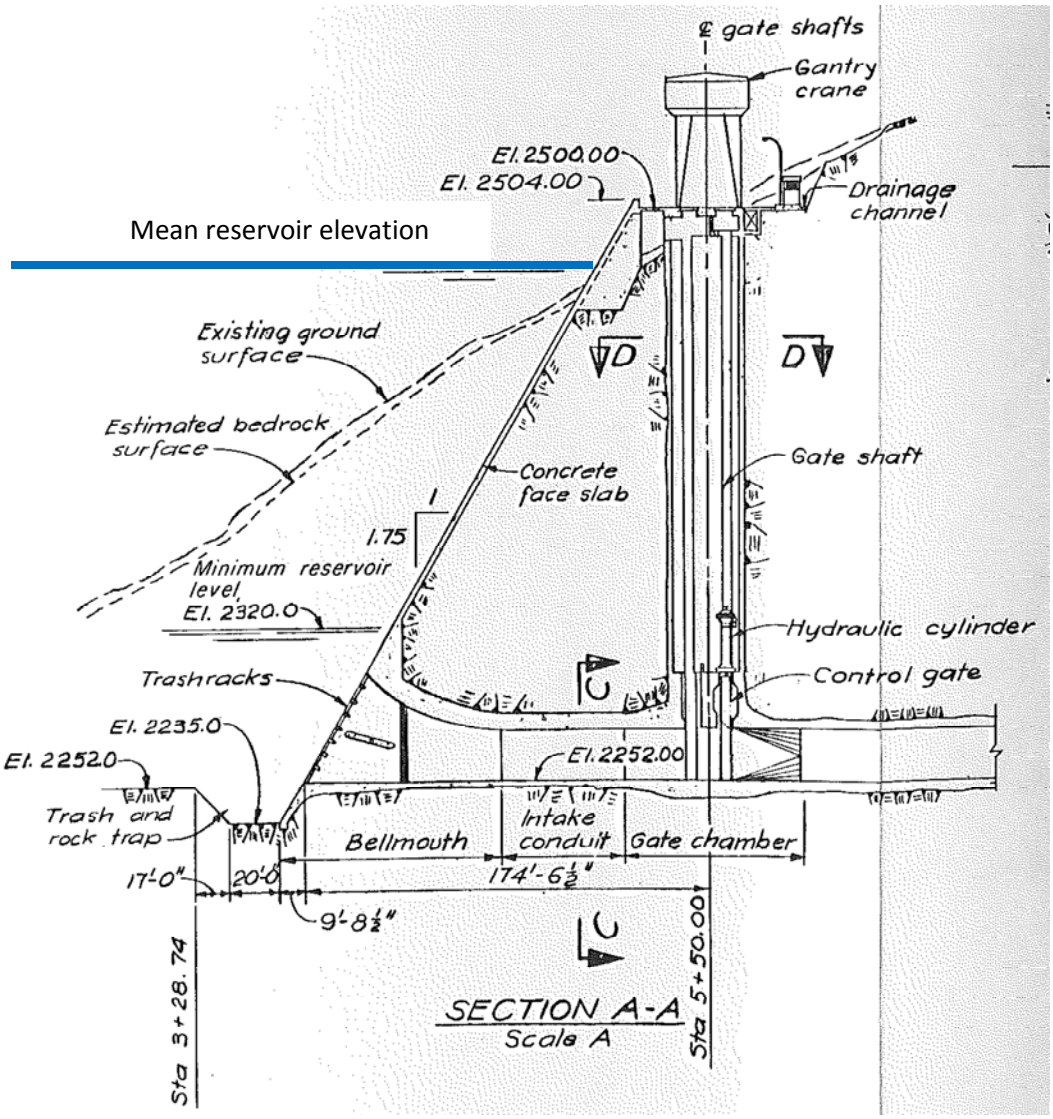

Figure 4.3 Profile view of an intake at MCA (from record drawing provided by BC Hydro).

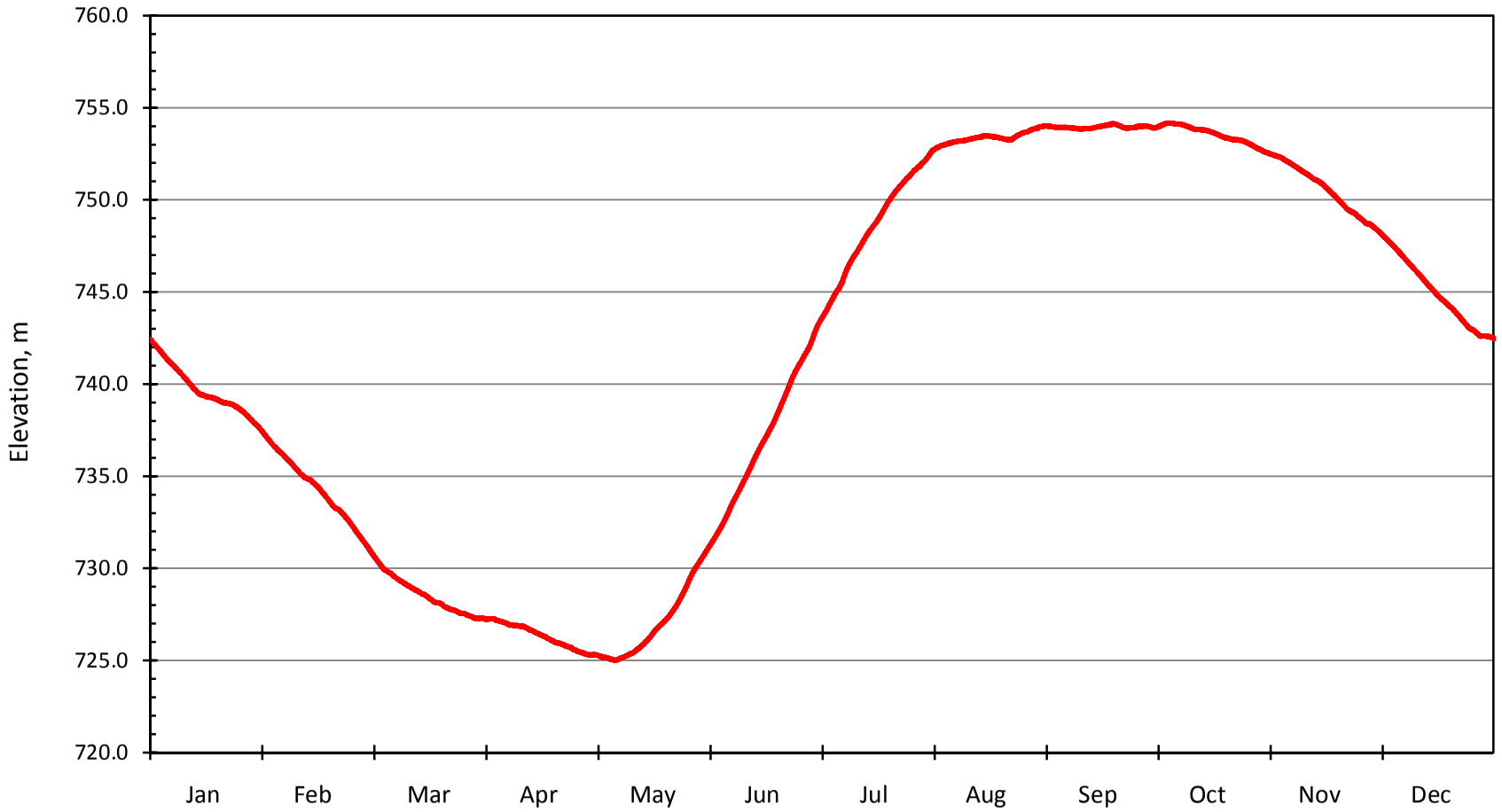

Figure 4.4 Water elevation in Kinbasket reservoir in 2011.

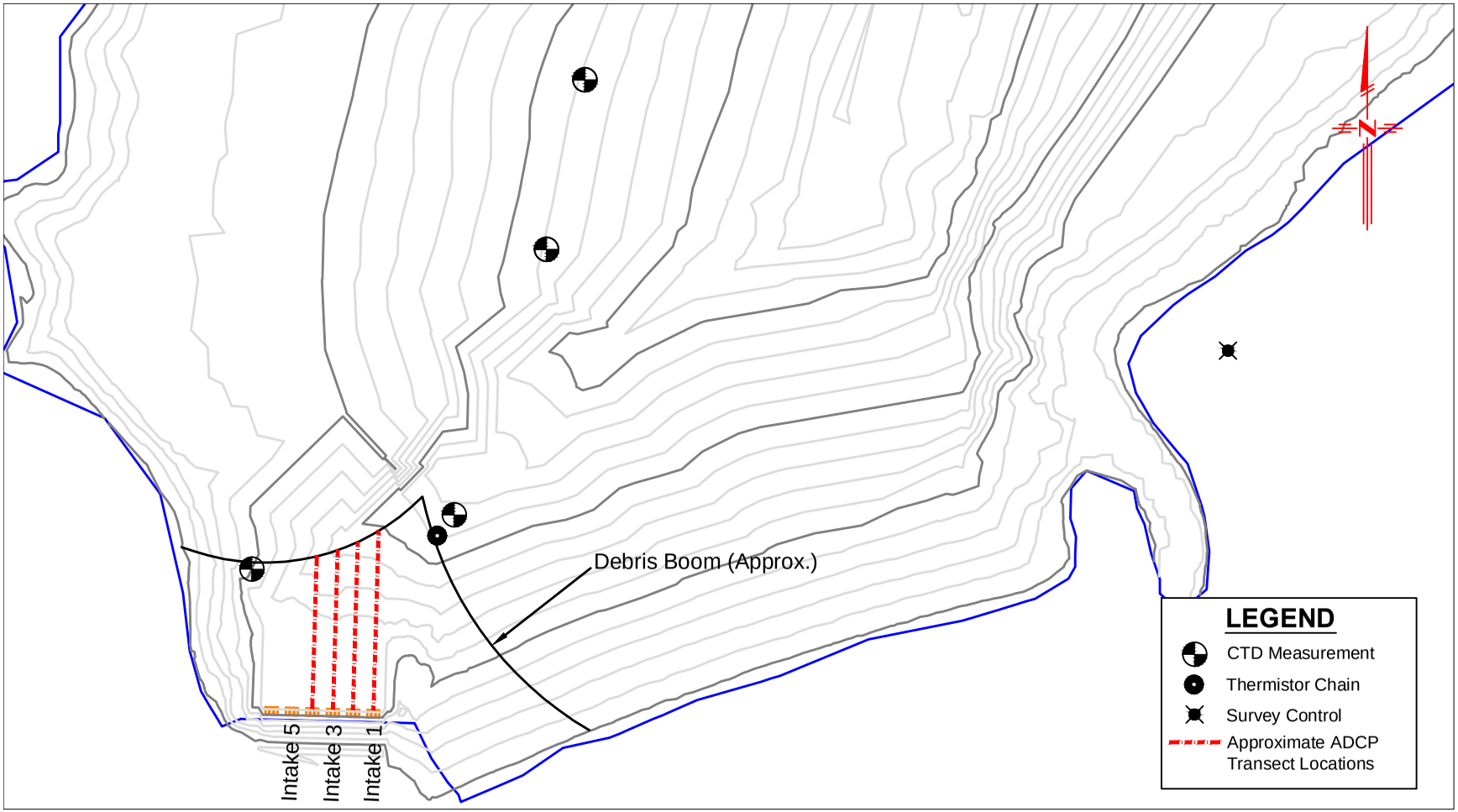

Figure 4.5 MCA forebay with CTD, thermistor chain, and approximate ADCP measurement locations and survey control point location.

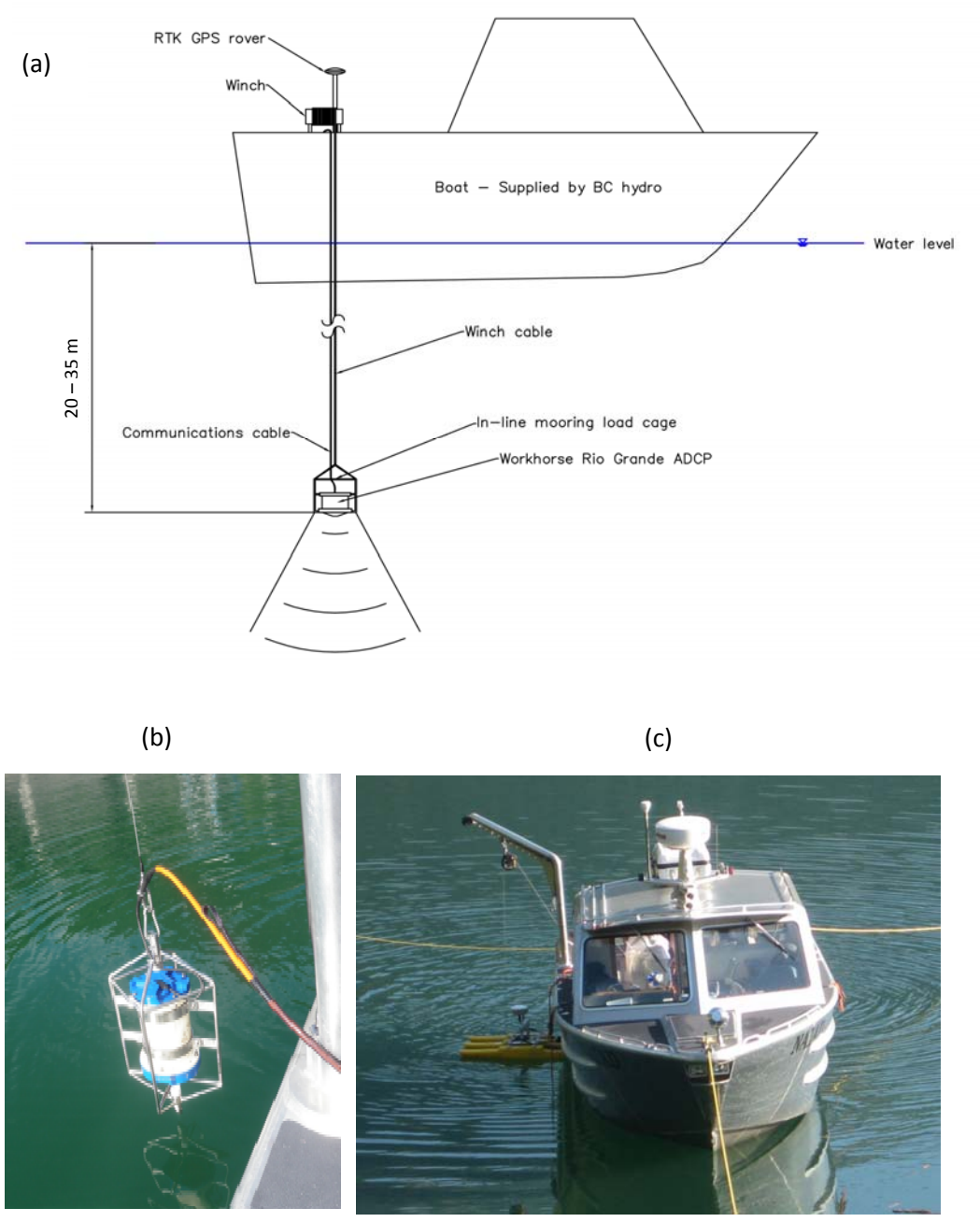

Figure 4.6 Sentinel ADCP measurement set-up: (a) schematic, (b) ADCP in mooring cage on hydraulic winch cable before deployment, and (c) deployed ADCP with RTK measurements from trimaran.

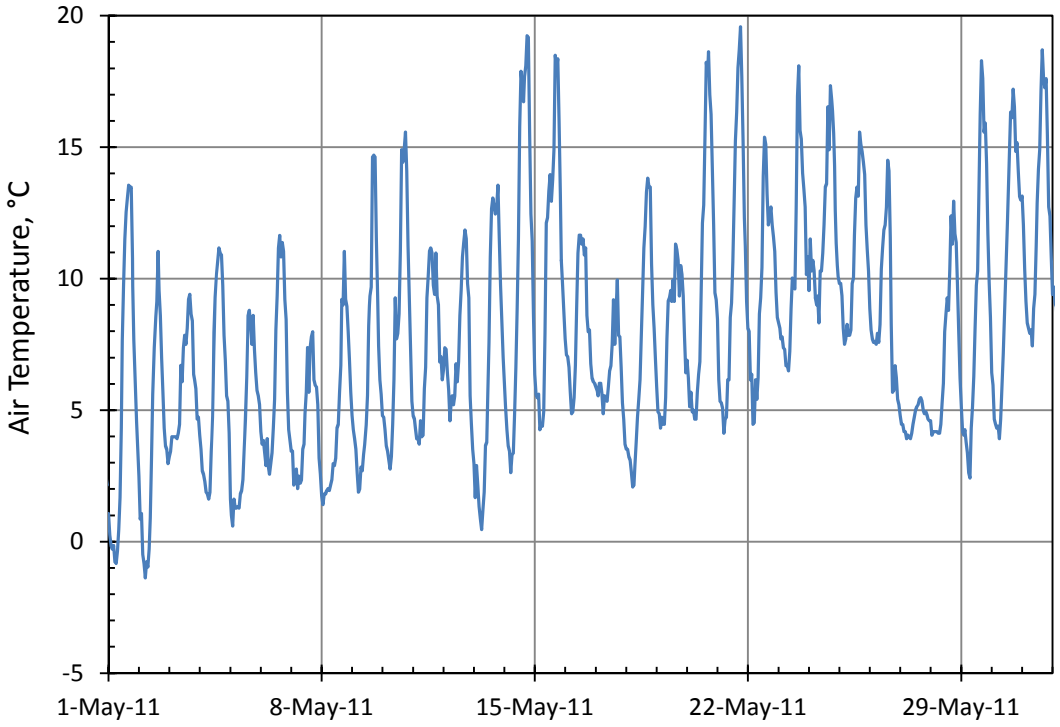

Figure 4.7a Air temperatures recorded at MCA meteorological station in May, 2011.

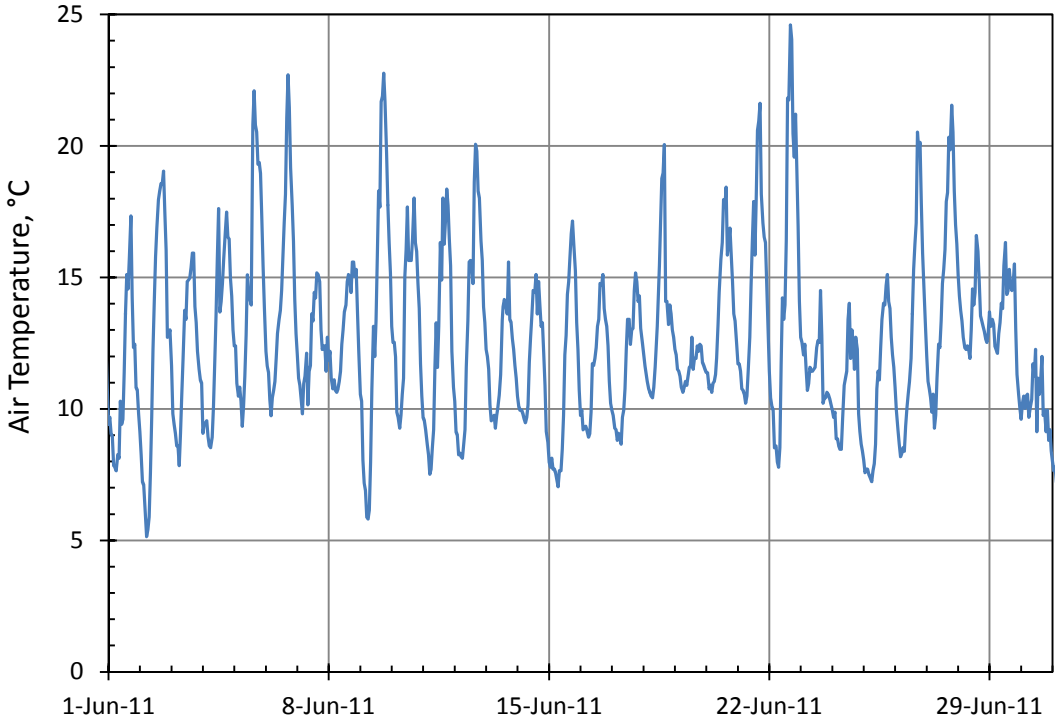

Figure 4.7b Air temperatures recorded at MCA meteorological station in June, 2011.

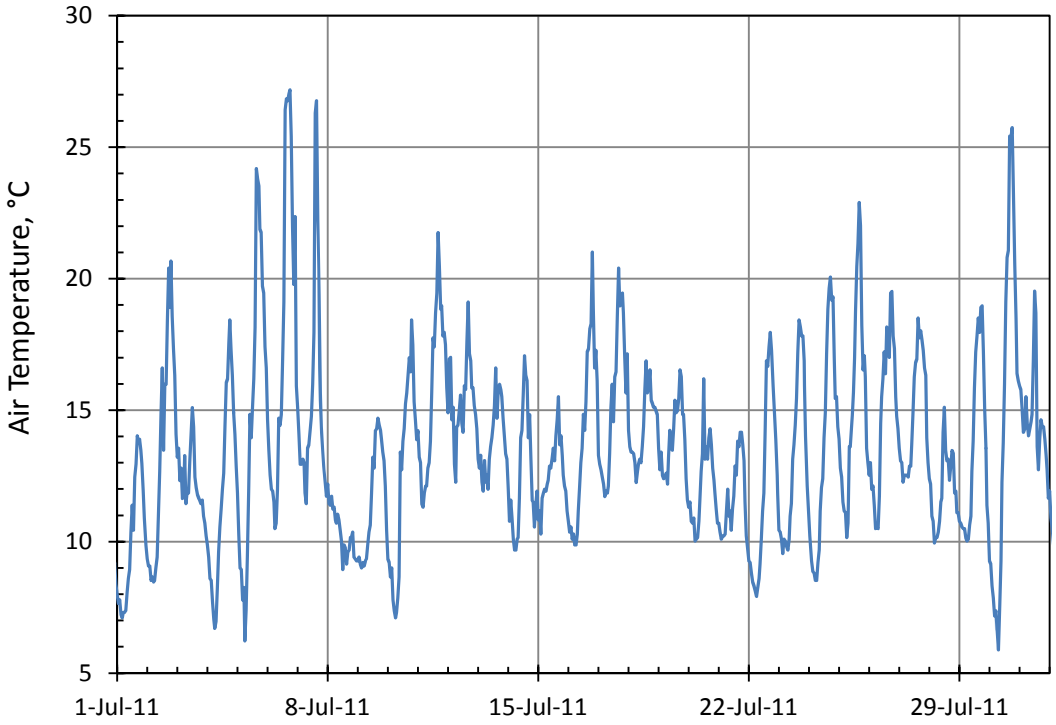

Figure 4.7c Air temperatures recorded at MCA meteorological station in July, 2011.

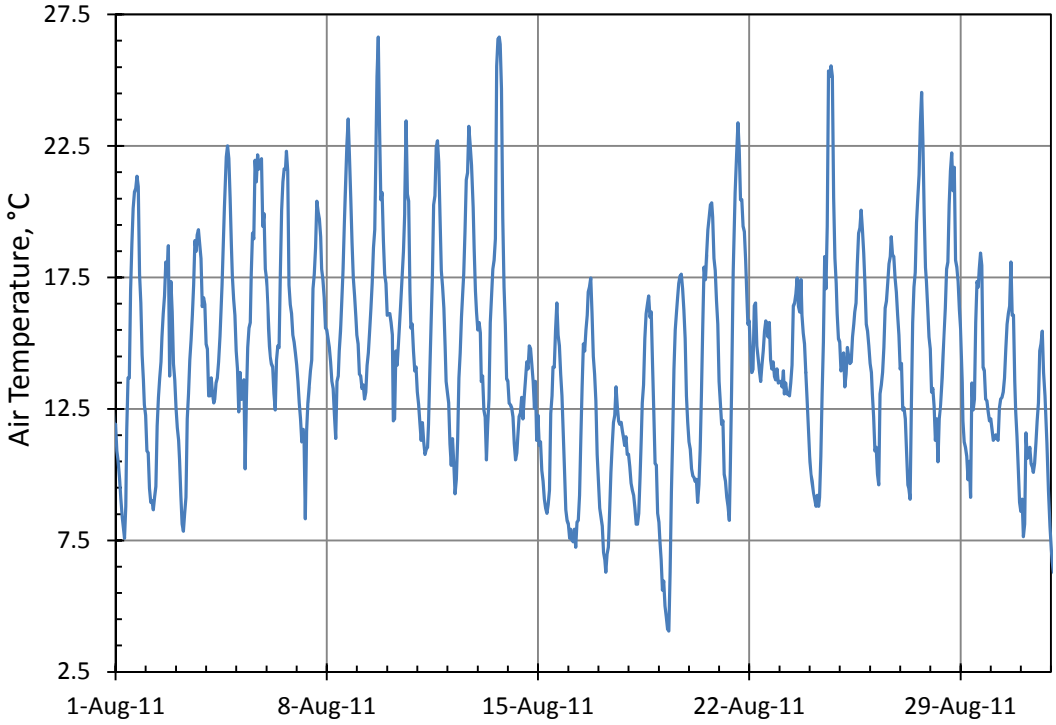

Figure 4.7d Air temperatures recorded at MCA meteorological station in August, 2011.

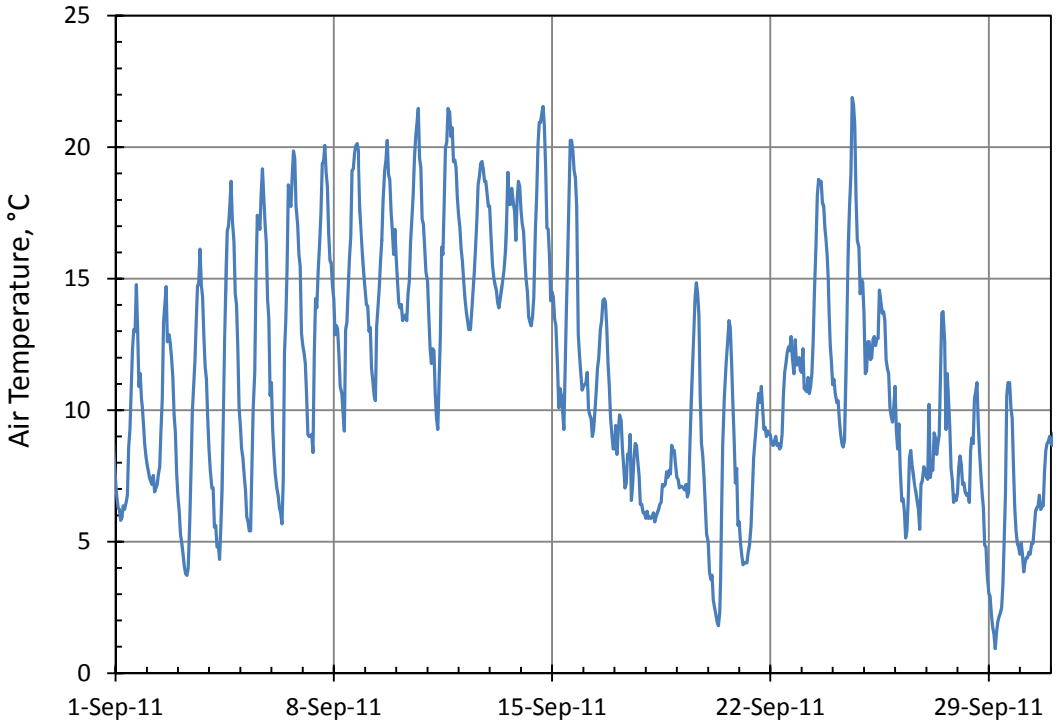

Figure 4.7e Air temperatures recorded at MCA meteorological station in September ,2011.

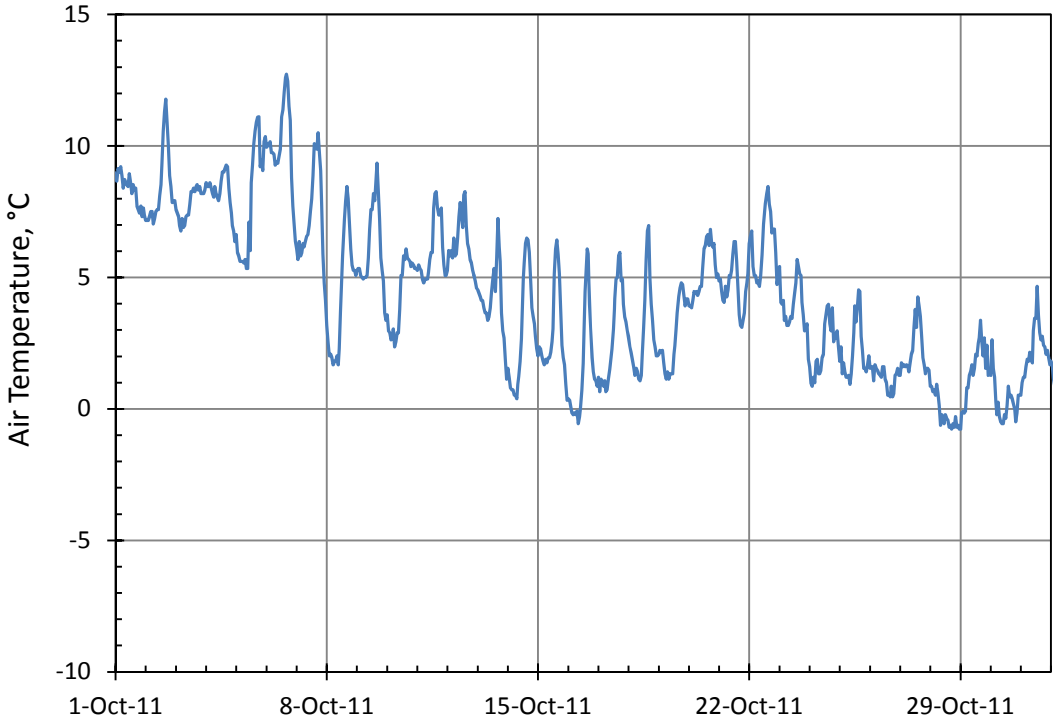

Figure 4.7f Air temperatures recorded at MCA meteorological station in October, 2011.

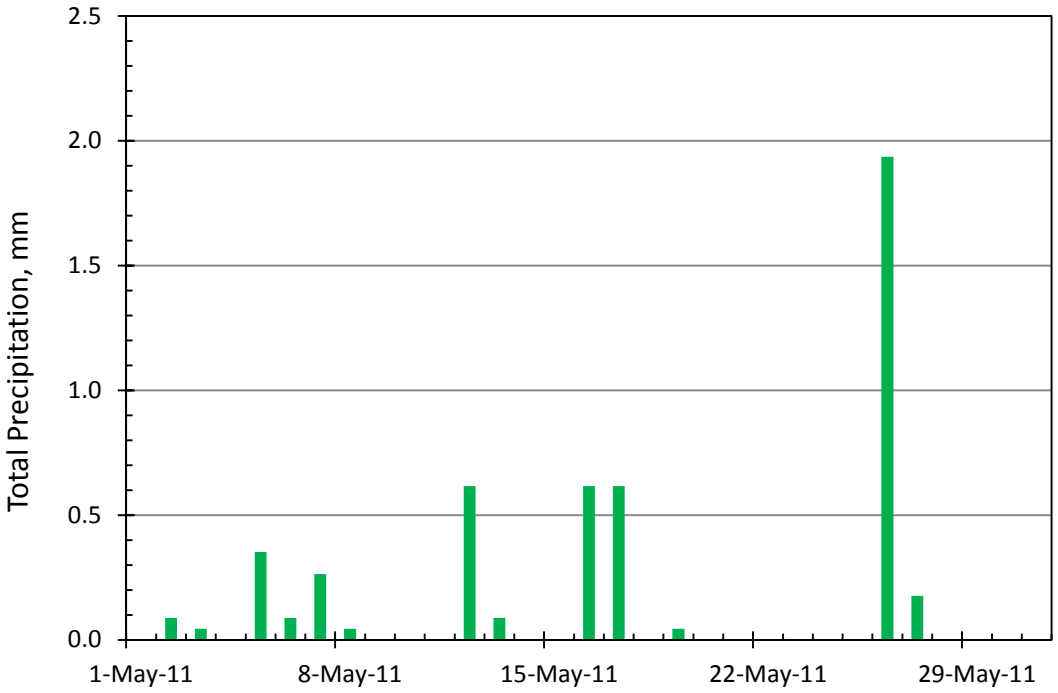

Figure 4.8a Precipitation recorded at MCA meteorological station in May, 2011.

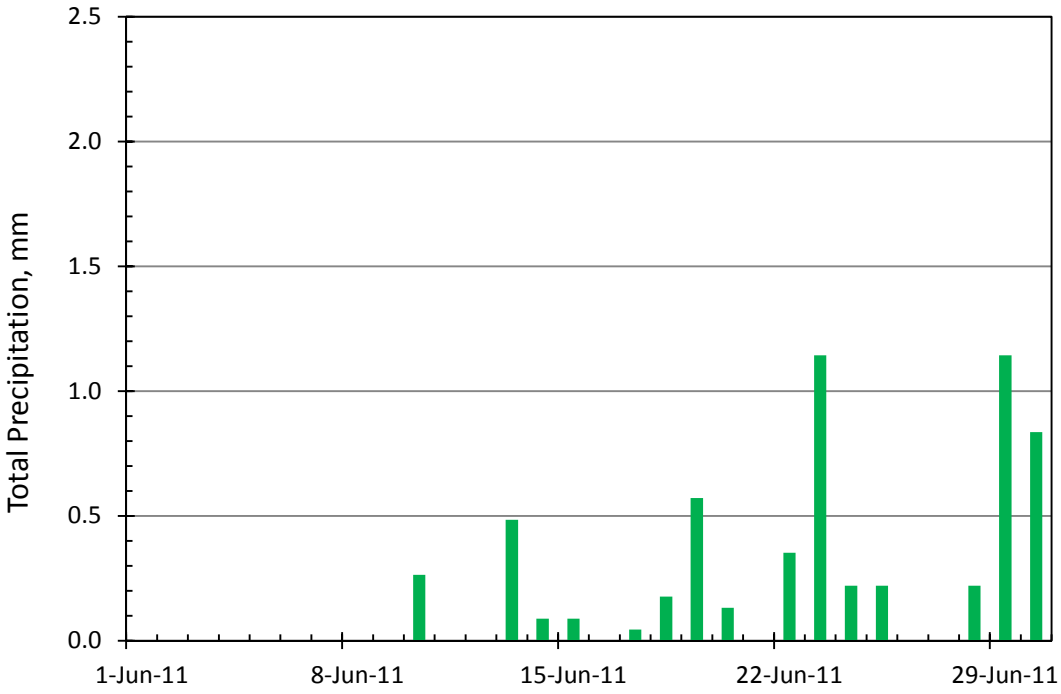

Figure 4.8b Precipitation recorded at MCA meteorological station in June, 2011.

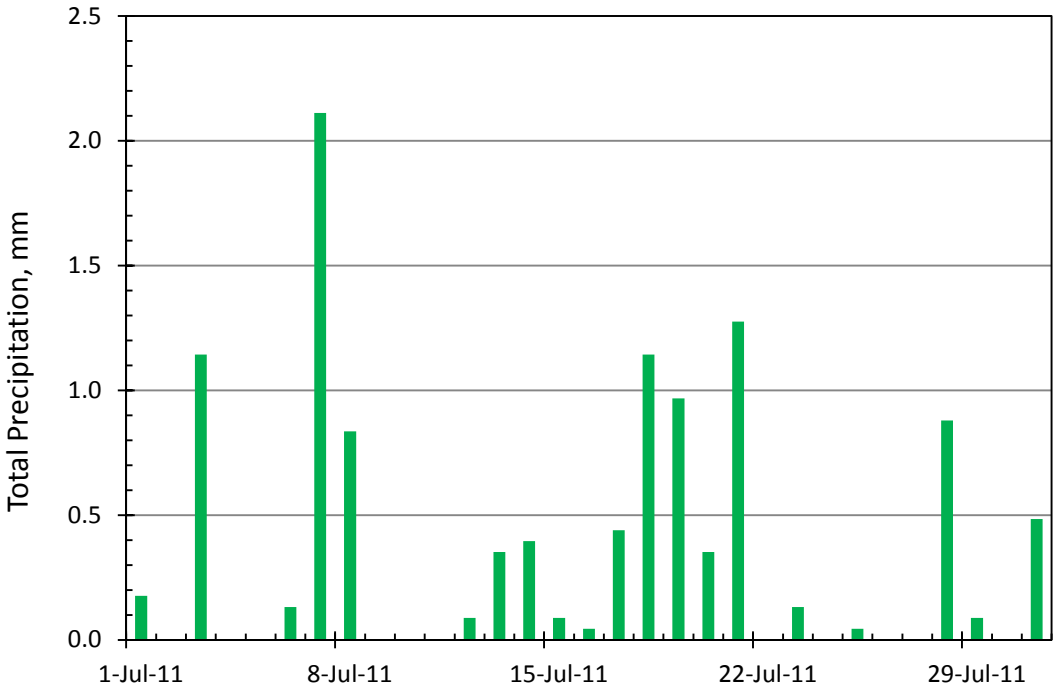

Figure 4.8c Precipitation recorded at MCA meteorological station in July, 2011.

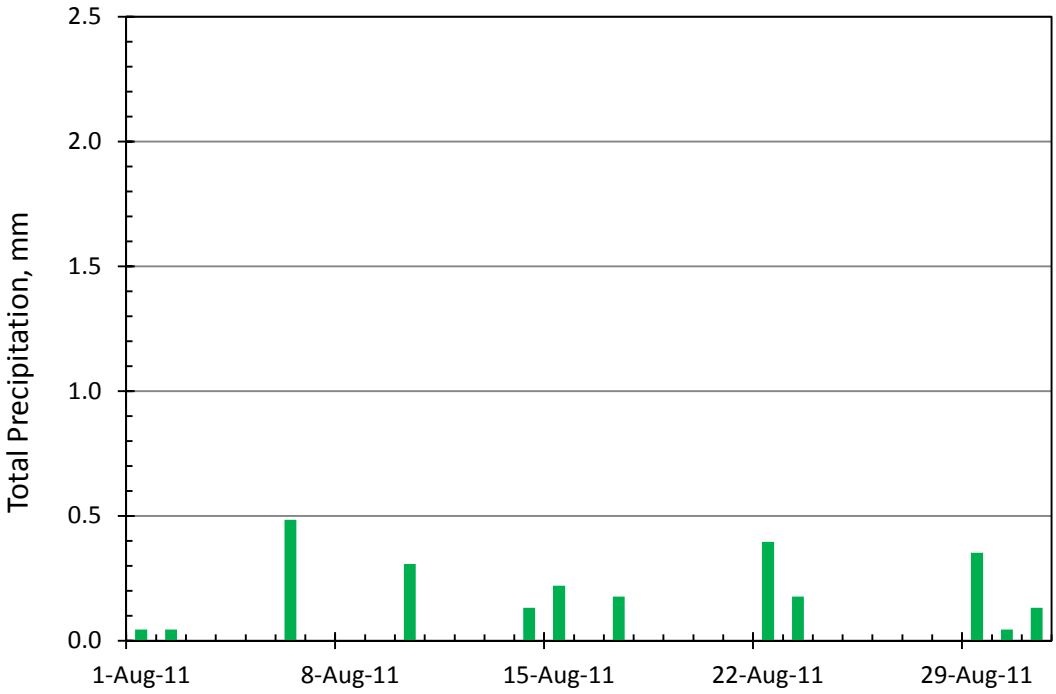

Figure 4.8d Precipitation recorded at MCA meteorological station in August , 2011.

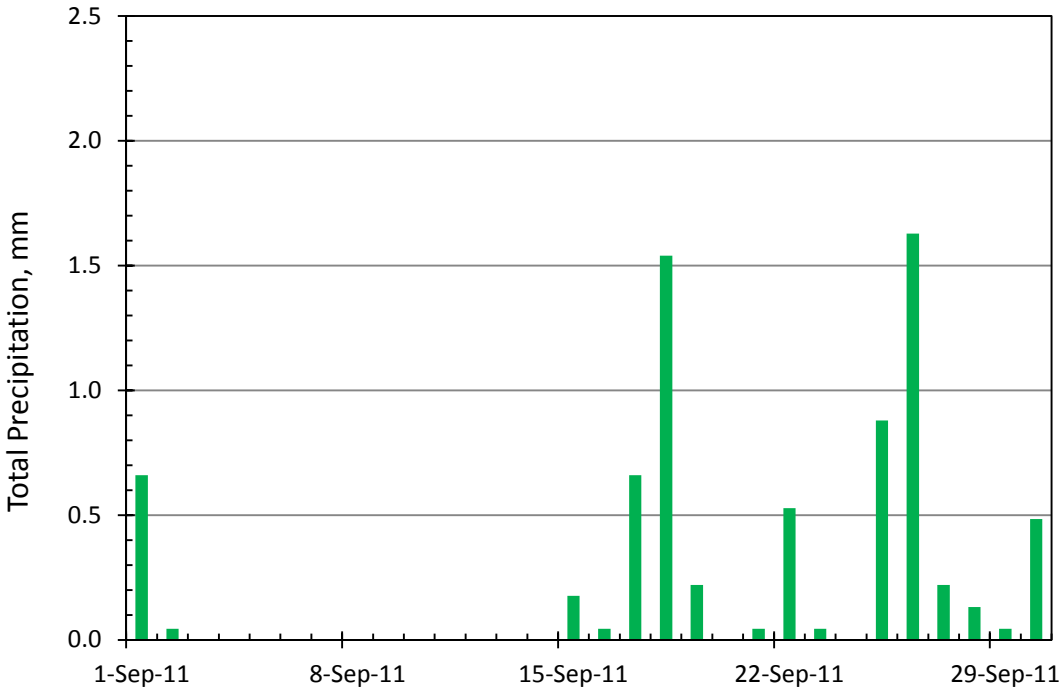

Figure 4.8e Precipitation recorded at MCA meteorological station in September, 2011.

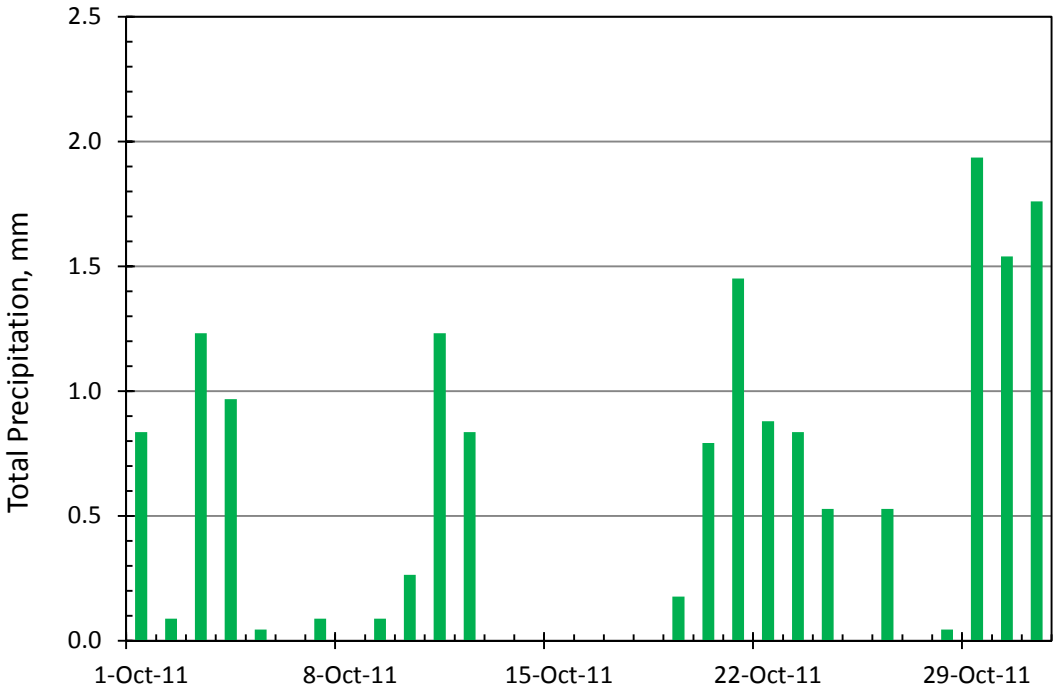

Figure 4.8f Precipitation recorded at MCA meteorological station in October, 2011.

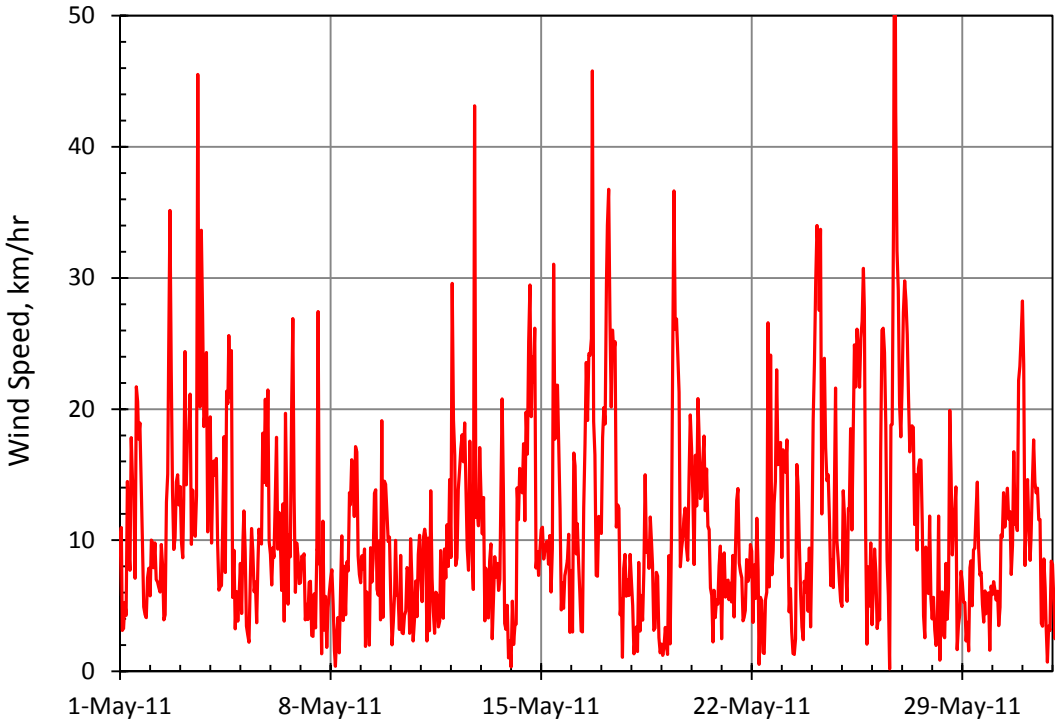

Figure 4.9a Wind speed recorded at MCA meteorological station in May, 2011.

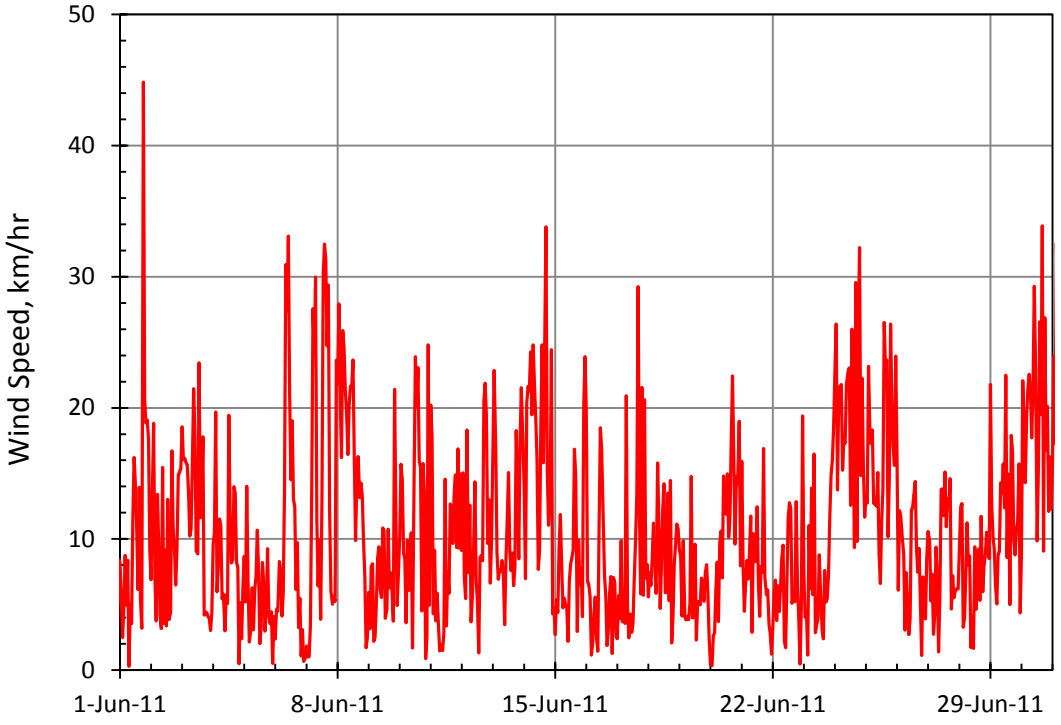

Figure 4.9b Wind speed recorded at MCA meteorological station in June, 2011.

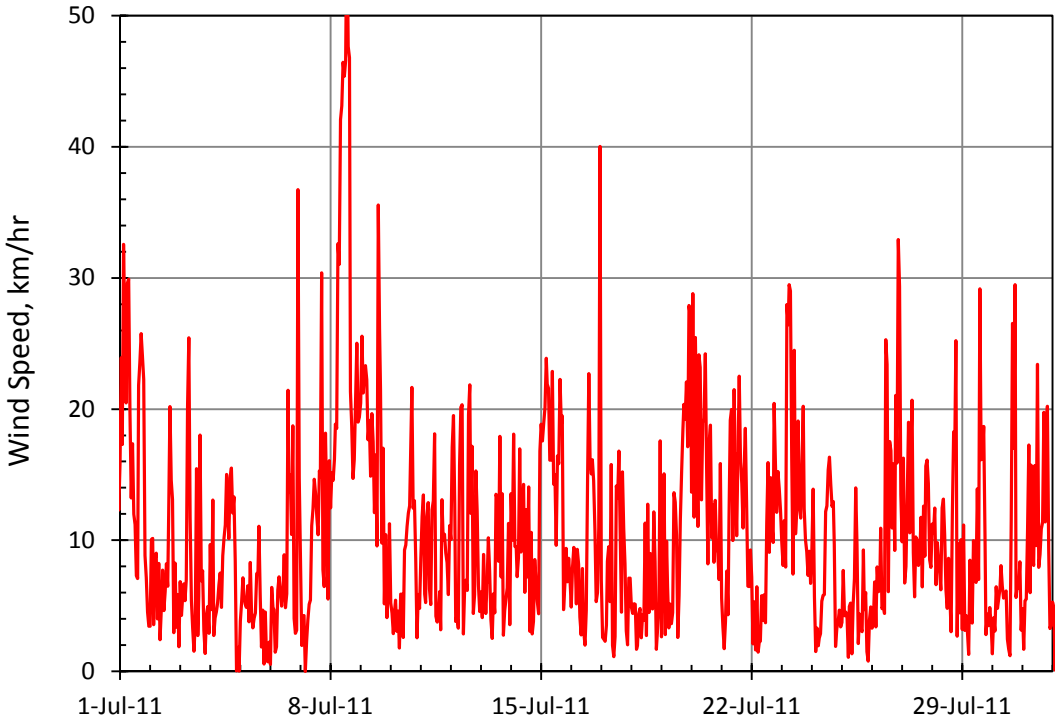

Figure 4.9c Wind speed recorded at MCA meteorological station in July, 2011.

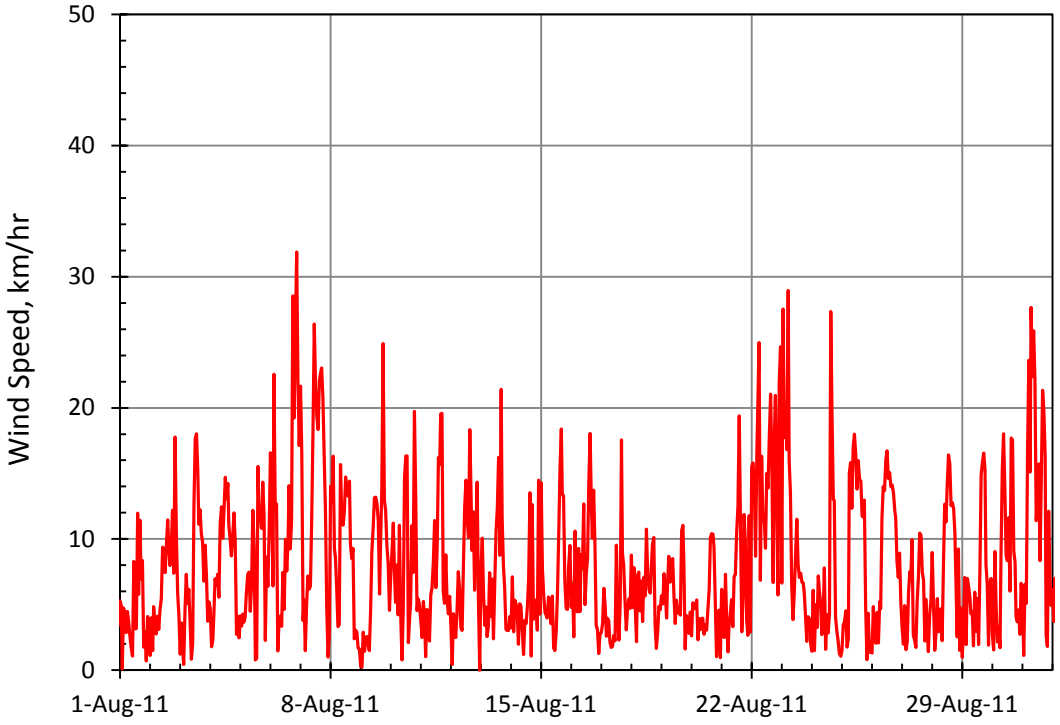

Figure 4.9d Wind speed recorded at MCA meteorological station in August, 2011.

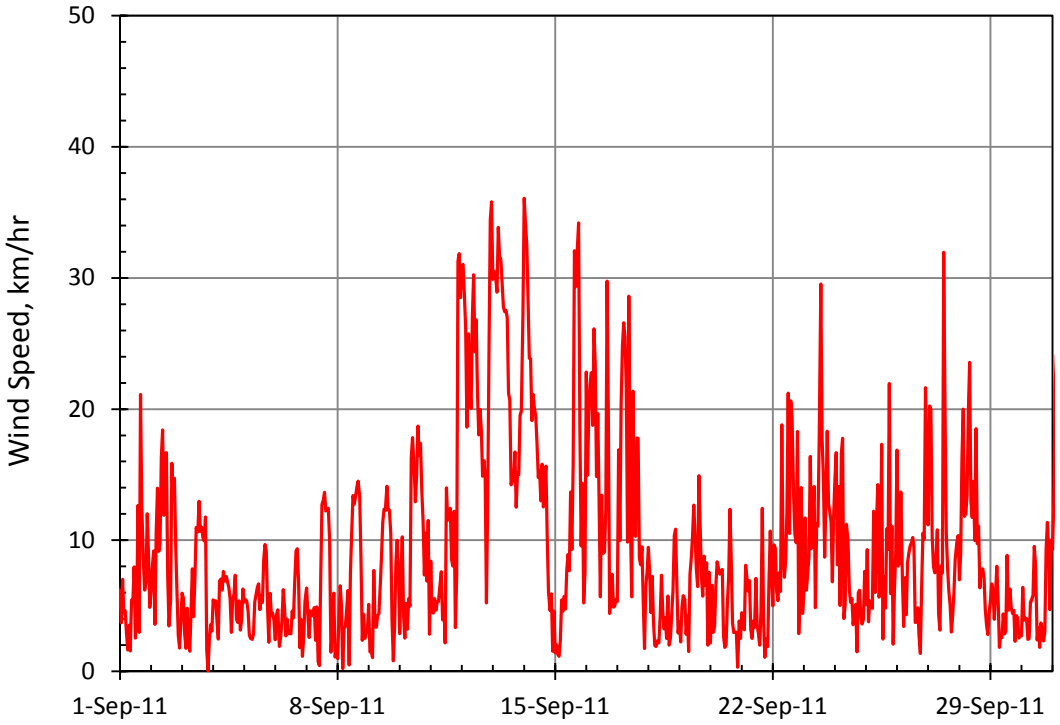

Figure 4.9e Wind speed recorded at MCA meteorological station in September, 2011.

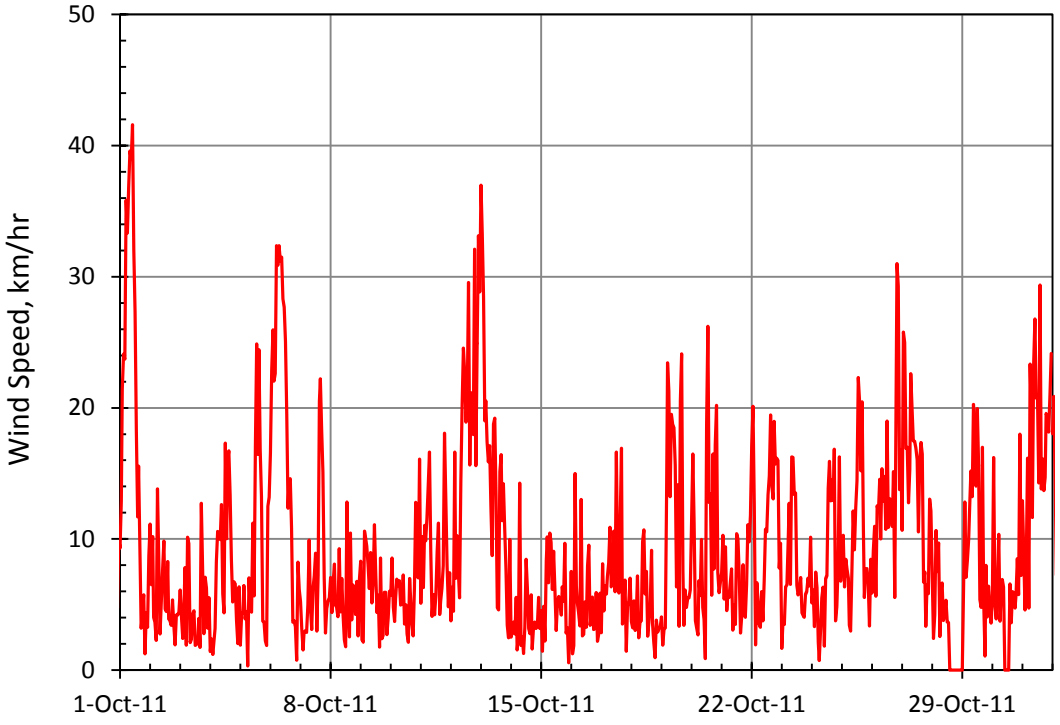

Figure 4.9f Wind speed recorded at MCA meteorological station in October, 2011.

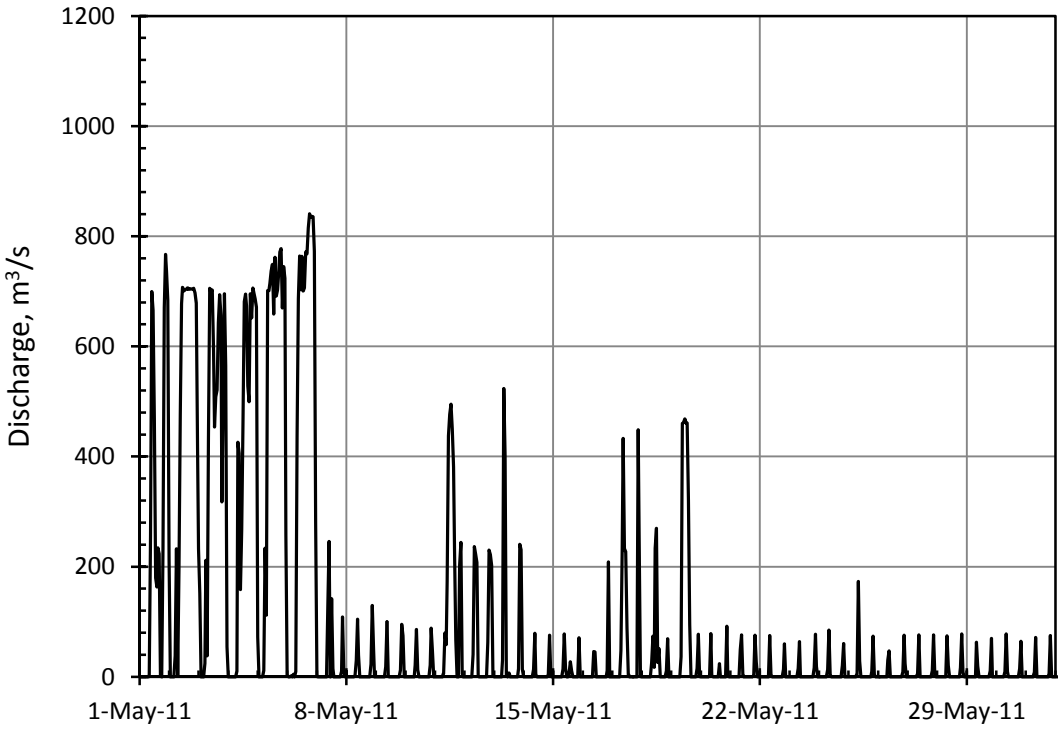

Figure 4.10a Total discharge of MCA intakes recorded in May, 2011.

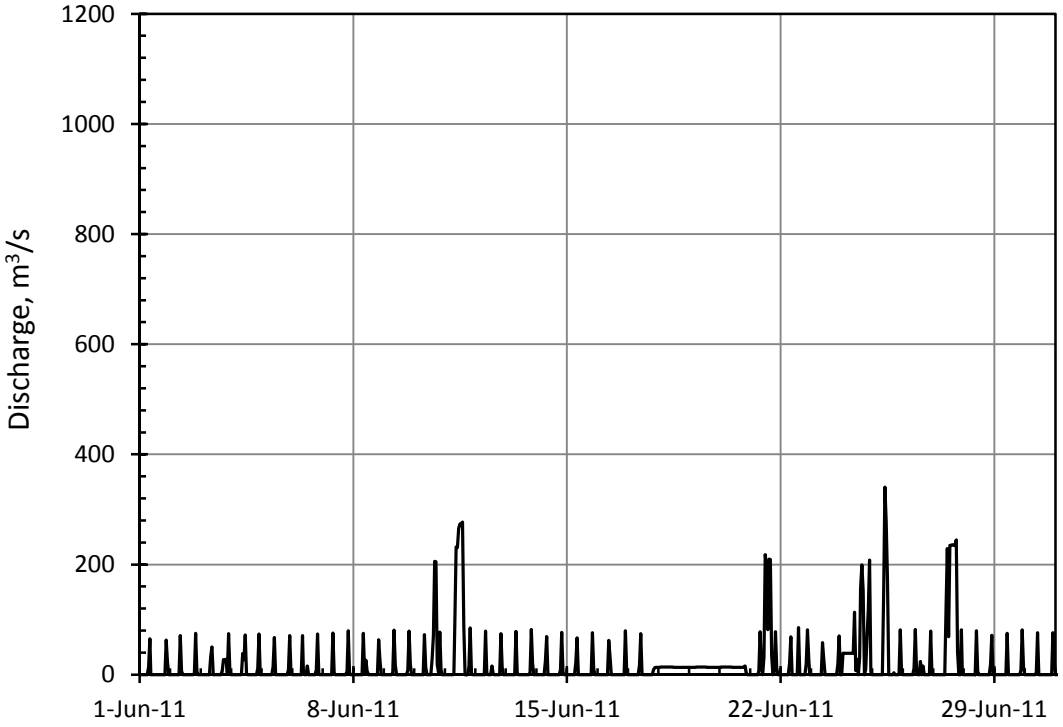

Figure 4.10b Total discharge of MCA intakes recorded in June, 2011.

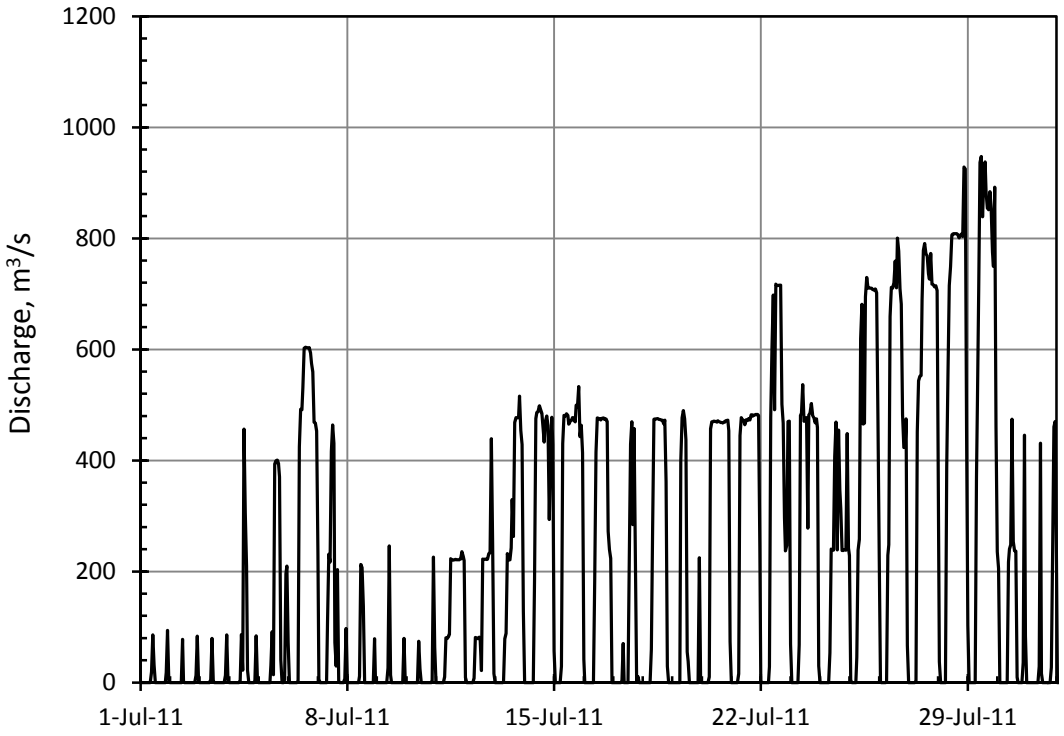

Figure 4.10c Total discharge of MCA intakes recorded in July, 2011.

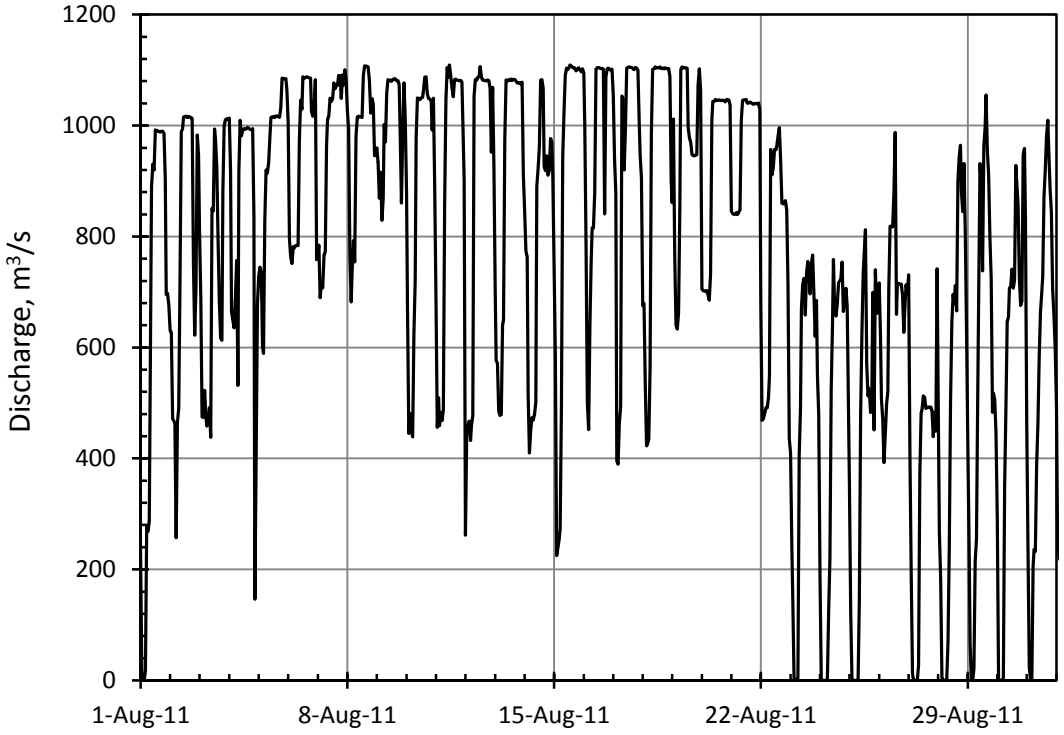

Figure 4.10d Total discharge of MCA intakes recorded in August, 2011.

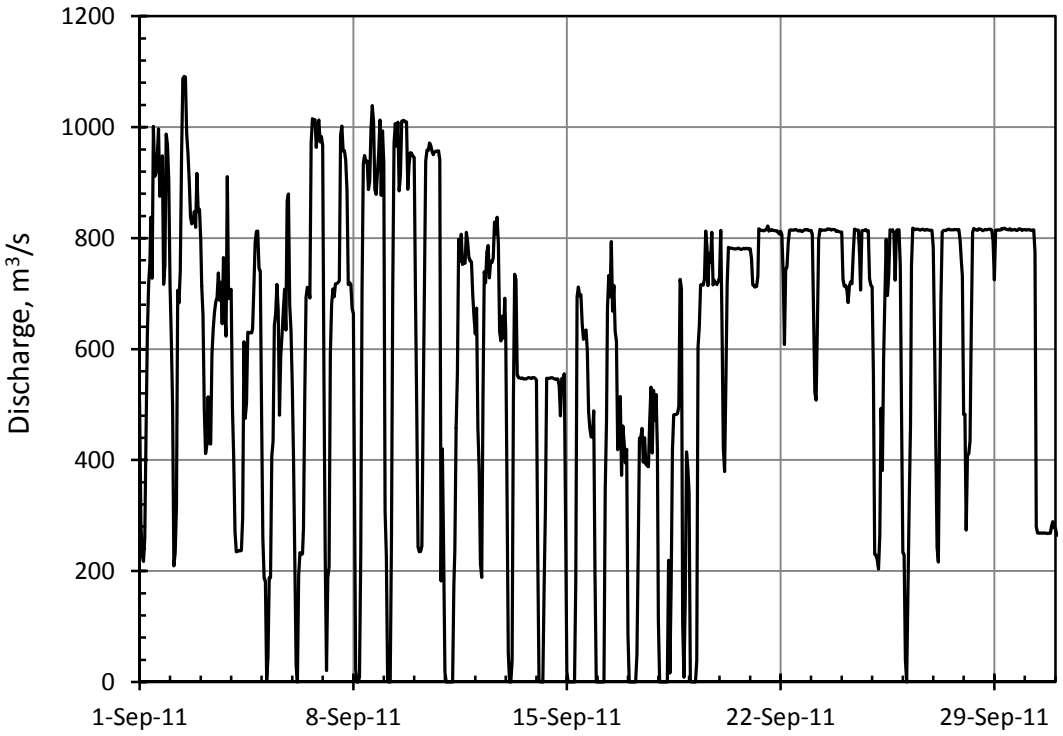

Figure 4.10e Total discharge of MCA intakes recorded in September, 2011.

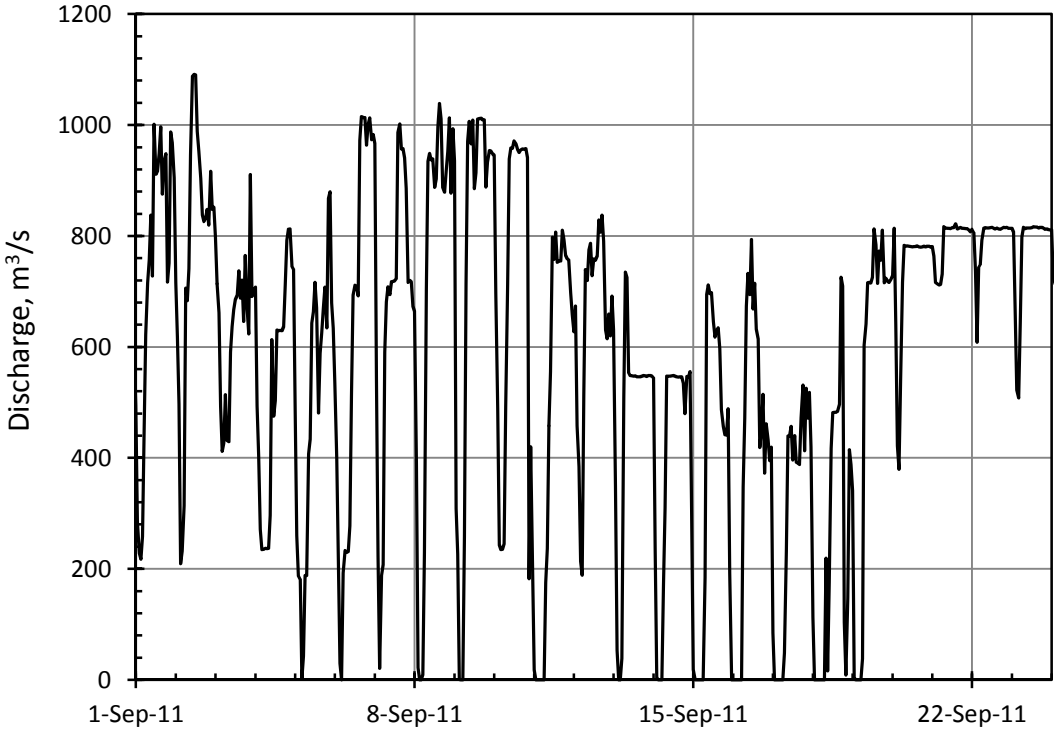

Figure 4.10f Total discharge of MCA intakes recorded in October, 2011.

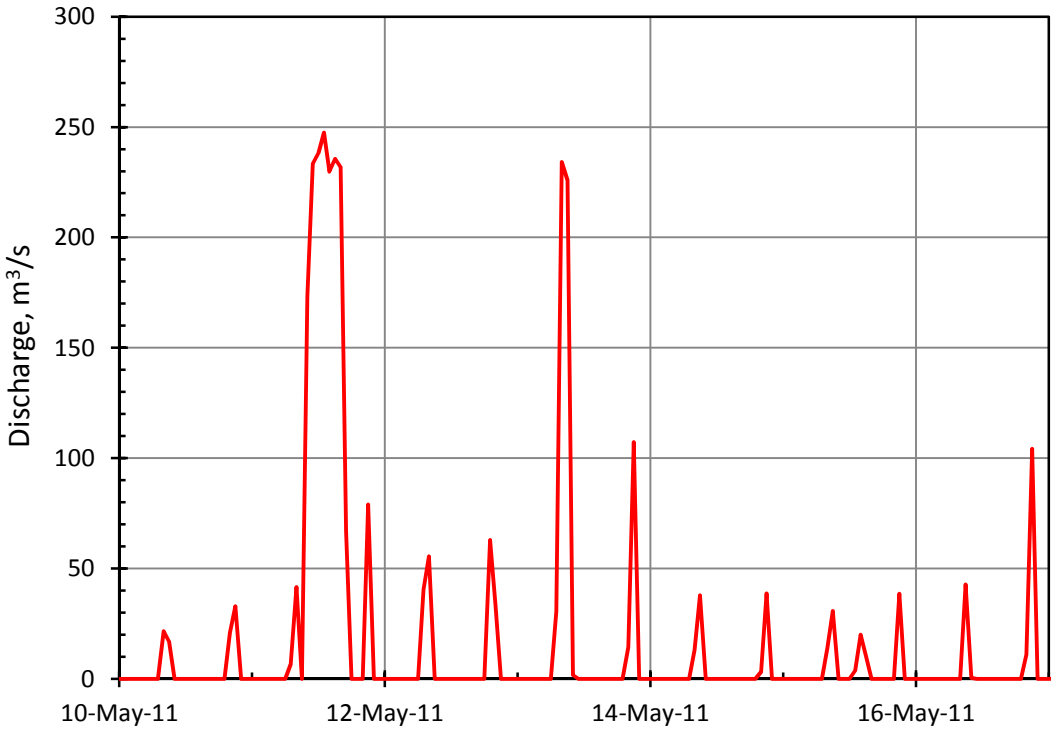

Figure 4.11a Discharge of Intake 1 recorded at MCA in May, 2011.

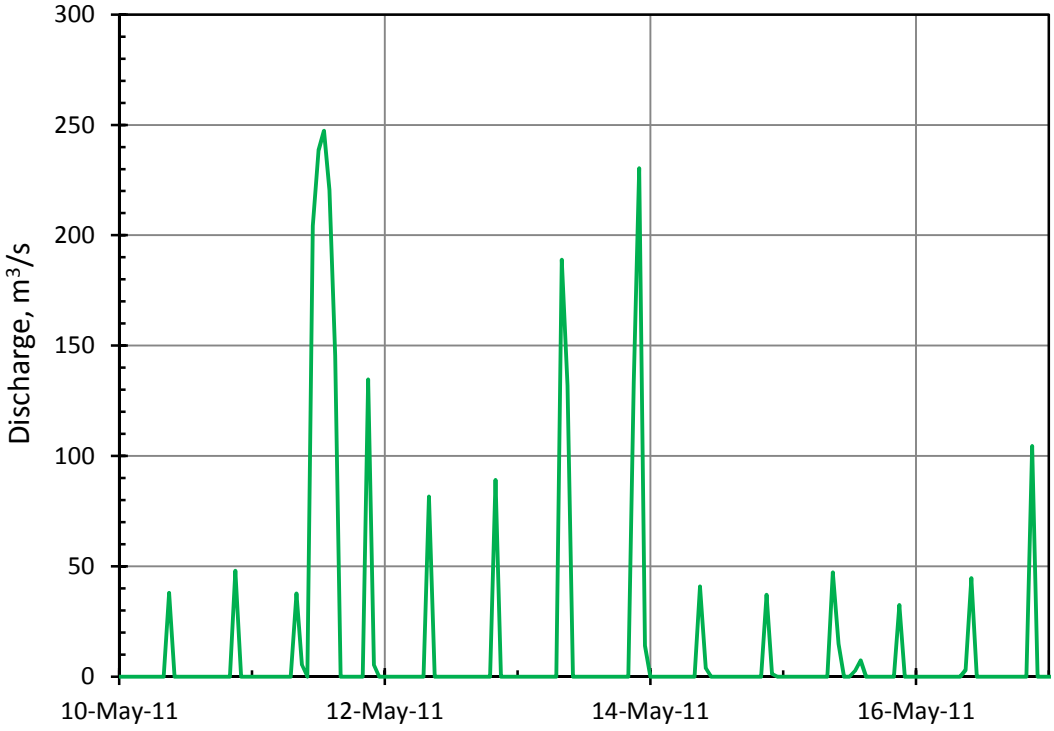

Figure 4.11b Discharge of Intake 2 recorded at MCA in May, 2011.

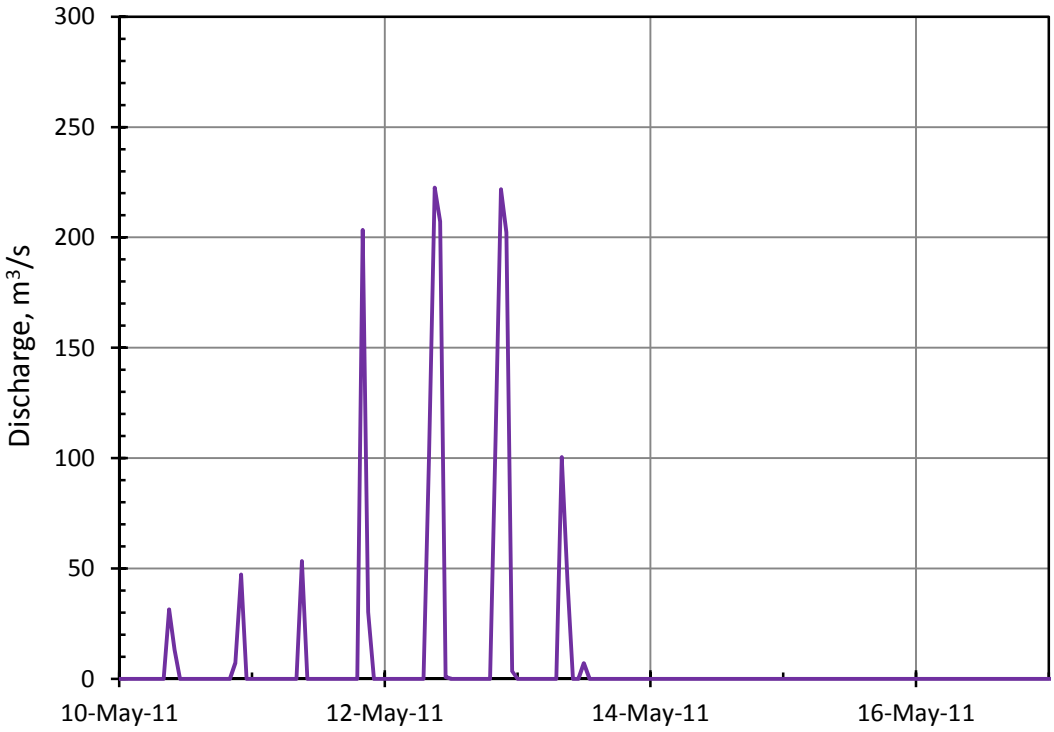

Figure 4.11c Discharge of Intake 3 recorded at MCA in May, 2011.

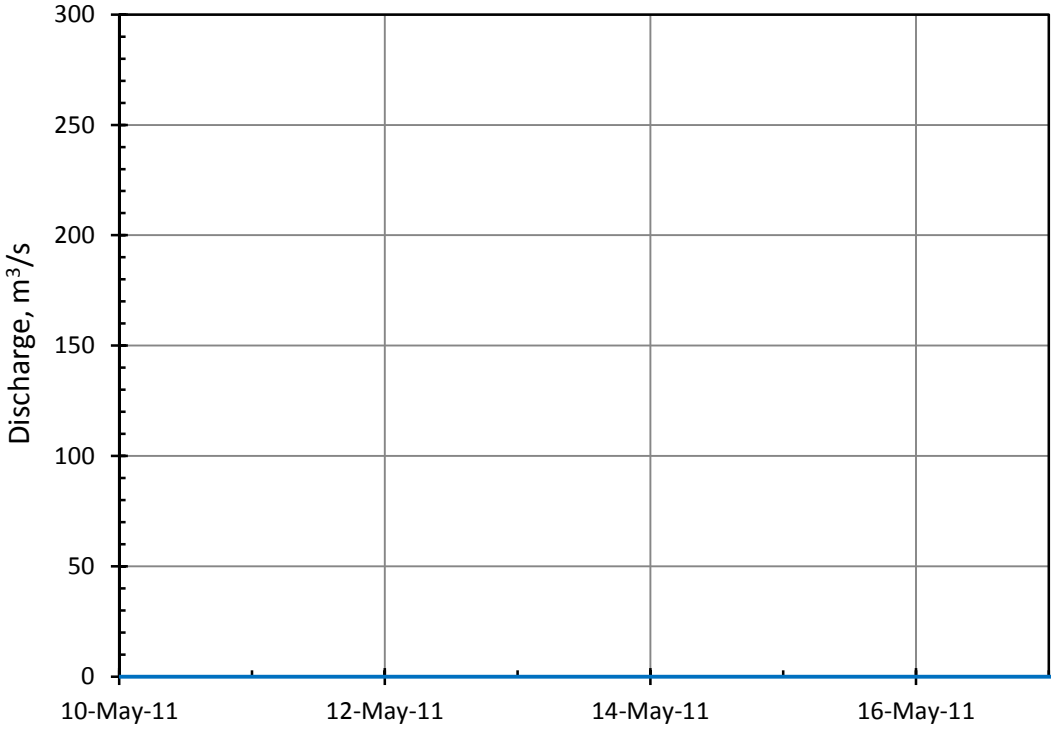

Figure 4.11d Discharge of Intake 4 recorded at MCA in May, 2011.

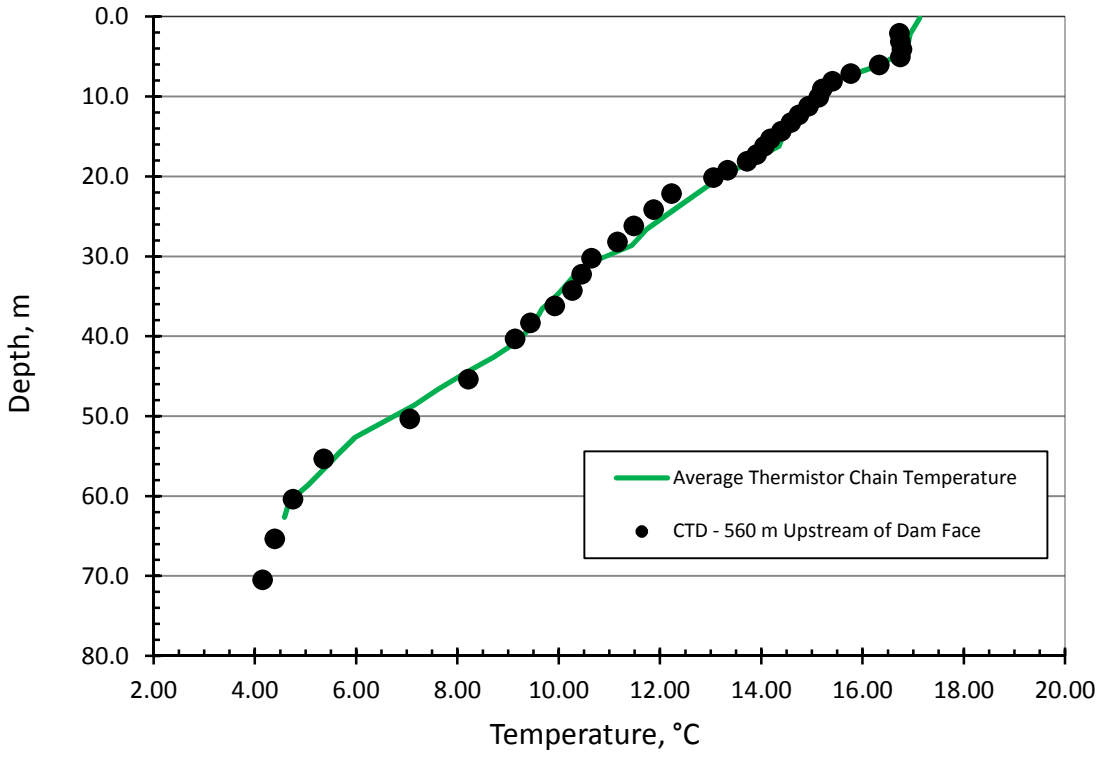

Figure 4.12a Comparison of average thermistor chain measurements and CTD measurement 560 m upstream of dam face, 09:30 August 8, 2011.

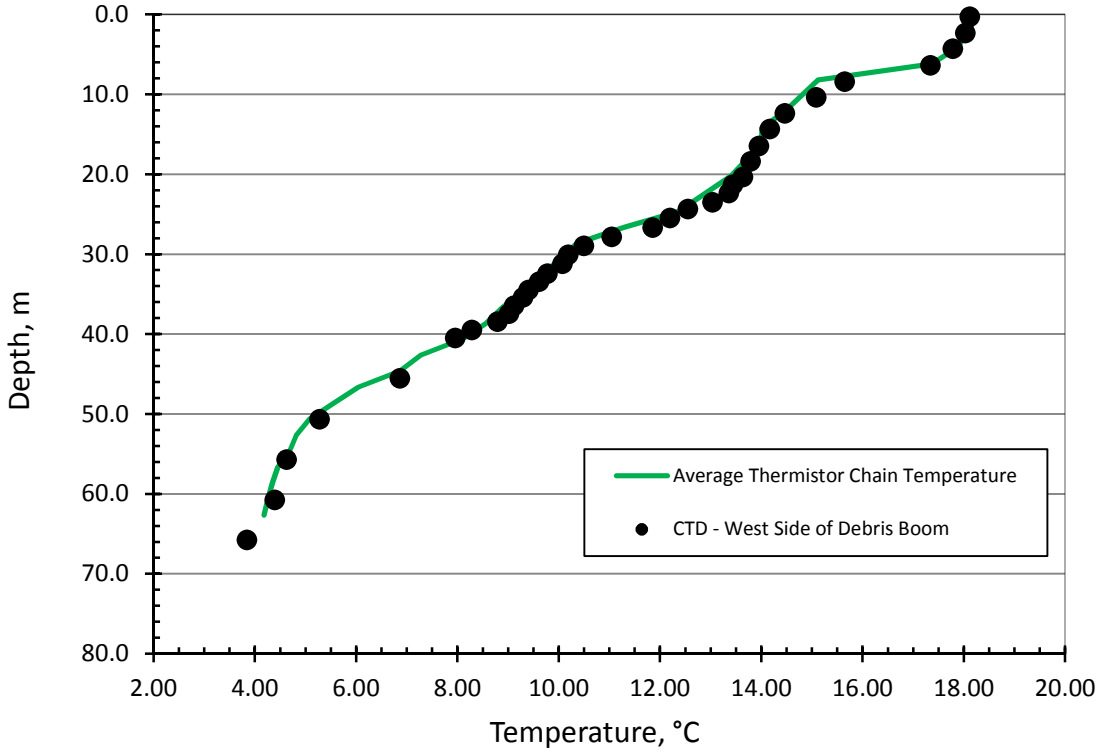

Figure 4.12b Comparison of average thermistor chain measurements and CTD measurement on west side of debris boom, 09:00 August 10, 2011.

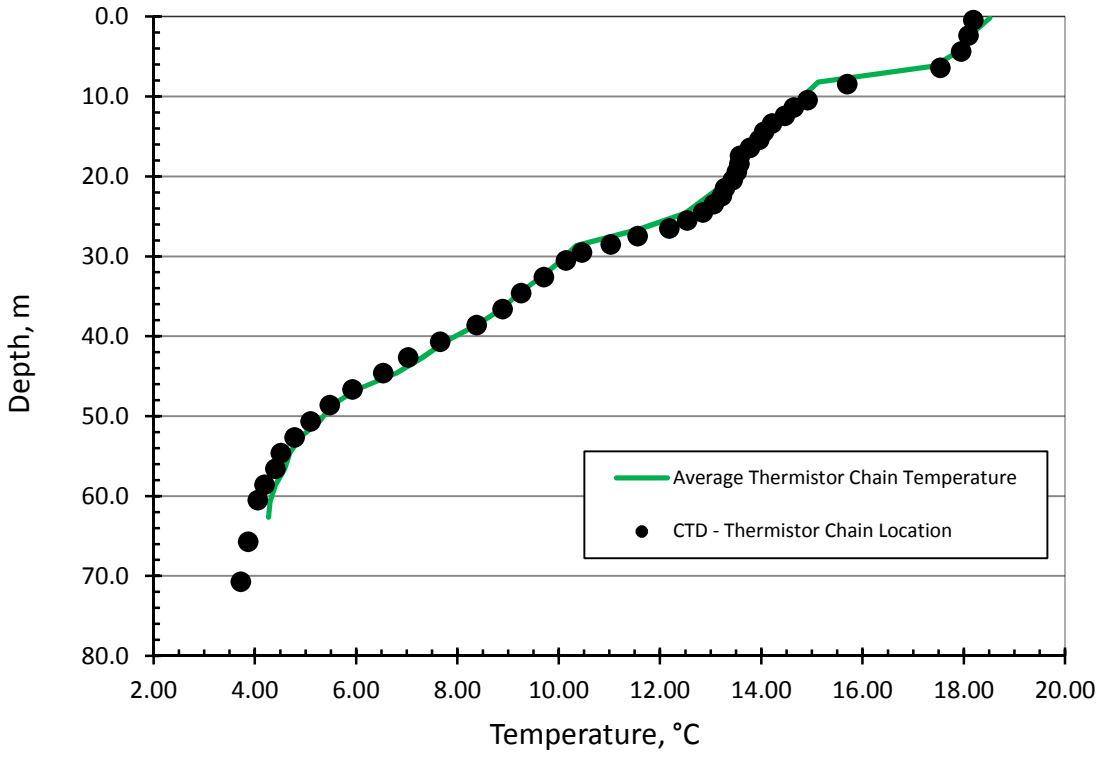

Figure 4.12c Comparison of average thermistor chain measurements (10:30) and CTD measurement at thermistor chain, 11:00 August 10, 2011.

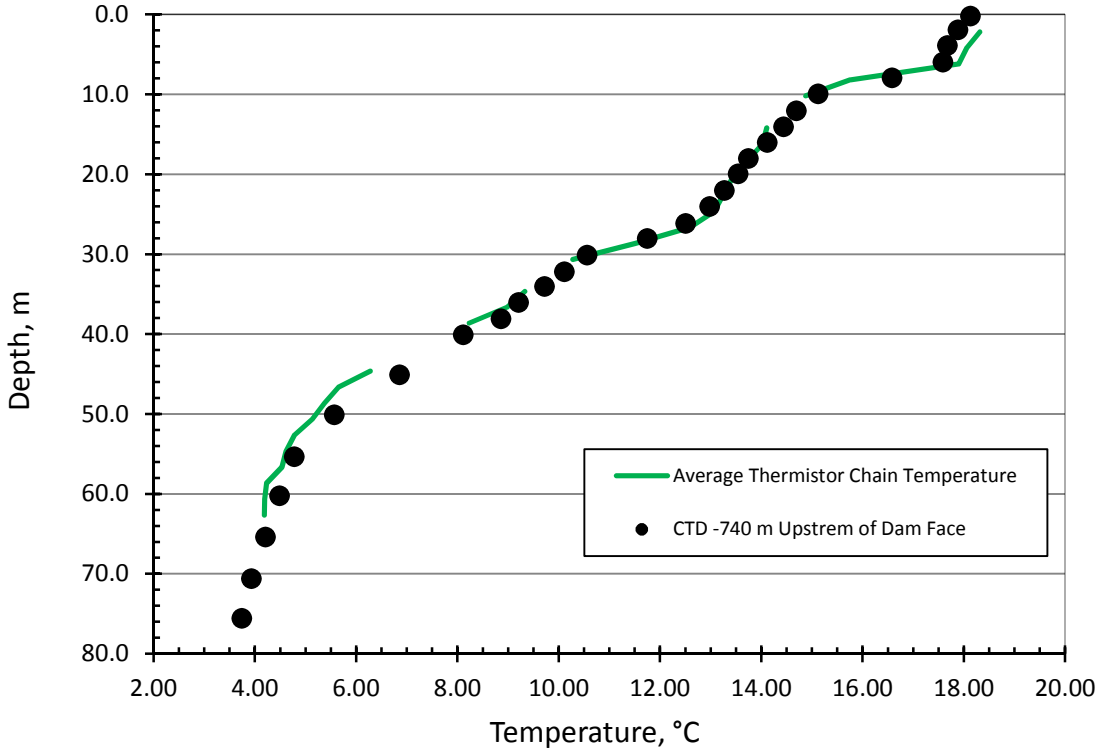

Figure 4.12d Comparison of average thermistor chain measurements and CTD measurement 740 m upstream of dam face, 13:25 August 10, 2011.

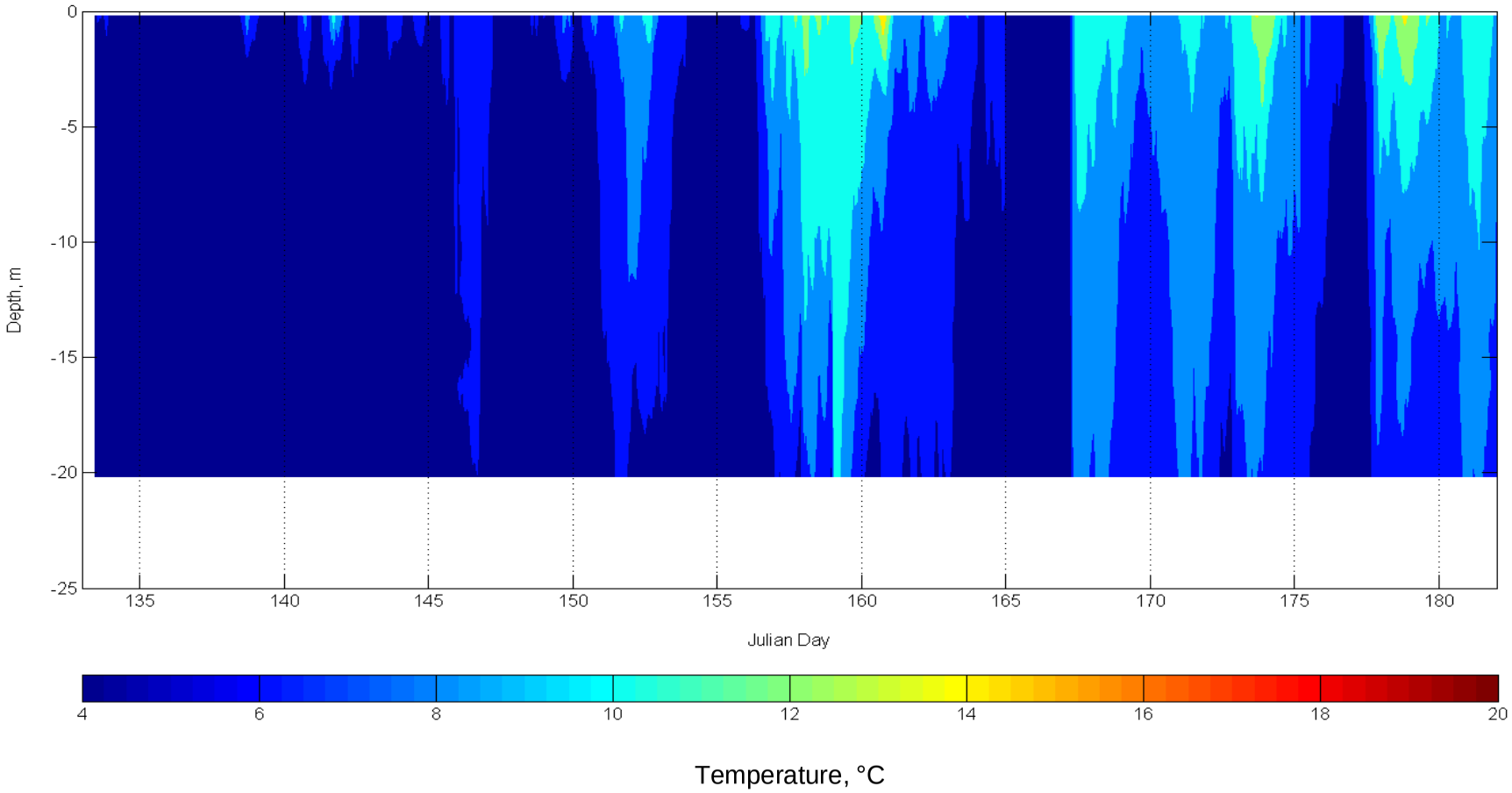

Figure 4.13a Thermistor chain mean hourly water temperature contours recorded in the MCA forebay in May and June, 2011.

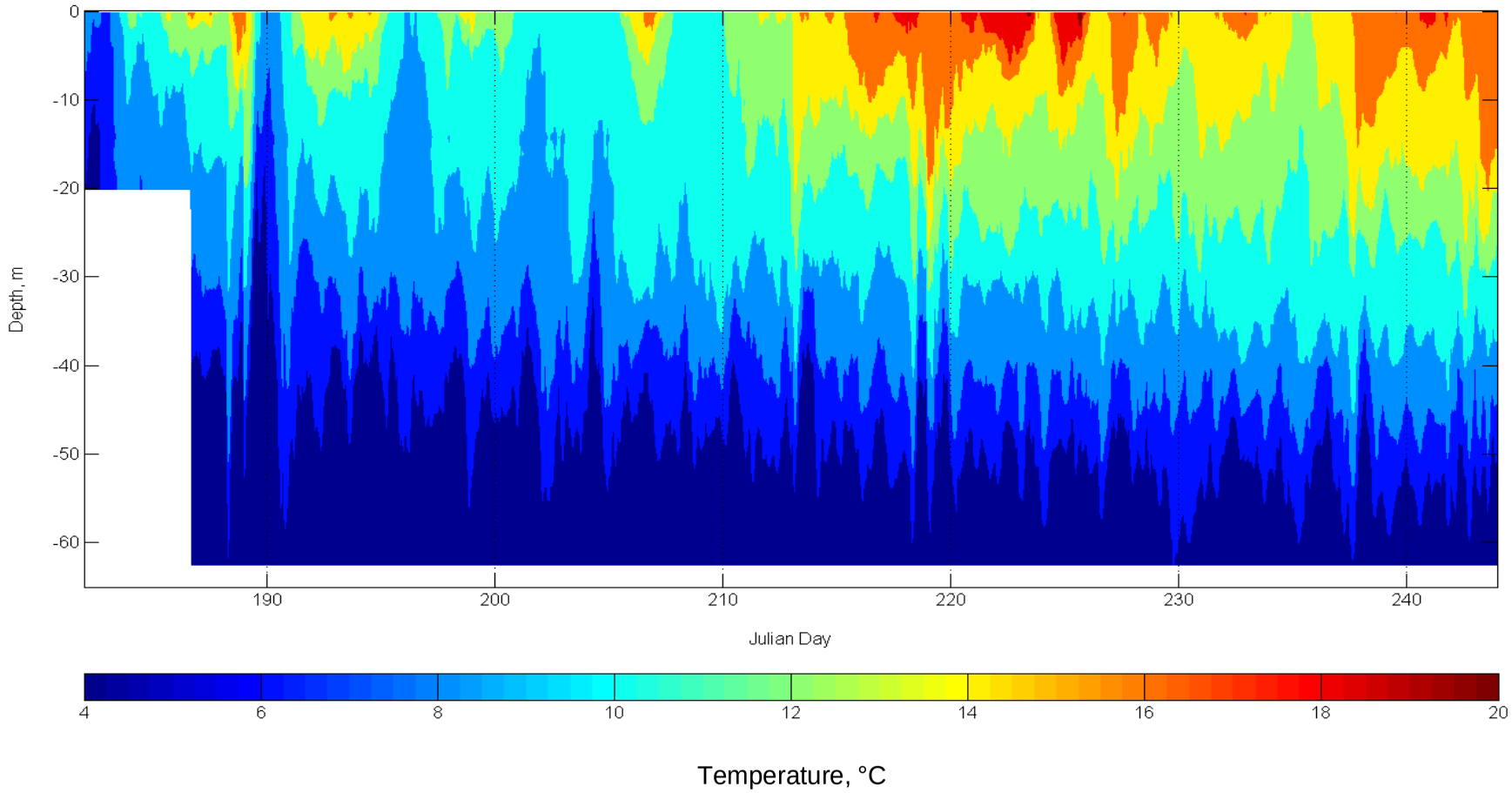

Figure 4.13b Thermistor chain mean hourly water temperature contours recorded in the MCA forebay in July and August 2011.

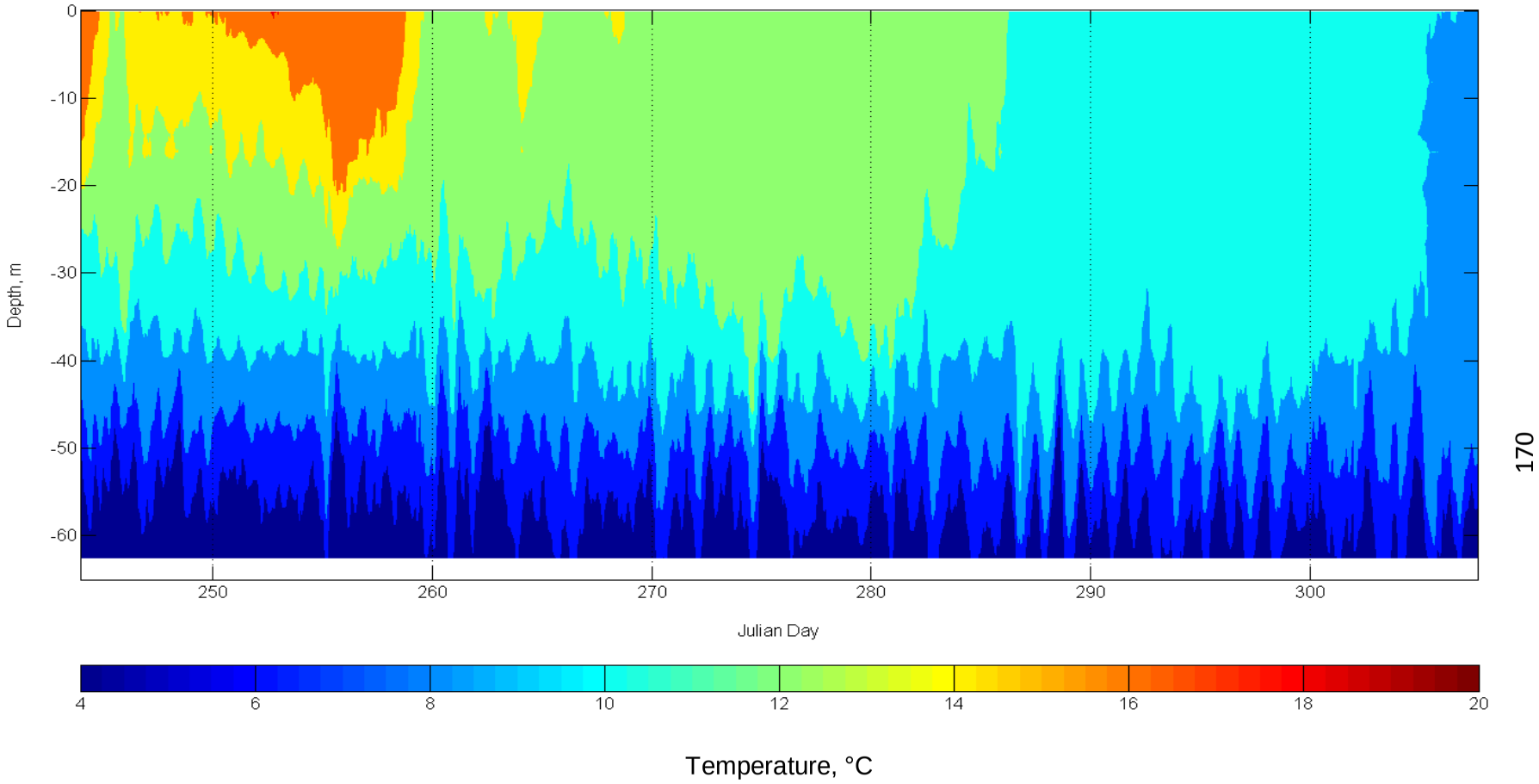

Figure 4.13b Thermistor chain mean hourly water temperature contours recorded in the MCA forebay in September and October, 2011.

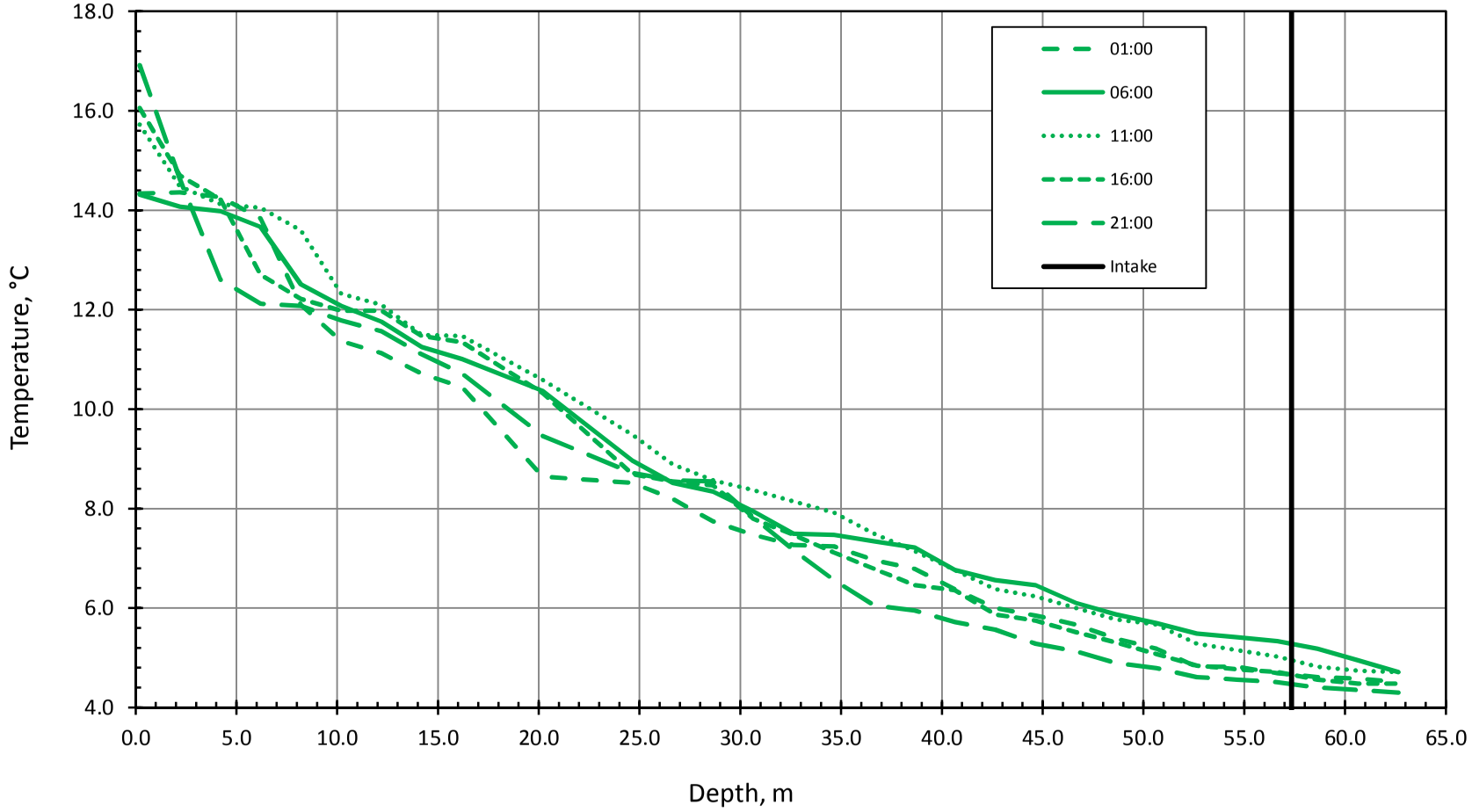

Figure 4.14a Typical hourly water temperature profiles in July (July 11, 2011).

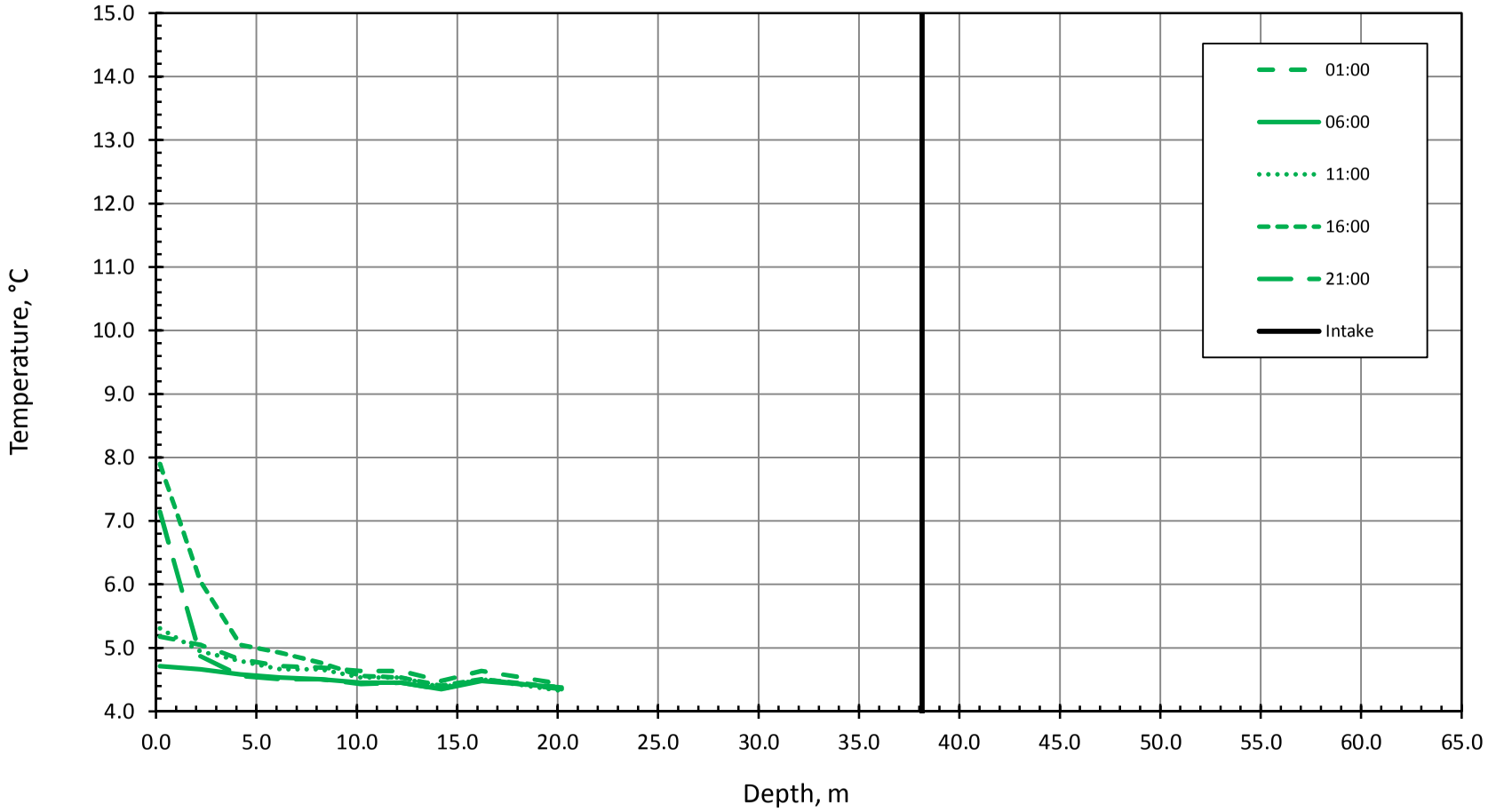

Figure 4.14b Typical hourly water temperature profiles in May (May 23, 2011).

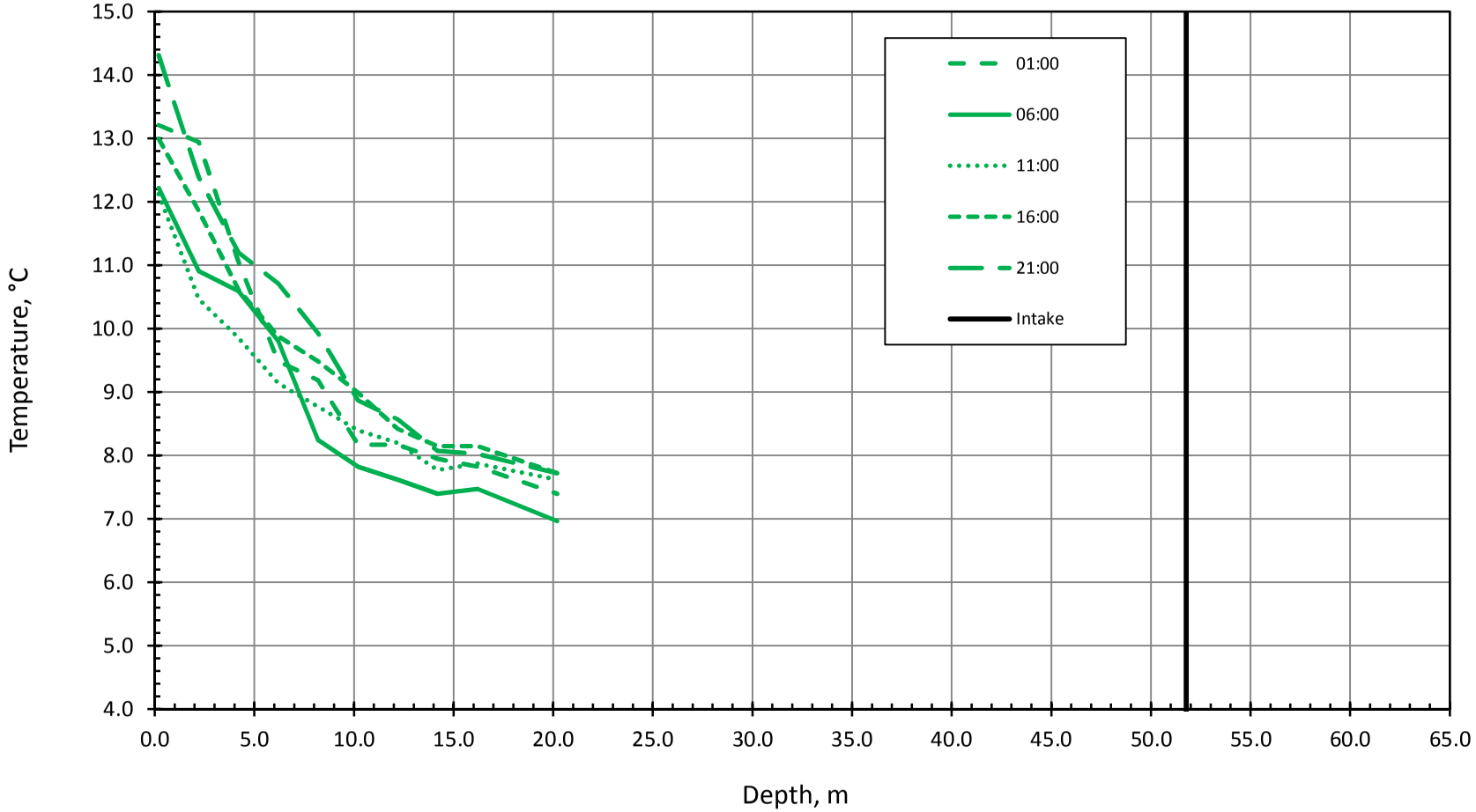

Figure 4.14c Typical hourly water temperature profiles in June (June 27, 2011).

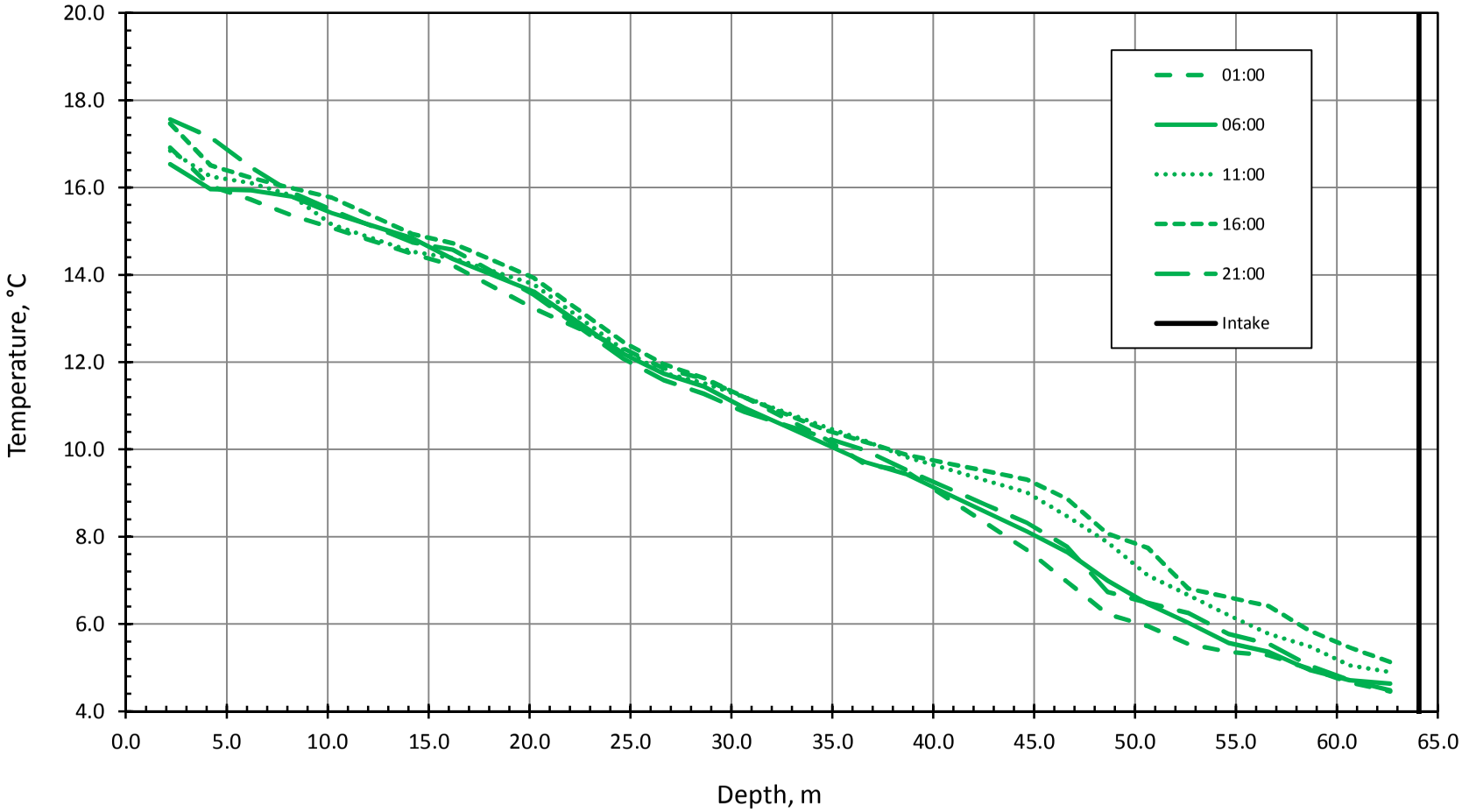

Figure 4.14d Typical hourly water temperature profiles in August (August 28, 2011).

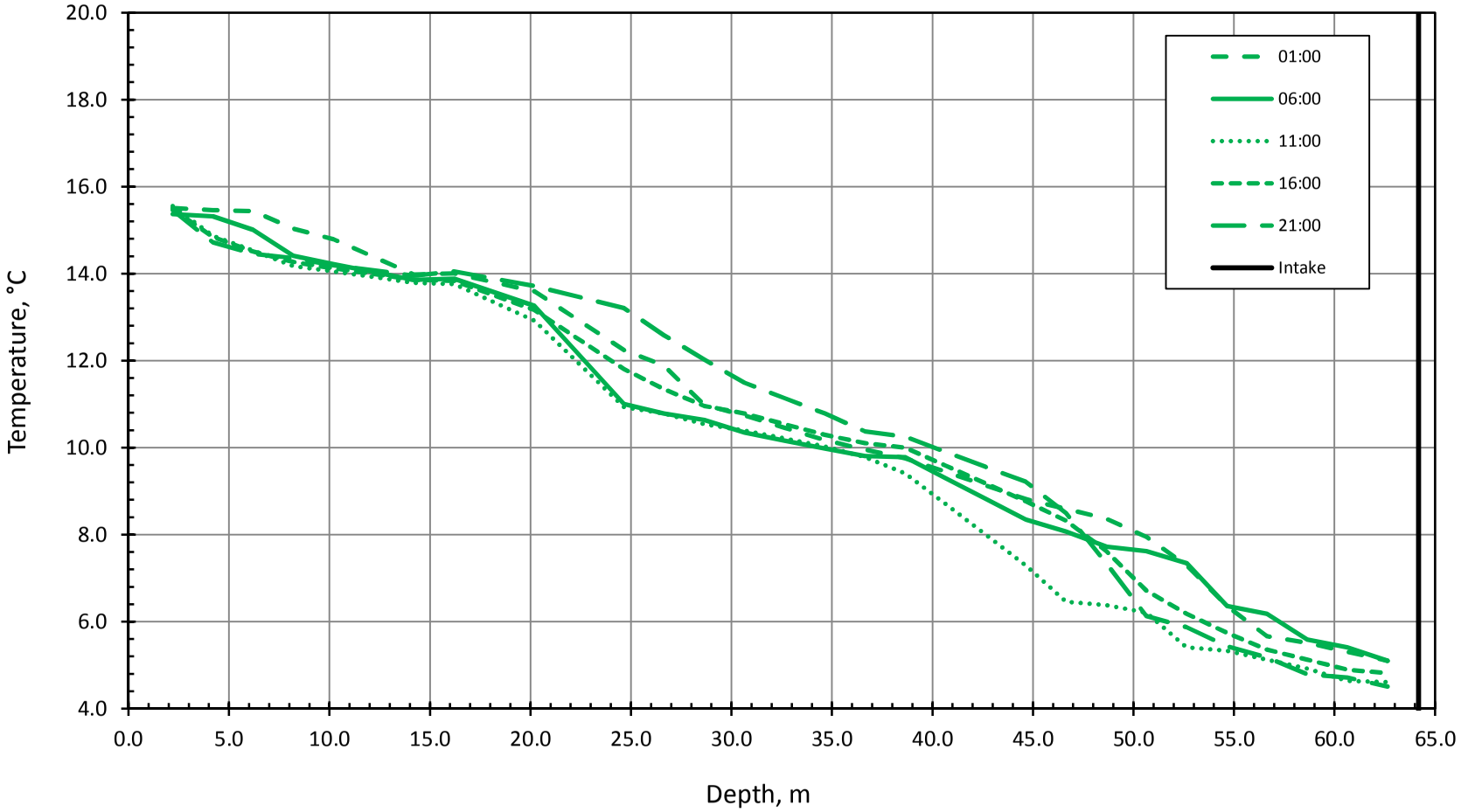

Figure 4.14e Typical hourly water temperature profiles in early September (September 4, 2011).

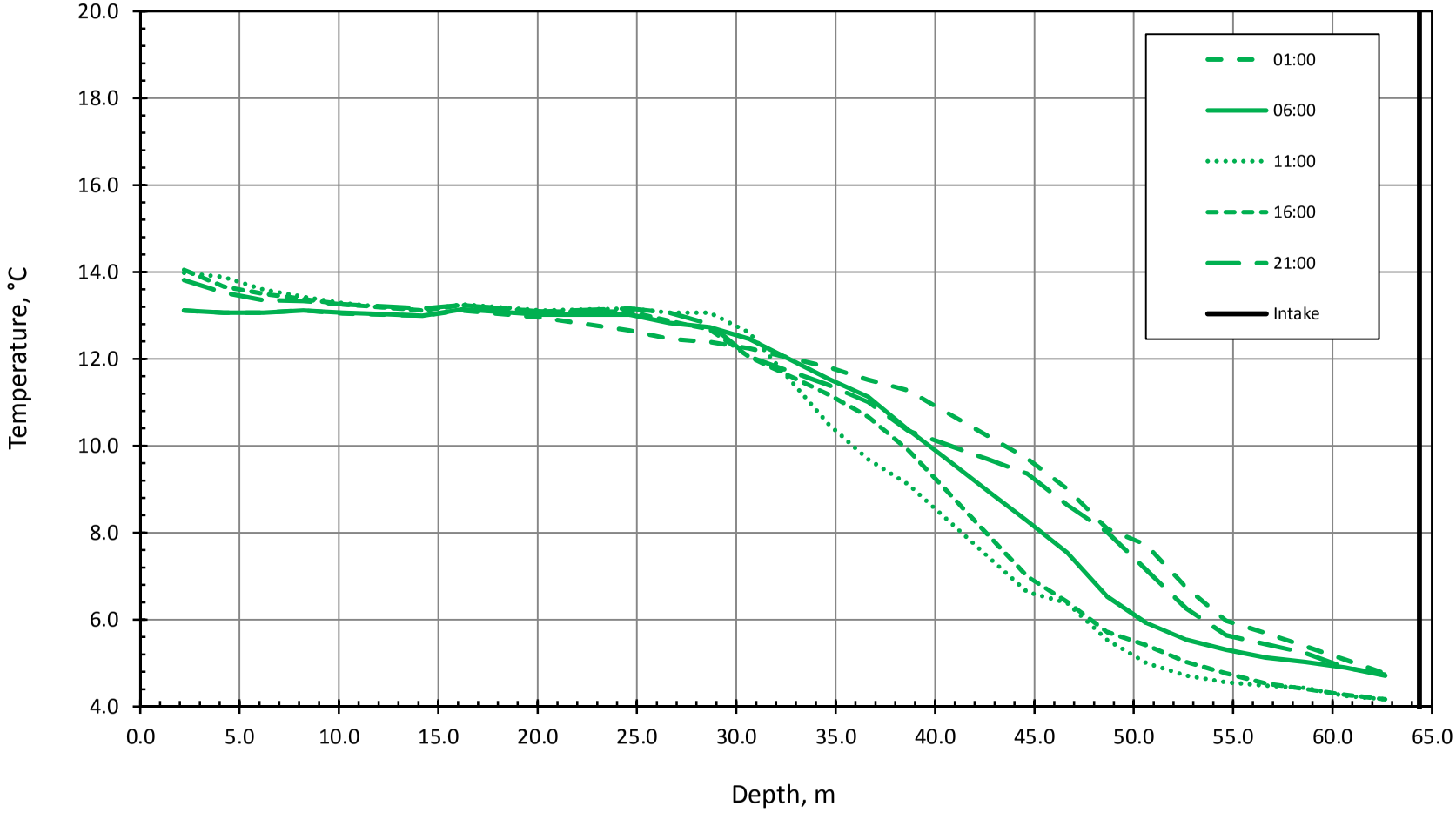

Figure 4.14f Typical hourly water temperature profiles in late September (September 19, 2011).

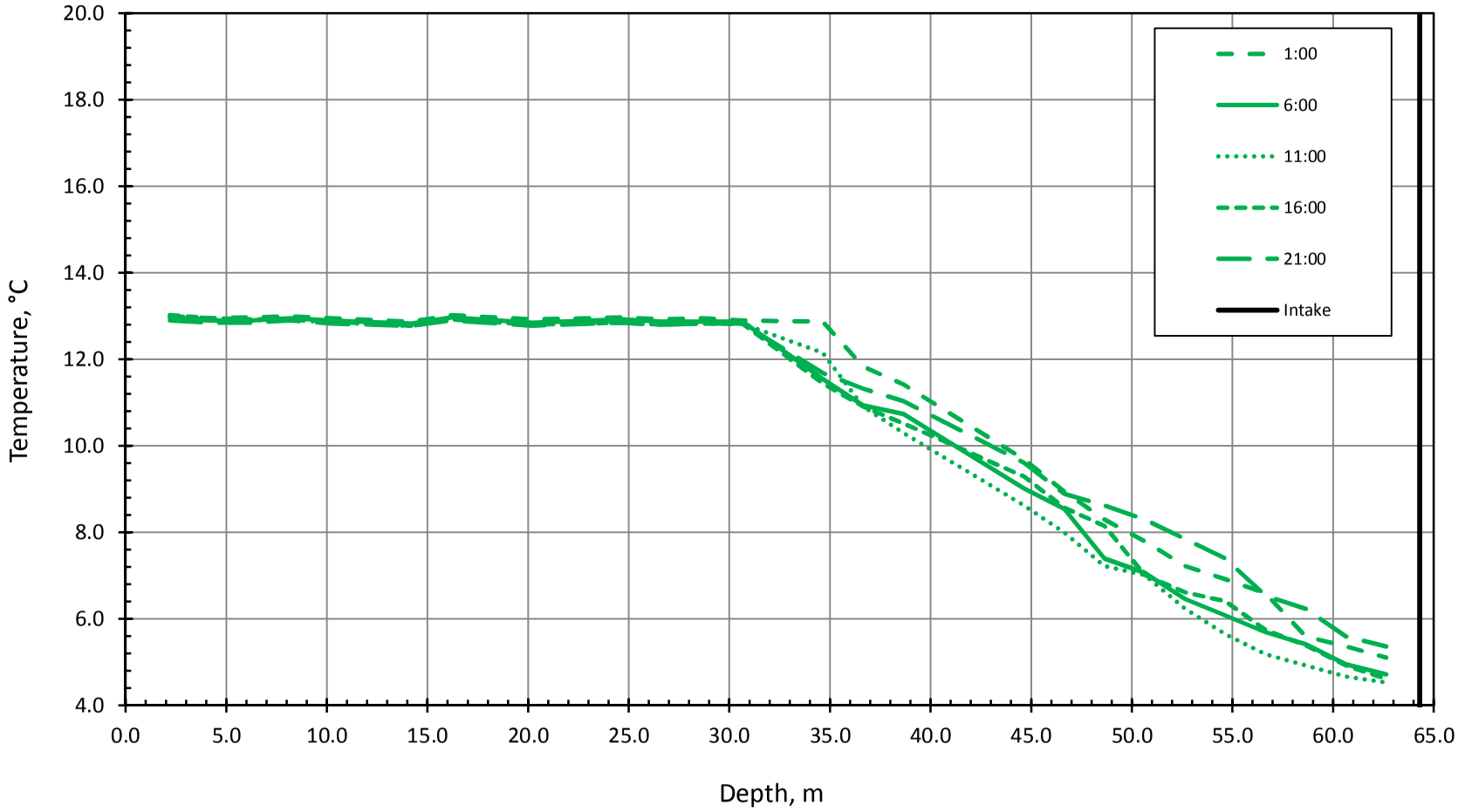

Figure 4.14g Typical hourly water temperature profiles in early October (October 8, 2011).

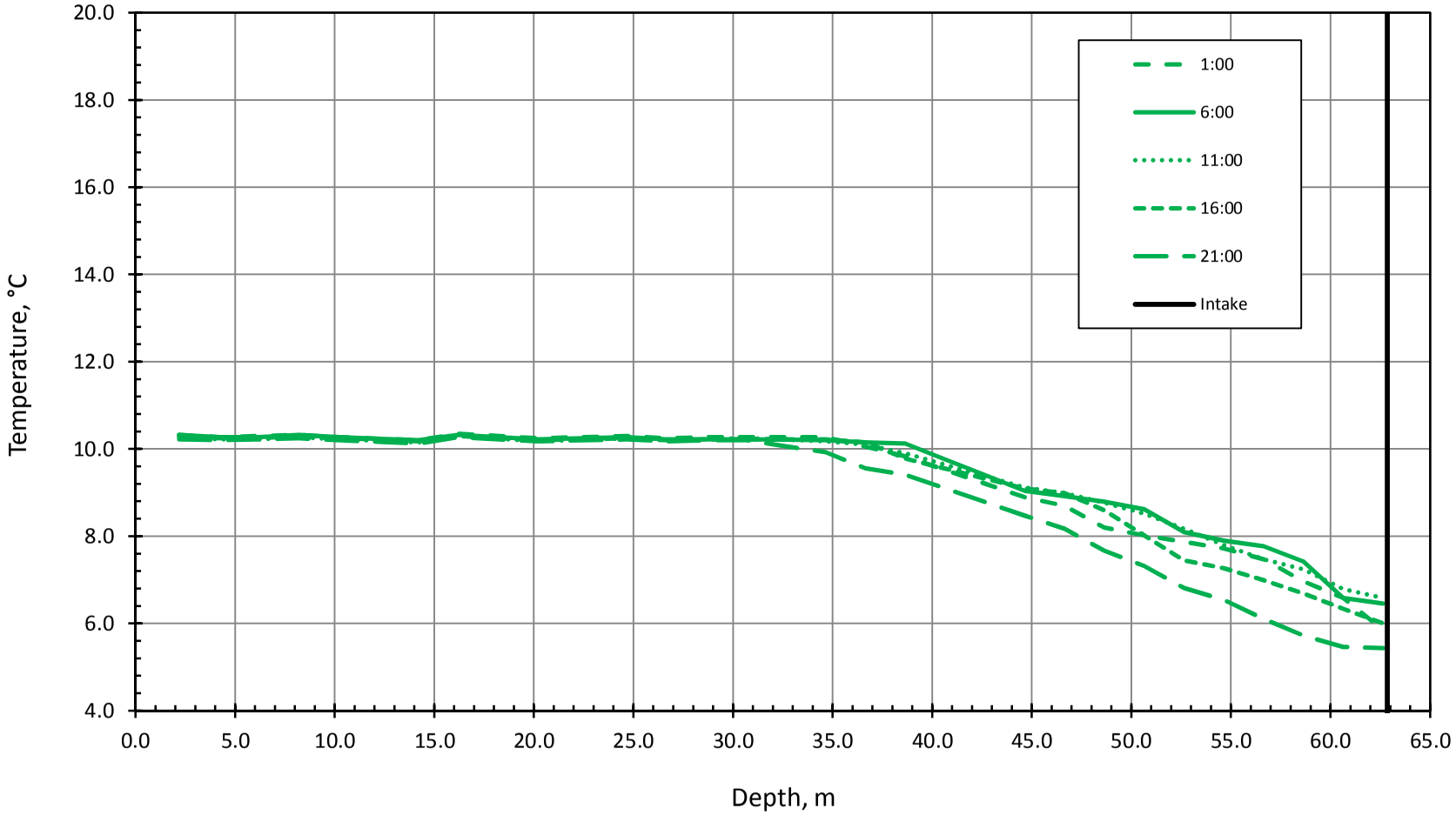

Figure 4.14h Typical hourly water temperature profiles in late October (October 30, 2011).

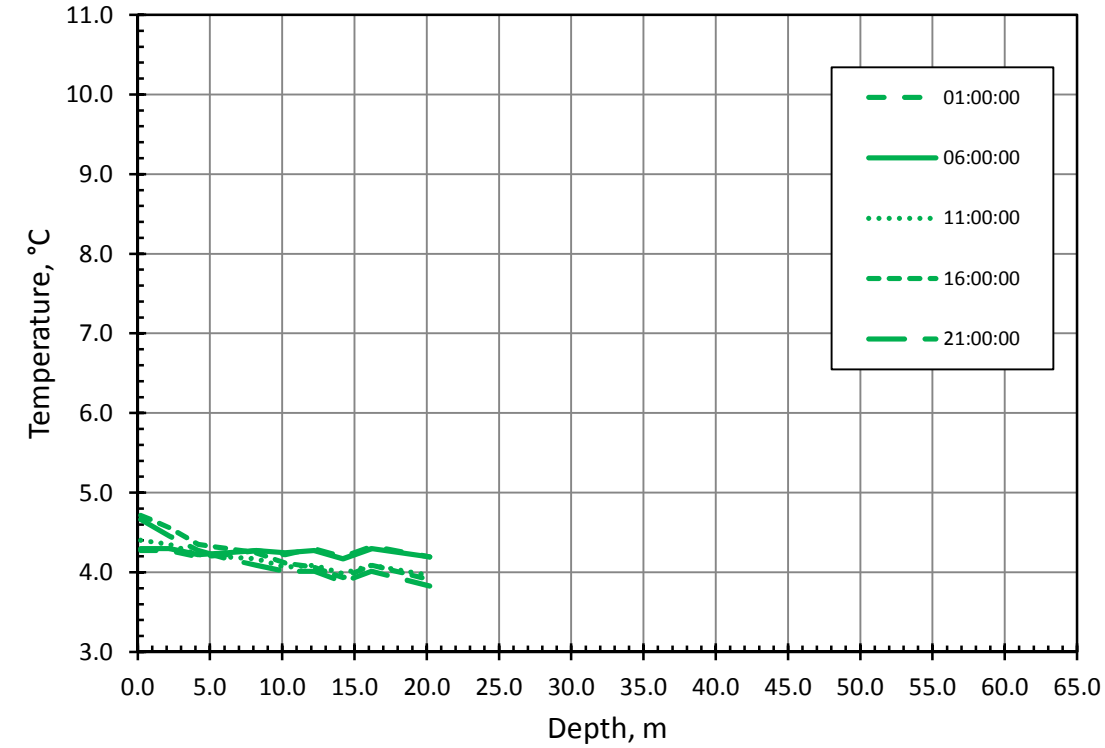

Figure 4.15a Water temperature profiles at MCA on May 17, 2011.

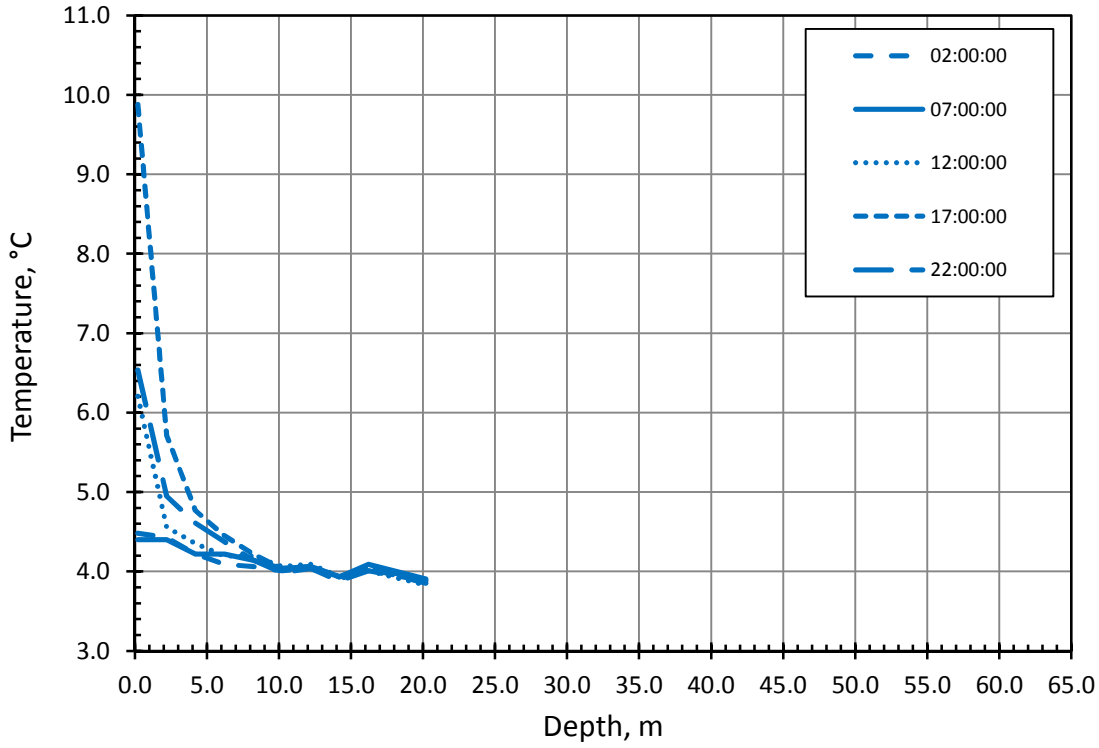

Figure 4.15b Water temperature profiles at MCA on May 18, 2011.

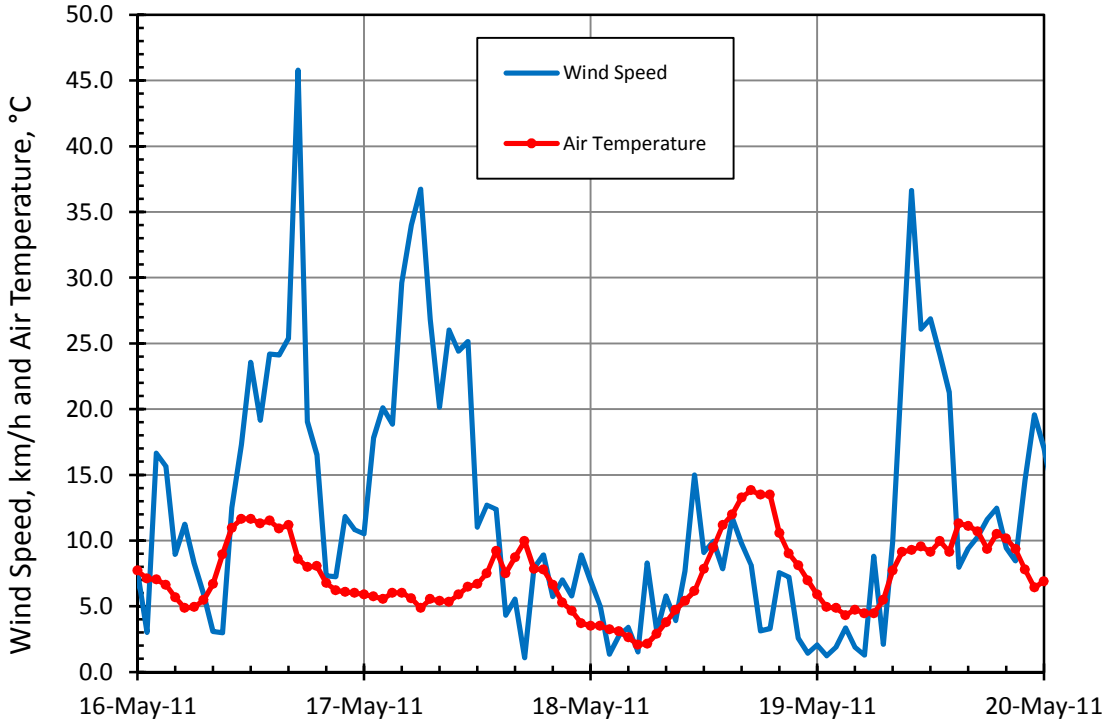

Figure 4.16a Air temperature and wind speed at MCA on May 16 - May 20, 2011.

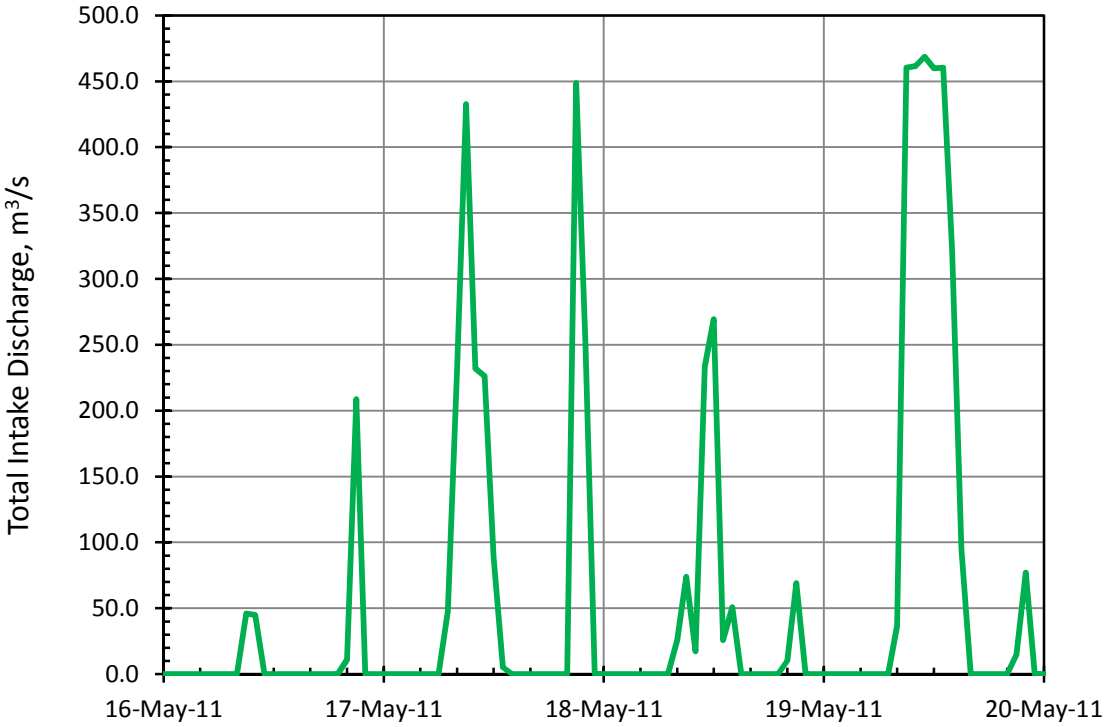

Figure 4.16b Total discharge from MCA on May 16 - May 20, 2011.

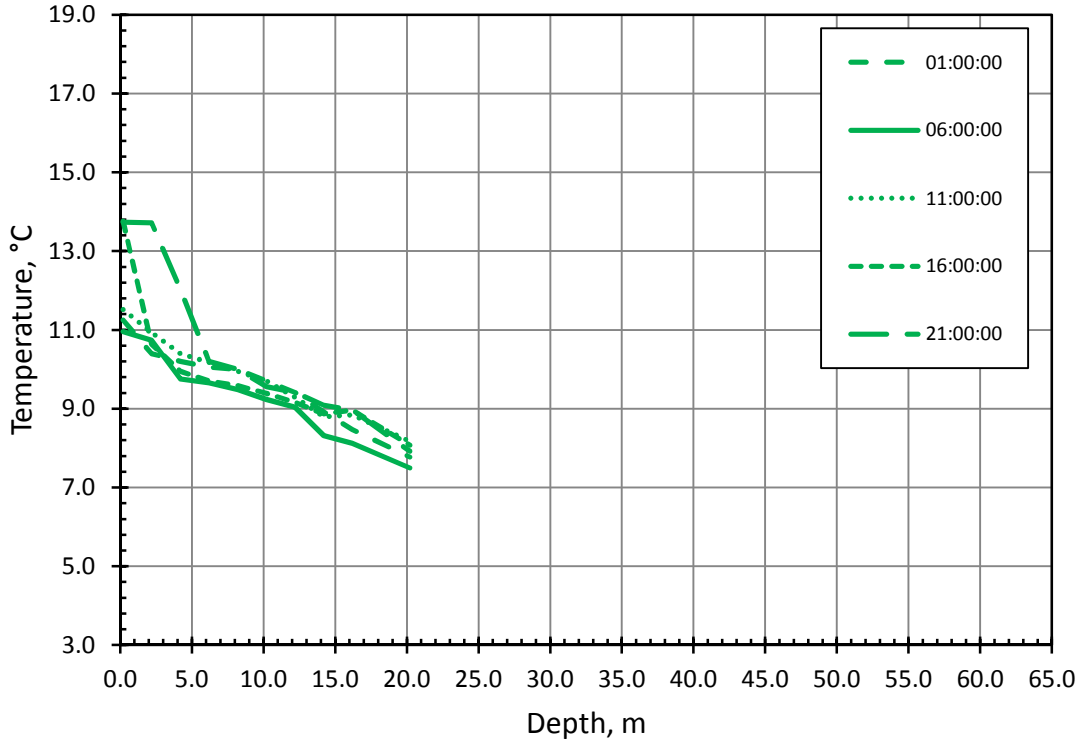

Figure 4.17 Water temperature profiles at MCA on June 22 2011.

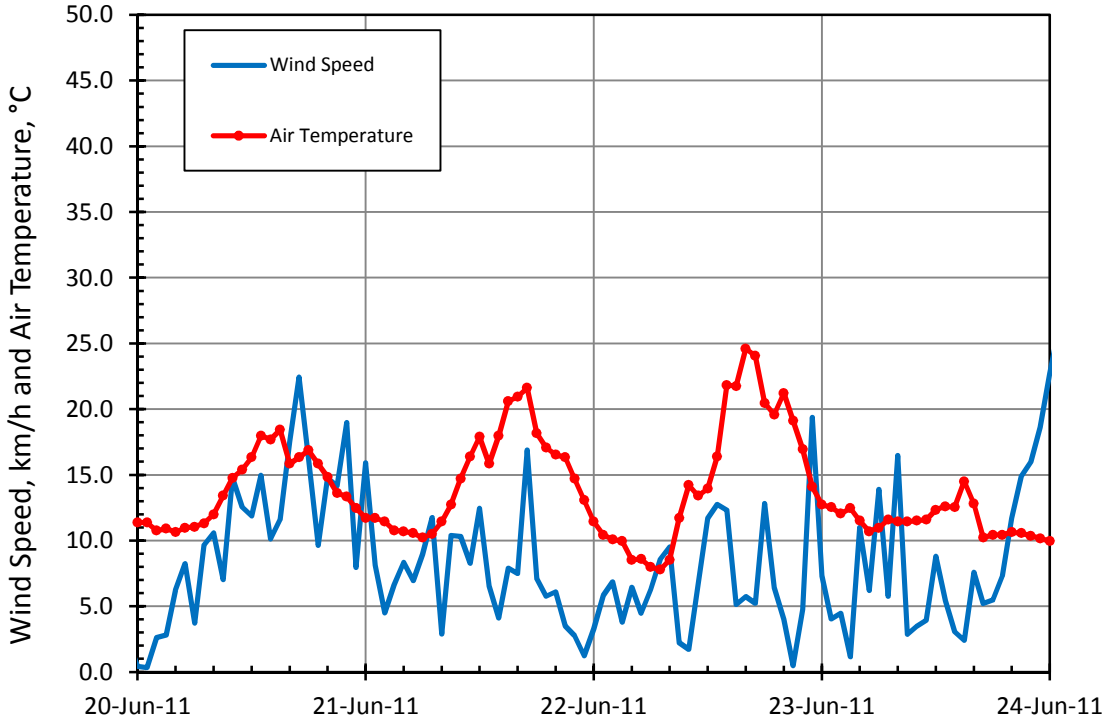

Figure 4.18a Air temperature and wind speed at MCA on June 20 - June 24, 2011.

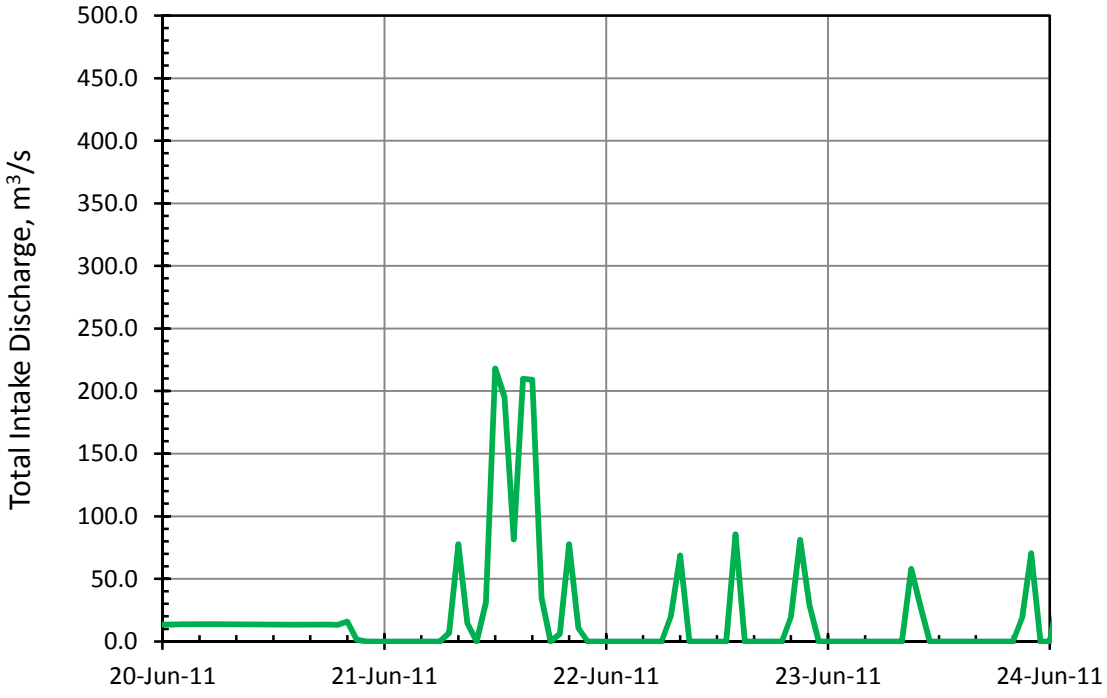

Figure 4.18b Total discharge from MCA on June 20 - June 24, 2011.

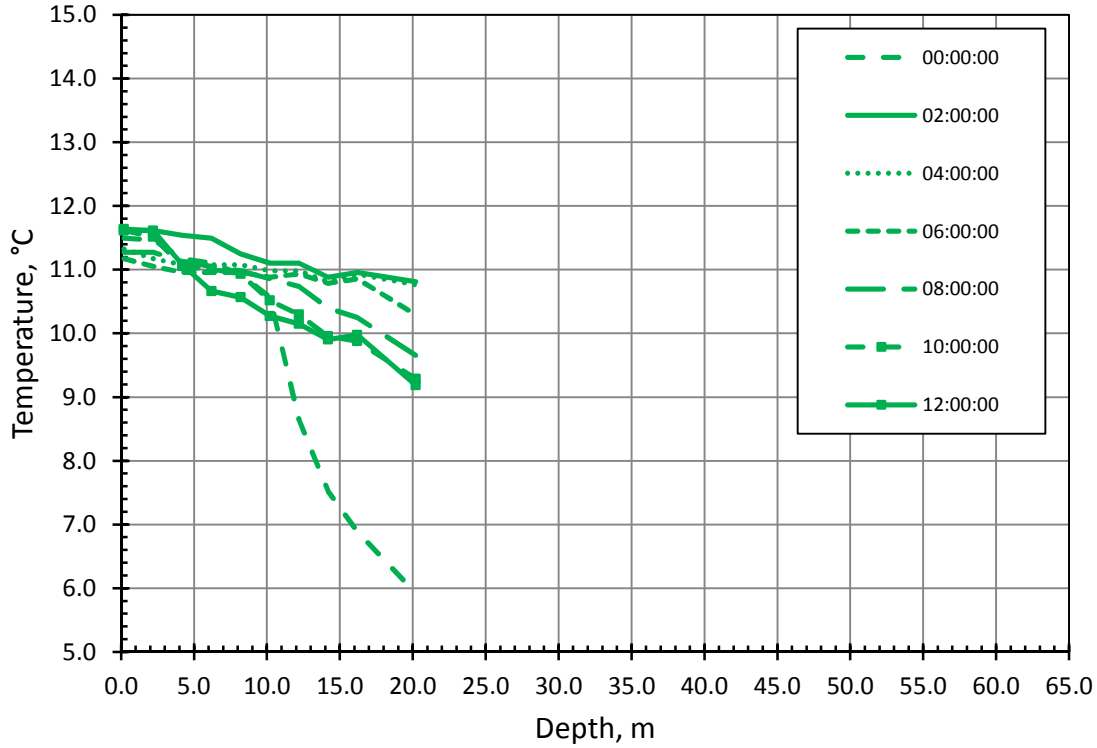

Figure 4.19a Water temperature profiles at MCA on morning of June 8, 2011.

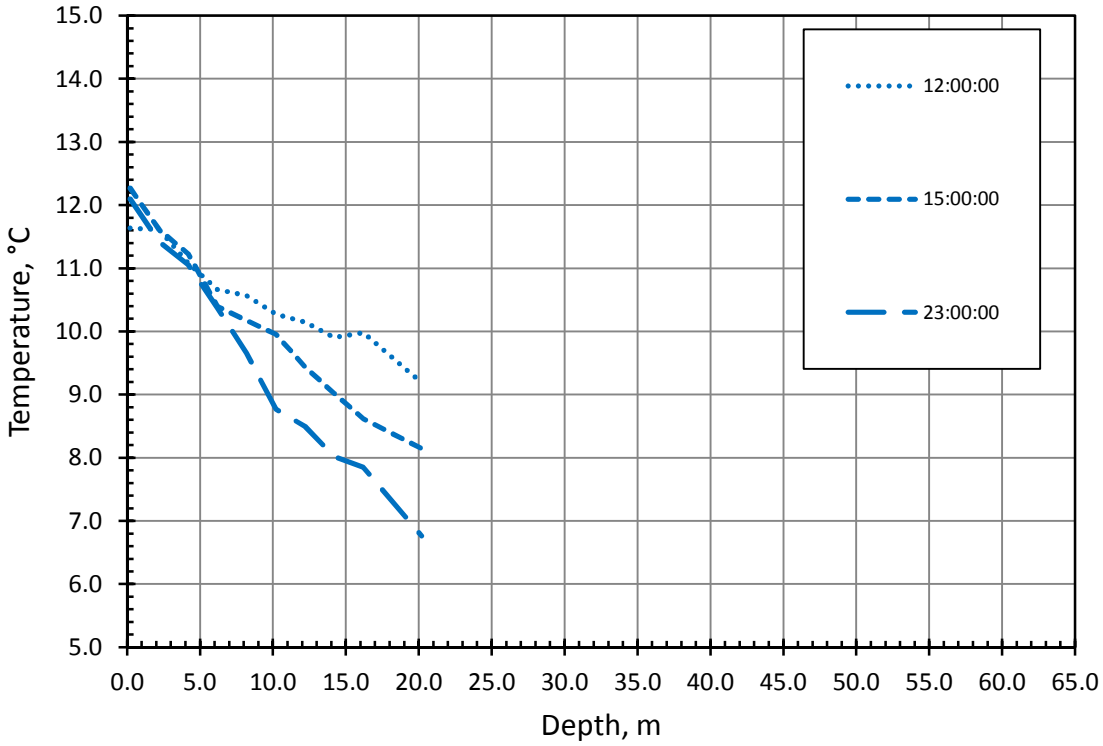

Figure 4.19b Water temperature profiles at MCA on afternoon of June 8, 2011.

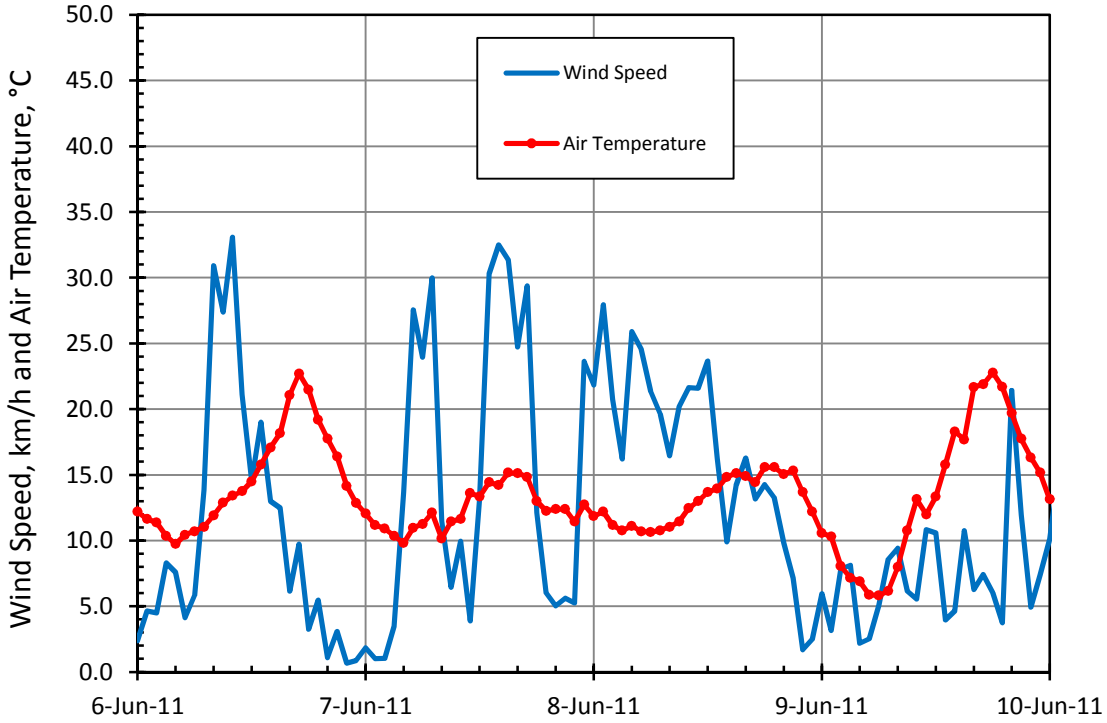

Figure 4.20a Air temperature and wind speed at MCA on June 6 - June 10, 2011.

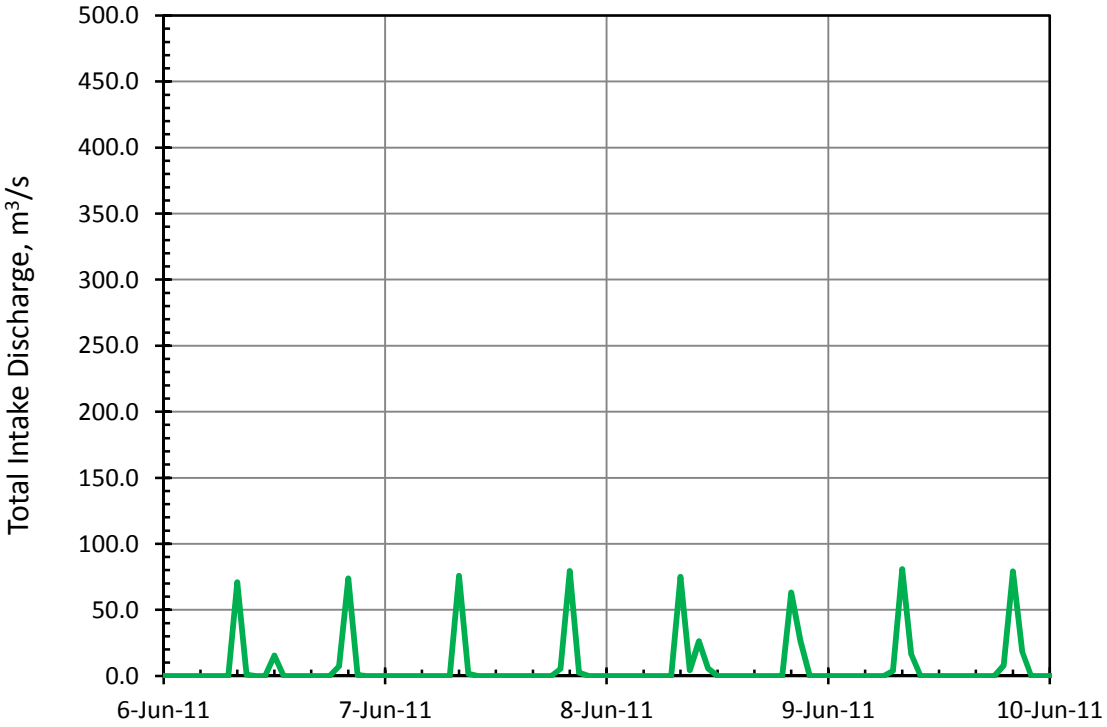

Figure 4.20b Total discharge from MCA on June 6 - June 10, 2011.

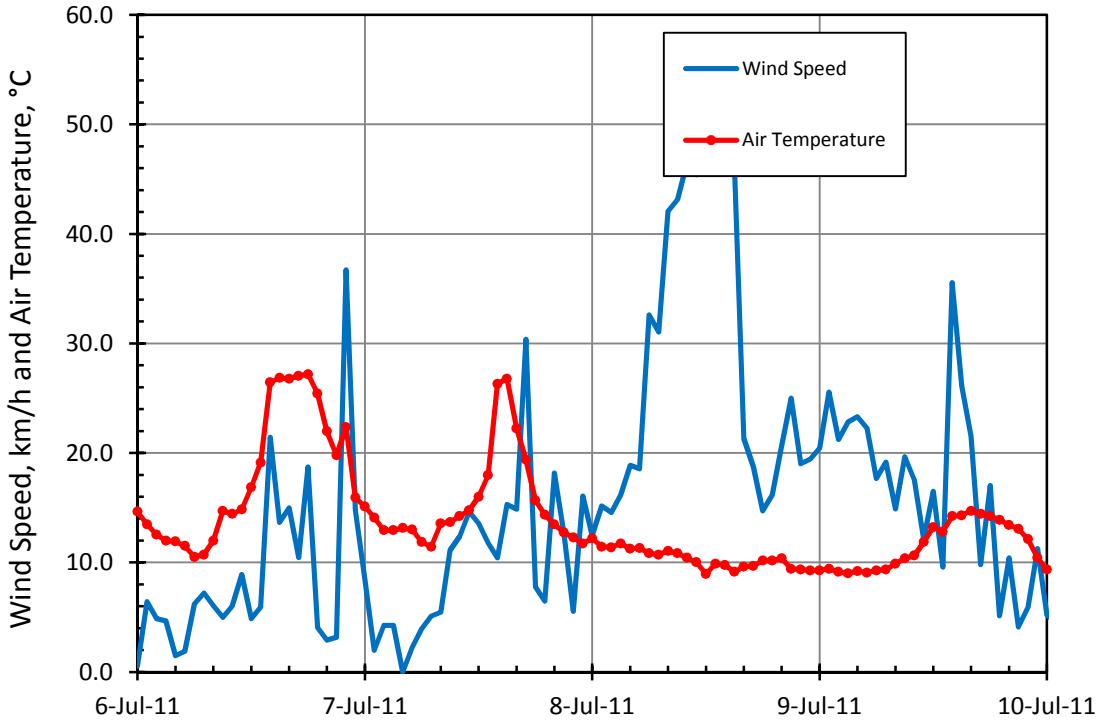

Figure 4.21a Air temperature and wind speed at MCA on July 6 - July 10, 2011.

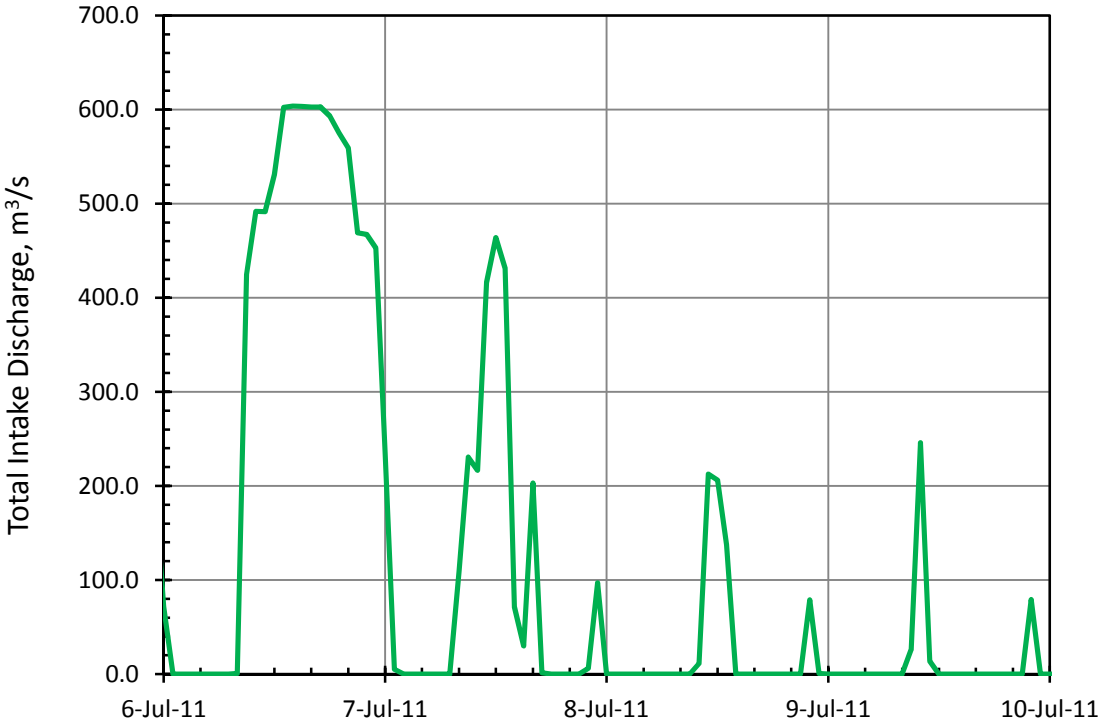

Figure 4.21b Total discharge from MCA on July 6 - July 10, 2011.

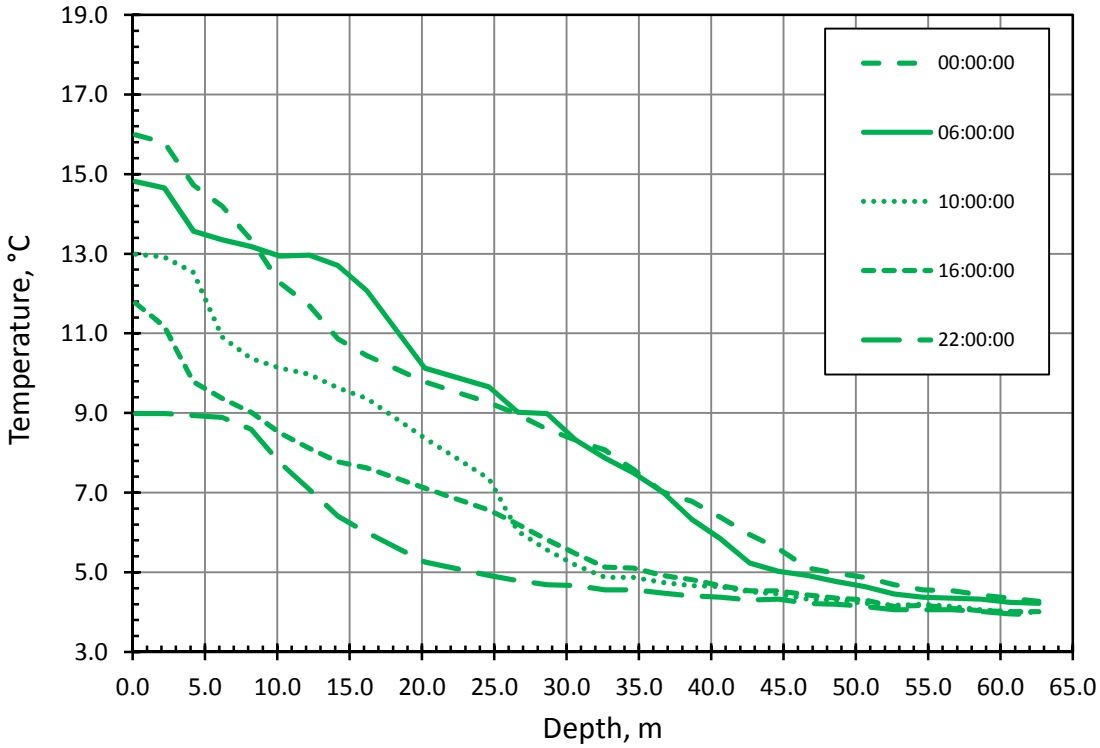

Figure 4.22 Water temperature profiles at MCA on July 8, 2011.

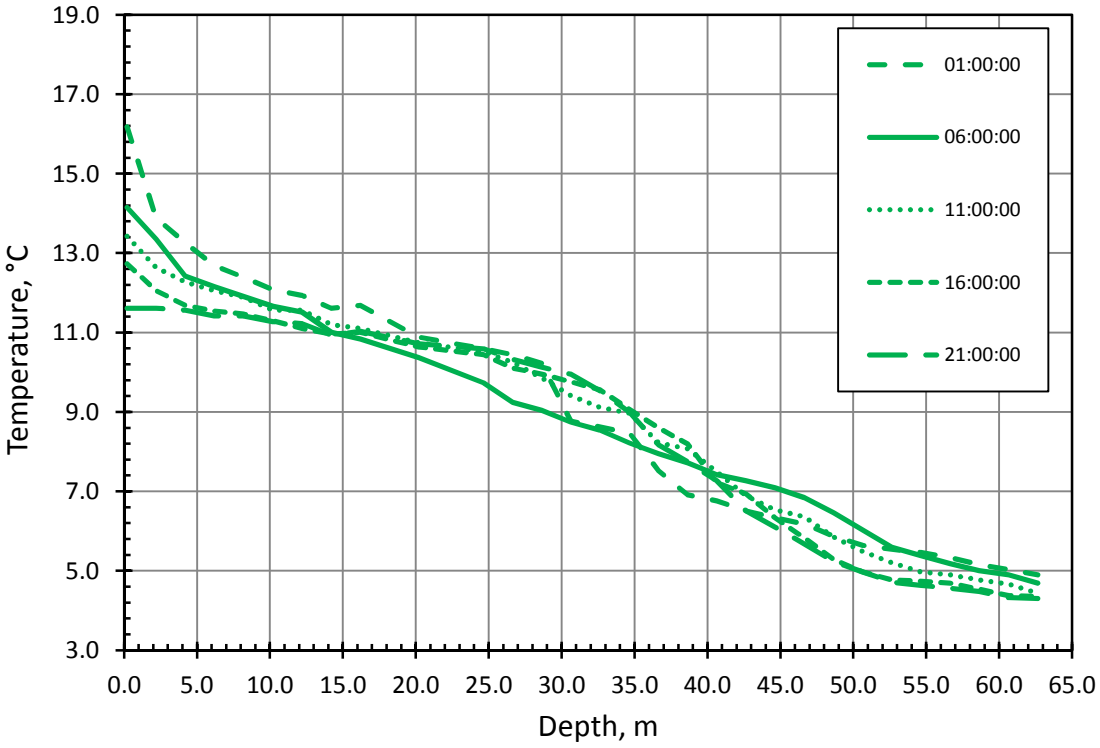

Figure 4.23a Water temperature profiles at MCA on July 26, 2011.

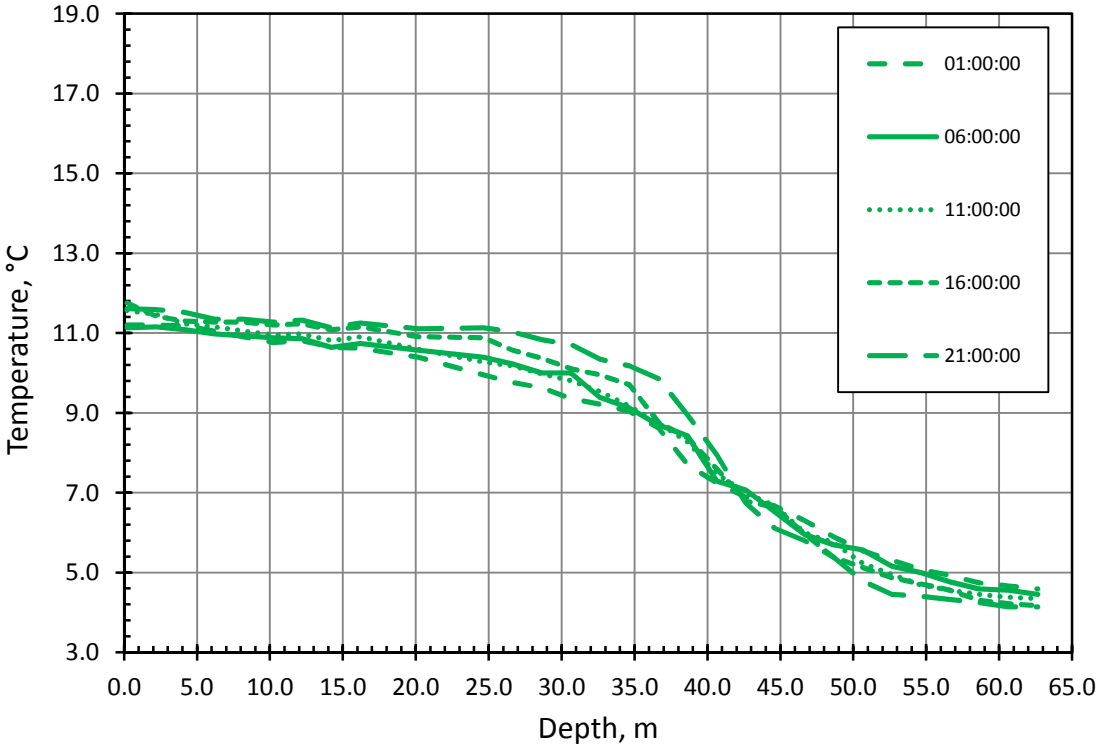

Figure 4.23b Water temperature profiles at MCA on July 28, 2011.

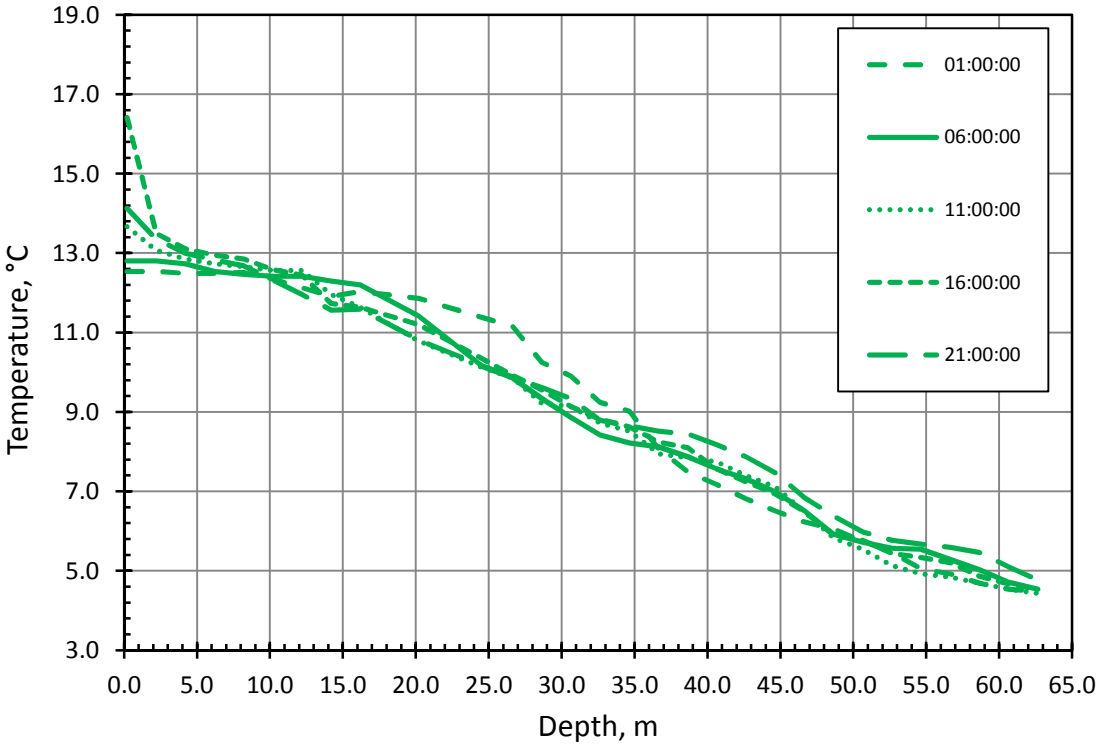

Figure 4.23c Water temperature profiles at MCA on July 30, 2011.

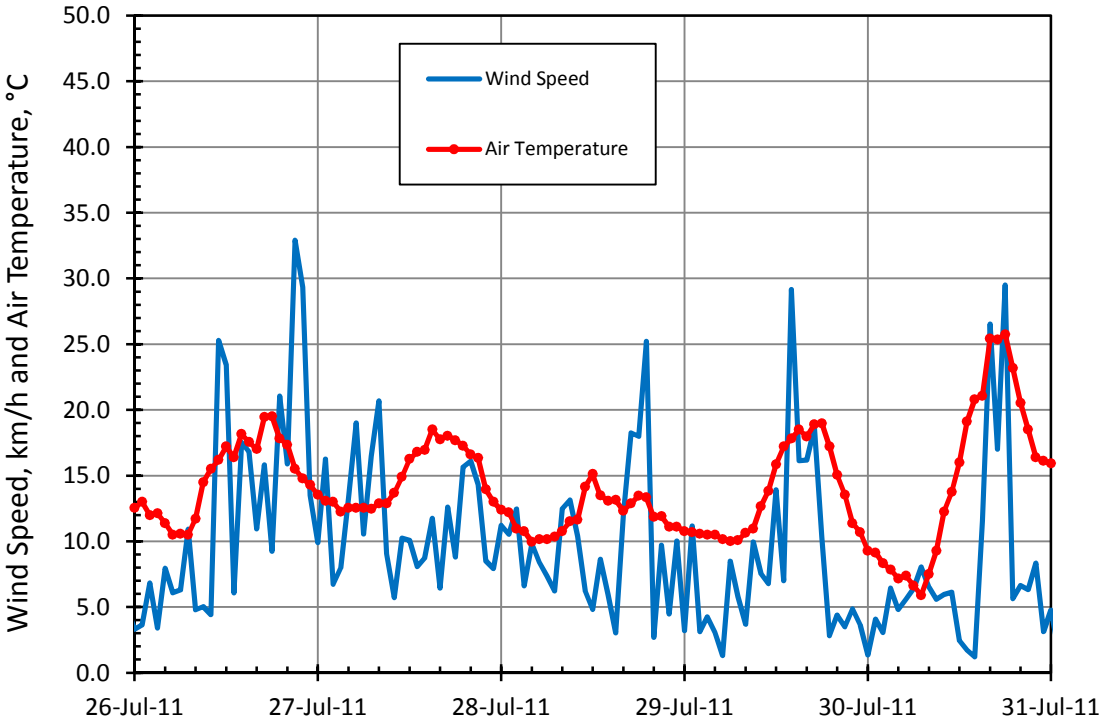

Figure 4.24 Air temperature and wind speed at MCA on July 26 - July 30, 2011.

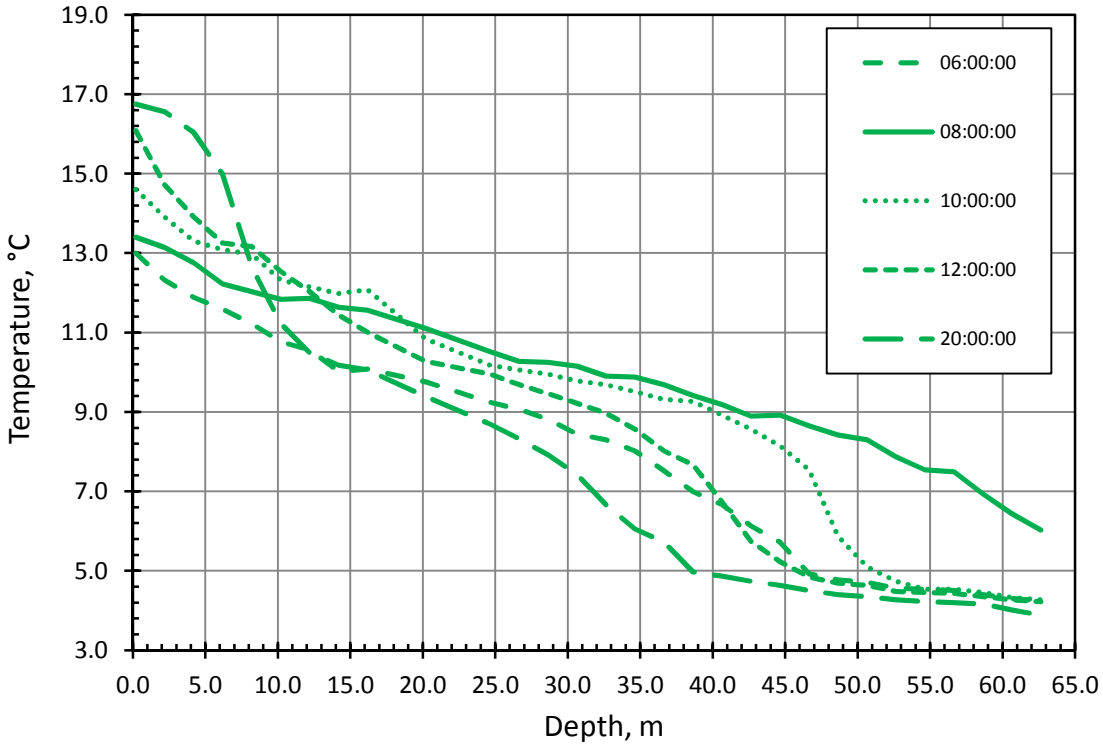

Figure 4.25a Water temperature profiles at MCA on July 7, 2011.

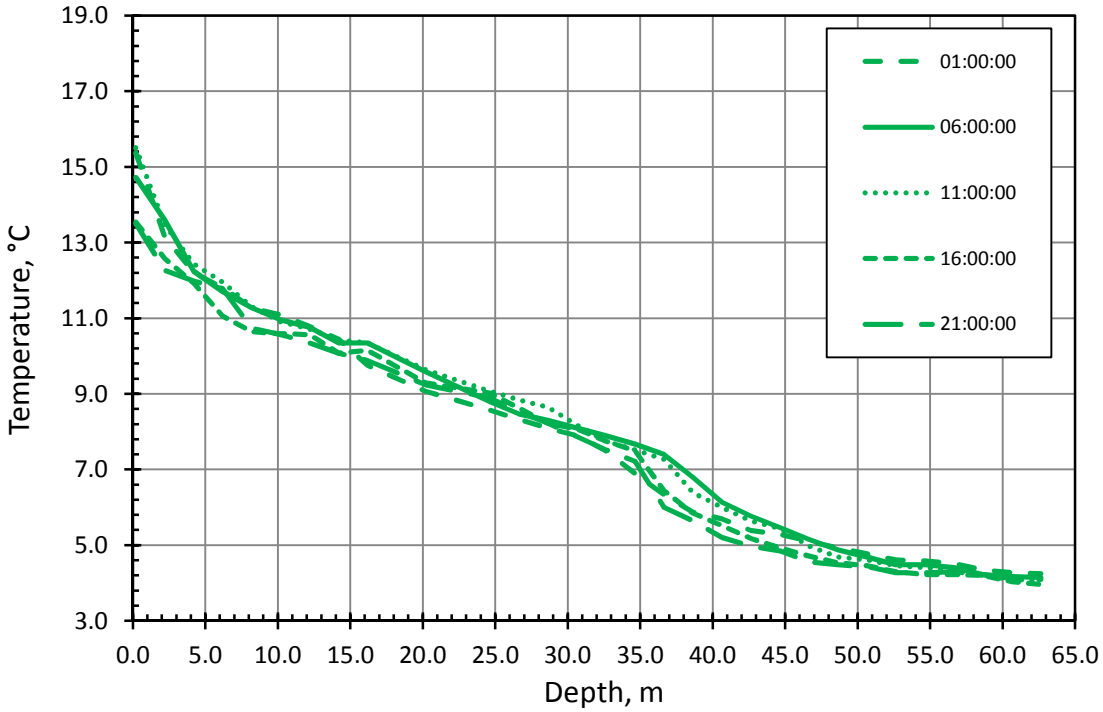

Figure 4.25b Water temperature profiles at MCA on July 6, 2011.

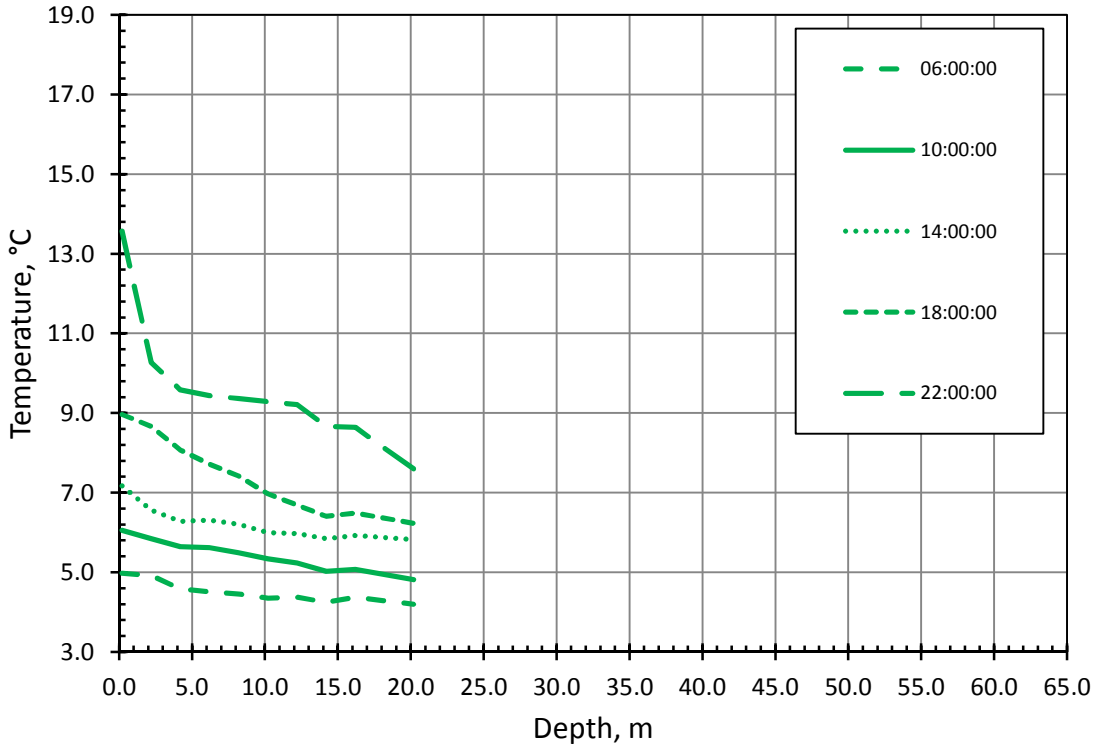

Figure 4.26a Water temperature profiles at MCA on June 26, 2011.

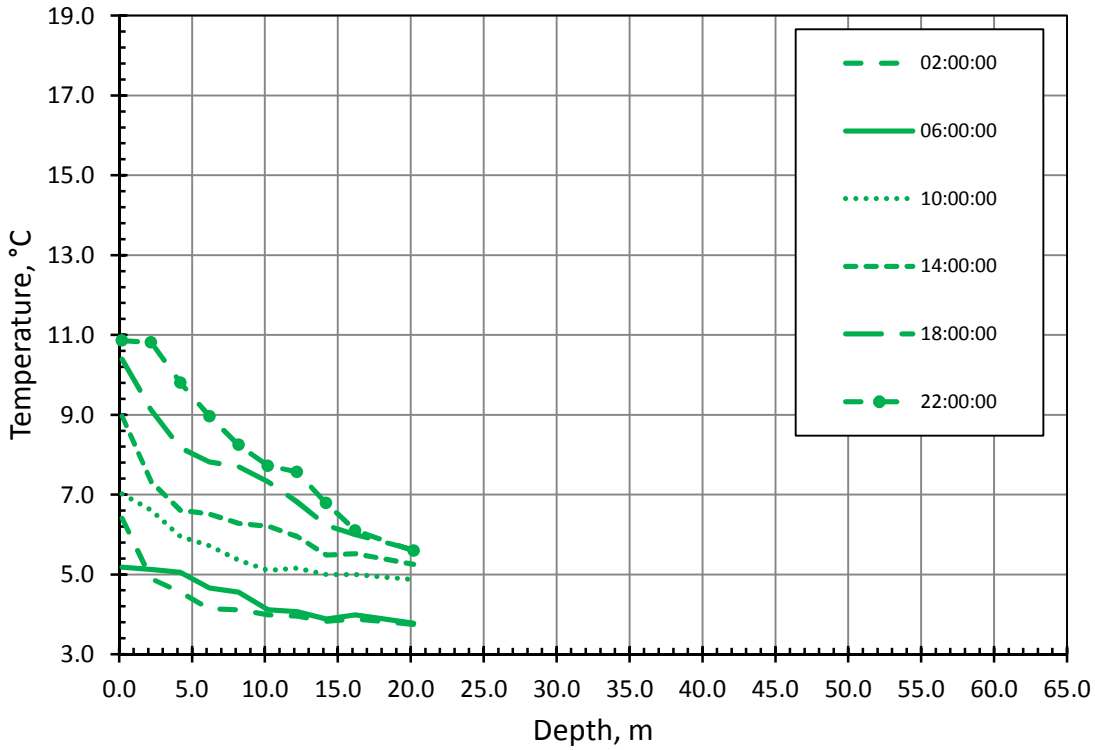

Figure 4.26b Water temperature profiles at MCA on June 5, 2011.

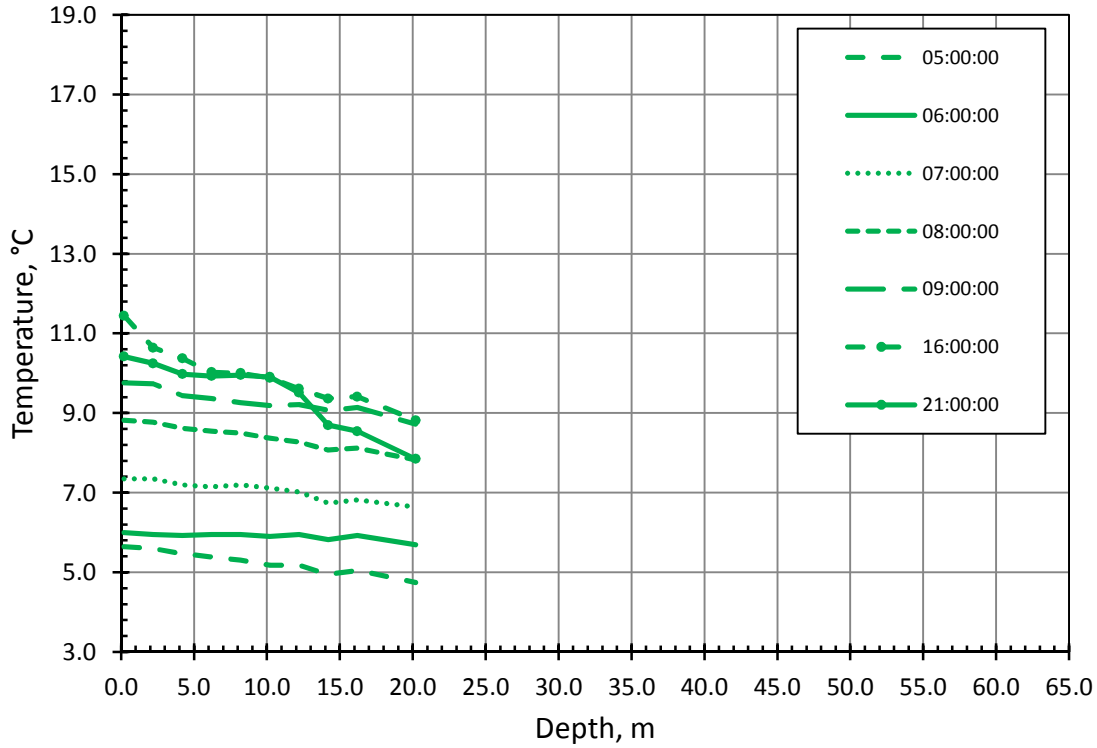

Figure 4.26c Water temperature profiles at MCA on June 16, 2011.

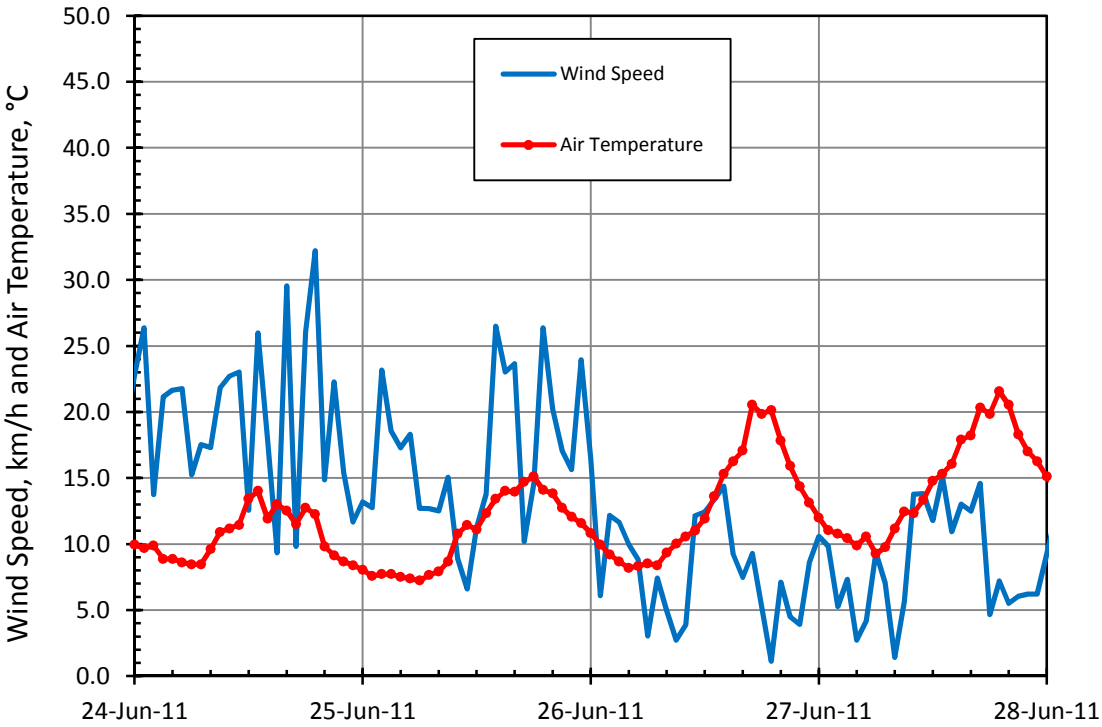

Figure 4.27a Air temperature and wind speed at MCA on June 24 - June 28, 2011.

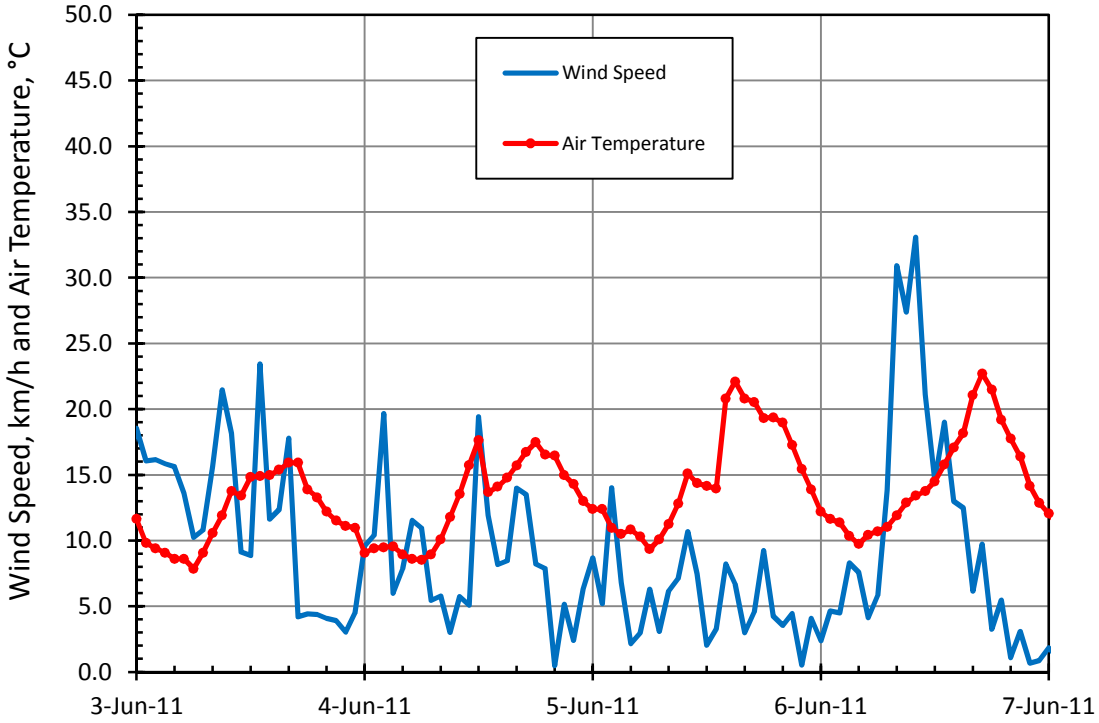

Figure 4.27b Air temperature and wind speed at MCA on June 3 - June 7, 2011.

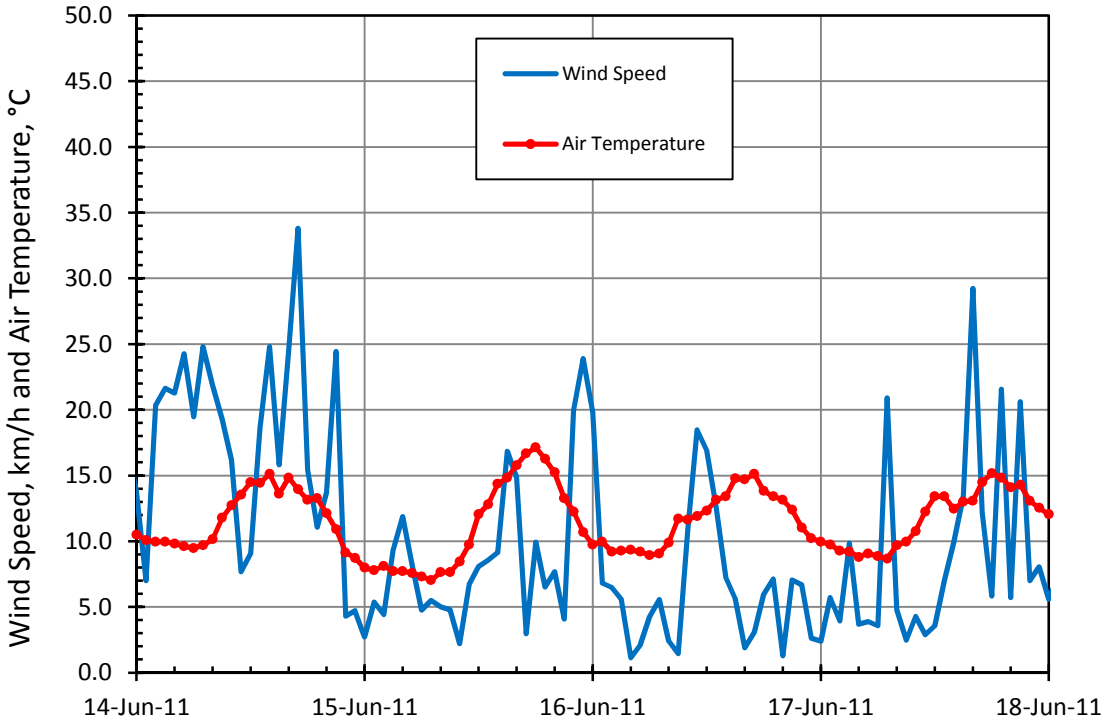

Figure 4.27c Air temperature and wind speed at MCA on June 14 - June 18, 2011.

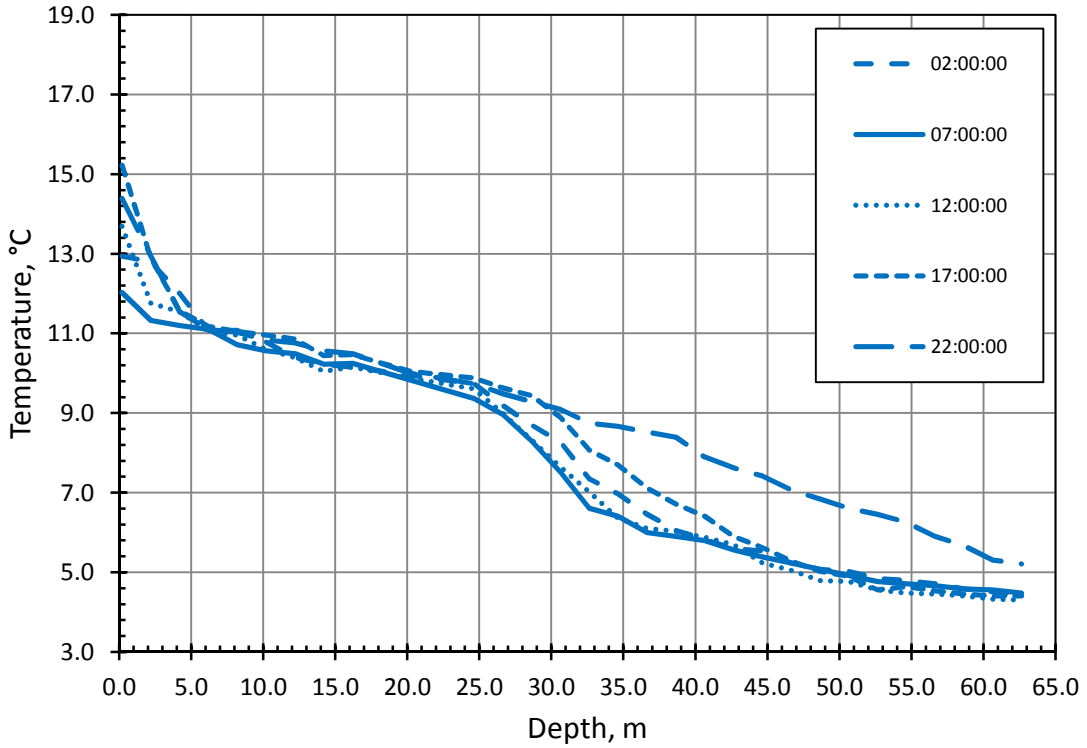

Figure 4.28a Water temperature profiles at MCA on the morning of July 17, 2011.

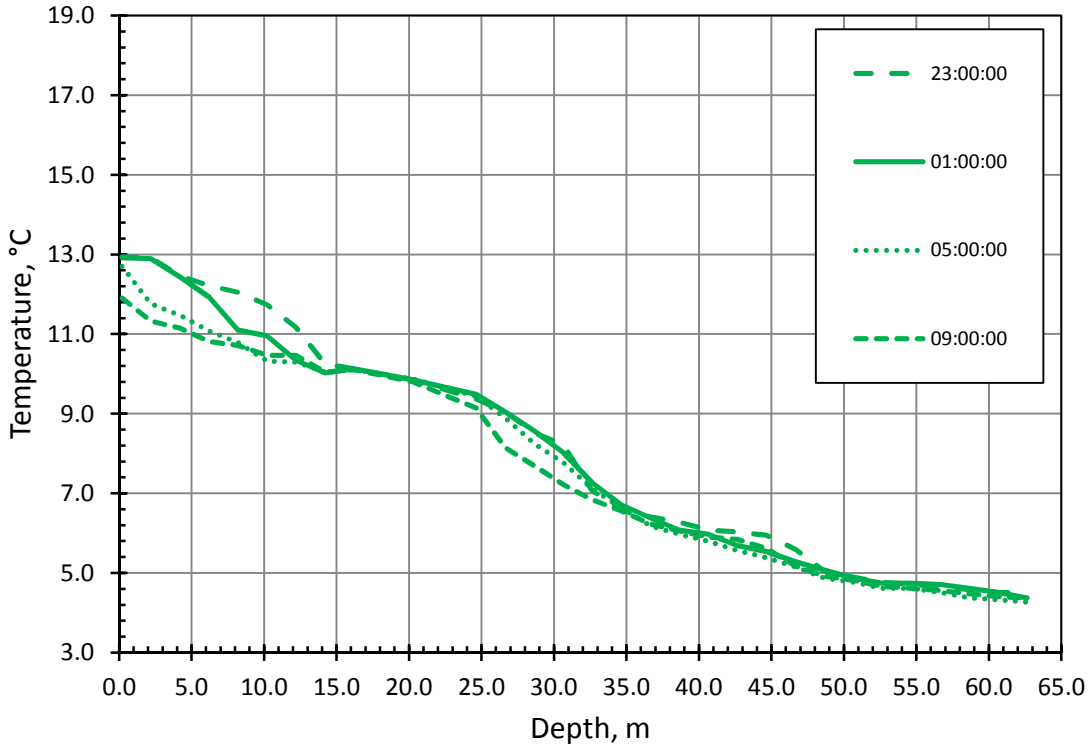

Figure 4.28b Water temperature profiles at MCA on the evening of July 16 and morning of July 17, 2011.

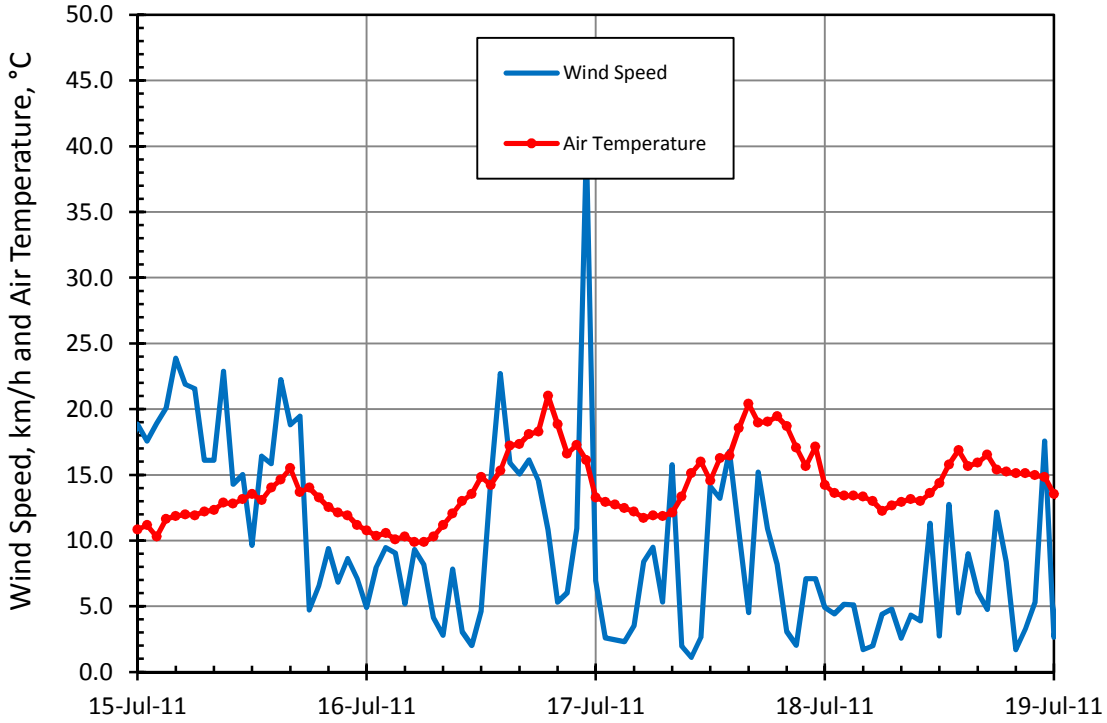

Figure 4.29a Air temperature and wind speed at MCA on July 15 - July 19, 2011.

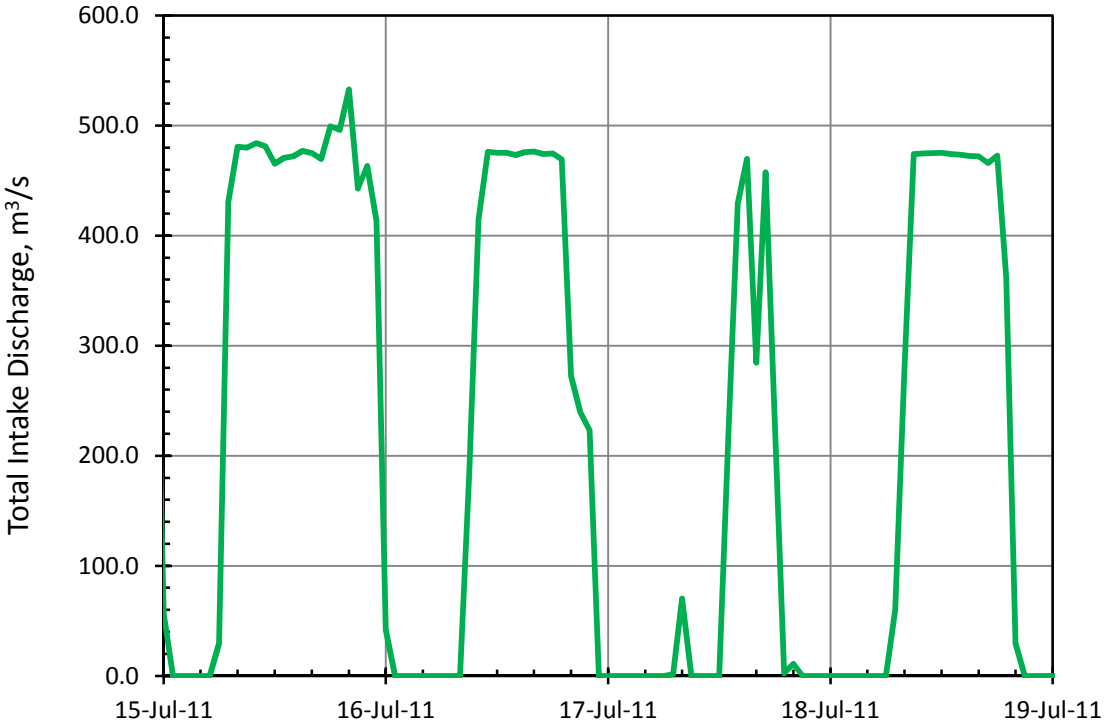

Figure 4.29b Total discharge from MCA on July 15 - July 19, 2011.

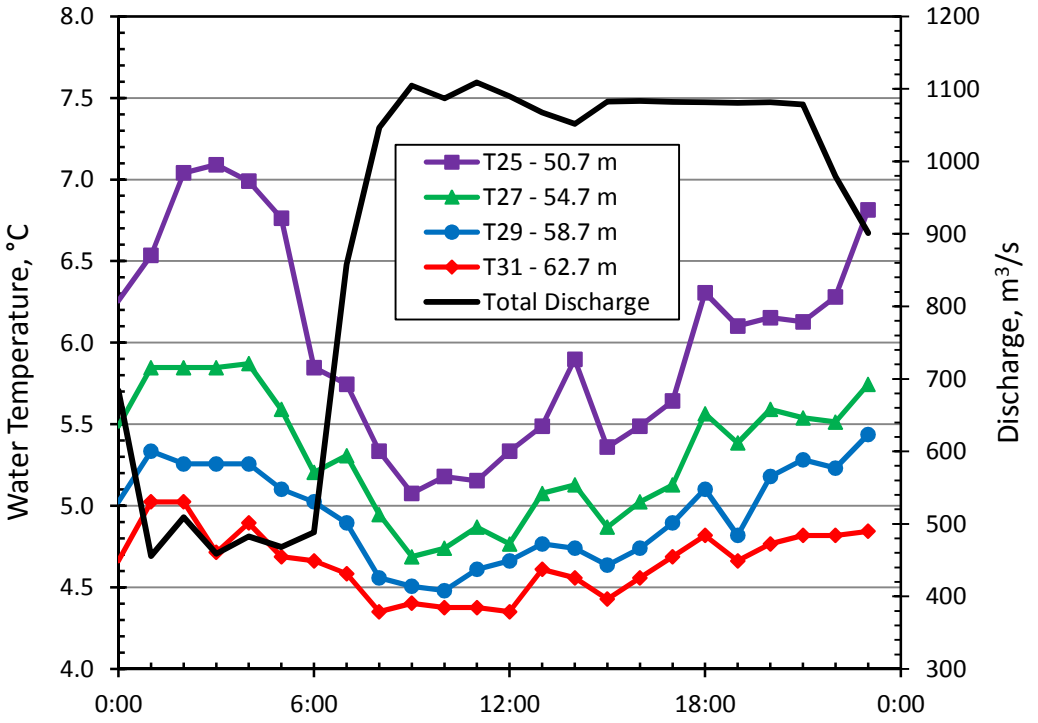

Figure 4.30a Comparison of MCA intake operations and bottom four thermistor water temperatures on August 11, 2011.

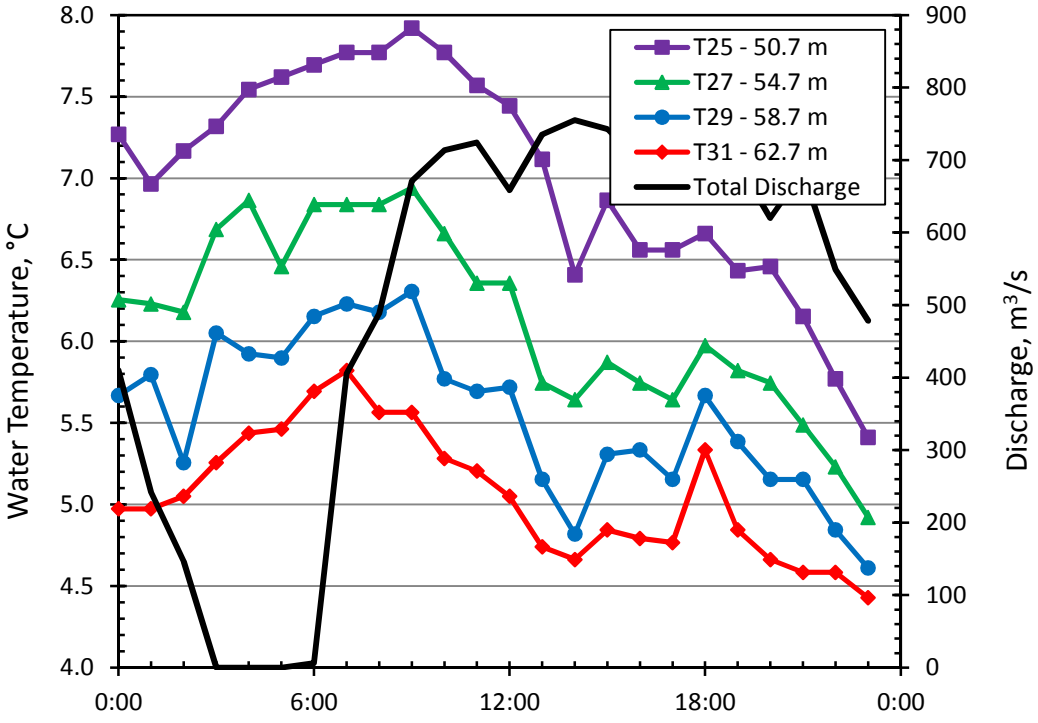

Figure 4.30b Comparison of MCA intake operations and bottom four thermistor water temperatures on August 23, 2011.

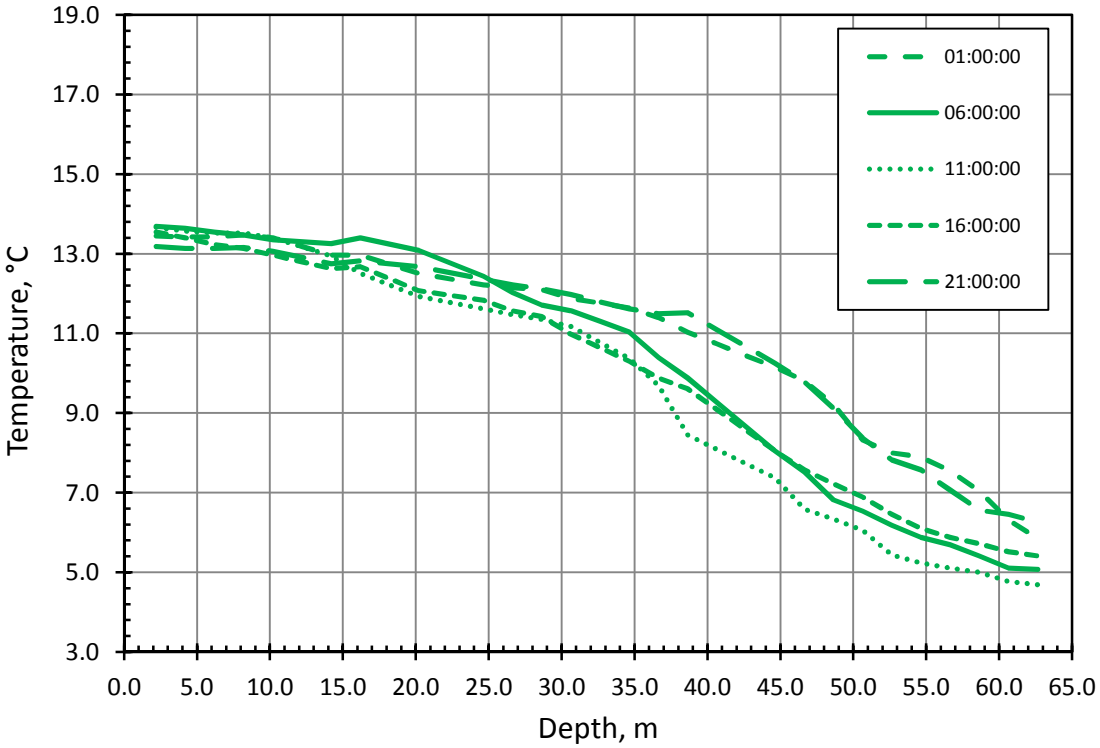

Figure 4.31a Water temperature profiles at MCA on September 17, 2011.

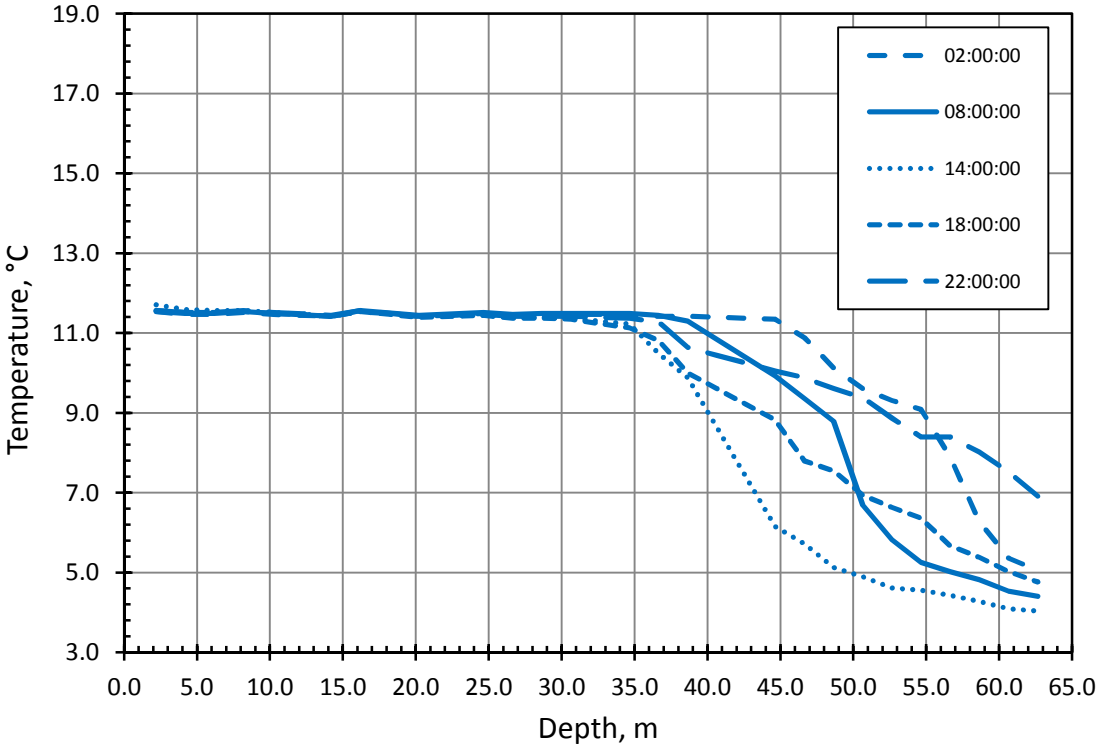

Figure 4.31b Water temperature profiles at MCA on October 15, 2011.

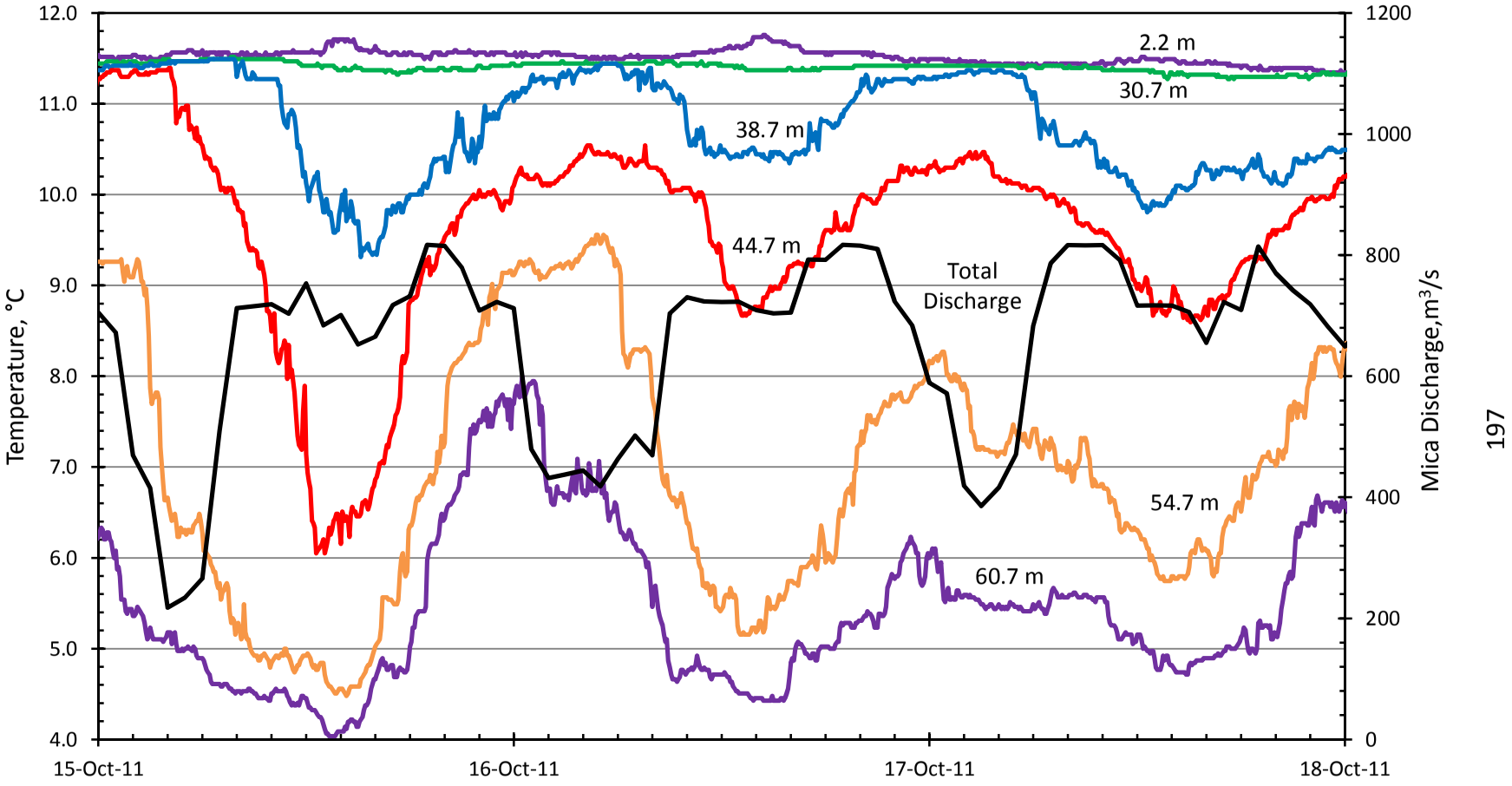

Figure 4.32 Comparison of total discharge at MCA and thermistor temperatures (October 15 - October 18, 2011).

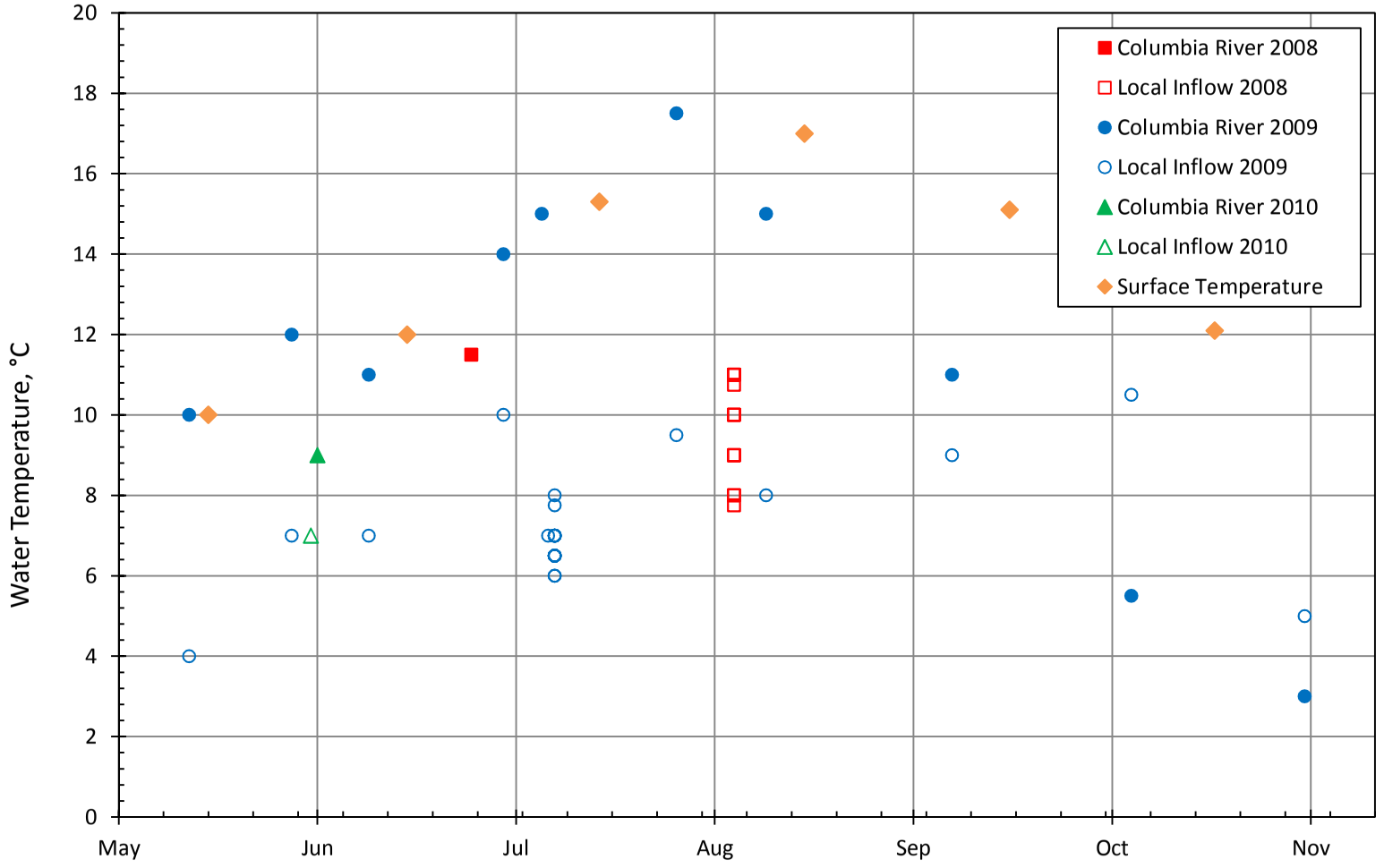

Figure 4.33 Columbia River inflow, local inflow and surface water temperatures for Kinbasket reservoir.

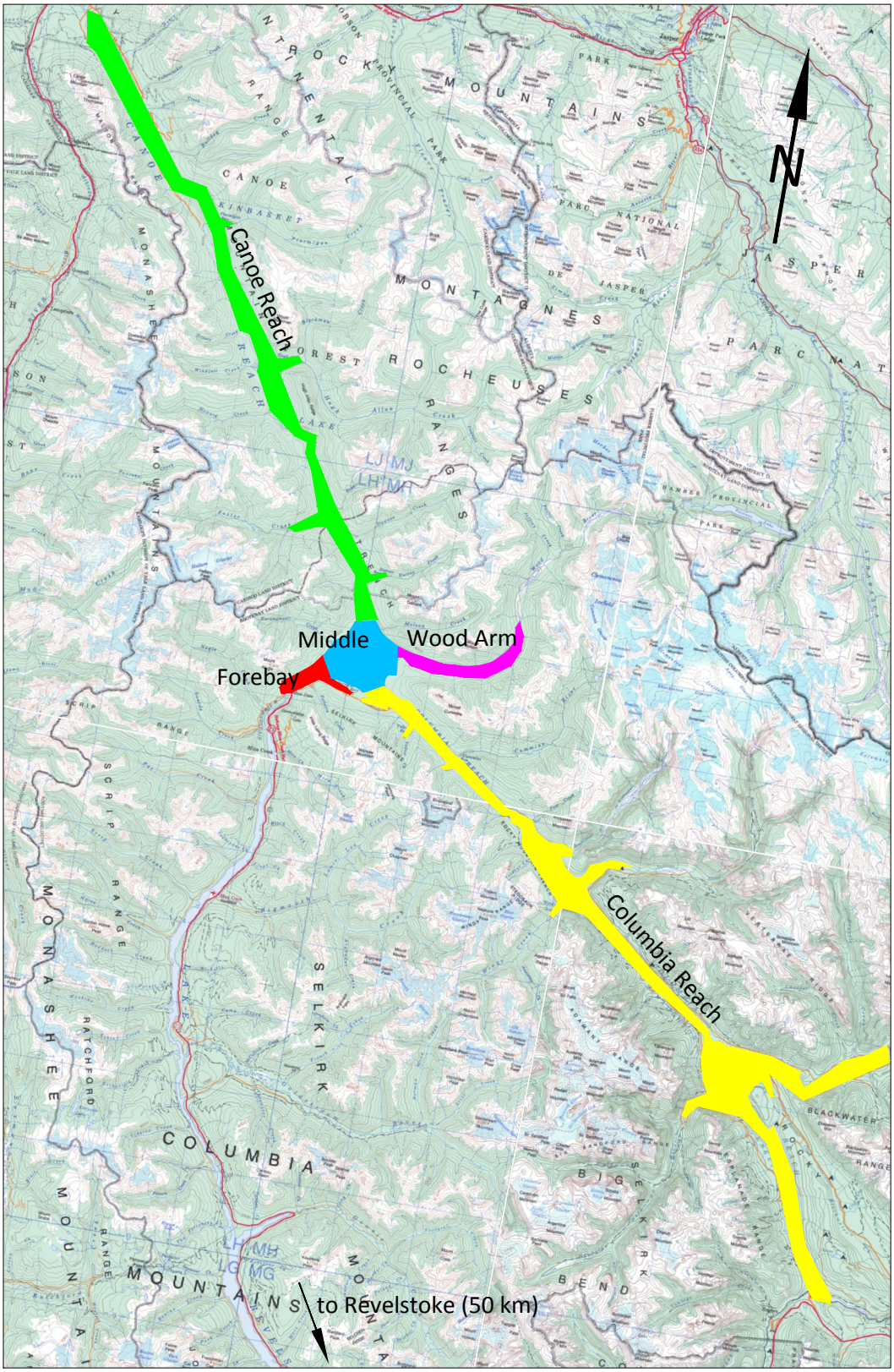

Figure 4.34 General locations of instantaneous temperature profiles at Kinbasket reservoir taken in 2008, 2009, and 2010.

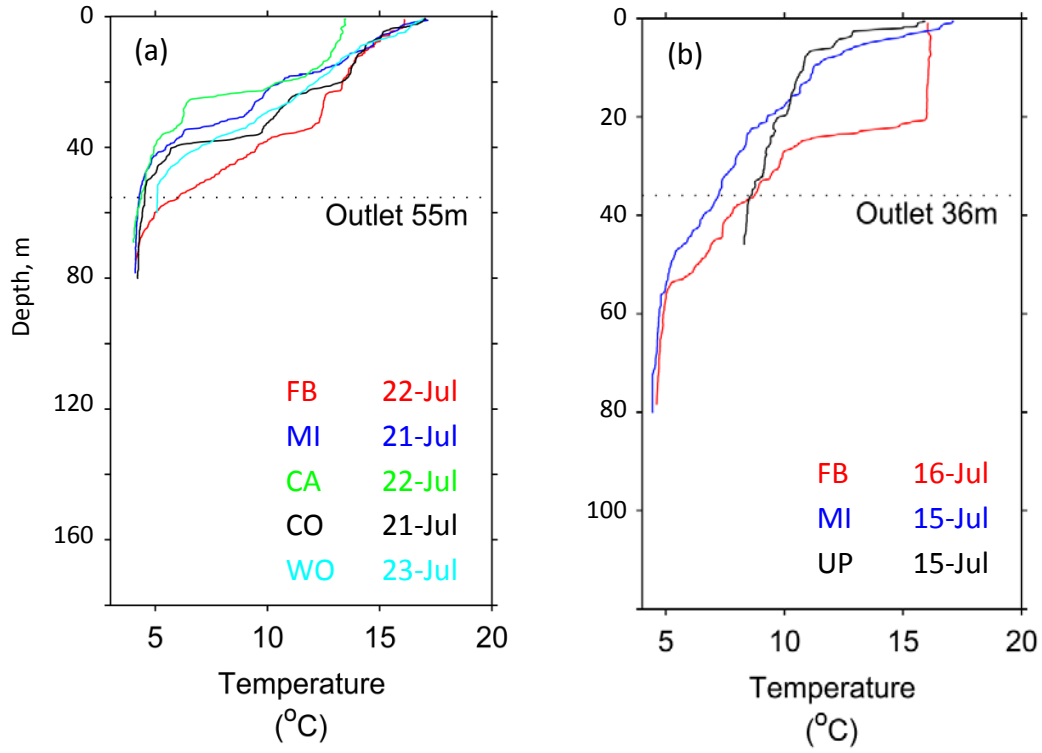

Figure 4.35 Instantaneous temperature profiles measured during July, 2008 in: (a) Kinbasket reservoir and (b) Revelstoke reservoir.

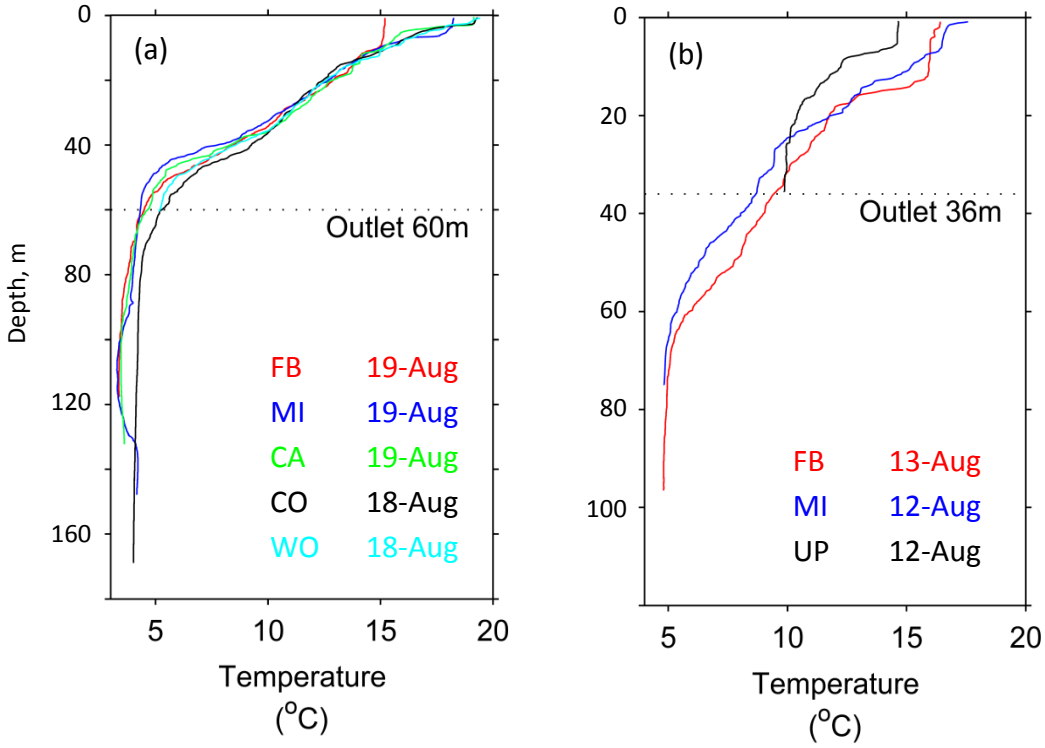

Figure 4.36 Instantaneous temperature profiles measured during August, 2008 in: (a) Kinbasket reservoir and (b) Revelstoke reservoir.

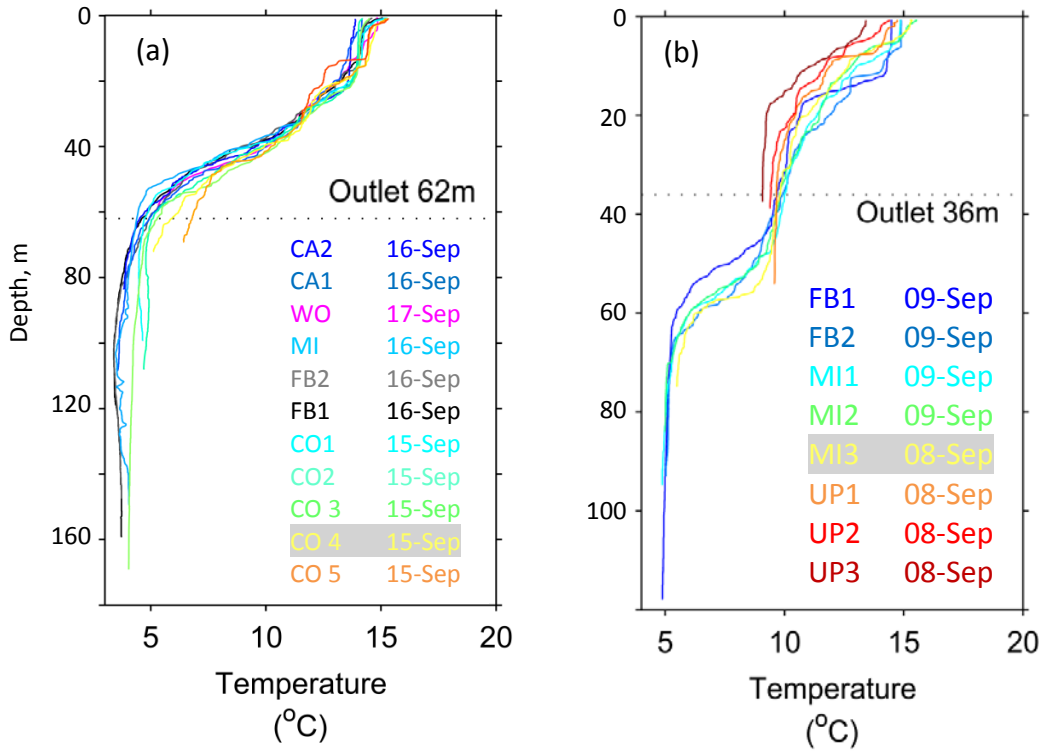

Figure 4.37 Instantaneous temperature profiles measured during September, 2008 in: (a) Kinbasket reservoir and (b) Revelstoke reservoir.

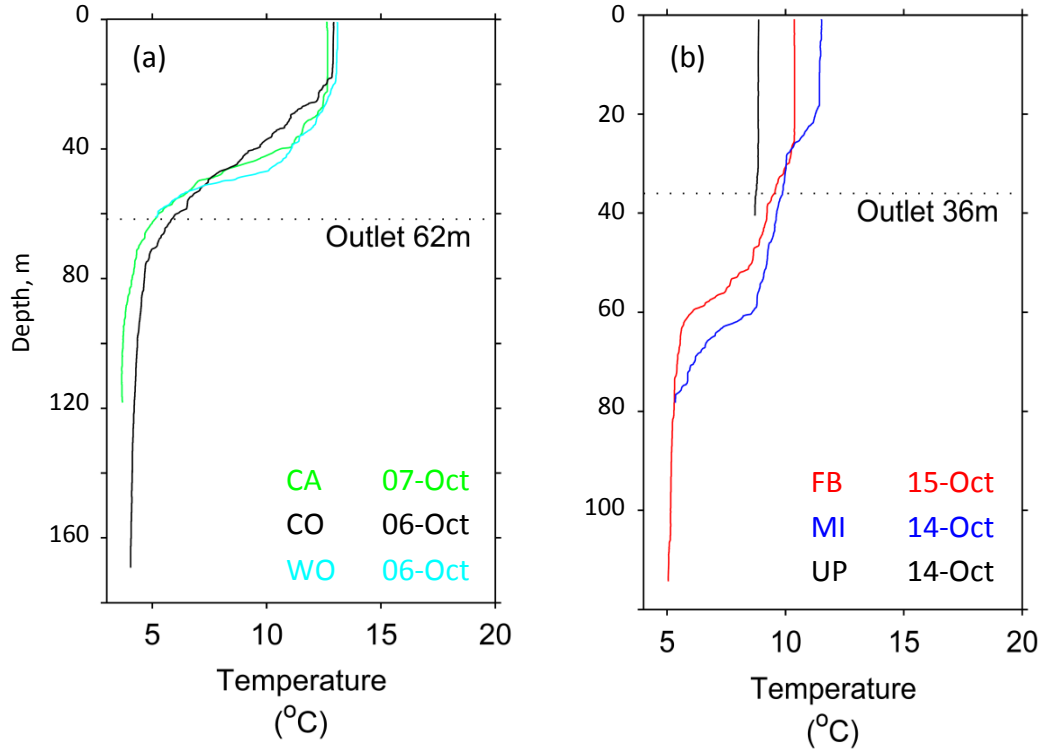

Figure 4.38 Instantaneous temperature profiles measured during October, 2008 in: (a) Kinbasket reservoir and (b) Revelstoke reservoir.

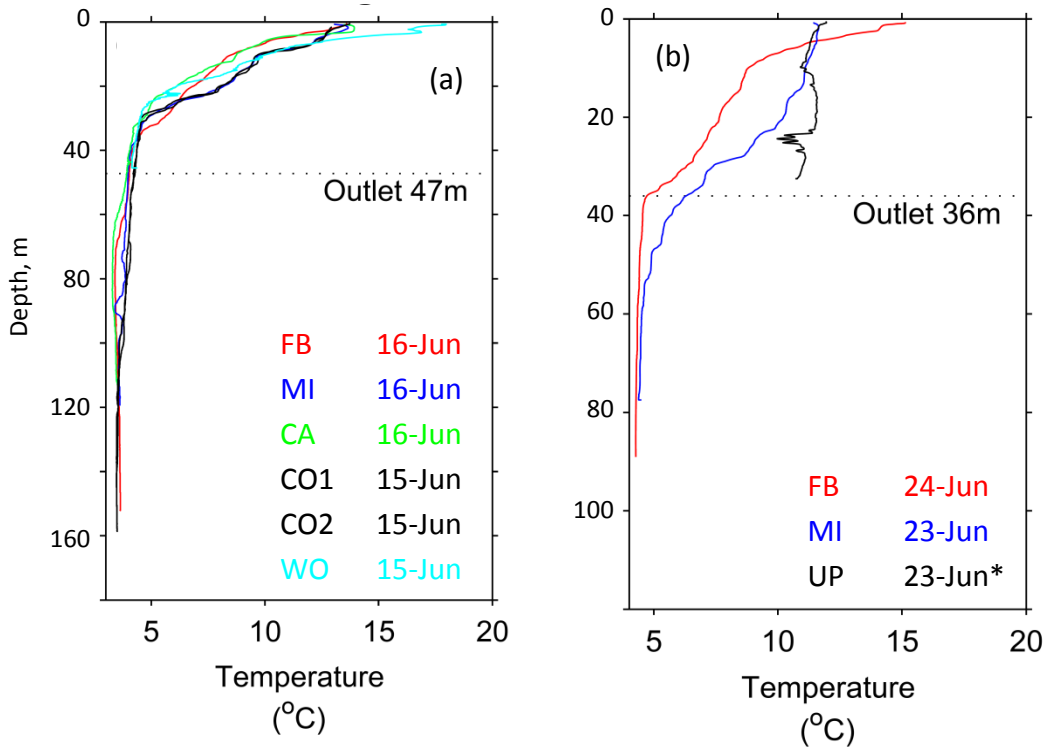

Figure 4.39 Instantaneous temperature profiles measured during June, 2009 in: (a) Kinbasket reservoir and (b) Revelstoke reservoir.

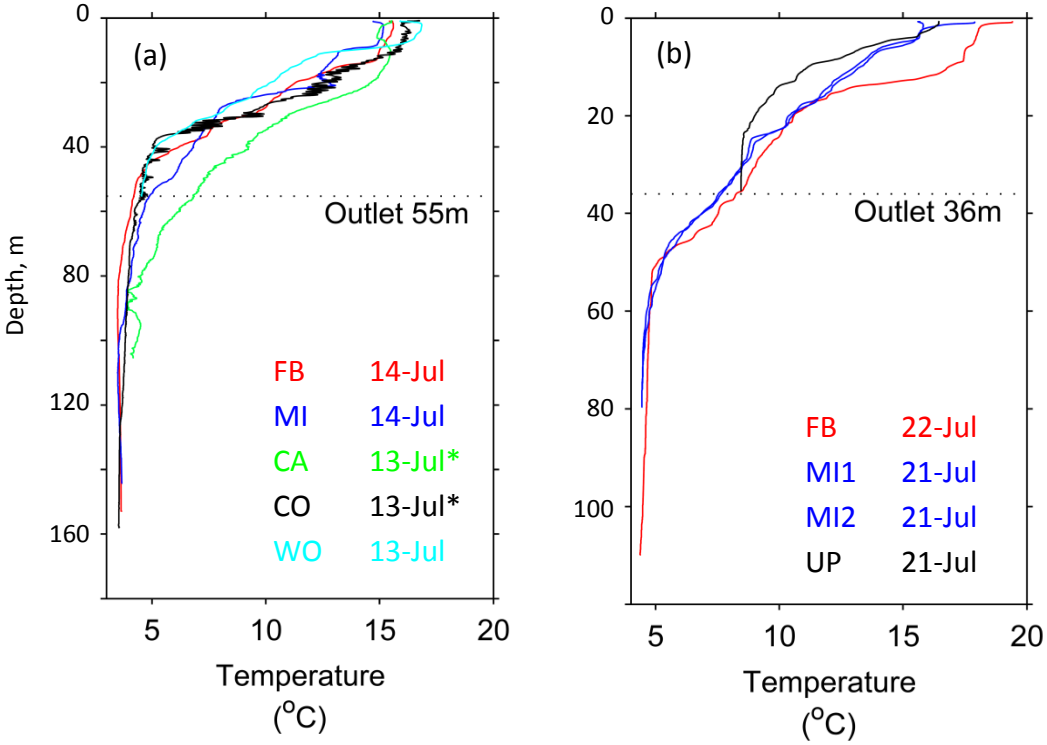

Figure 4.40 Instantaneous temperature profiles measured during July, 2009 in: (a) Kinbasket reservoir and (b) Revelstoke reservoir.

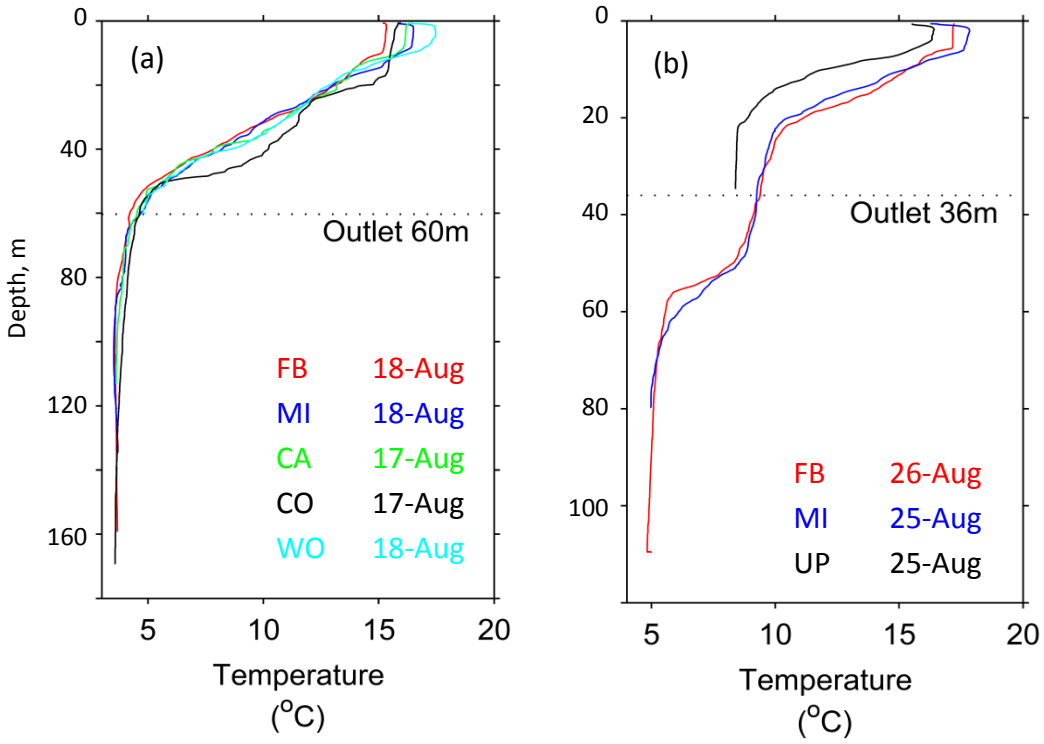

Figure 4.41 Instantaneous temperature profiles measured during August, 2009 in: (a) Kinbasket reservoir and (b) Revelstoke reservoir.

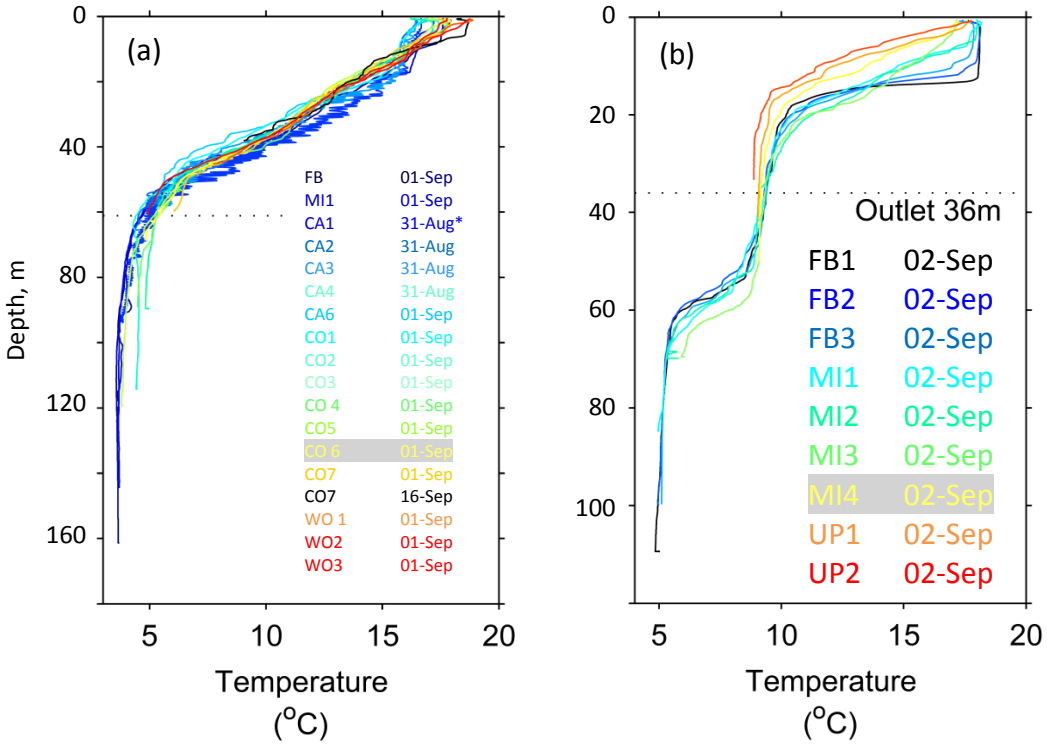

Figure 4.42 Instantaneous temperature profiles measured during late August and early September, 2009 in: (a) Kinbasket reservoir and (b) Revelstoke reservoir.

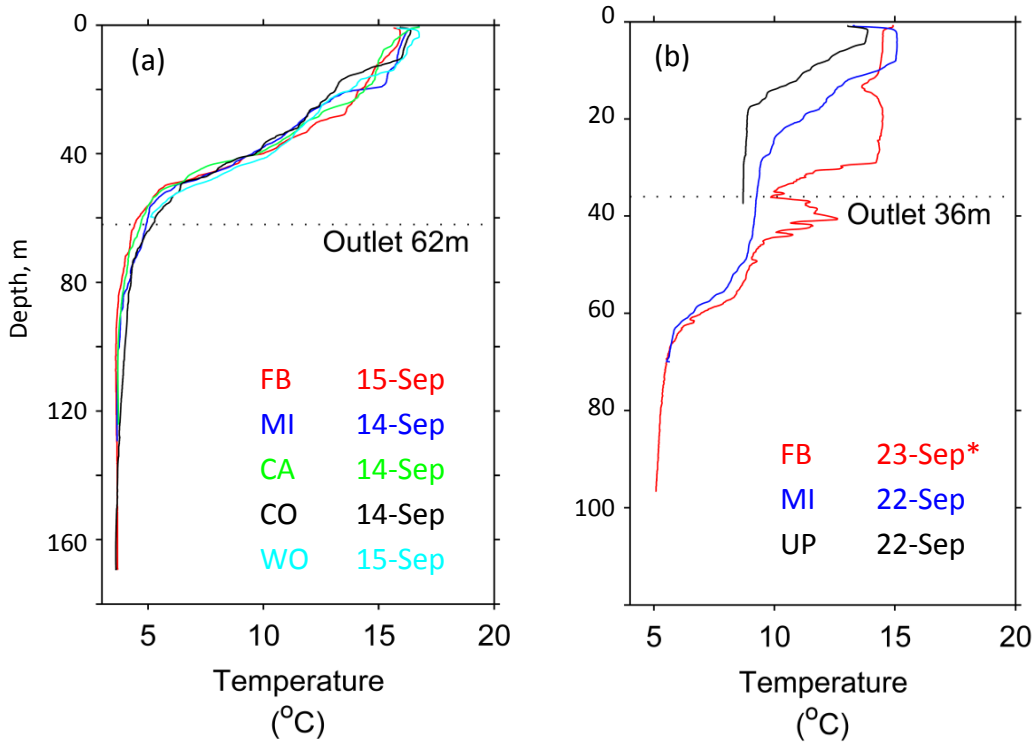

Figure 4.43 Instantaneous temperature profiles measured during mid-September, 2009 in: (a) Kinbasket reservoir and (b) Revelstoke reservoir.

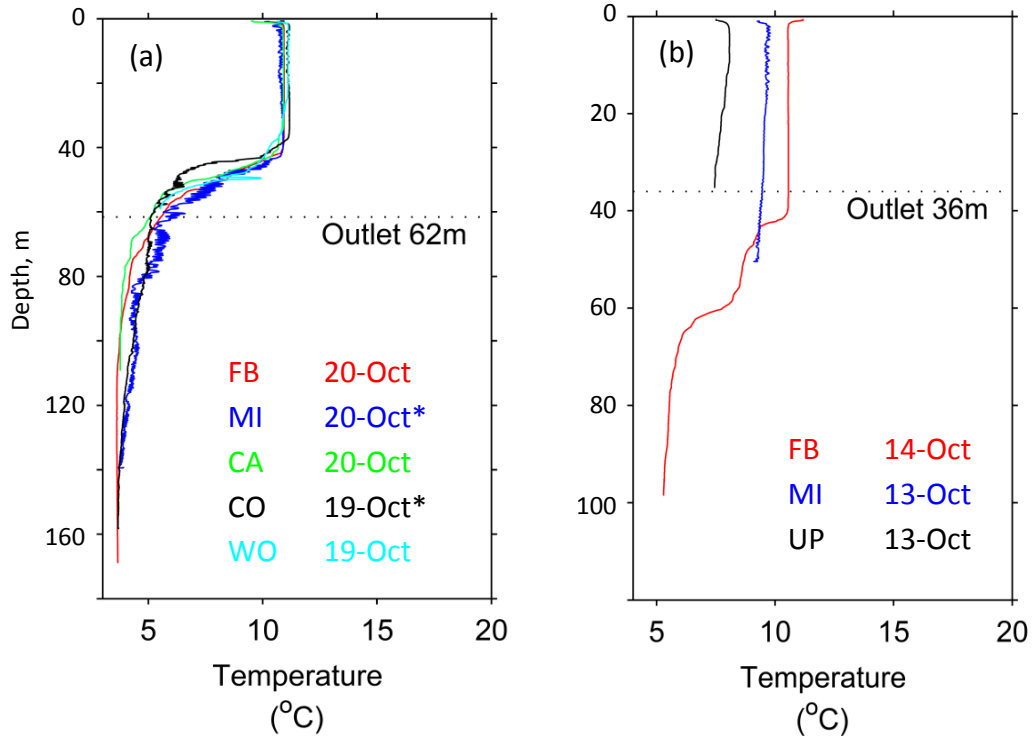

Figure 4.44 Instantaneous temperature profiles measured during October, 2009 in: (a) Kinbasket reservoir and (b) Revelstoke reservoir.

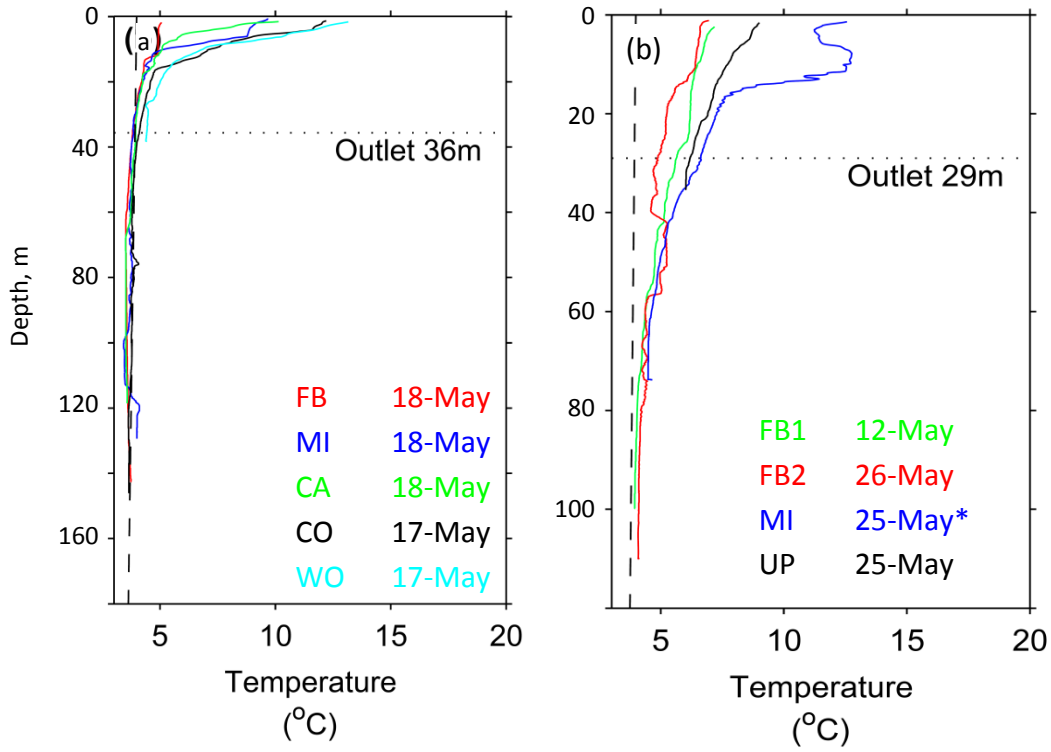

Figure 4.45 Instantaneous temperature profiles measured during May, 2010 in: (a) Kinbasket reservoir and (b) Revelstoke reservoir.

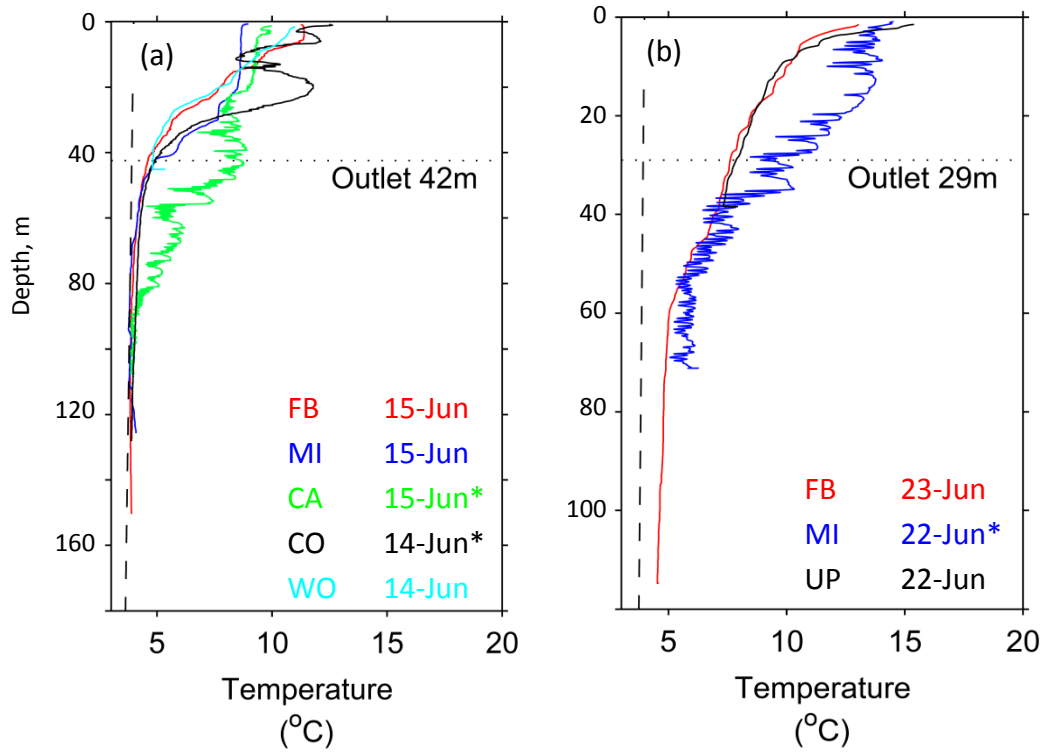

Figure 4.46 Instantaneous temperature profiles measured during June, 2010 in: (a) Kinbasket reservoir and (b) Revelstoke reservoir.

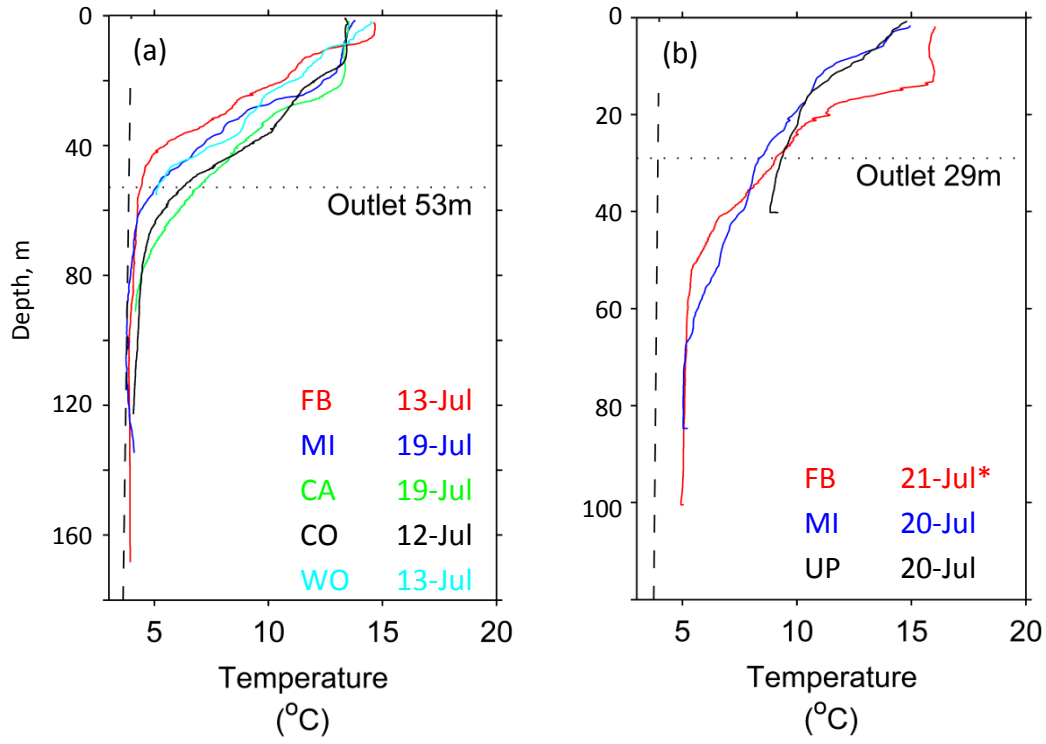

Figure 4.47 Instantaneous temperature profiles measured during July, 2010 in: (a) Kinbasket reservoir and (b) Revelstoke reservoir.

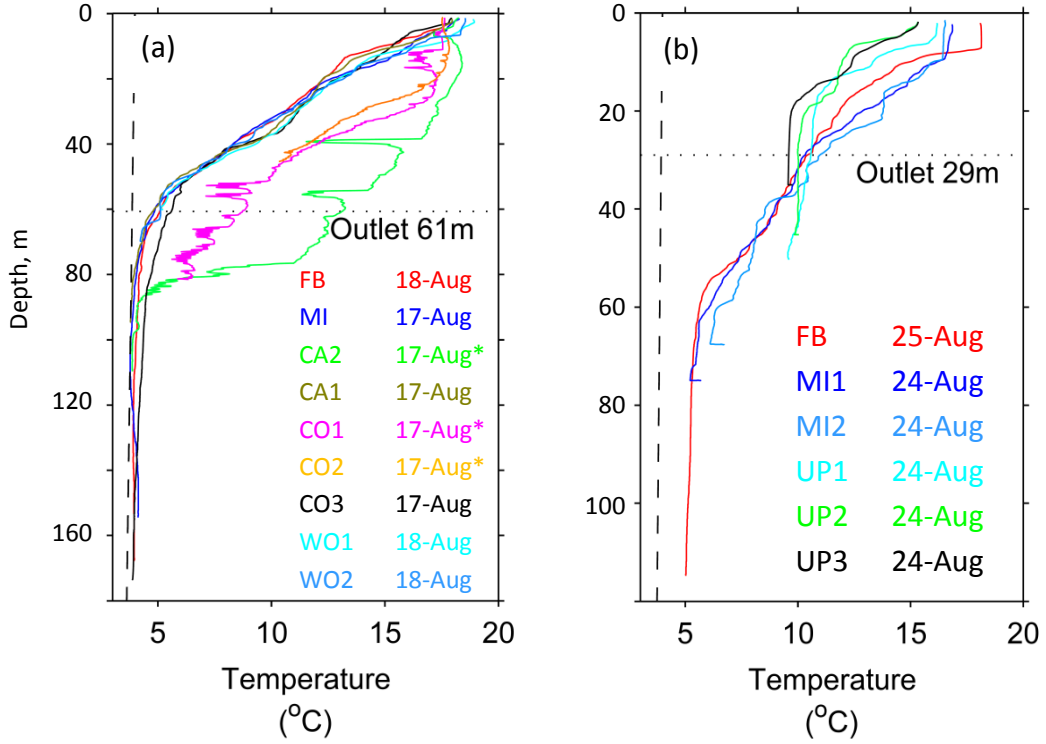

Figure 4.48 Instantaneous temperature profiles measured during August, 2010 in: (a) Kinbasket reservoir and (b) Revelstoke reservoir.

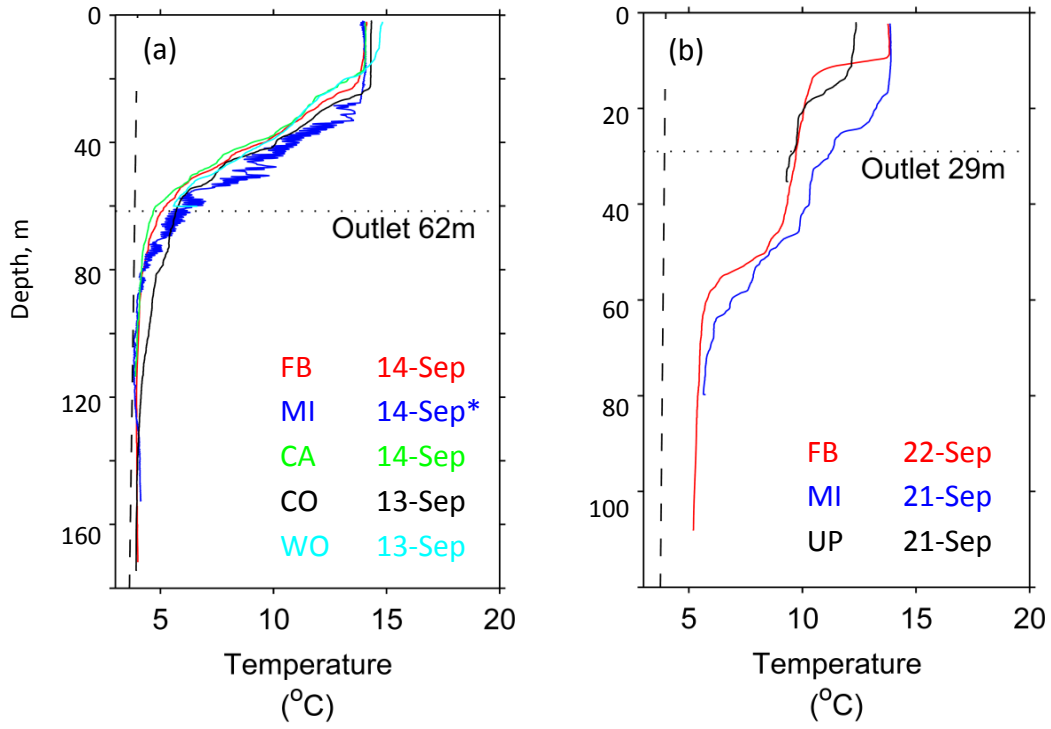

Figure 4.49 Instantaneous temperature profiles measured during September, 2010 in: (a) Kinbasket reservoir and (b) Revelstoke reservoir.

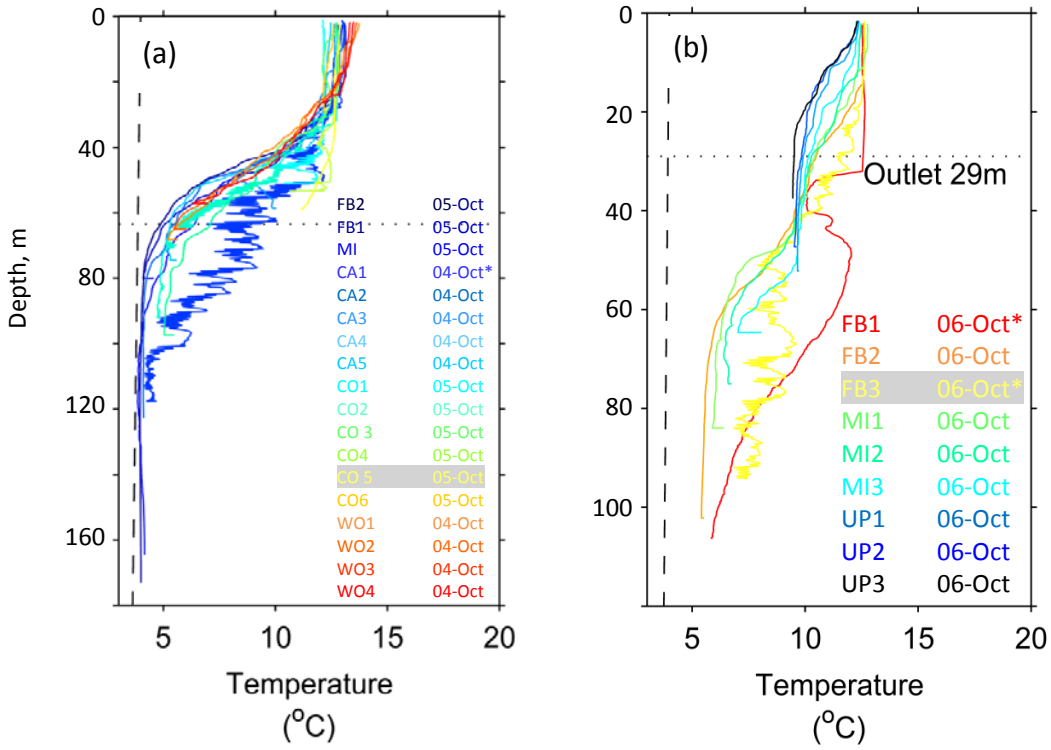

Figure 4.50 Instantaneous temperature profiles measured during early October, 2010 in: (a) Kinbasket reservoir and (b) Revelstoke reservoir.

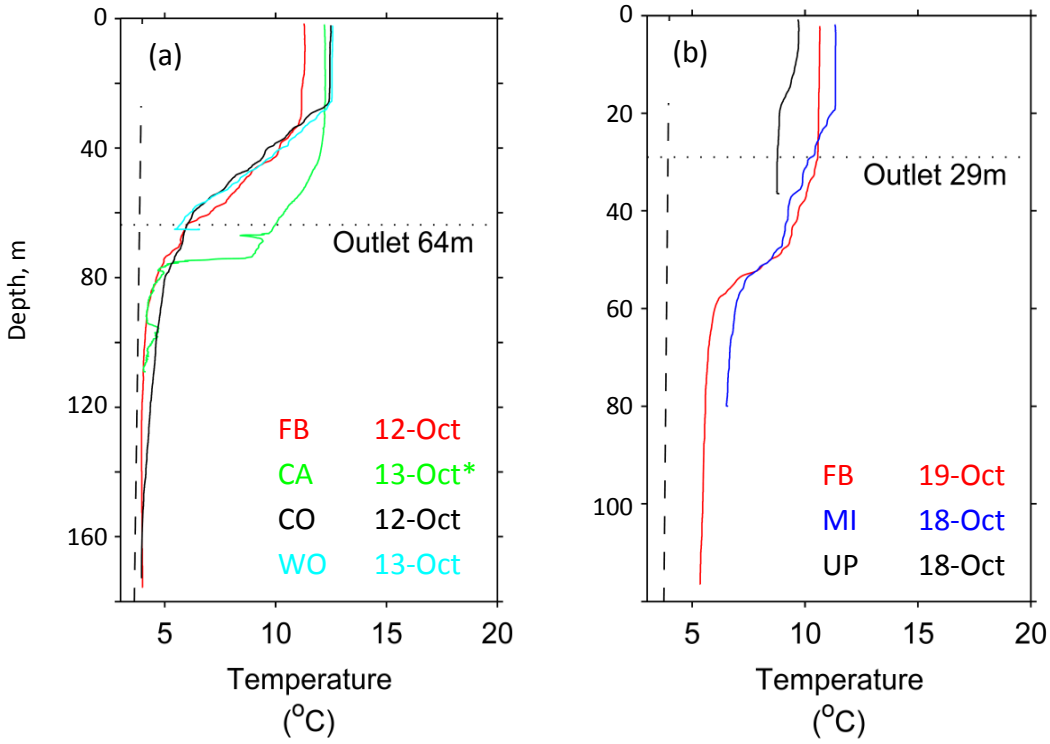

Figure 4.51 Instantaneous temperature profiles measured during mid-October, 2010 in: (a) Kinbasket reservoir and (b) Revelstoke reservoir.

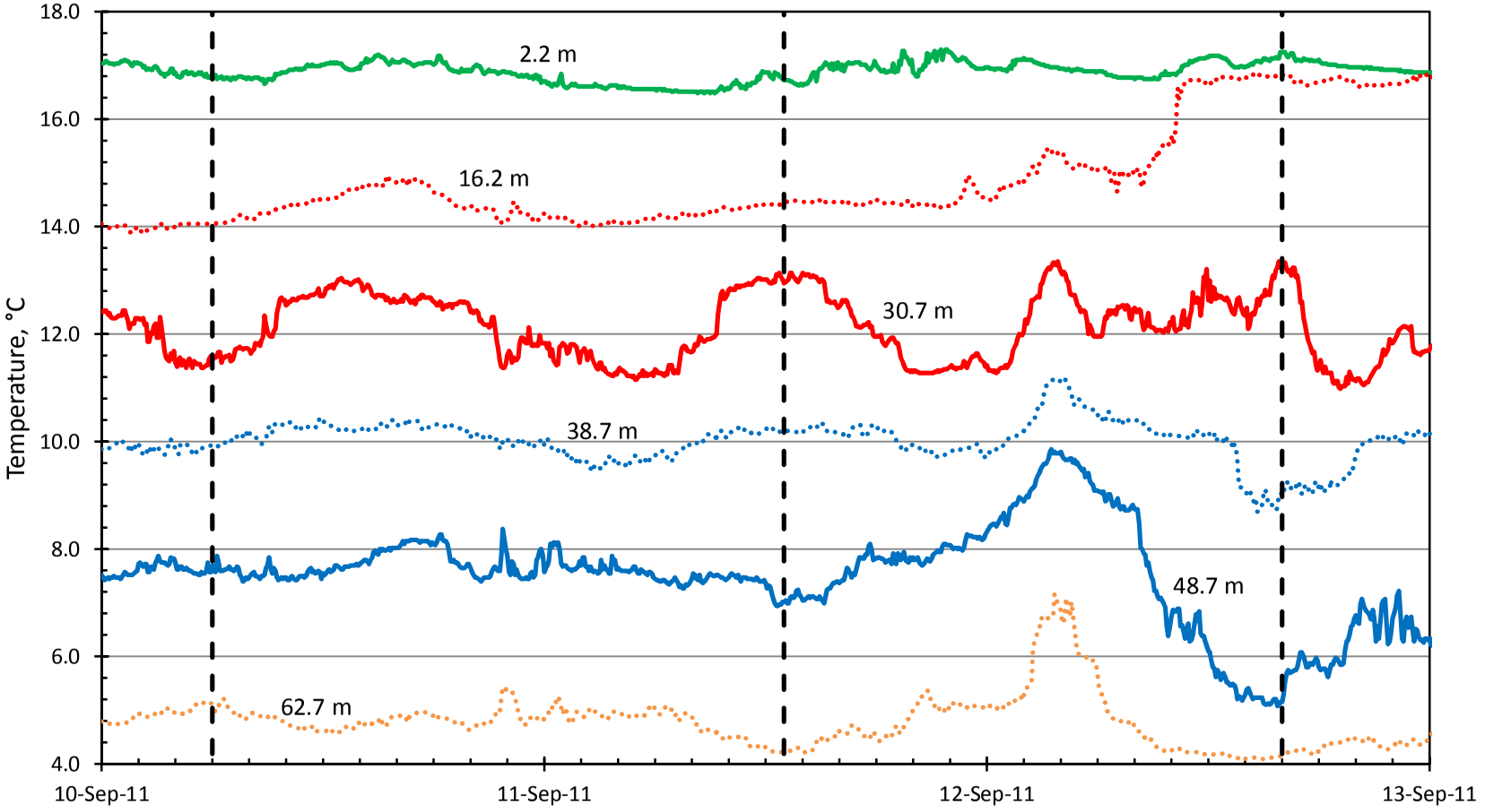

Figure 4.52 Evidence of a second vertical mode occuring (at dashed lines) at MCA in September, 2011.

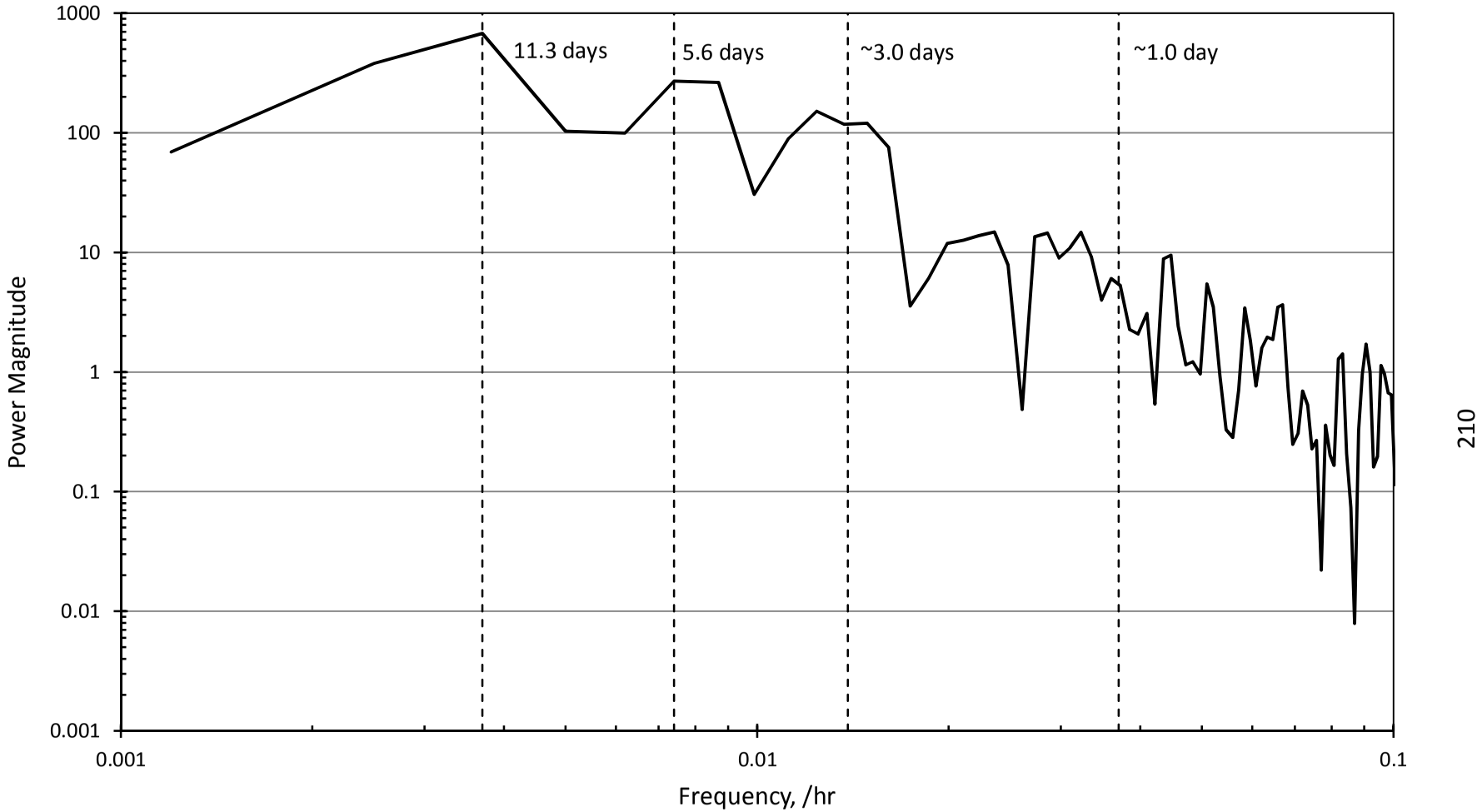

Figure 4.53 Periodogram of the MCA thermistor 3 time series from June 1 - 30, 2011.

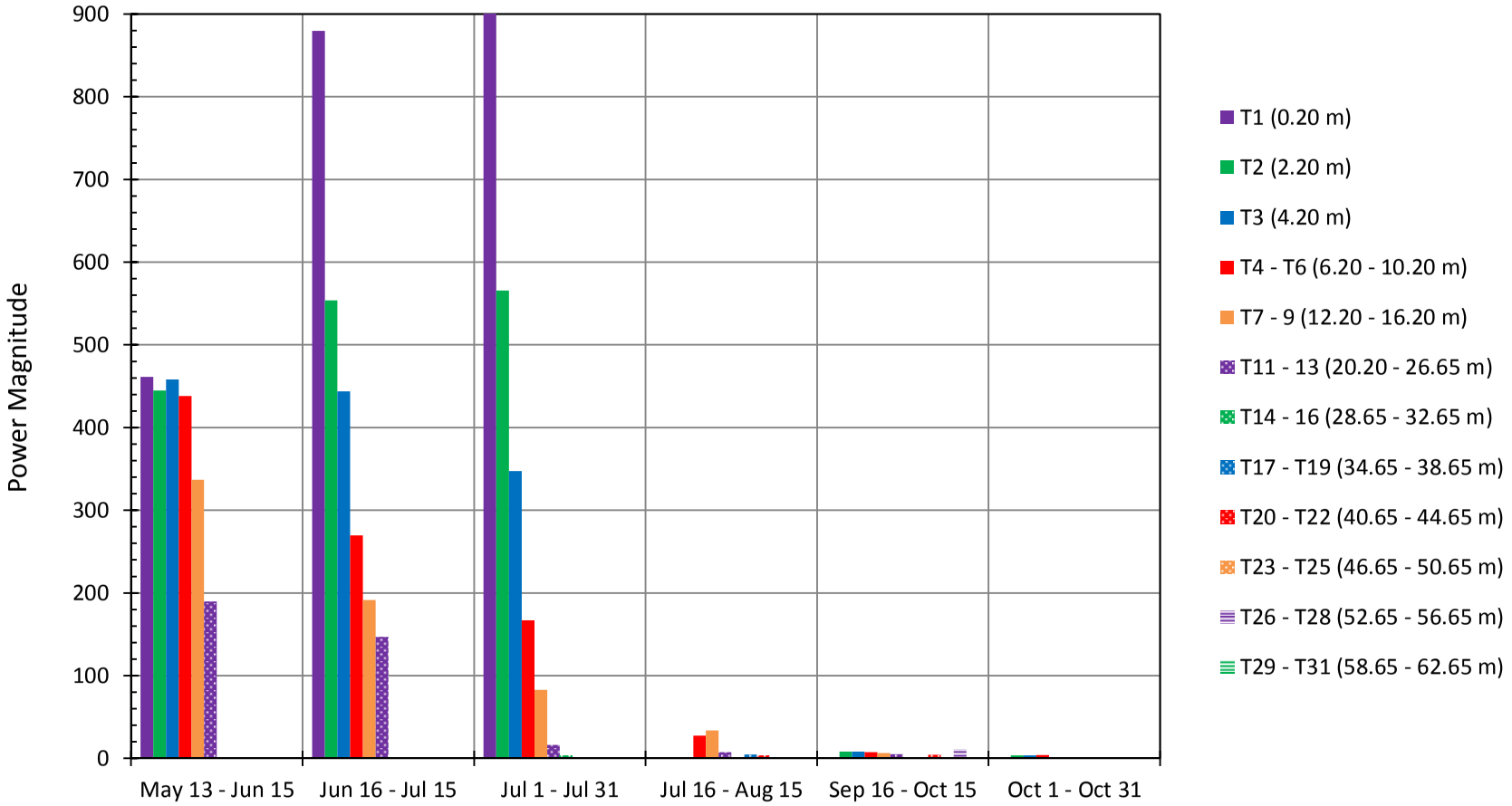

Figure 4.54a Power magnitudes of 6.7 day result of low frequency waveform analysis on MCA thermistor time series.

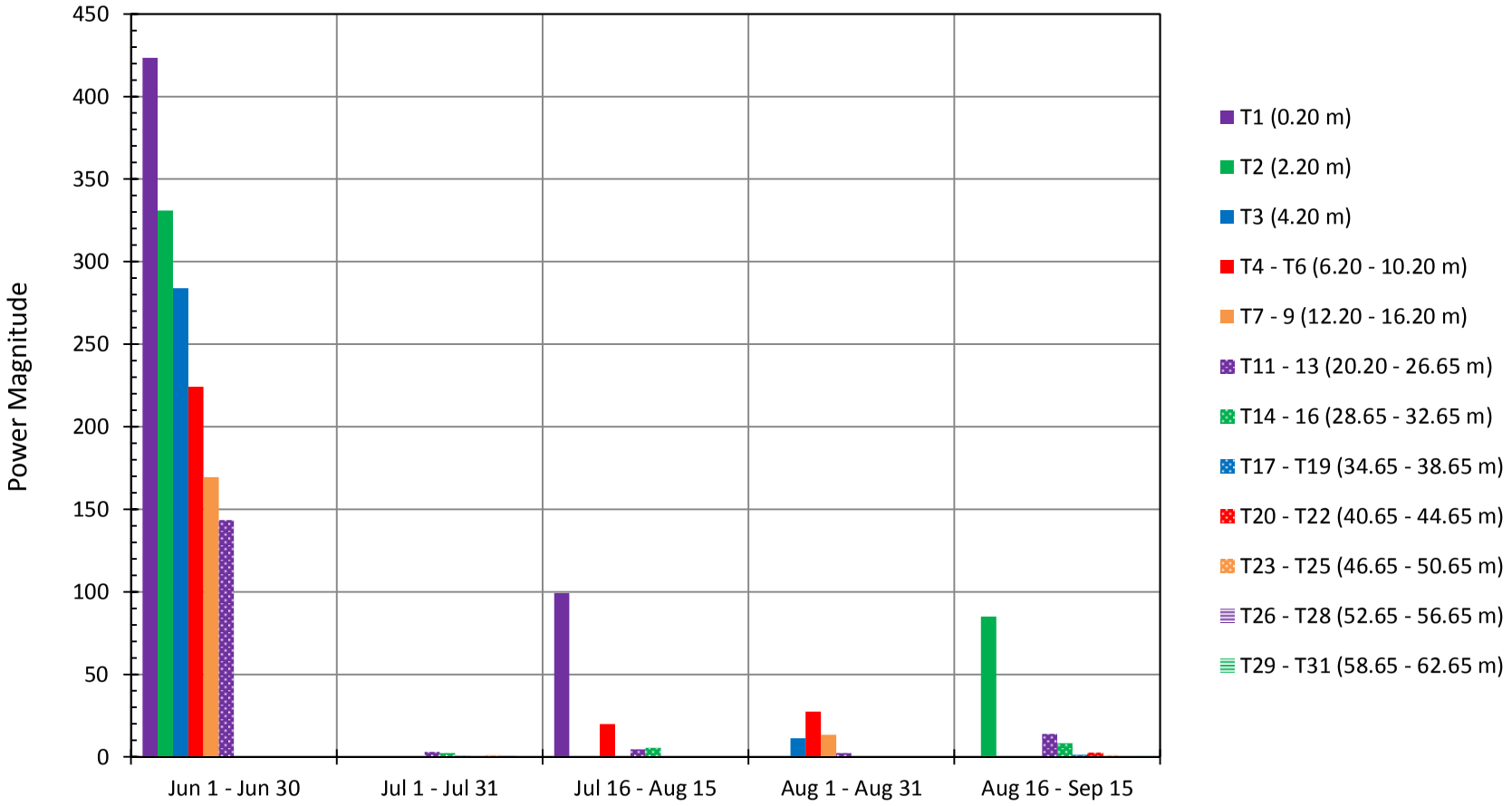

Figure 4.54b Power magnitudes of 11.3 day result of low frequency waveform analysis on MCA thermistor time series.

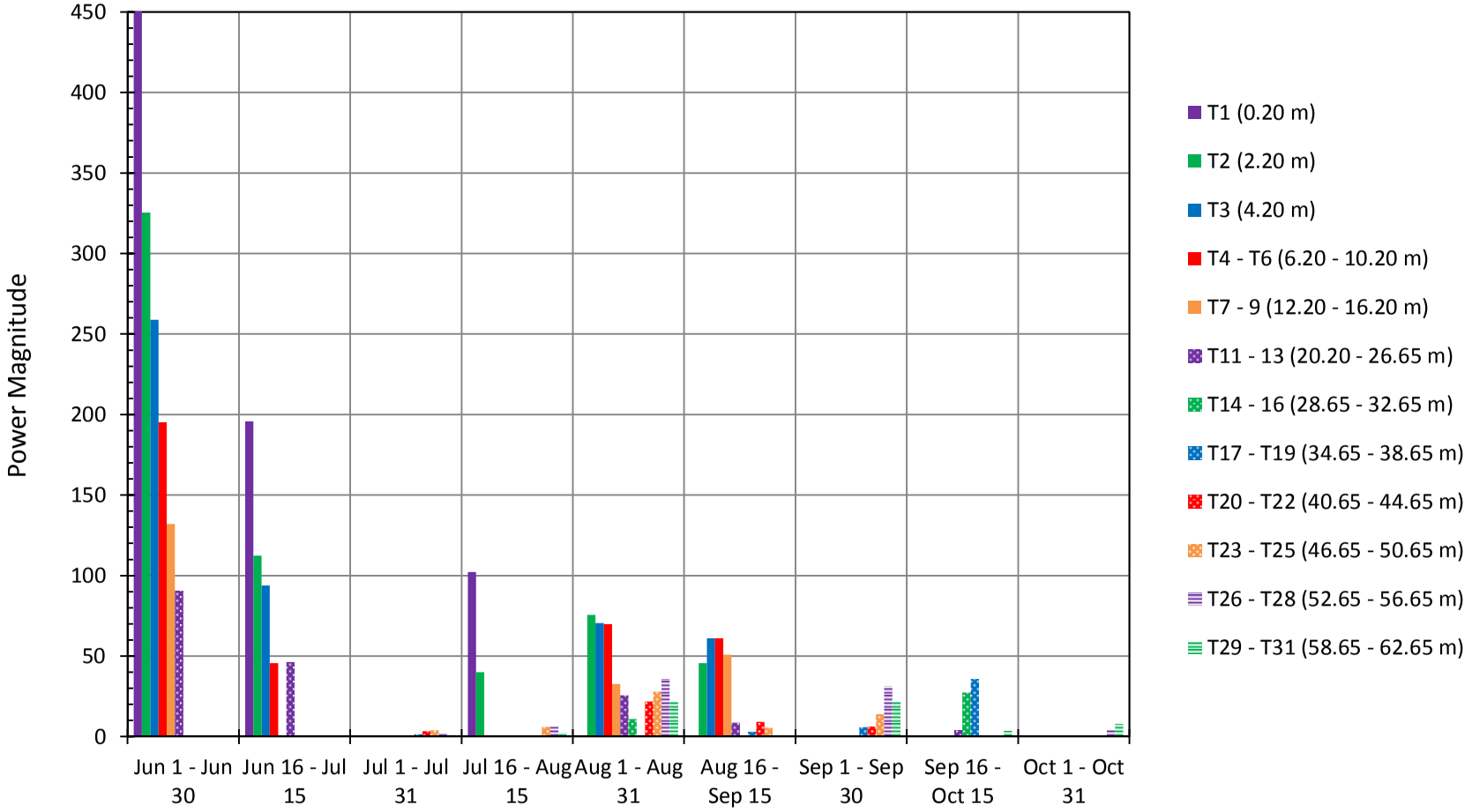

Figure 4.54c Power magnitudes of 5.6 day result of low frequency waveform analysis on MCA thermistor time series.

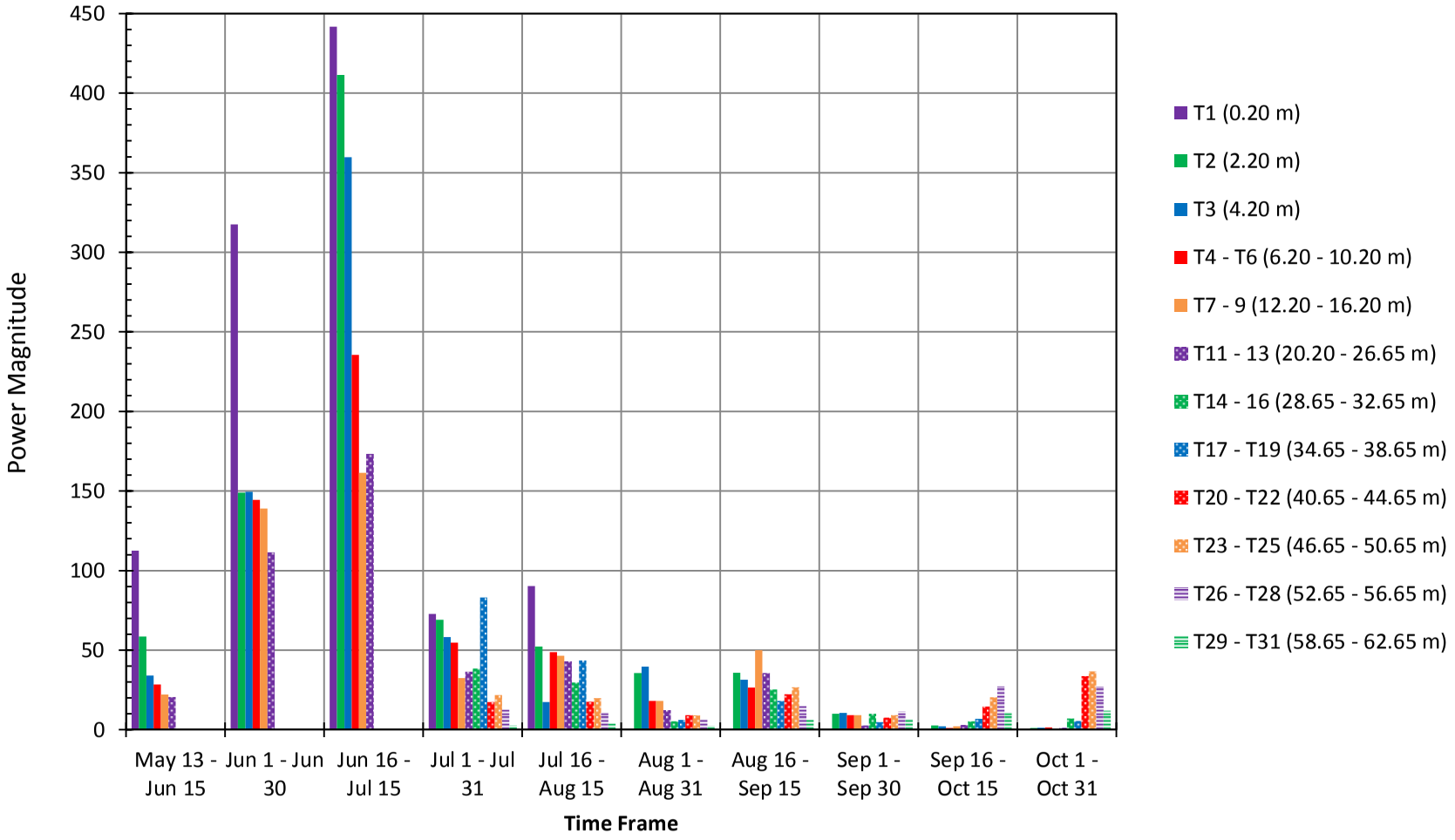

Figure 4.54d Power magnitudes of ~3 day result of low frequency waveform analysis on MCA thermistor time series.

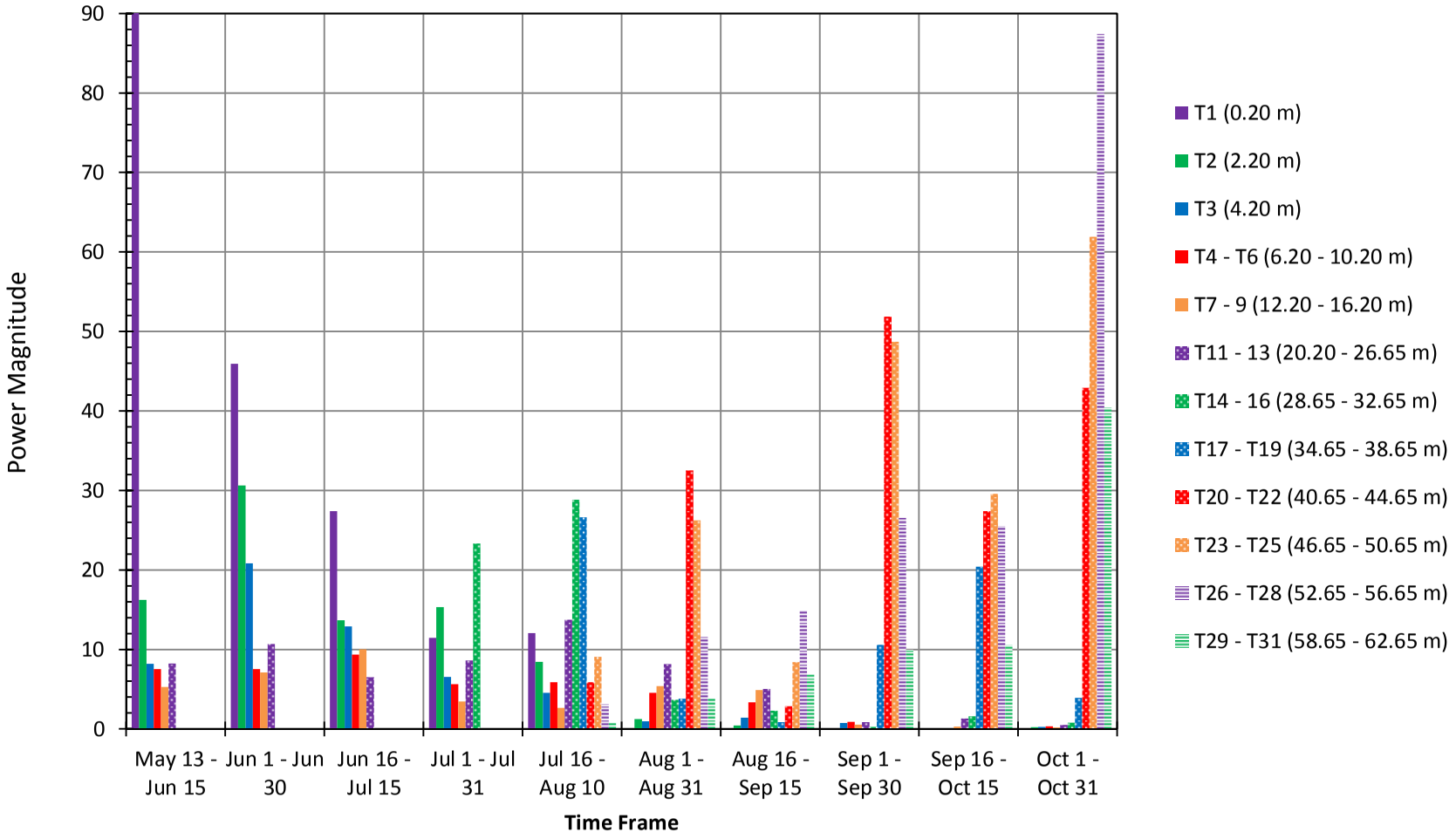

Figure 4.54e Power magnitudes of ~1 day result of low frequency waveform analysis on MCA thermistor time series.

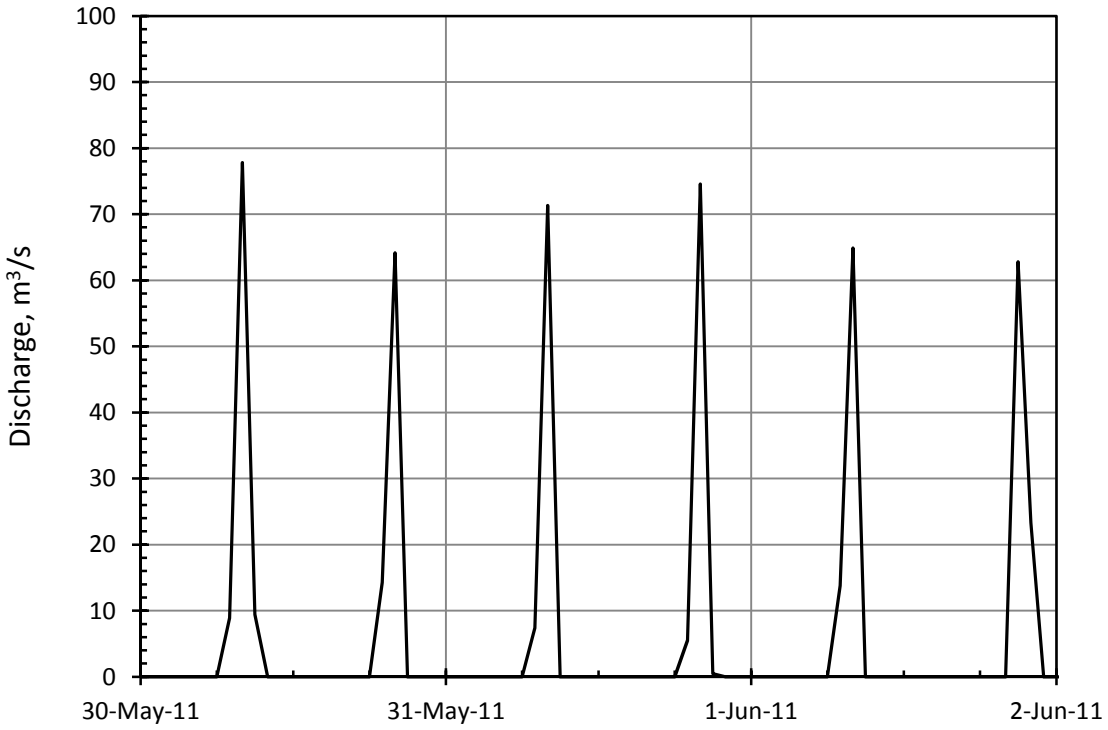

Figure 4.55a Example of approximately 12 hour cycle of total discharge at MCA.

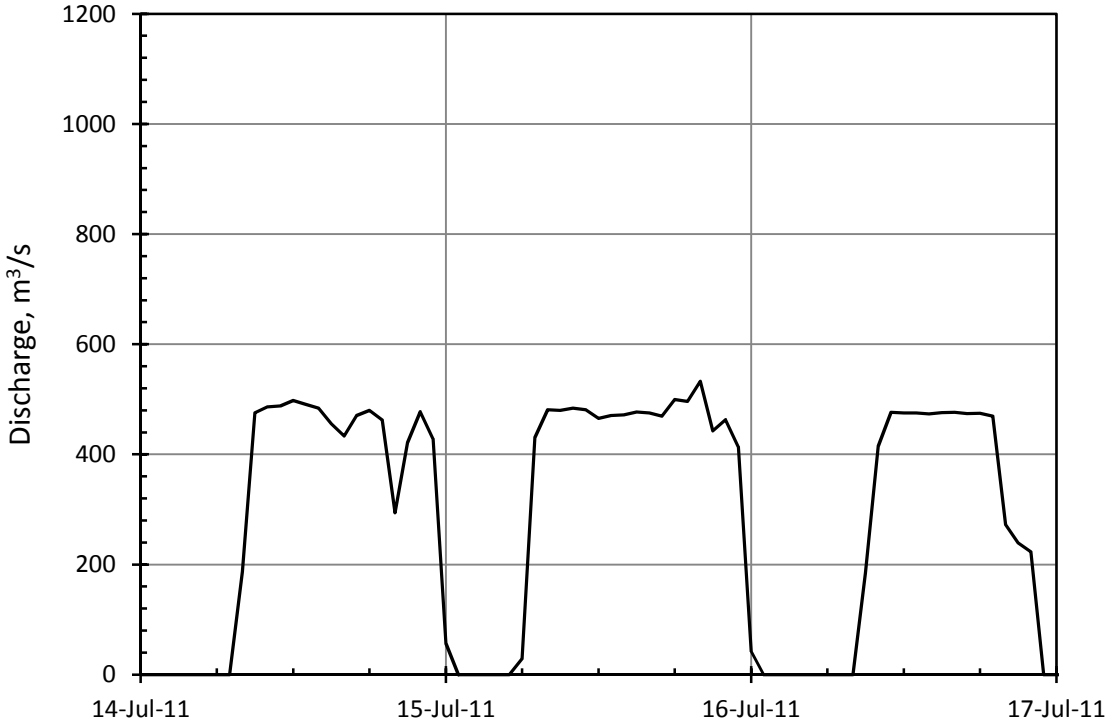

Figure 4.55b Example of approximately 1 day cycle of total discharge at MCA.

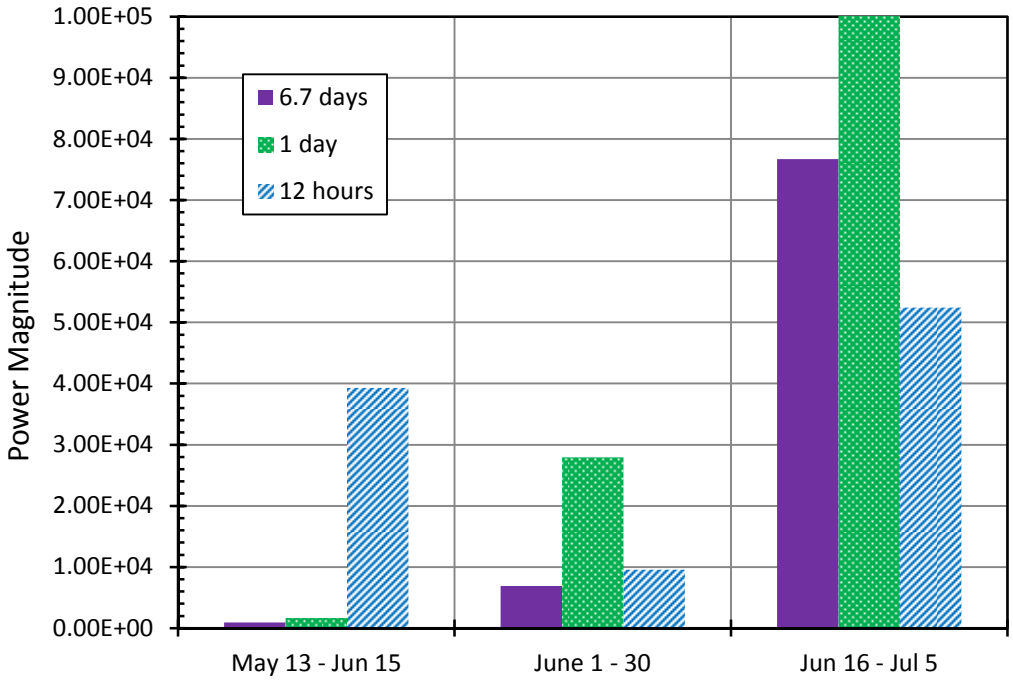

Figure 4.56a Dominant periods of oscillation in MCA dam operations during May 13 - July 5, 2011.

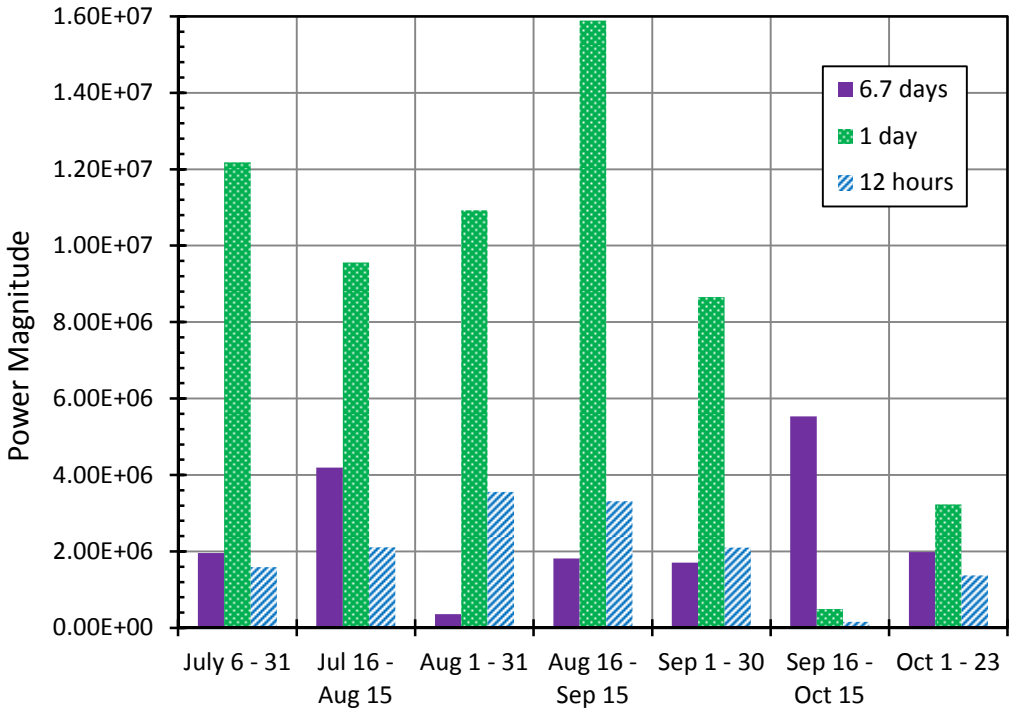

Figure 4.56b Dominant periods of oscillation in MCA dam operations during July 6 - October 23, 2011.

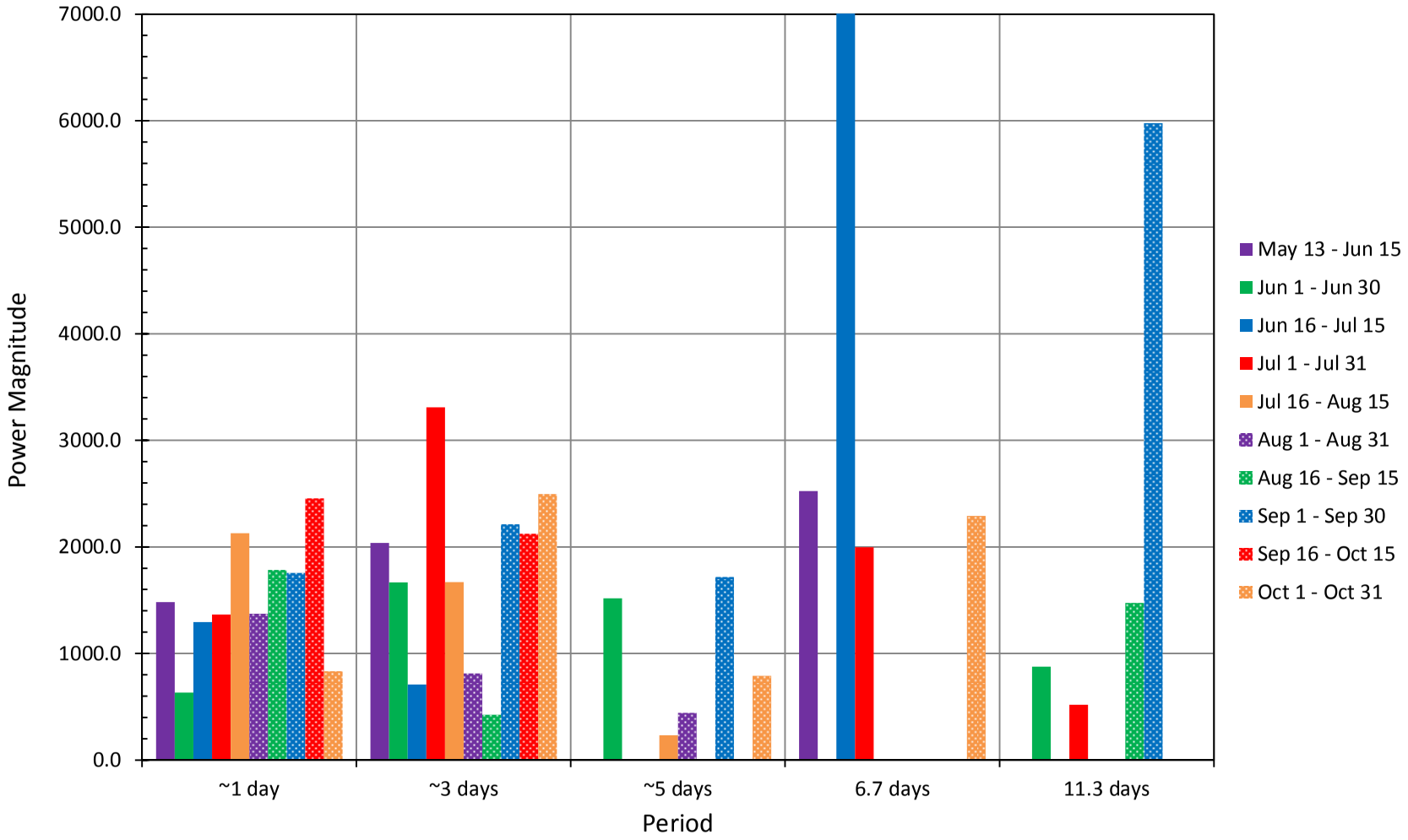

Figure 4.57 Dominant periods (order of days) in the wind speed time series data at MCA.

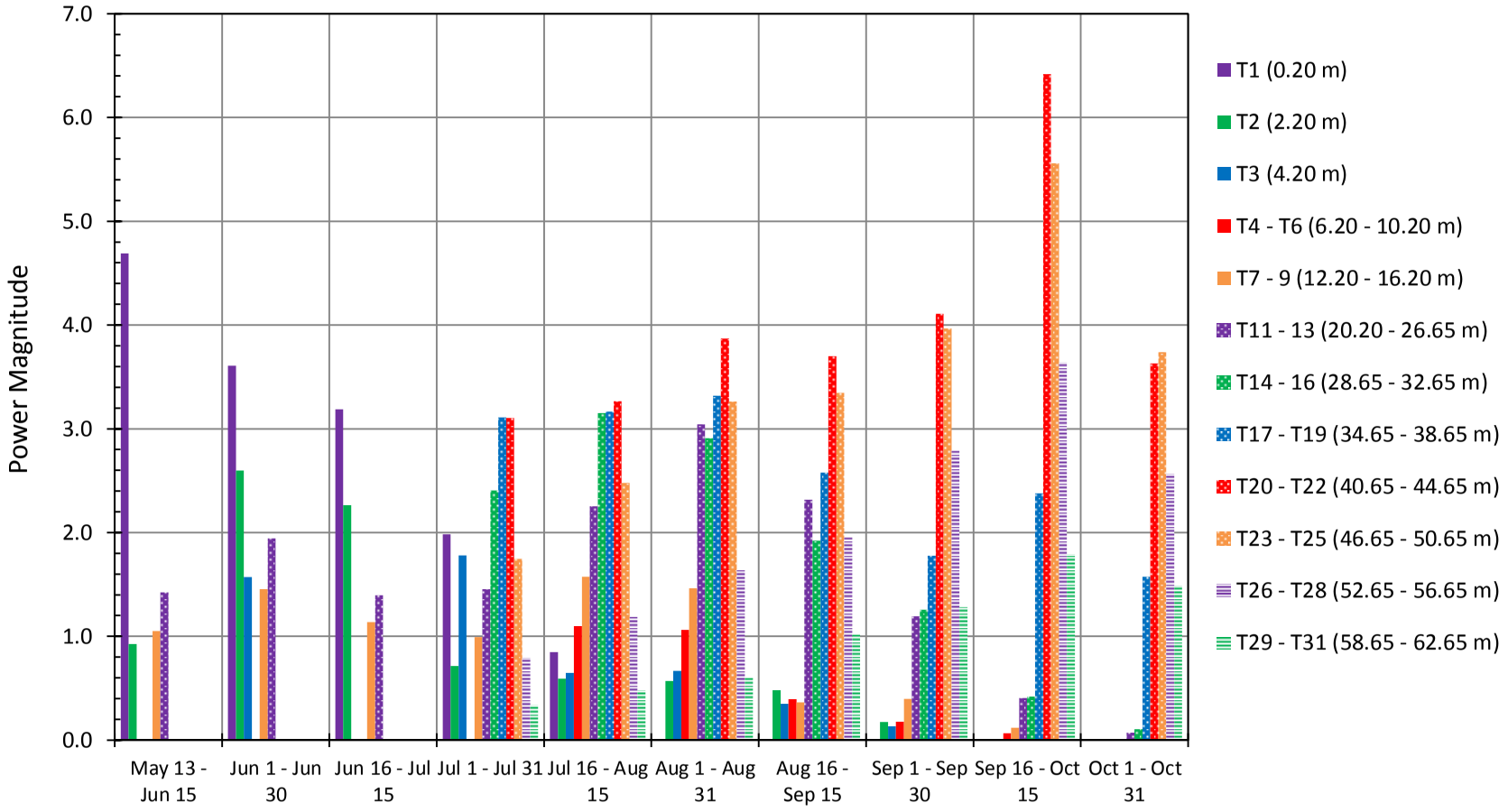

Figure 4.58a Power magnitudes of 18 - 22 hour result of high frequency waveform analysis on MCA thermistor time series.

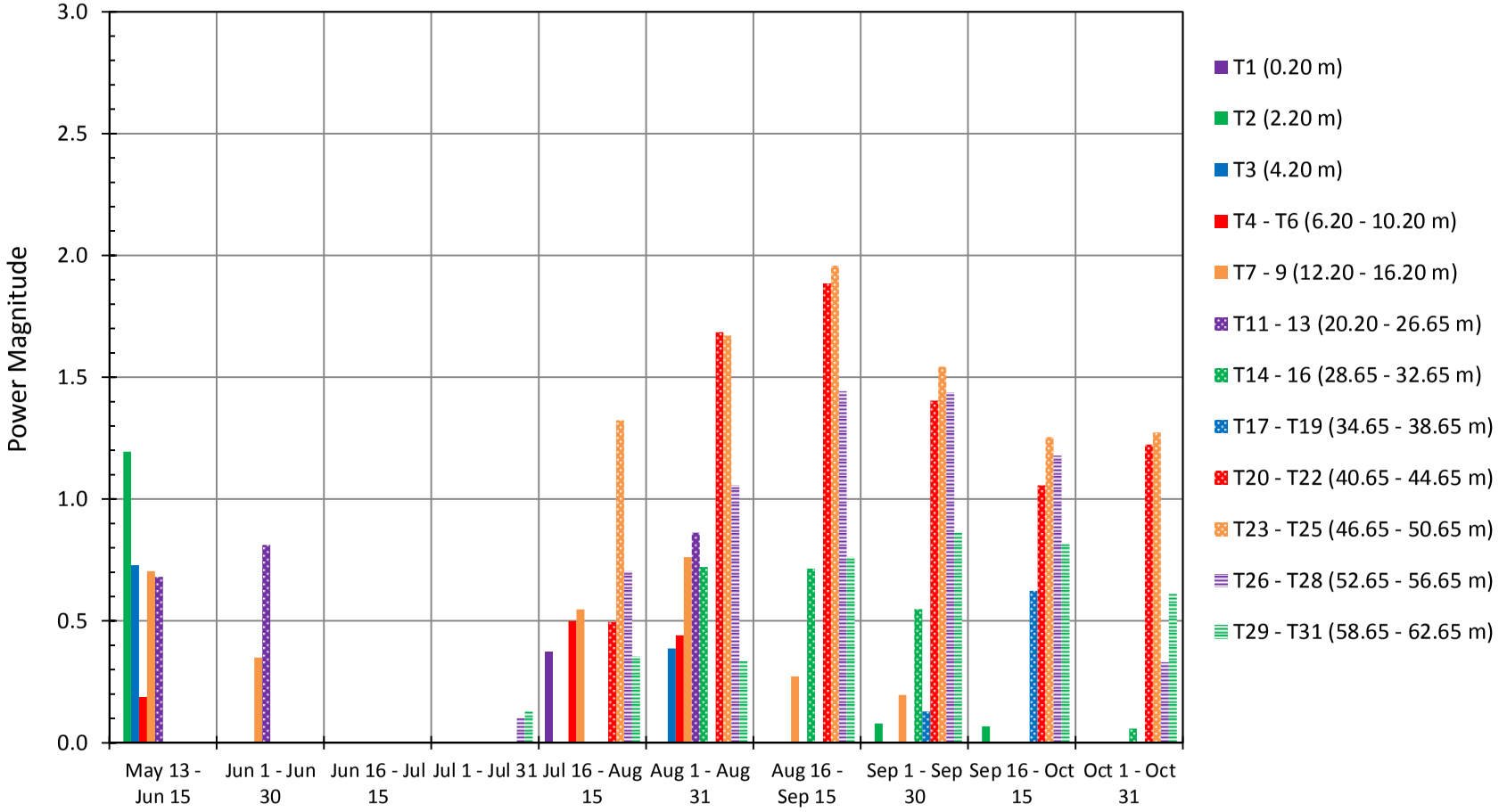

Figure 4.58b Power magnitudes of 11 - 14 hour result of high frequency waveform analysis on MCA thermistor time series.

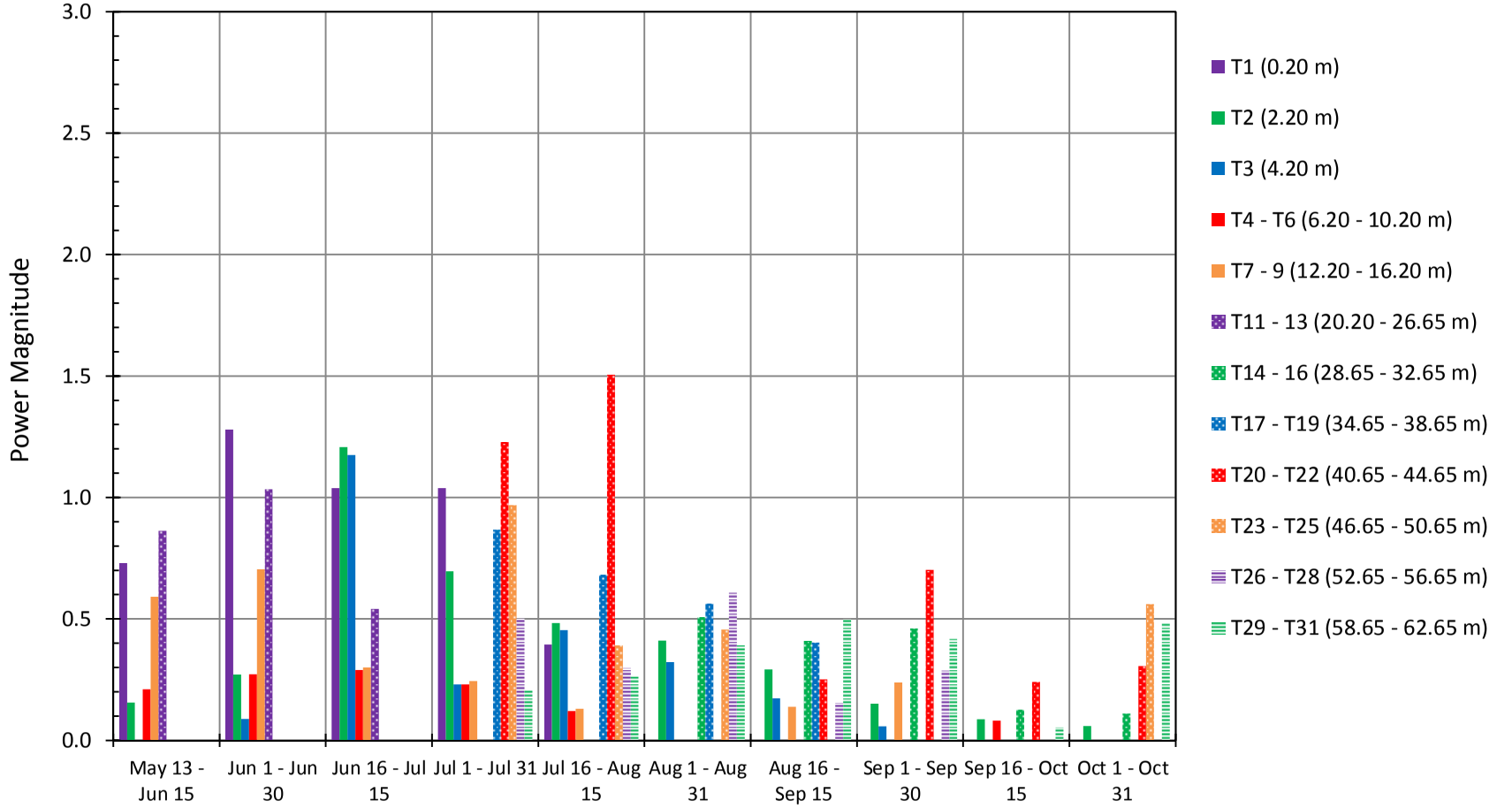

Figure 4.58c Power magnitudes of 6 - 10 hour result of high frequency waveform analysis on MCA thermistor time series.

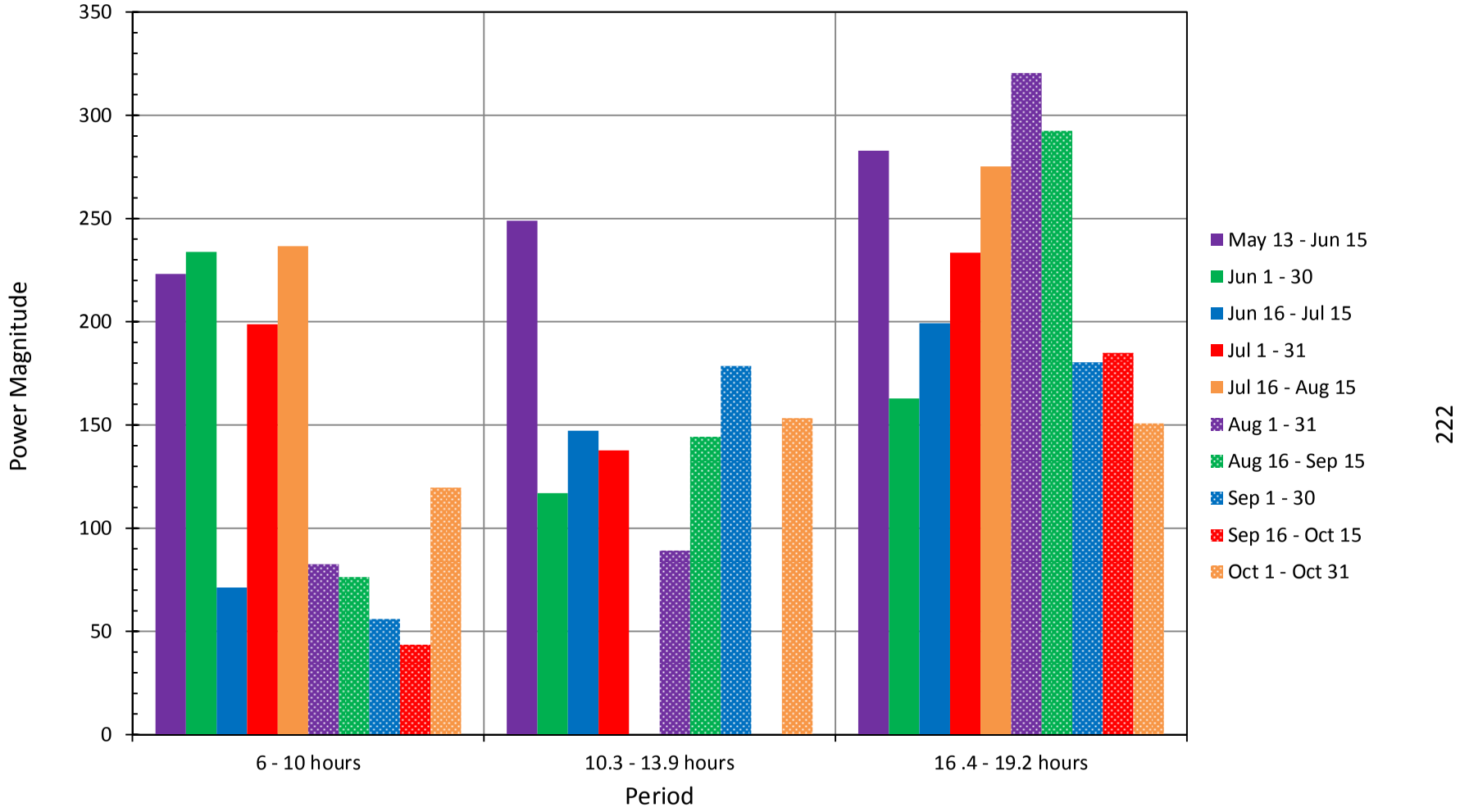

Figure 4.59 Dominant periods (order of hours) in the wind speed time series data at MCA.

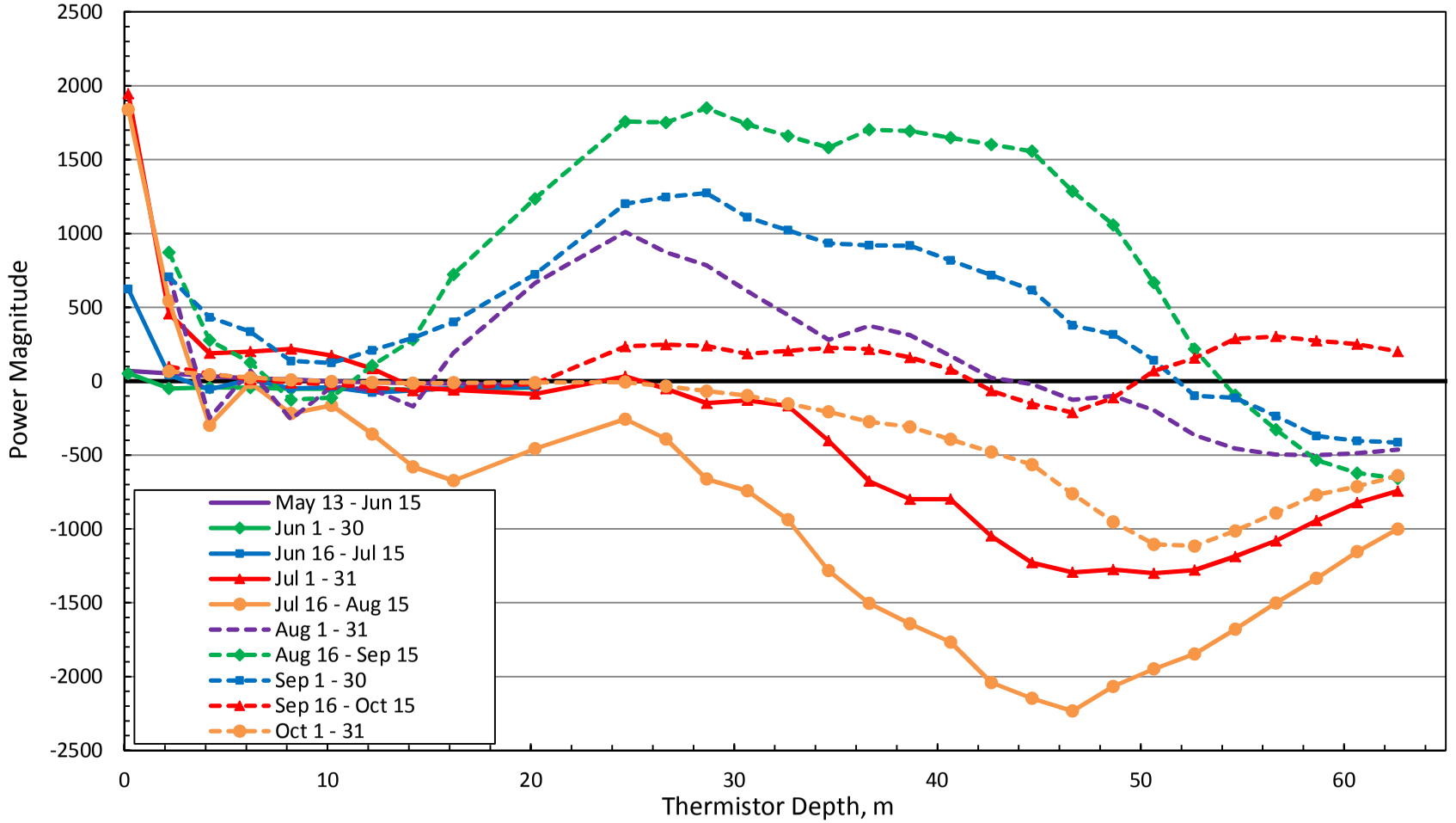

Figure 4.60 Power magnitudes of cross spectral density analysis at 1.0 day between thermistor time series and operations time series at MCA.

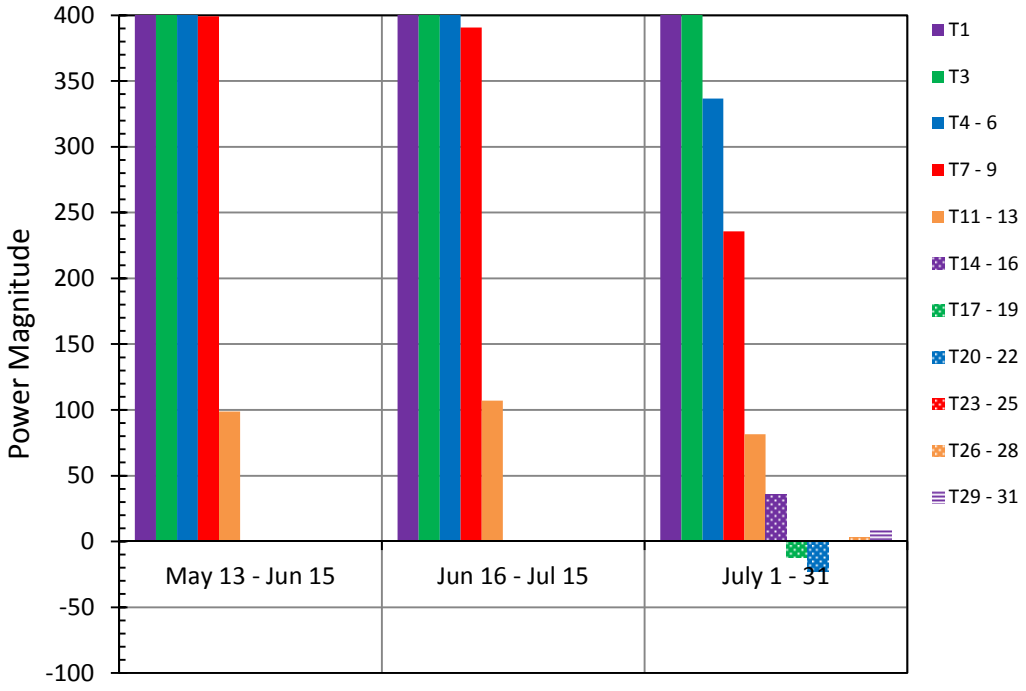

Figure 4.61a Power magnitudes of 6.7 day result of cross spectral density analysis between T2 and all other thermistors in May, June, and July.

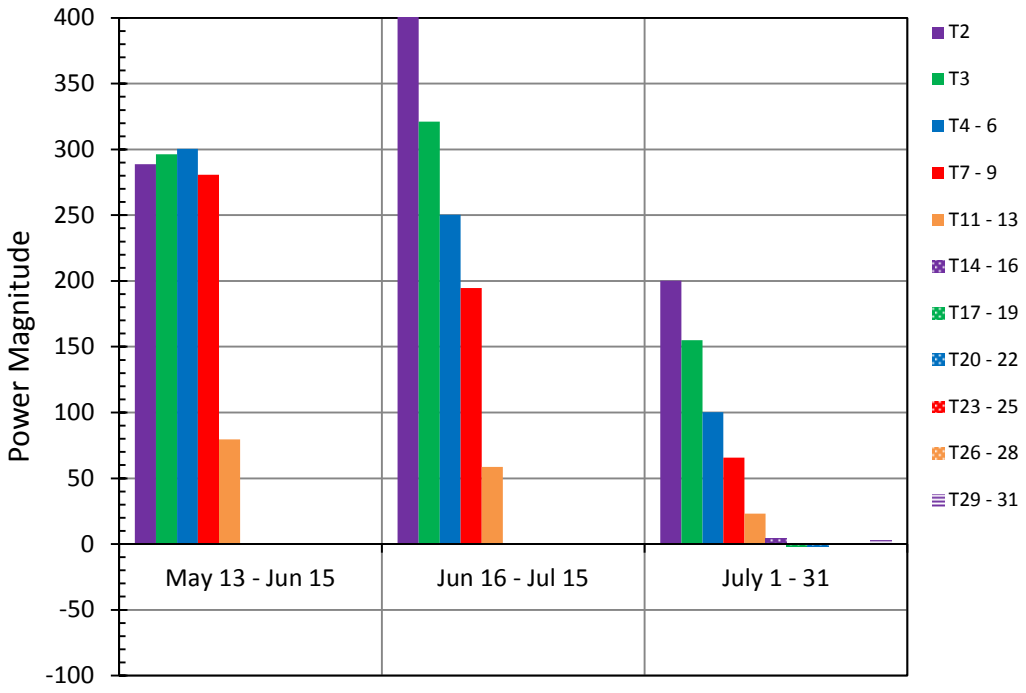

Figure 4.61b Power magnitudes of 6.7 day result of cross spectral density analysis between T11 and all other thermistors in May, June, and July.

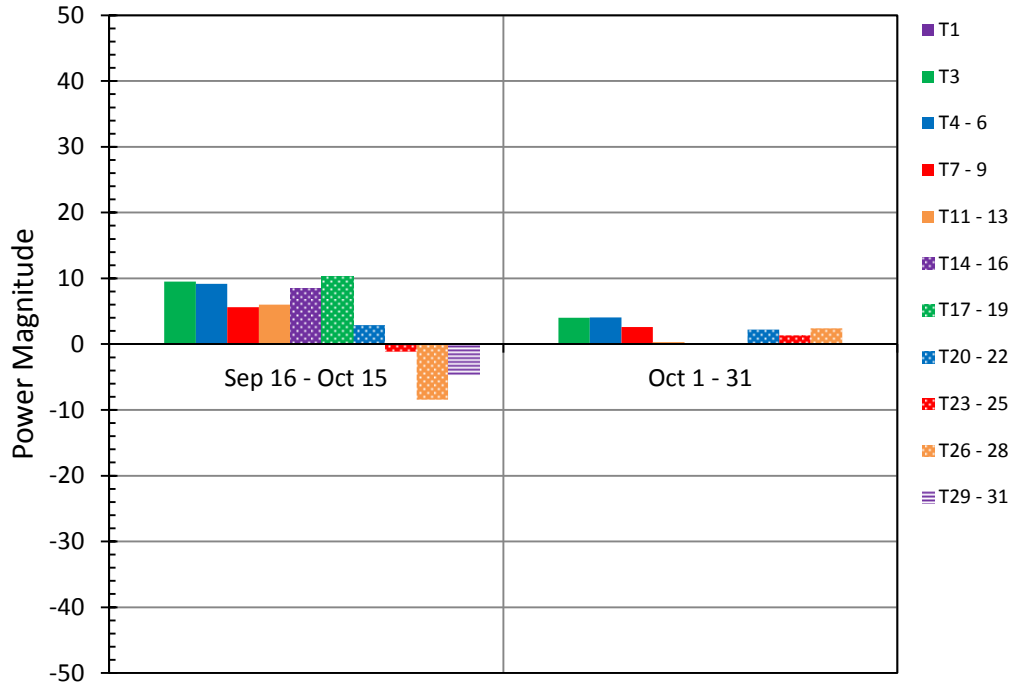

Figure 4.62a Power magnitudes of 6.7 day result of cross spectral density analysis between T2 and all other thermistors in September and October.

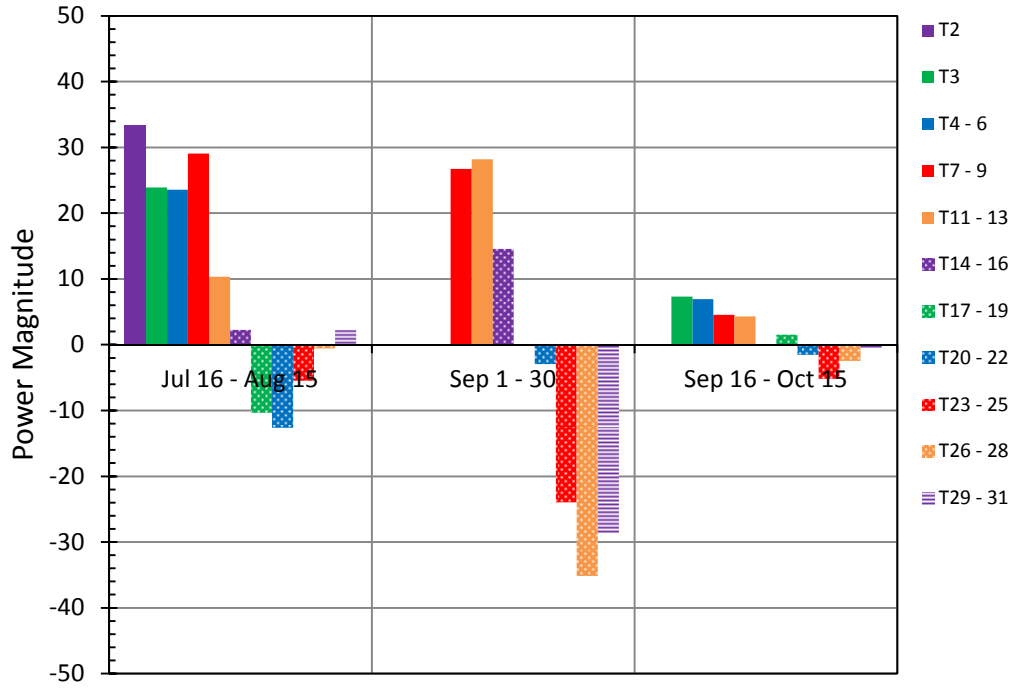

Figure 4.62b Power magnitudes of 6.7 day result of cross spectral density analysis between T11 and all other thermistors in September and October.

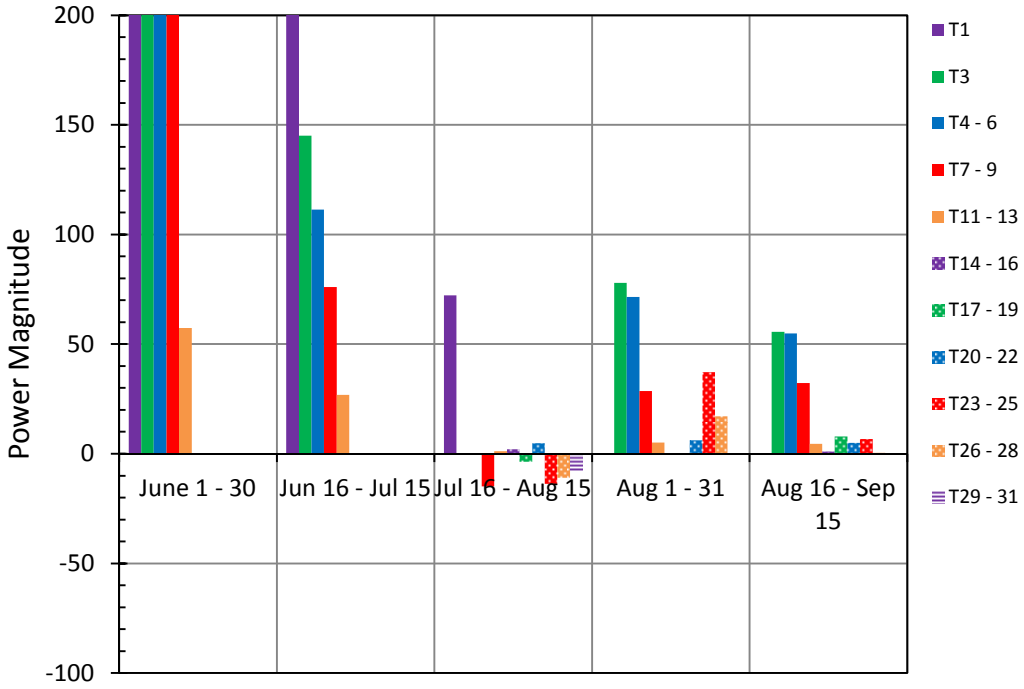

Figure 4.63a Power magnitudes of ~5 day result of cross spectral density analysis between T2 and all other thermistors.

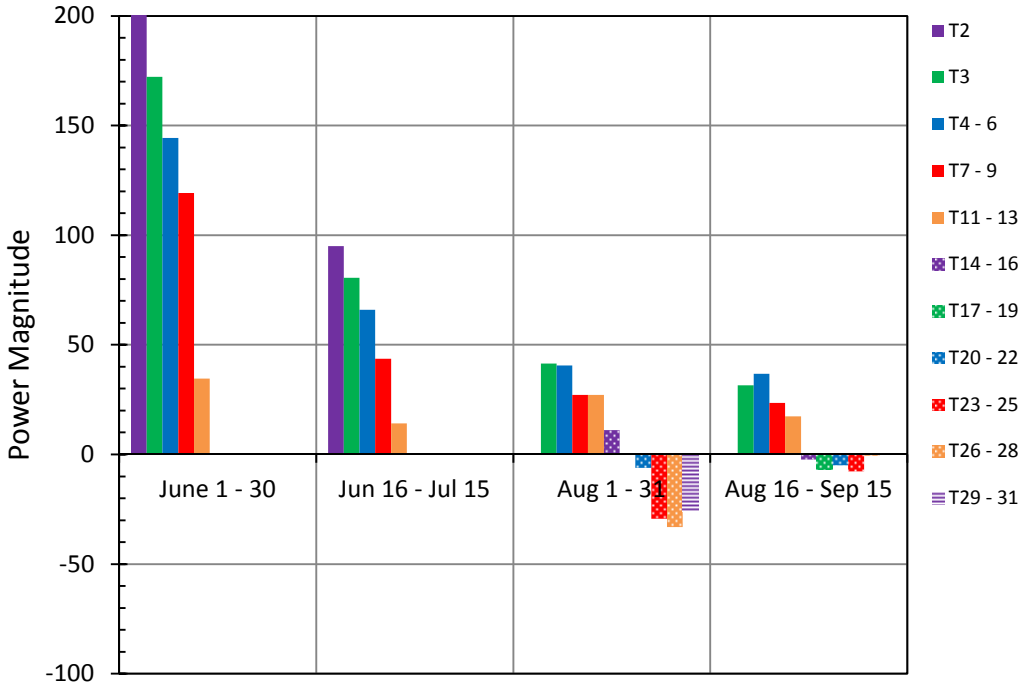

Figure 4.63b Power magnitudes of ~5 day result of cross spectral density analysis between T11 and all other thermistors.

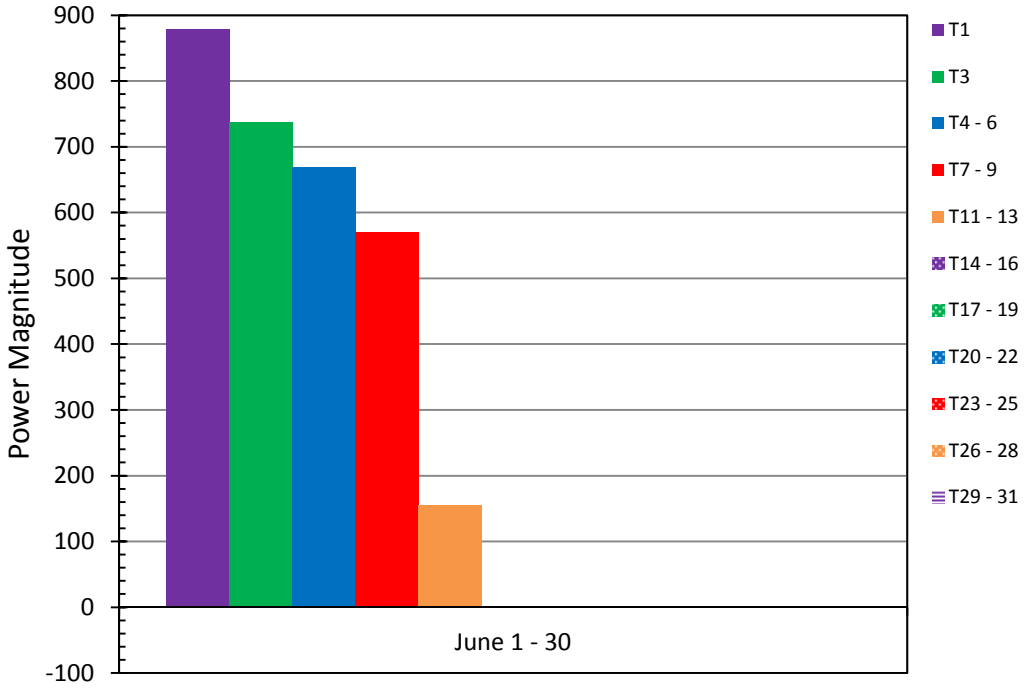

Figure 4.64a Power magnitudes of 11.3 day result of cross spectral density analysis between T2 and all other thermistors.

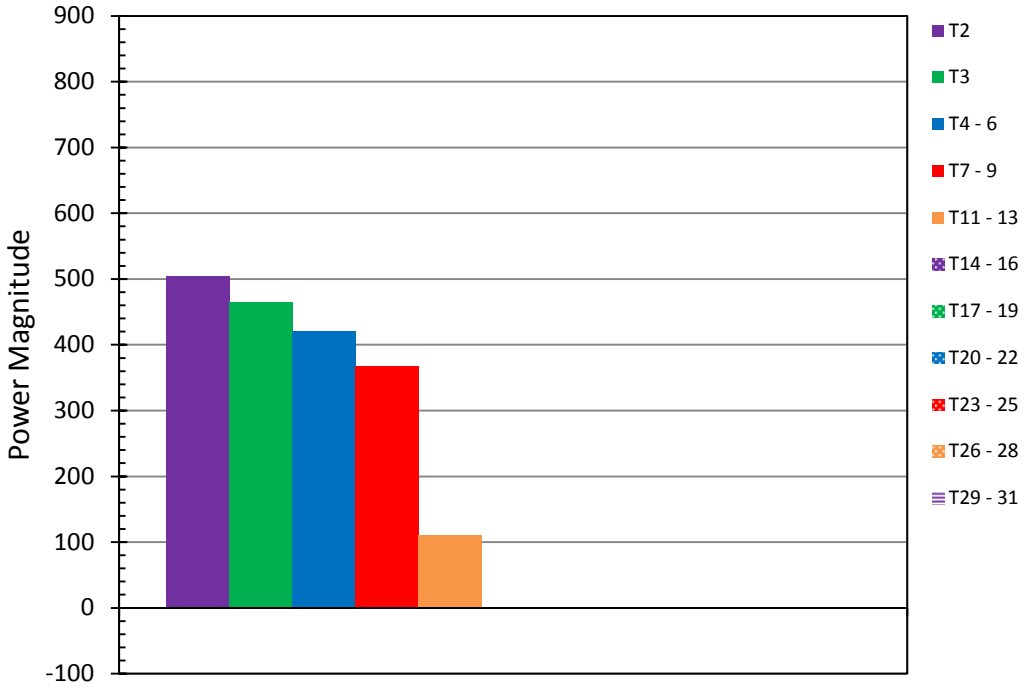

Figure 4.64b Power magnitudes of 11.3 day result of cross spectral density analysis between T11 and all other thermistors.

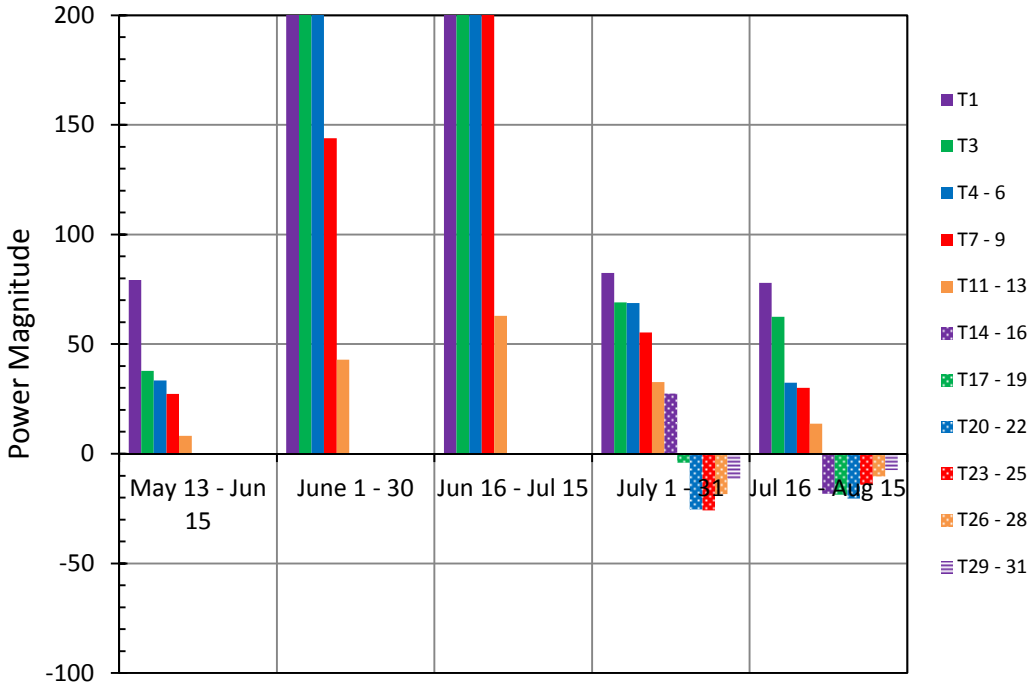

Figure 4.65a Power magnitudes of ~3 day result of cross spectral density analysis between T2 and all other thermistors in May, June, July, and August.

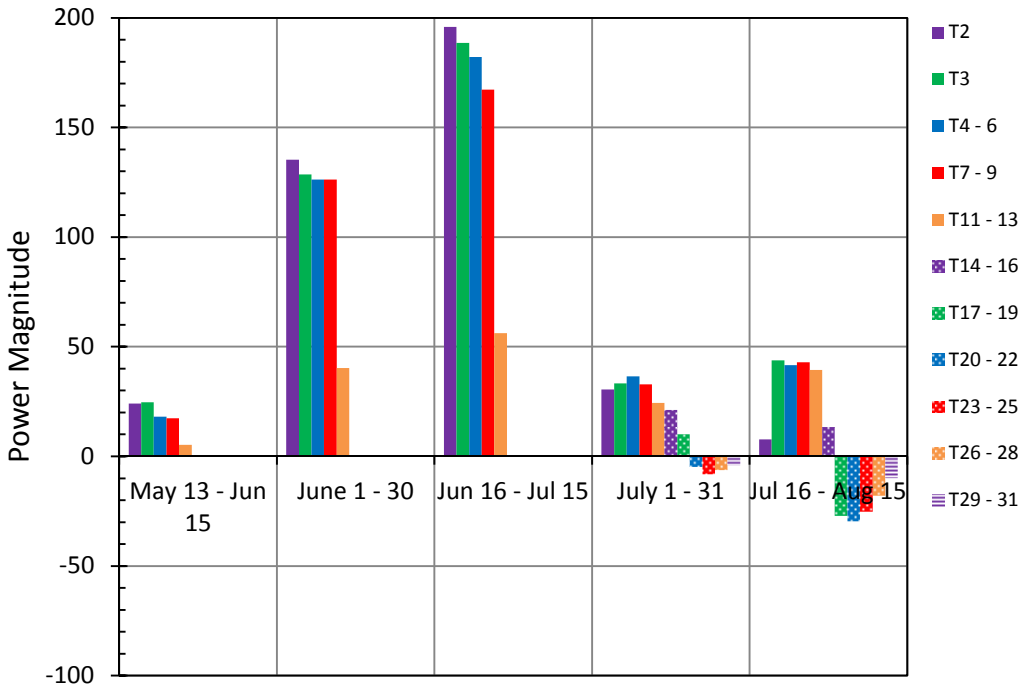

Figure 4.65b Power magnitudes of ~3 day result of cross spectral density analysis between T11 and all other thermistors in May, June, July, and August.

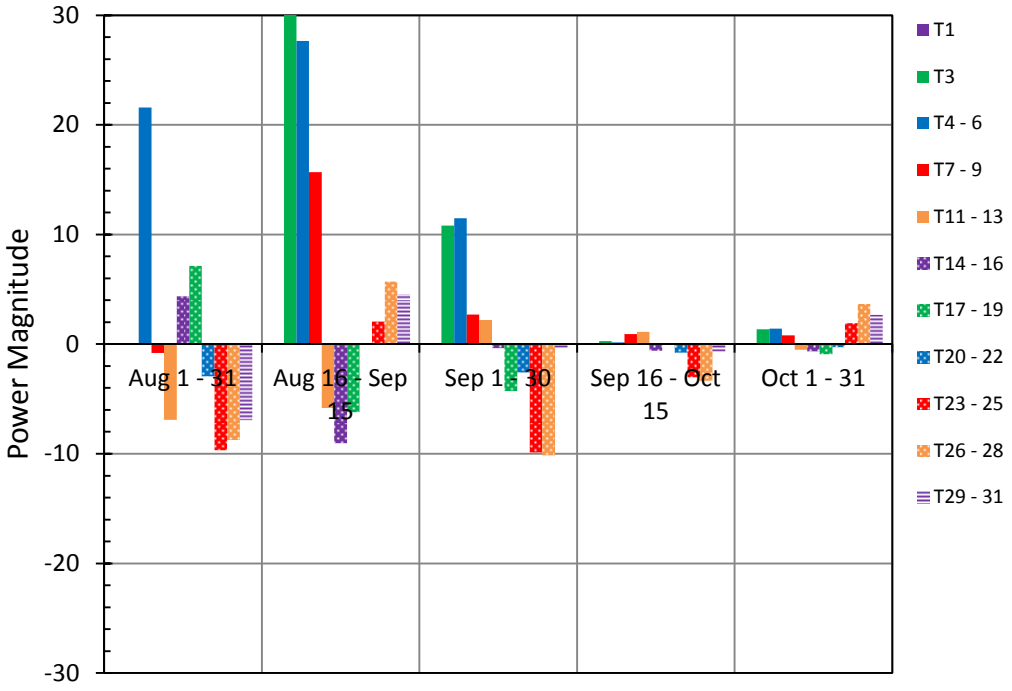

Figure 4.66a Power magnitudes of ~3 day result of cross spectral density analysis between T2 and all other thermistors in August, September, and October.

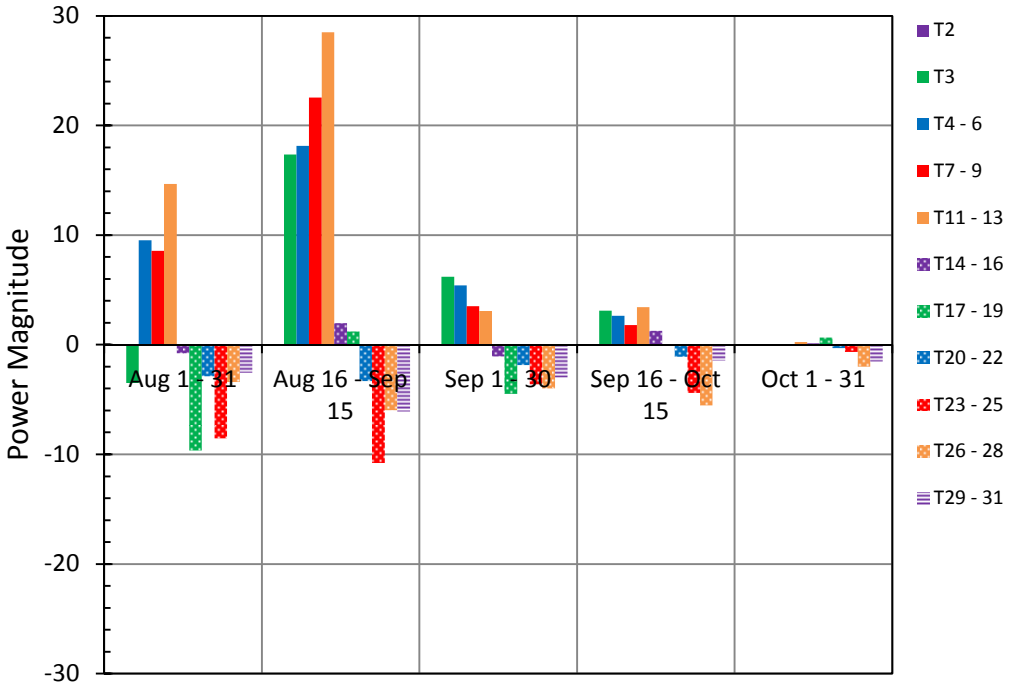

Figure 4.66b Power magnitudes of ~3 day result of cross spectral density analysis between T11 and all other thermistors in August, September, and October.

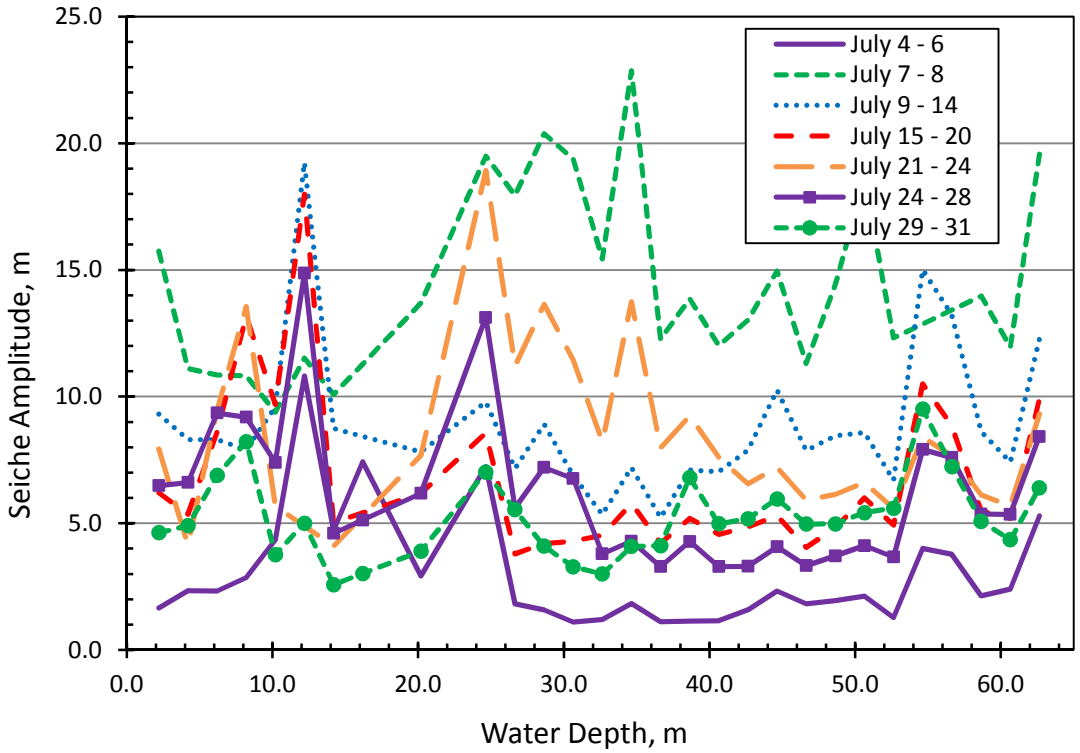

Figure 4.67a Calculated seiche amplitudes for the MCA forebay in July.

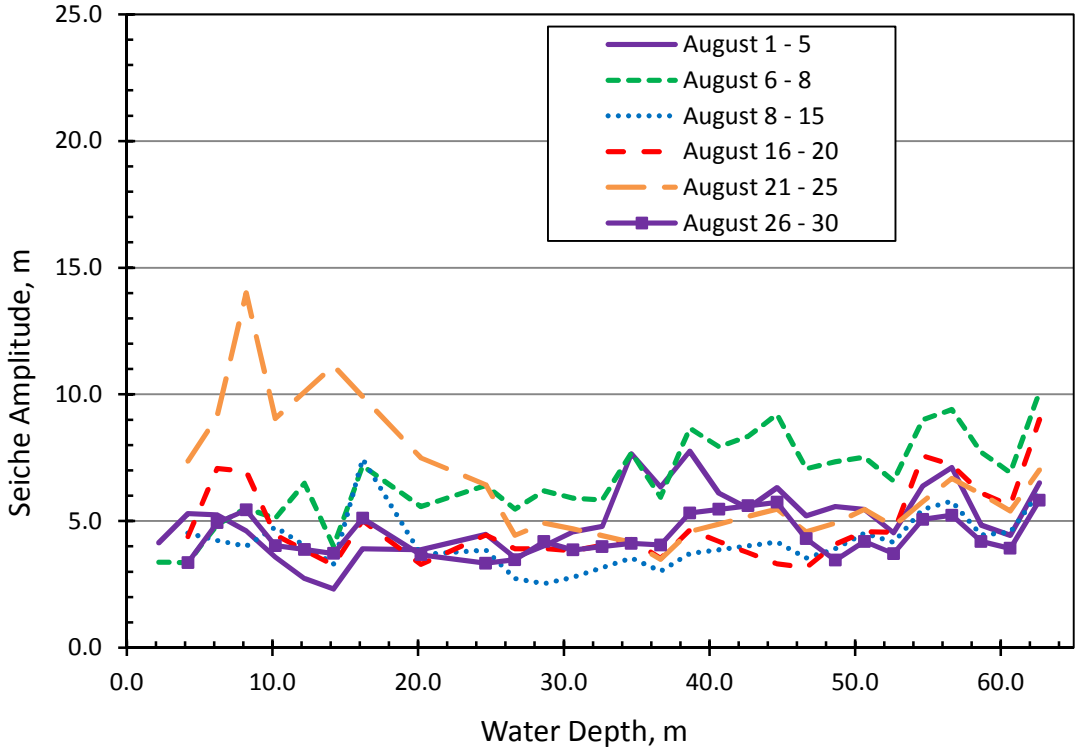

Figure 4.67b Calculated seiche amplitudes for the MCA forebay in August.

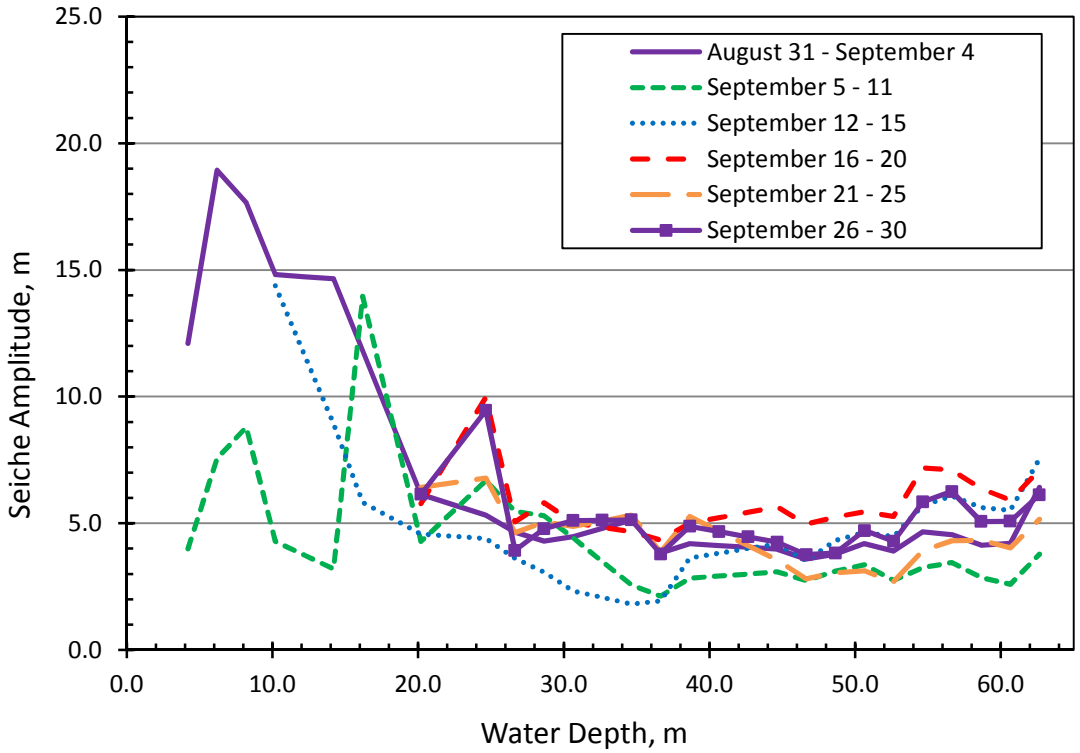

Figure 4.67c Calculated seiche amplitudes for the MCA forebay in September.

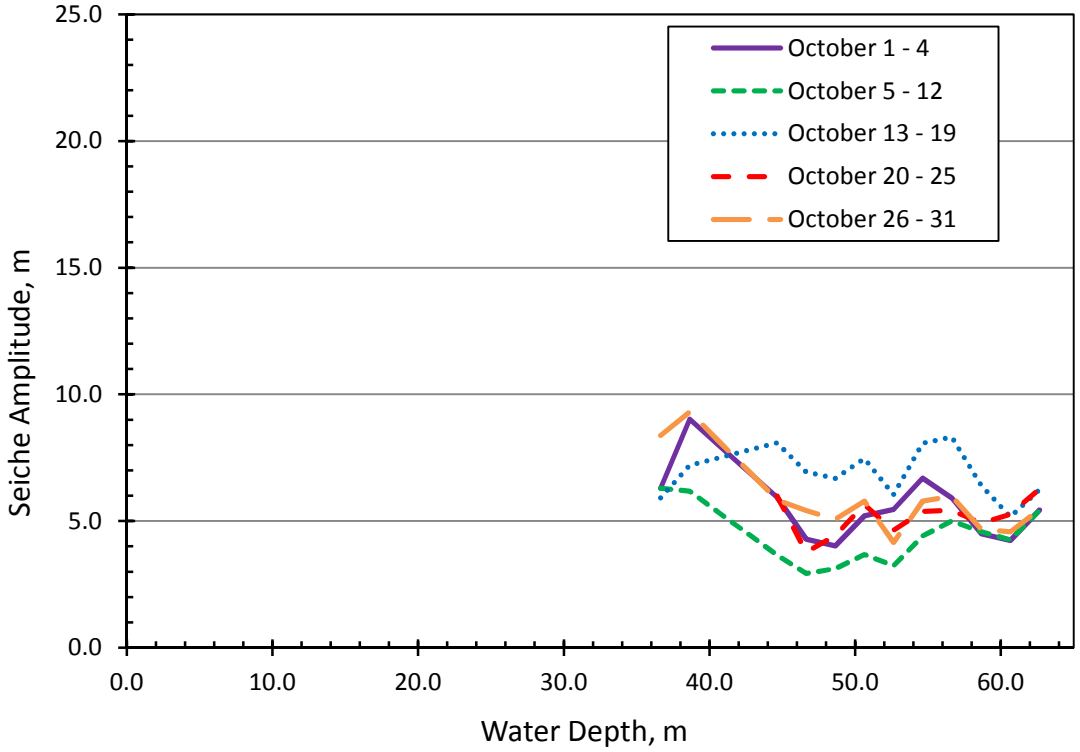

Figure 4.67d Calculated seiche amplitudes for the MCA forebay in October.

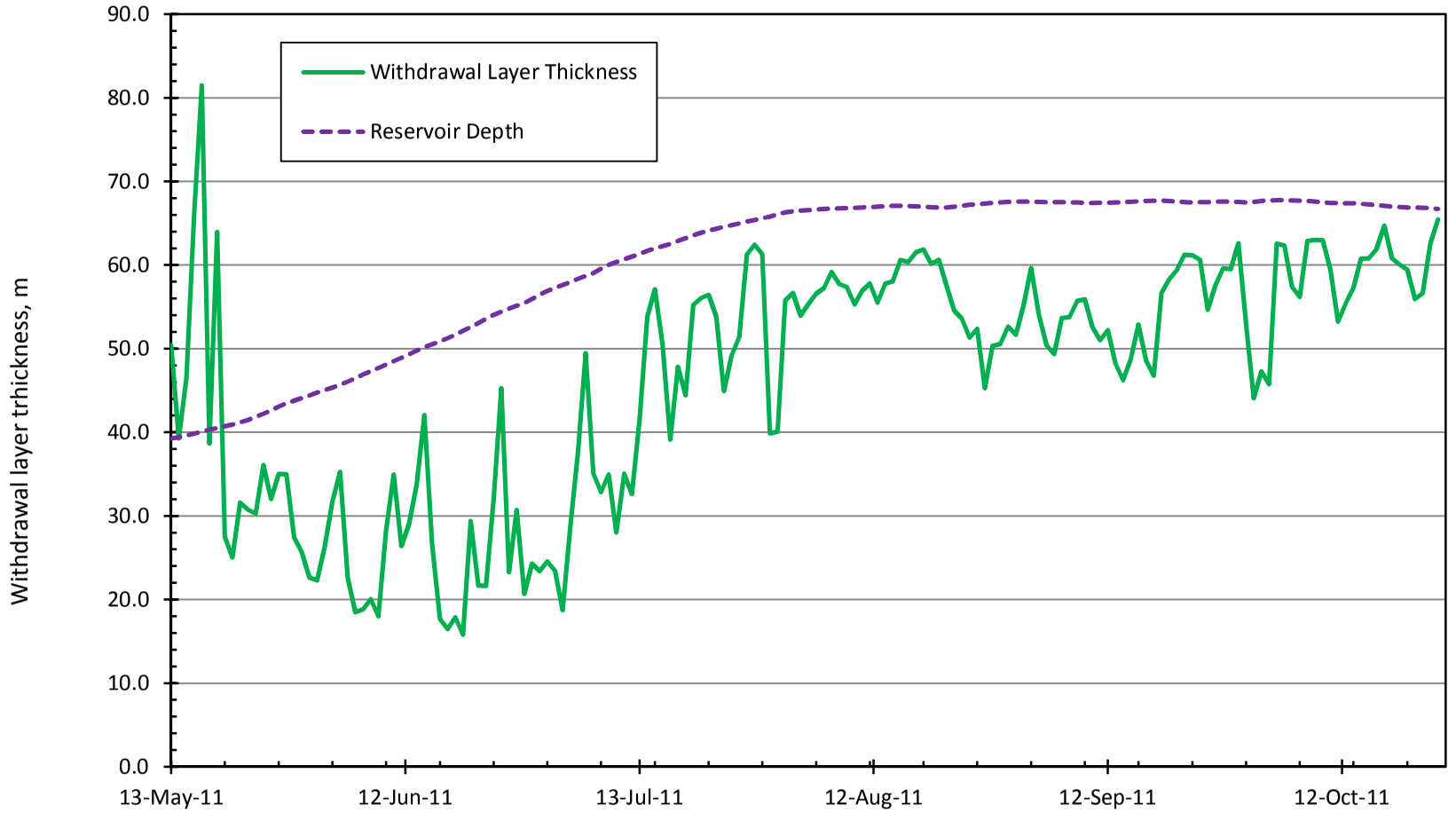

Figure 4.68 Calculated withdrawal layer thickness and reservoir depth per day at MCA.

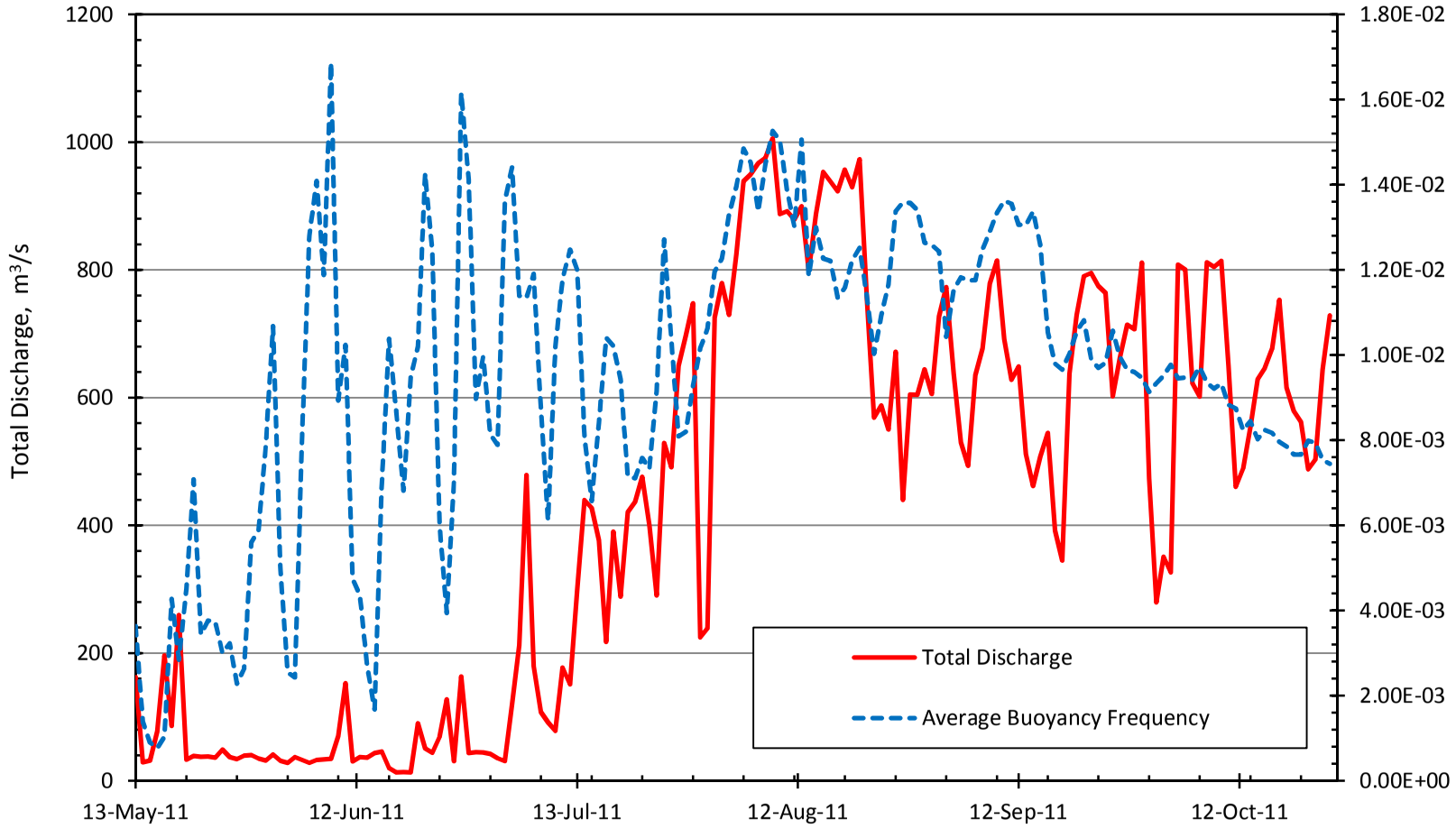

Figure 4.69 Total discharge and calculated average buoyancy frequency per day at MCA.

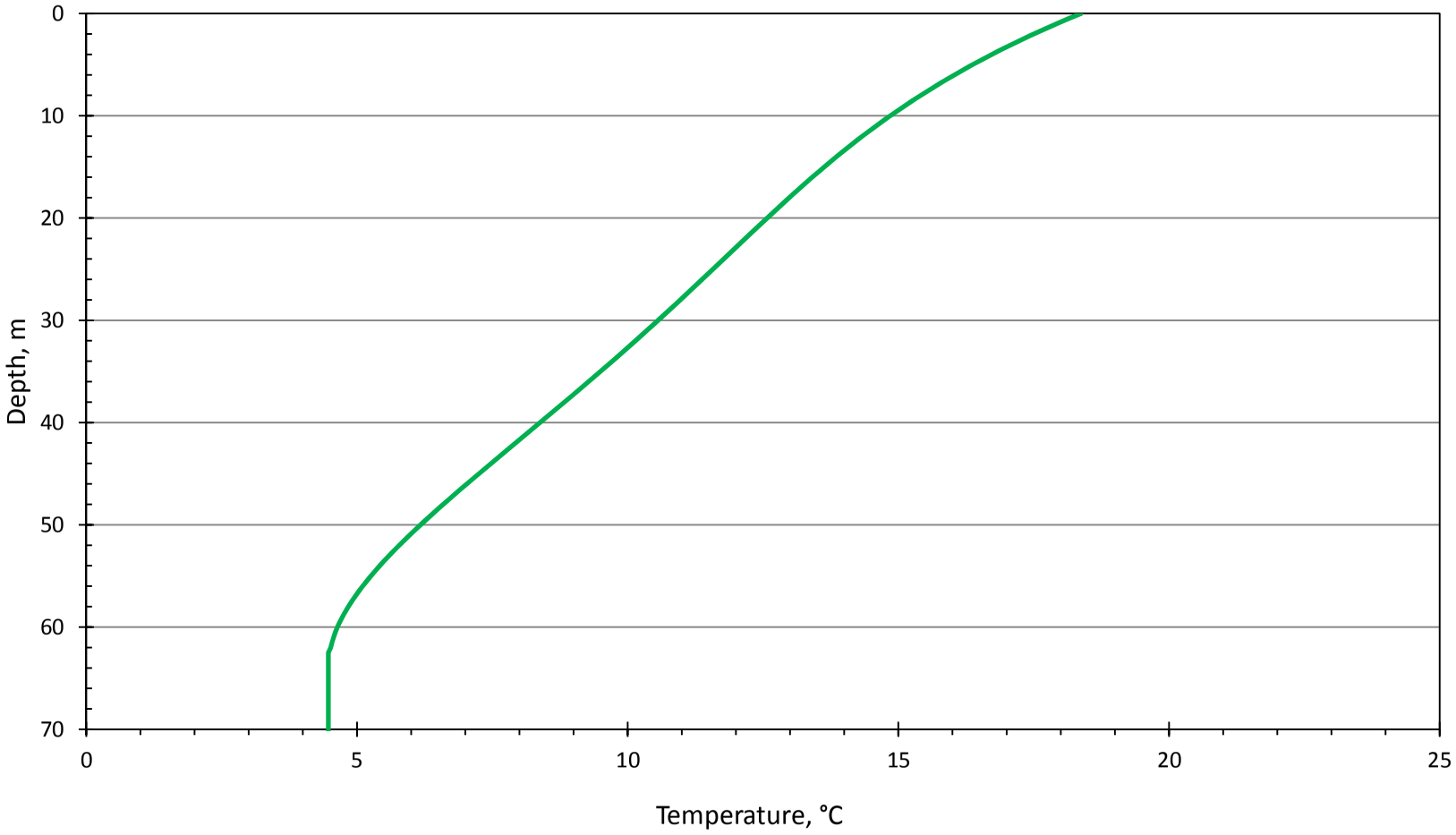

Figure 4.70 Temperature stratification used in the MCA CFD model simulations.

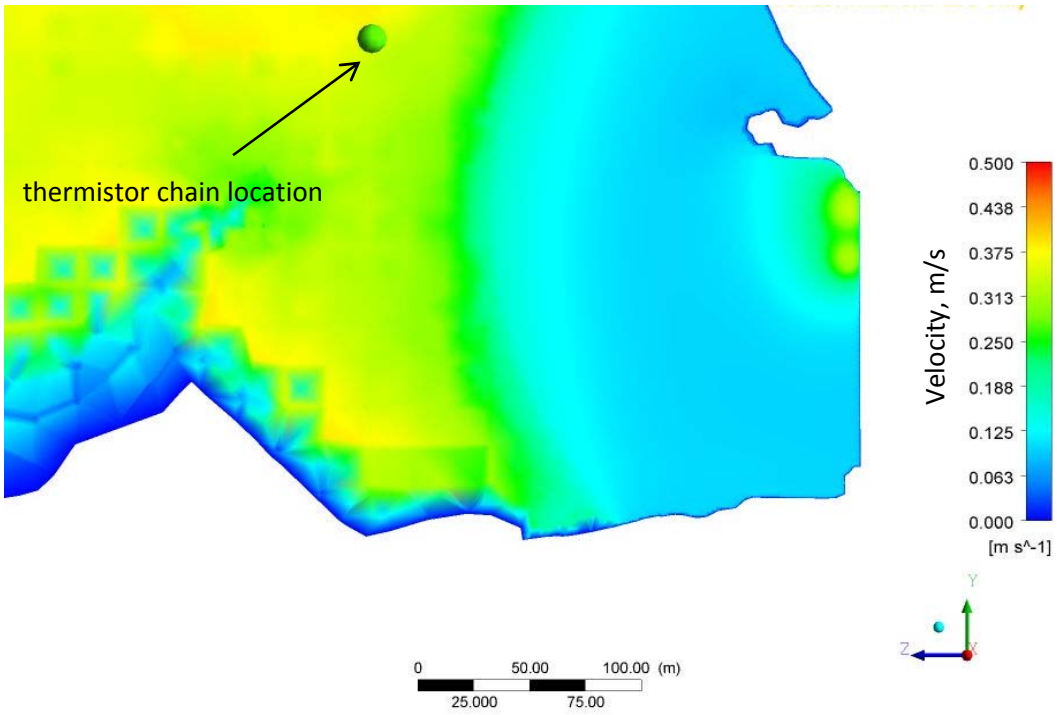

Figure 4.71a Modelled velocity magnitudes in the MCA forebay for discharges of 235 m^3/s from Intakes 1 and 2 (plane elevation is 706 m).

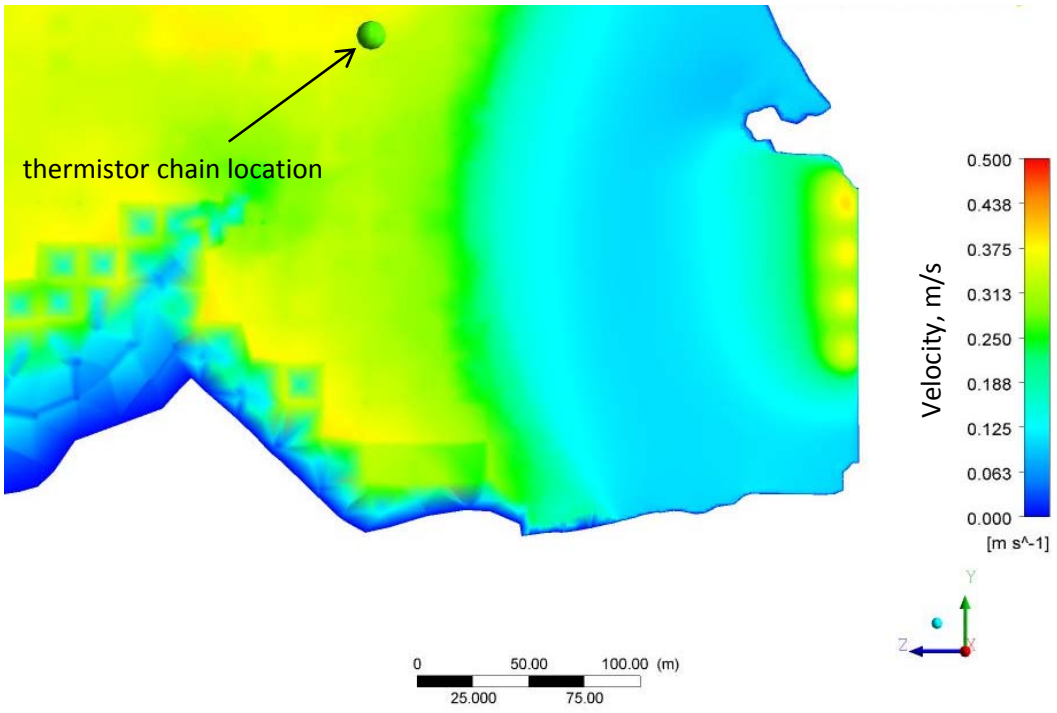

Figure 4.71b Modelled velocity magnitudes in the MCA forebay for discharges of 257 m^3/s from Intakes 1 - 4 (plane elevation is 706 m).

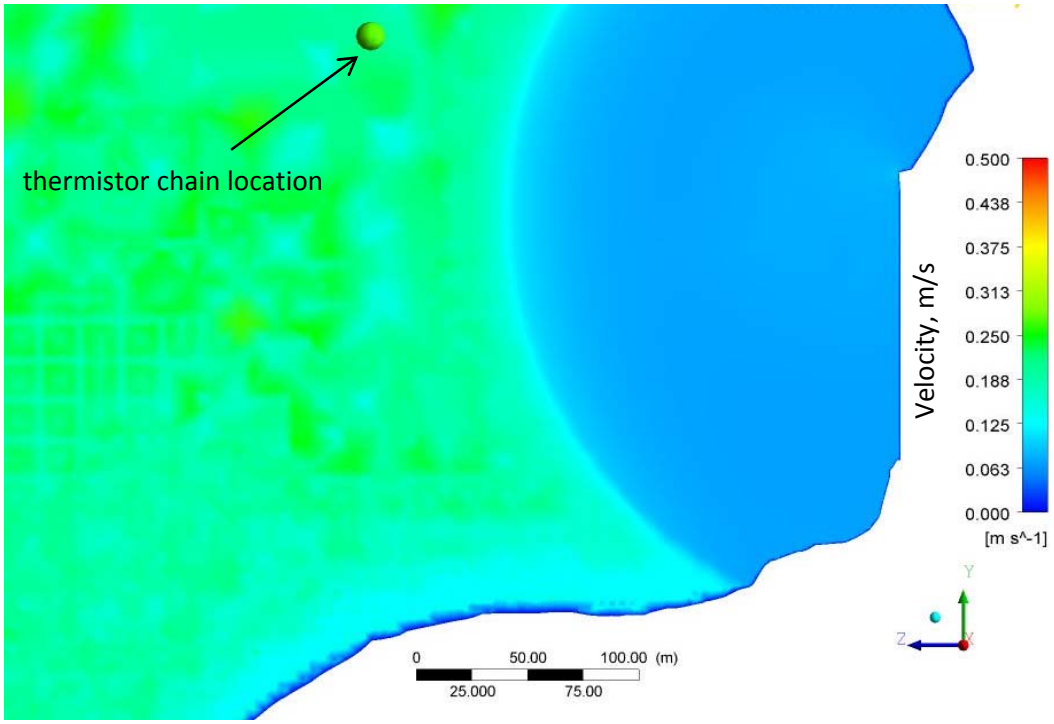

Figure 4.71c Modelled velocity magnitudes in the MCA forebay for discharges of 235 m^3/s from Intakes 1 and 2 (plane elevation is 740 m).

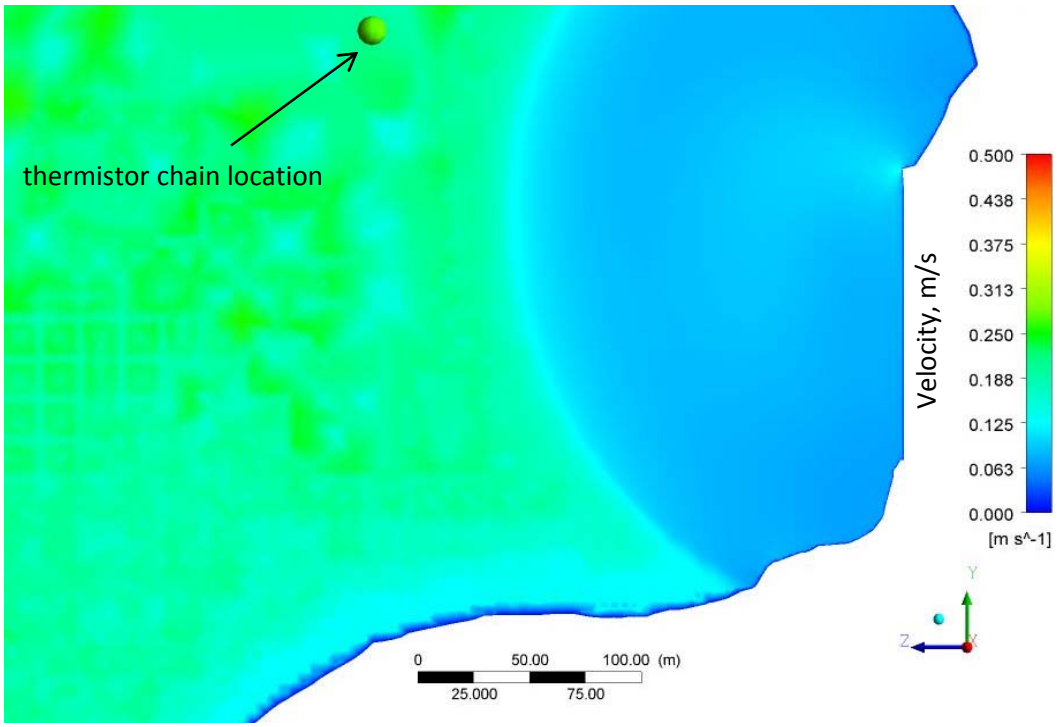

Figure 4.71d Modelled velocity magnitudes in the MCA forebay for discharges of 257 m^3/s from Intakes 1 - 4 (plane elevation is 740 m).

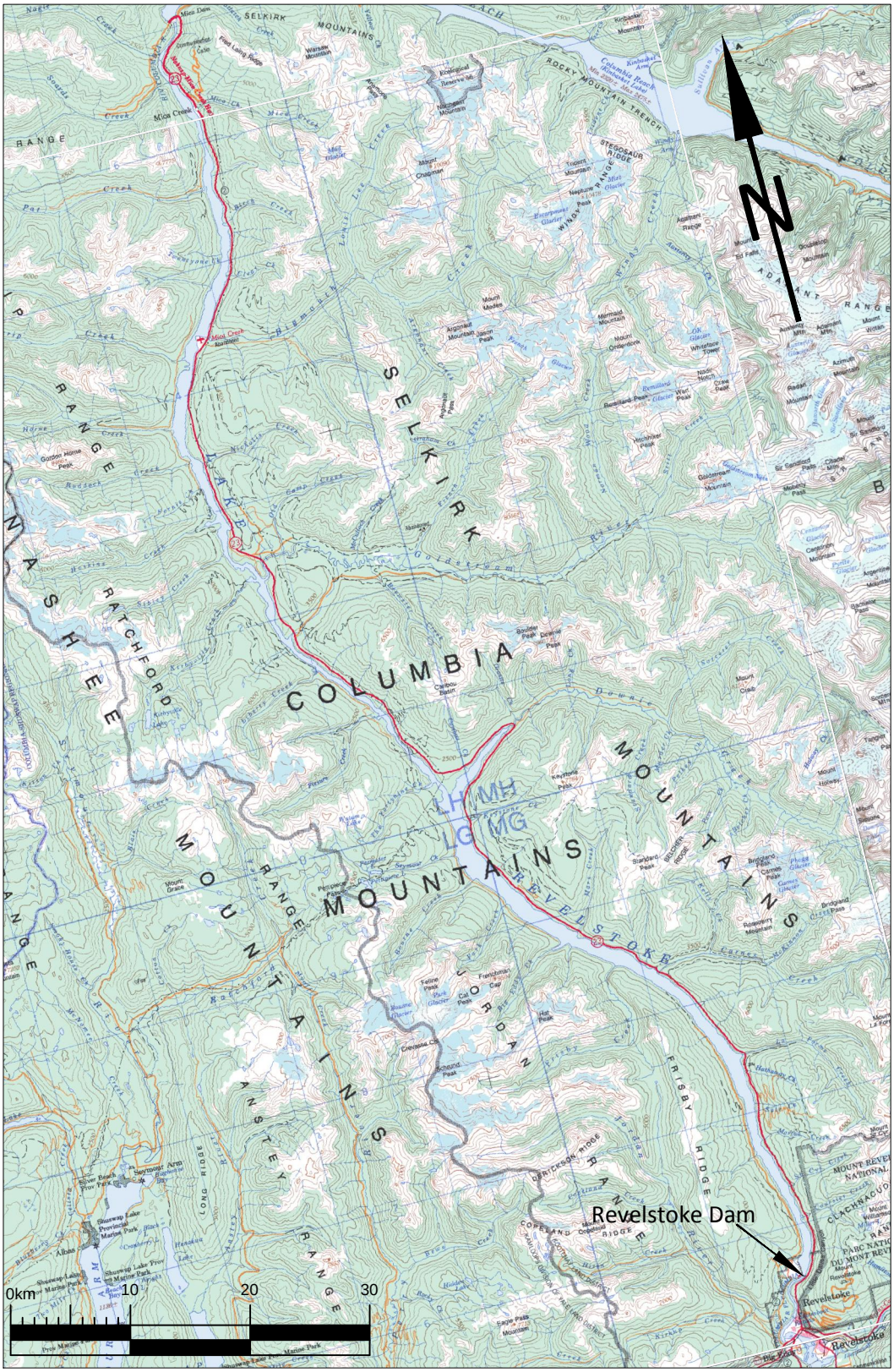

Figure 5.1 Overall site plan of Revelstoke reservoir.

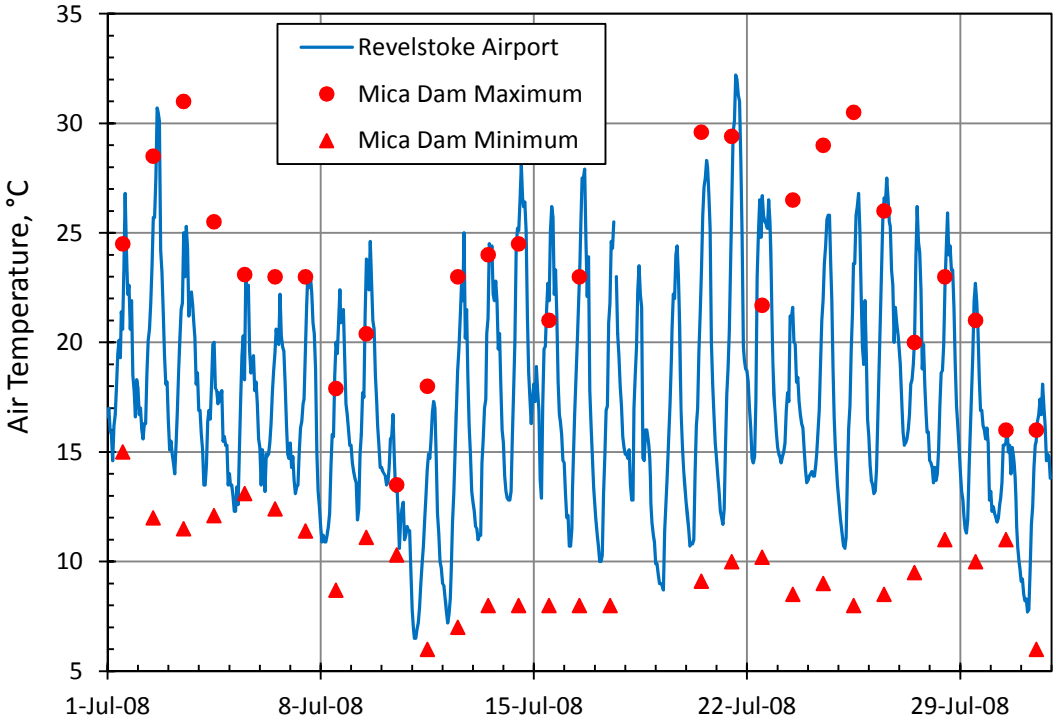

Figure 5.2a Air temperatures recorded at Revelstoke Airport and Mica Dam meteorological stations in July, 2008.

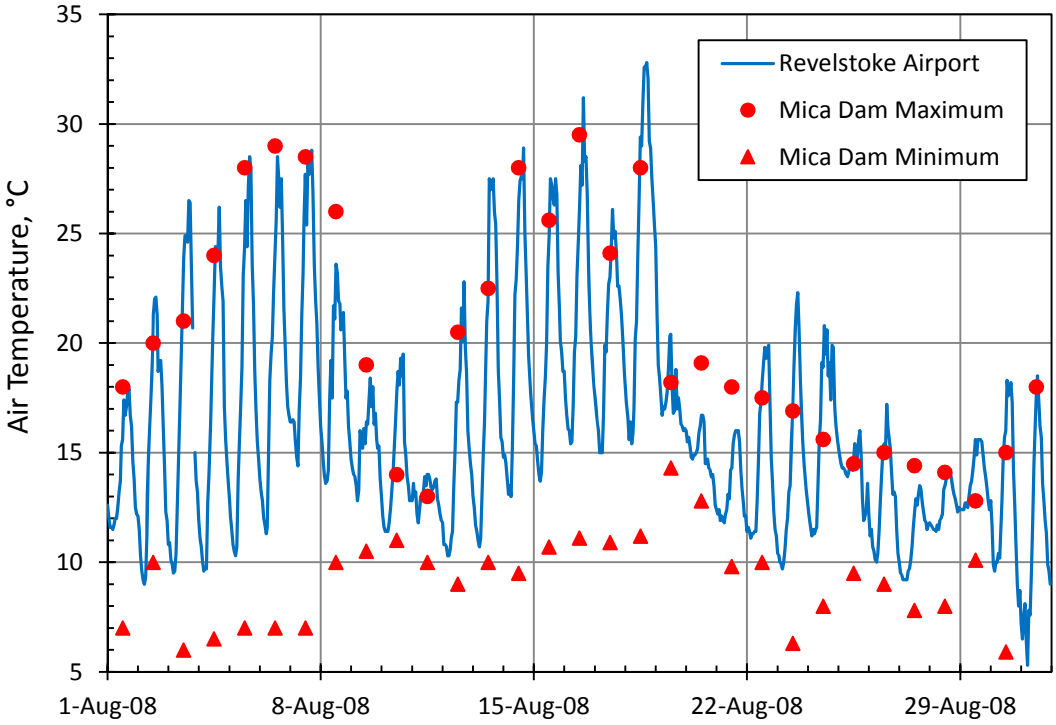

Figure 5.2b Air temperatures recorded at Revelstoke Airport and Mica Dam meteorological stations in August, 2008.

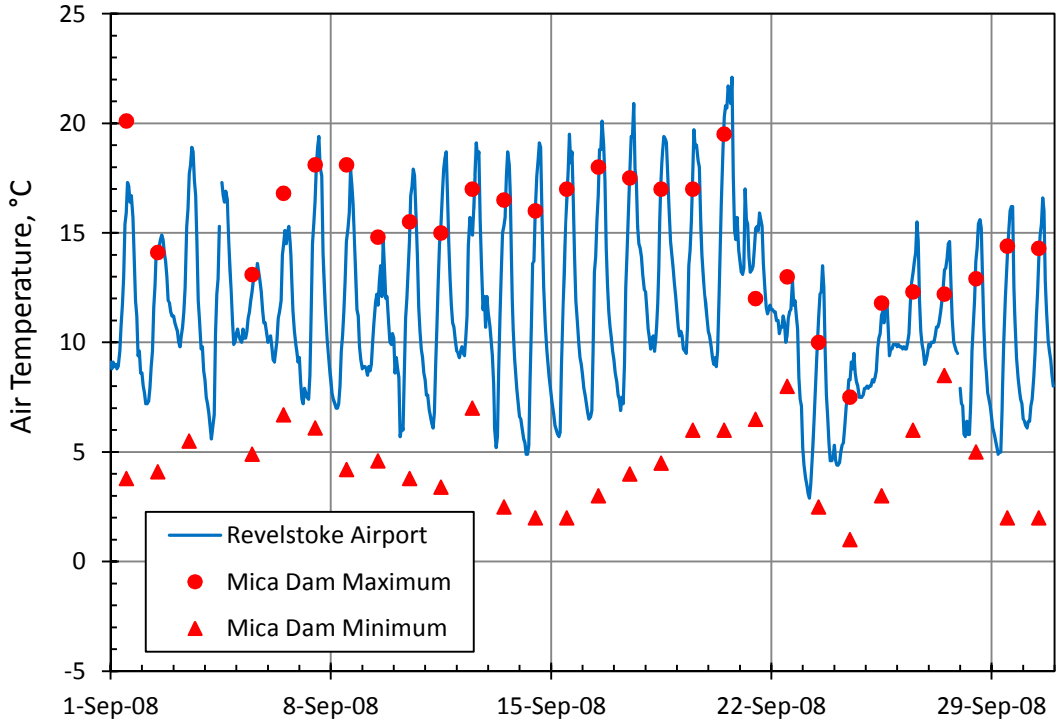

Figure 5.2c Air temperatures recorded at Revelstoke Airport and Mica Dam meteorological stations in September 2008.

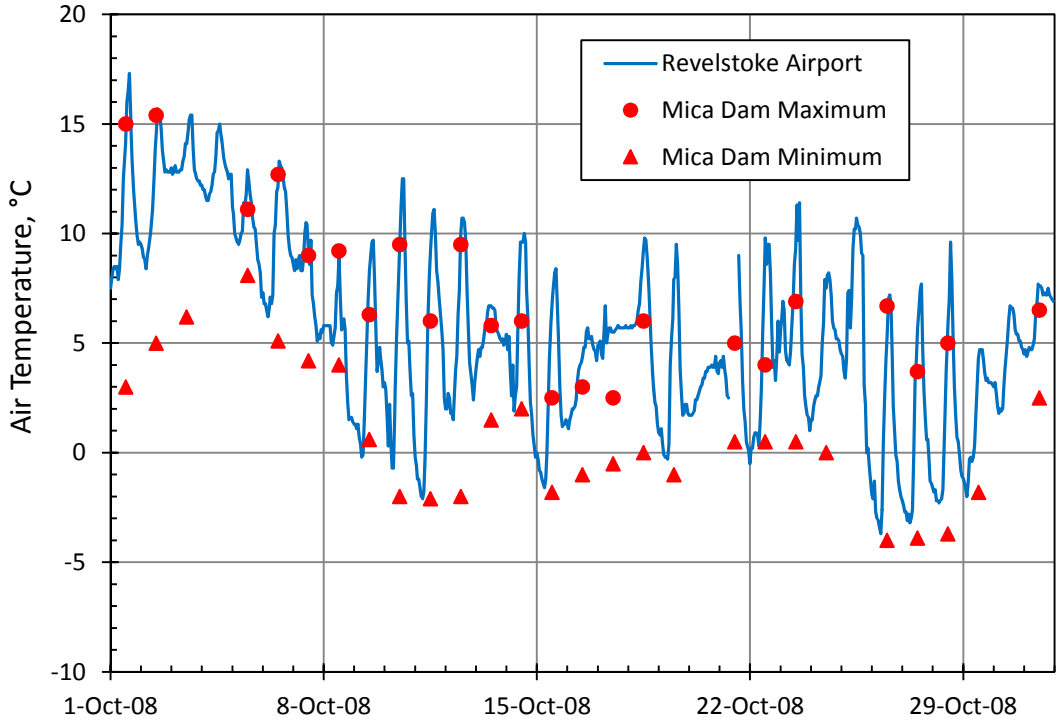

Figure 5.2d Air temperatures recorded at Revelstoke Airport and Mica Dam meteorological stations in October, 2008.

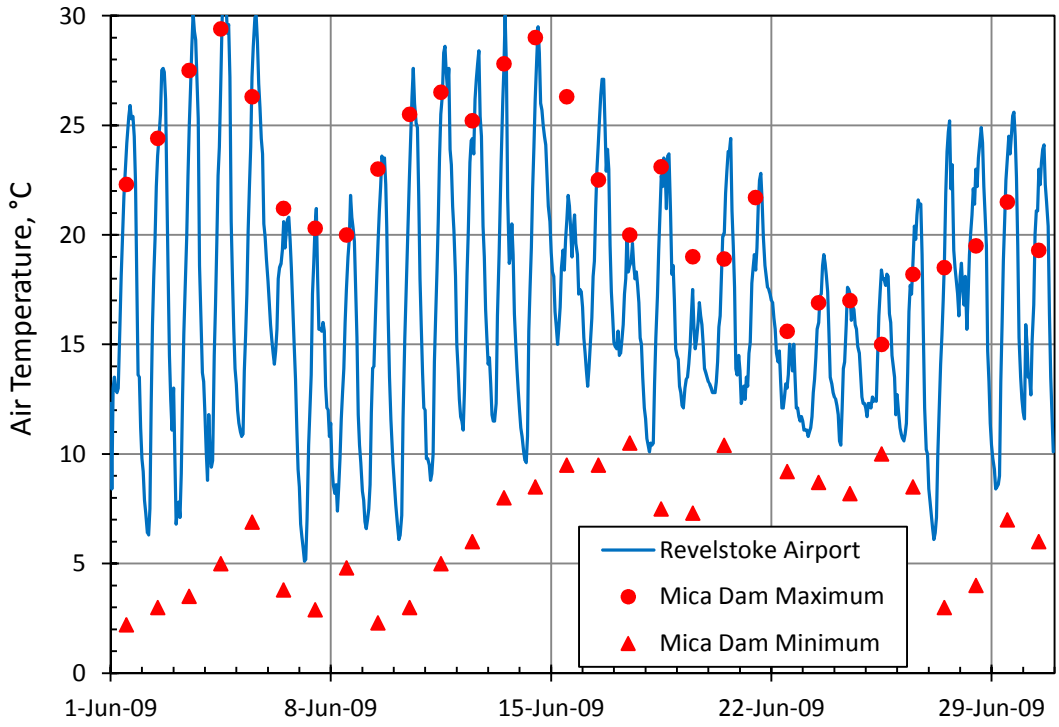

Figure 5.3a Air temperatures recorded at Revelstoke Airport and Mica Dam meteorological stations in June, 2009.

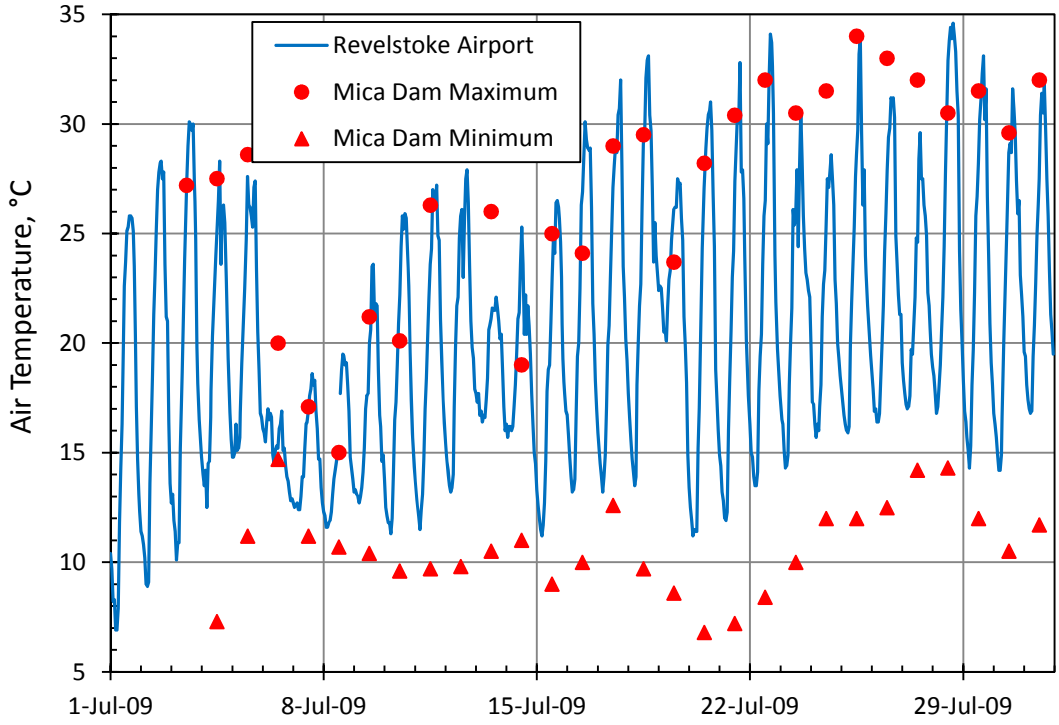

Figure 5.3b Air temperatures recorded at Revelstoke Airport and Mica Dam meteorological stations in July, 2009.

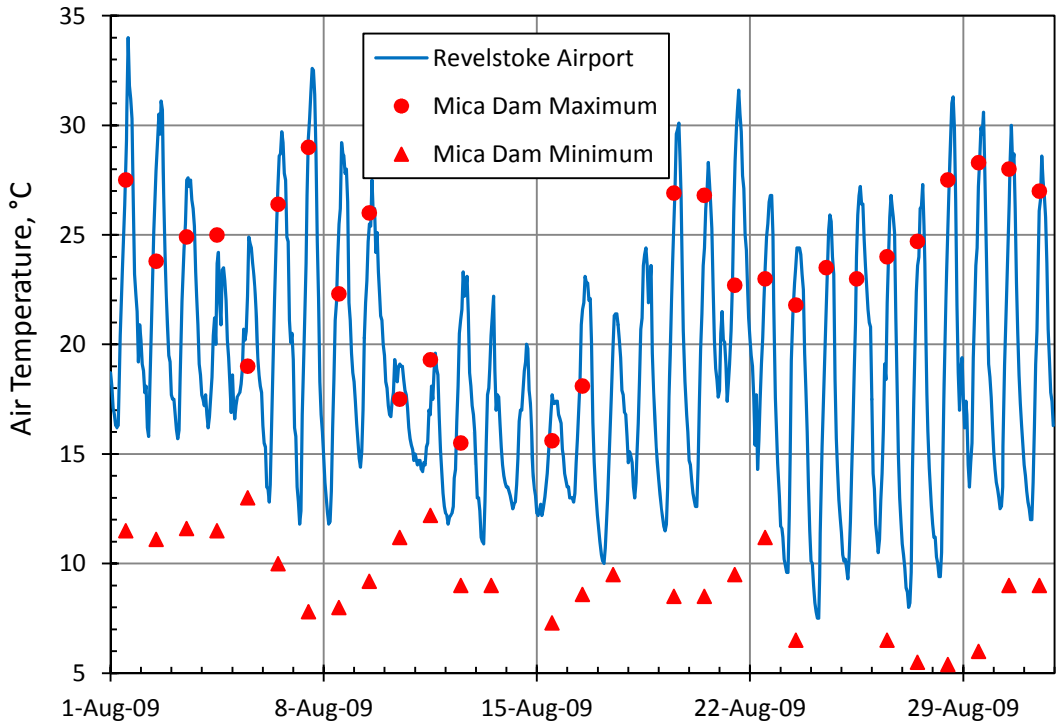

Figure 5.3c Air temperatures recorded at Revelstoke Airport and Mica Dam meteorological stations in August, 2009.

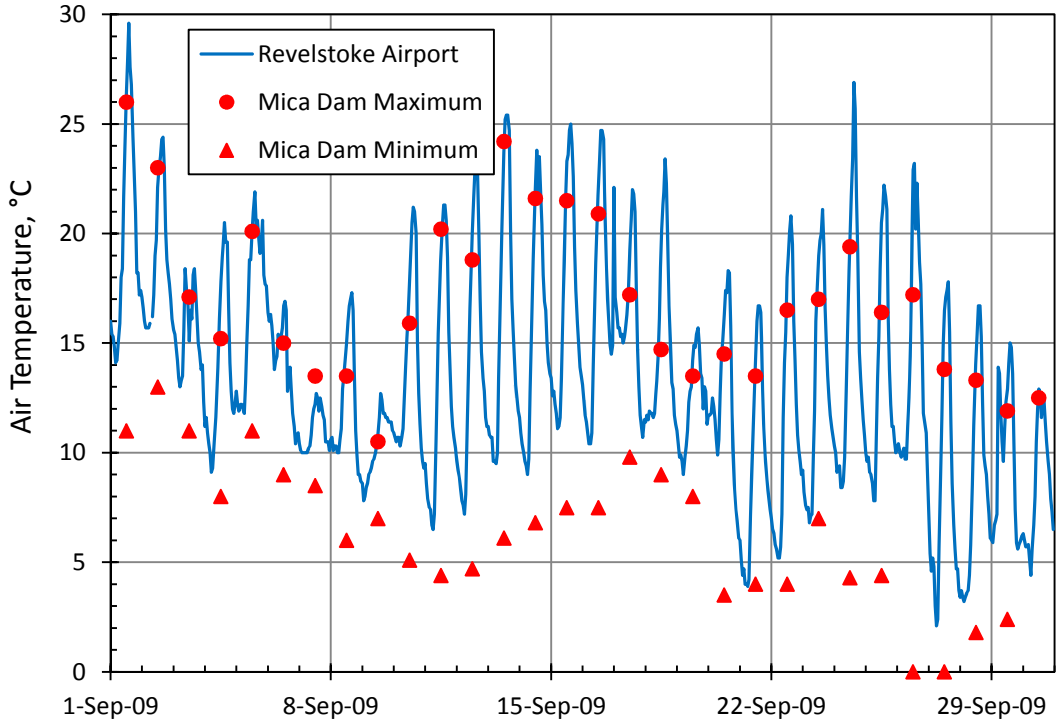

Figure 5.3d Air temperatures recorded at Revelstoke Airport and Mica Dam meteorological stations in September, 2009.

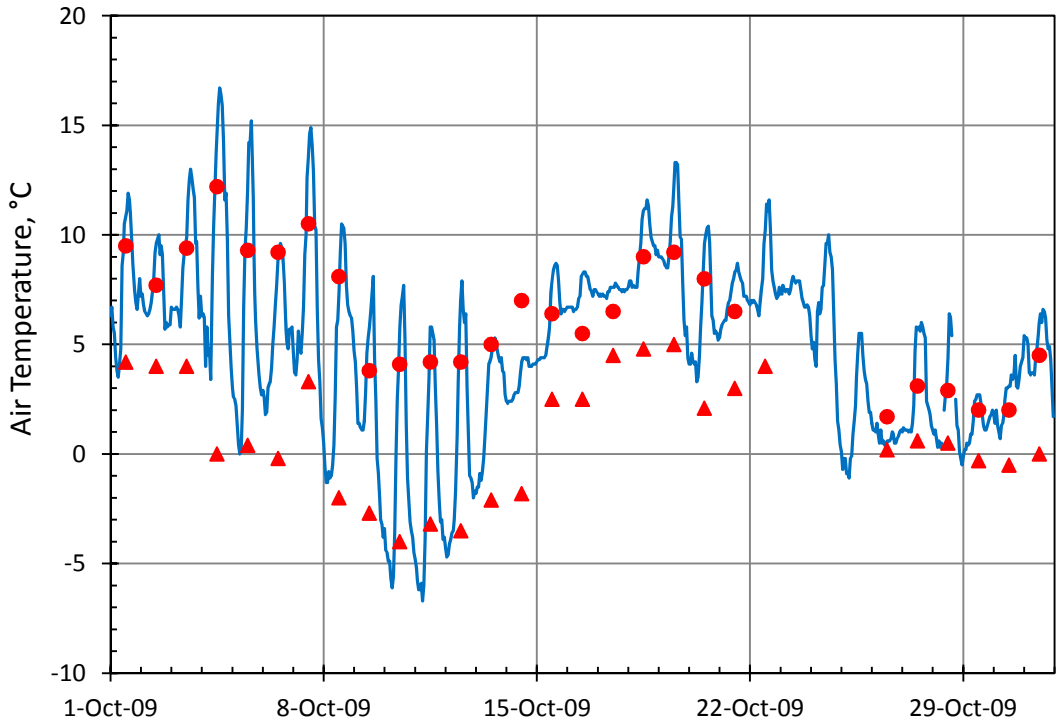

Figure 5.3e Air temperatures recorded at Revelstoke Airport and Mica Dam meteorological stations in October, 2009.

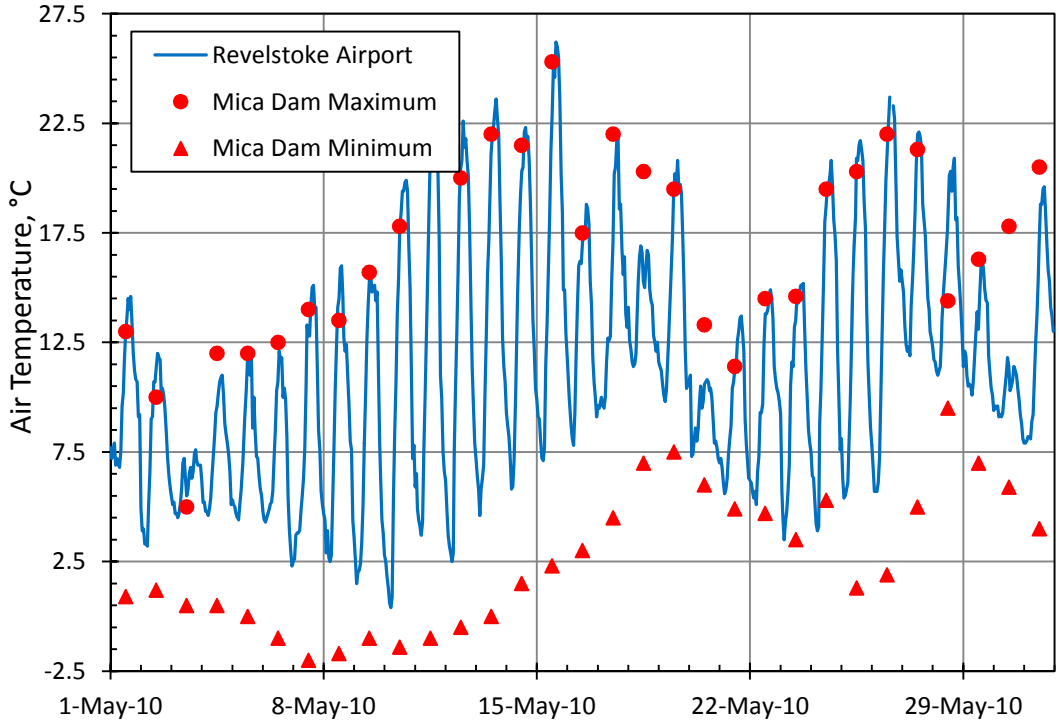

Figure 5.4a Air temperatures recorded at Revelstoke Airport and Mica Dam meteorological stations in May, 2010.

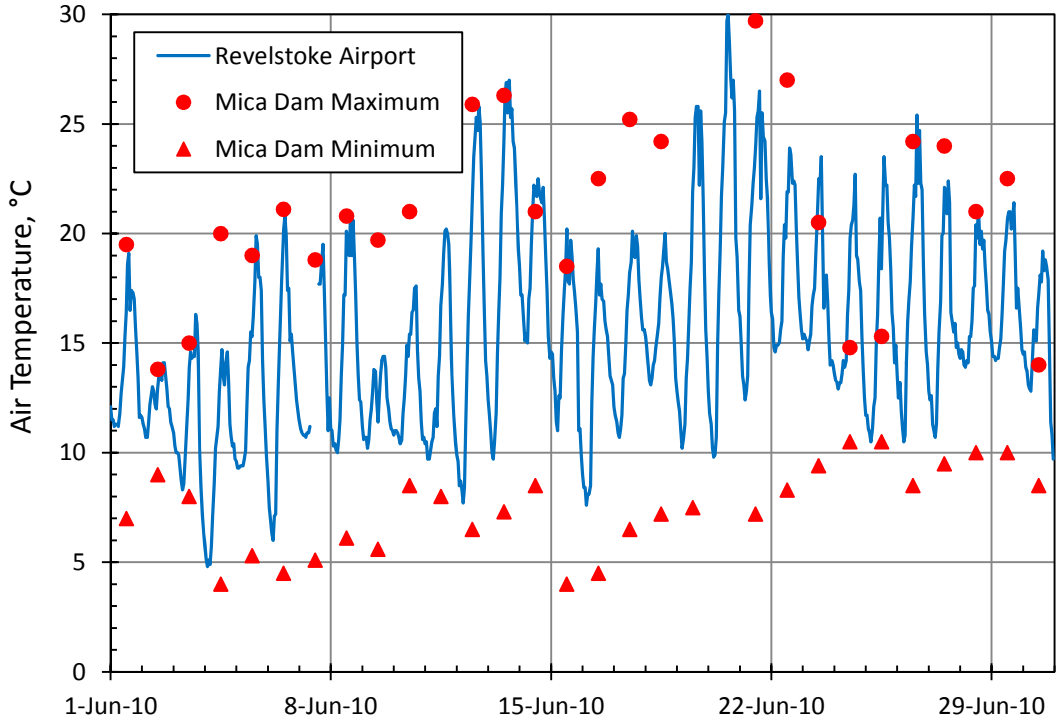

Figure 5.4b Air temperatures recorded at Revelstoke Airport and Mica Dam meteorological stations in June, 2010.

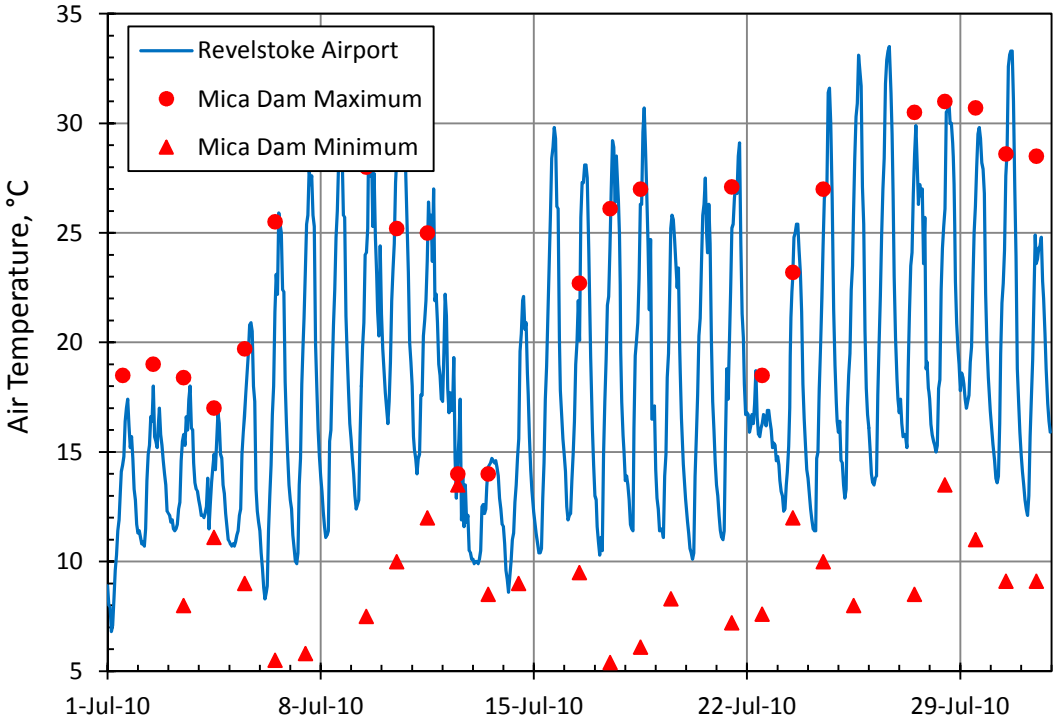

Figure 5.4c Air temperatures recorded at Revelstoke Airport and Mica Dam meteorological stations in July, 2010.

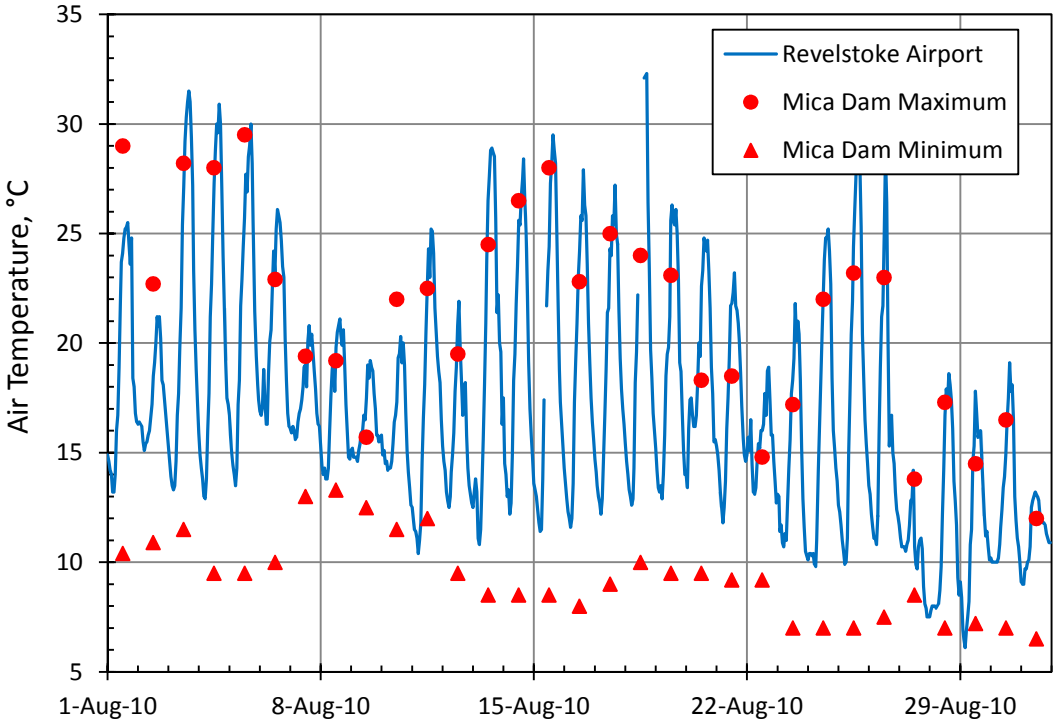

Figure 5.4d Air temperatures recorded at Revelstoke Airport and Mica Dam meteorological stations in August, 2010.

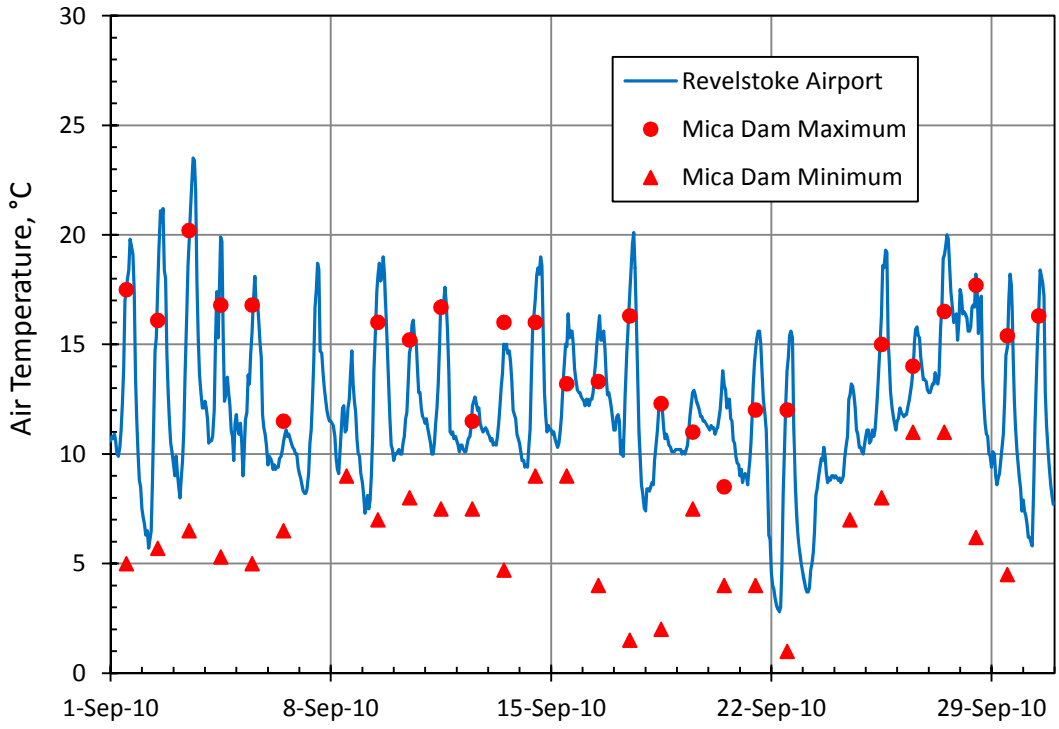

Figure 5.4e Air temperatures recorded at Revelstoke Airport and Mica Dam meteorological stations in September, 2010.

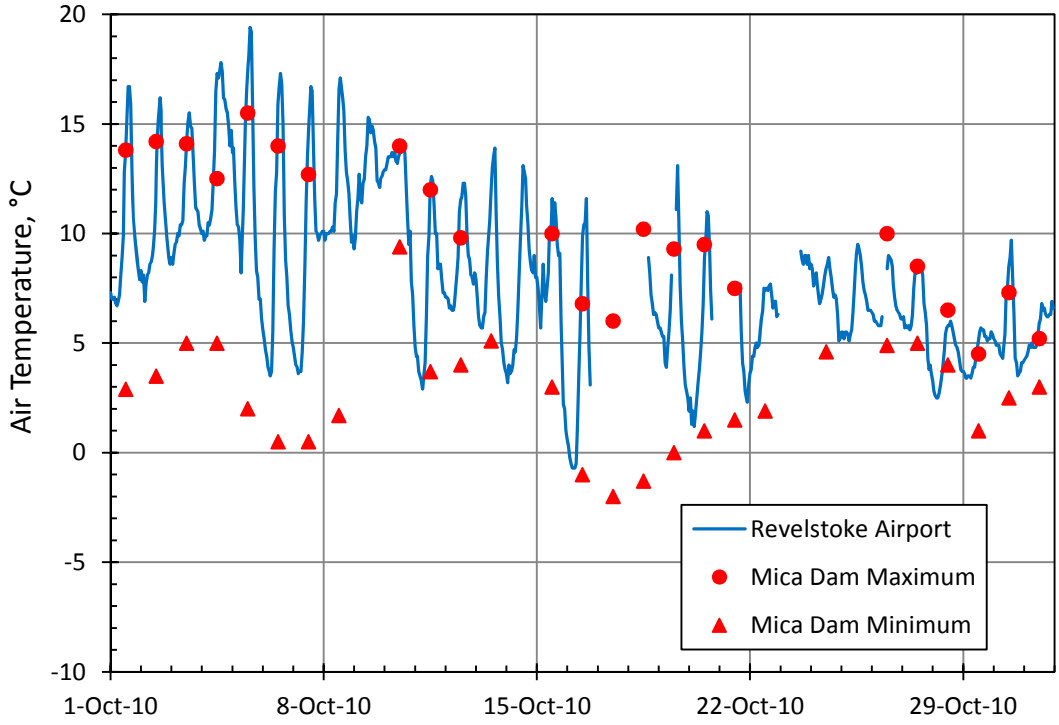

Figure 5.4f Air temperatures recorded at Revelstoke Airport and Mica Dam meteorological stations in October, 2010.

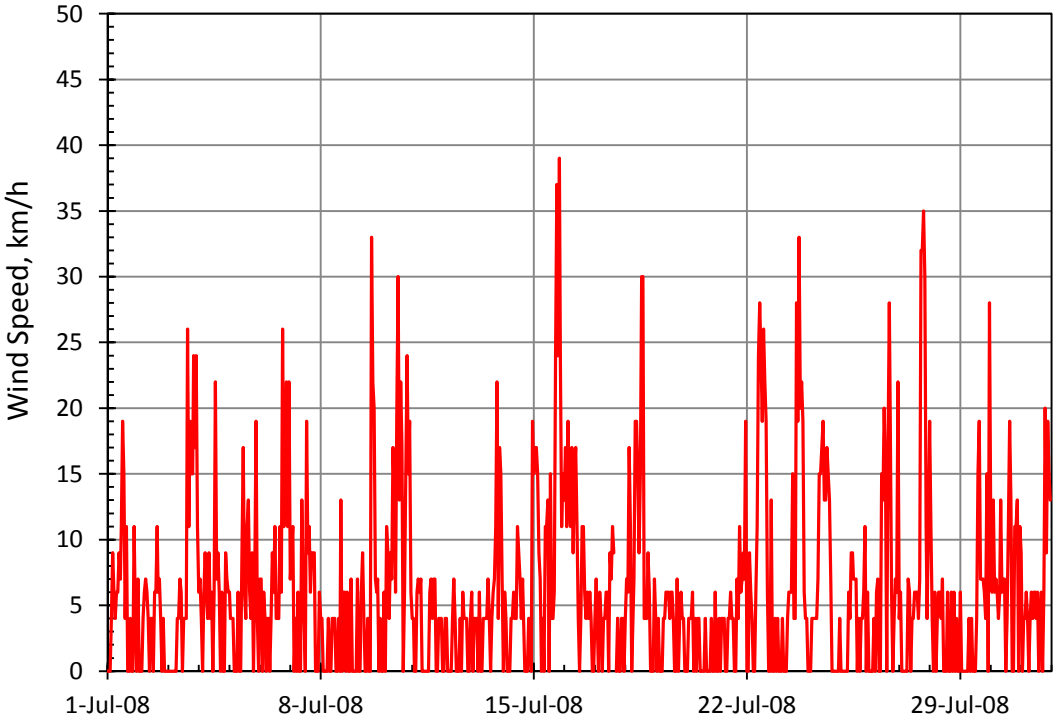

Figure 5.5a Wind speeds recorded at Revelstoke Airport meteorological station in July, 2008.

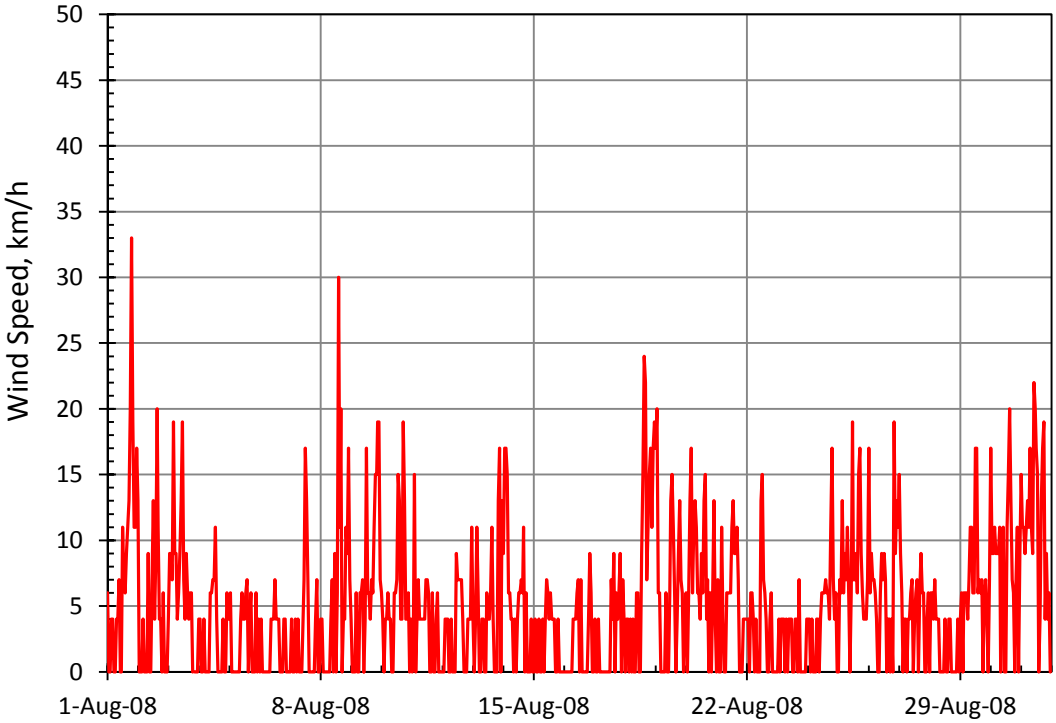

Figure 5.5b Wind speeds recorded at Revelstoke Airport meteorological station in August, 2008.

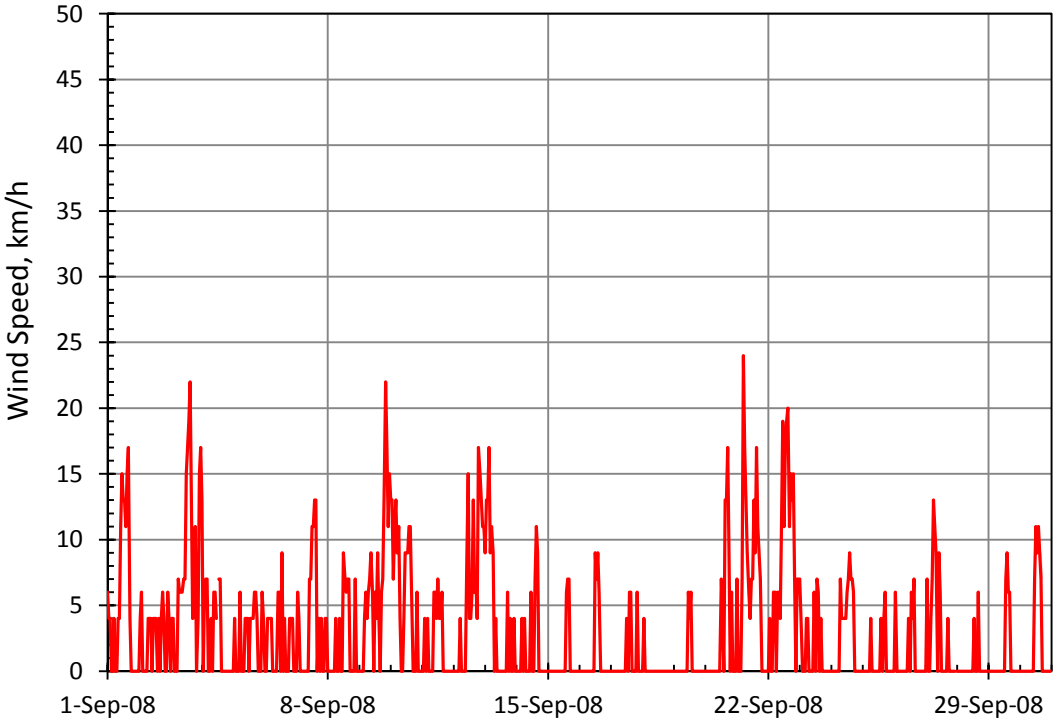

Figure 5.5c Wind speeds recorded at Revelstoke Airport meteorological station in September, 2008.

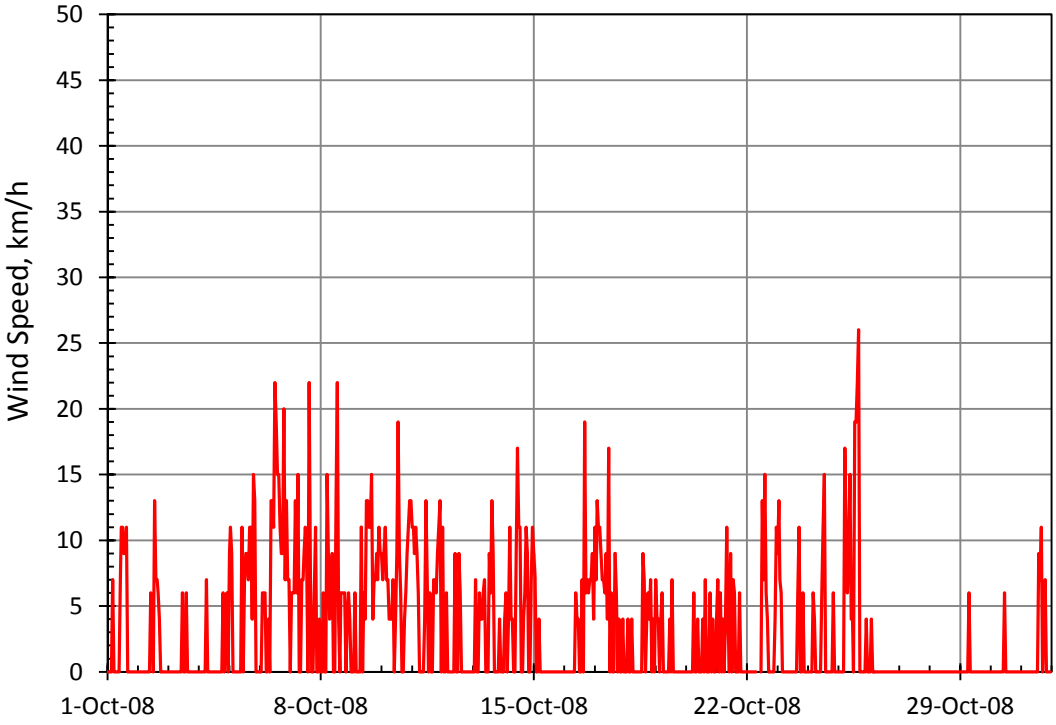

Figure 5.5d Wind speeds recorded at Revelstoke Airport meteorological station in October, 2008.

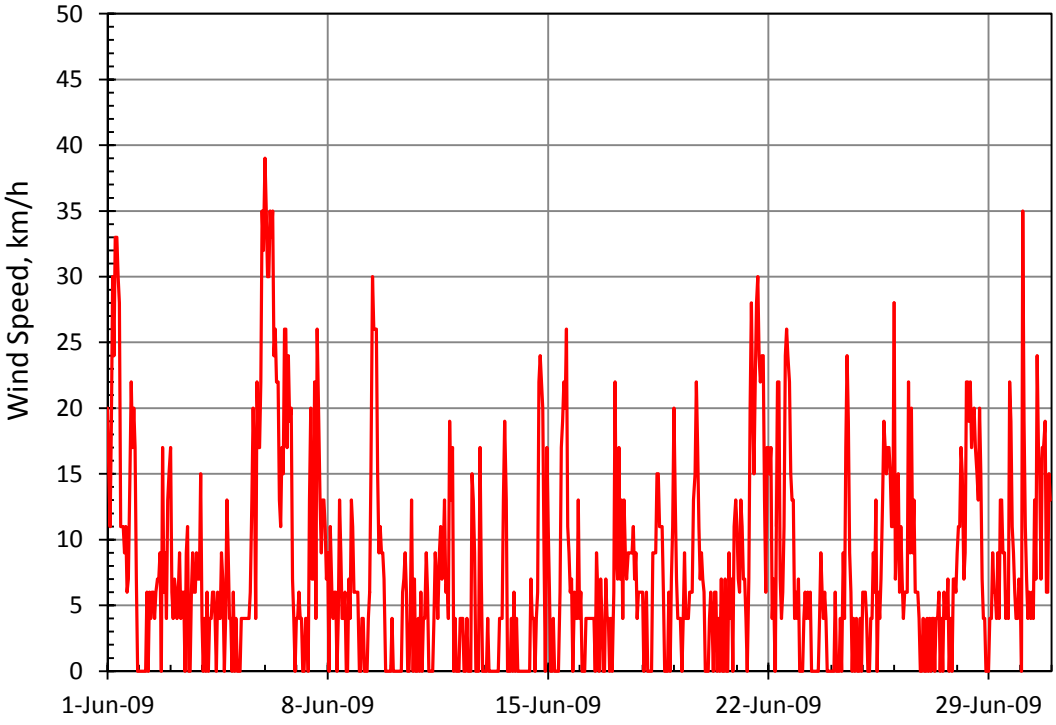

Figure 5.6a Wind speeds recorded at Revelstoke Airport meteorological station in June, 2009.

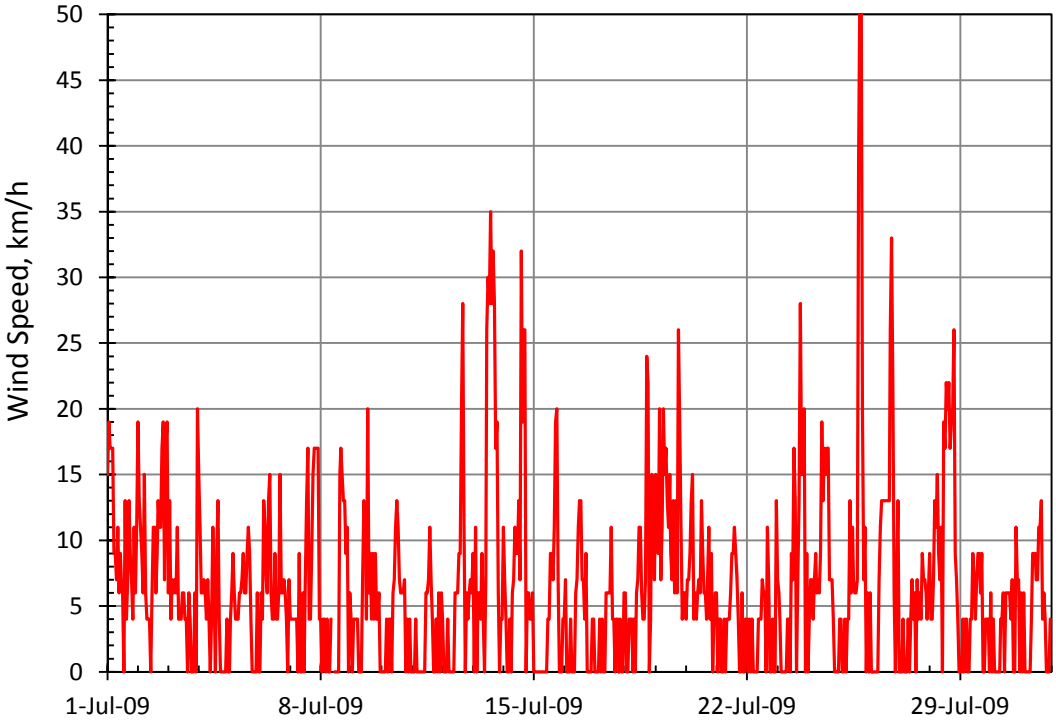

Figure 5.6b Wind speeds recorded at Revelstoke Airport meteorological station in July, 2009.

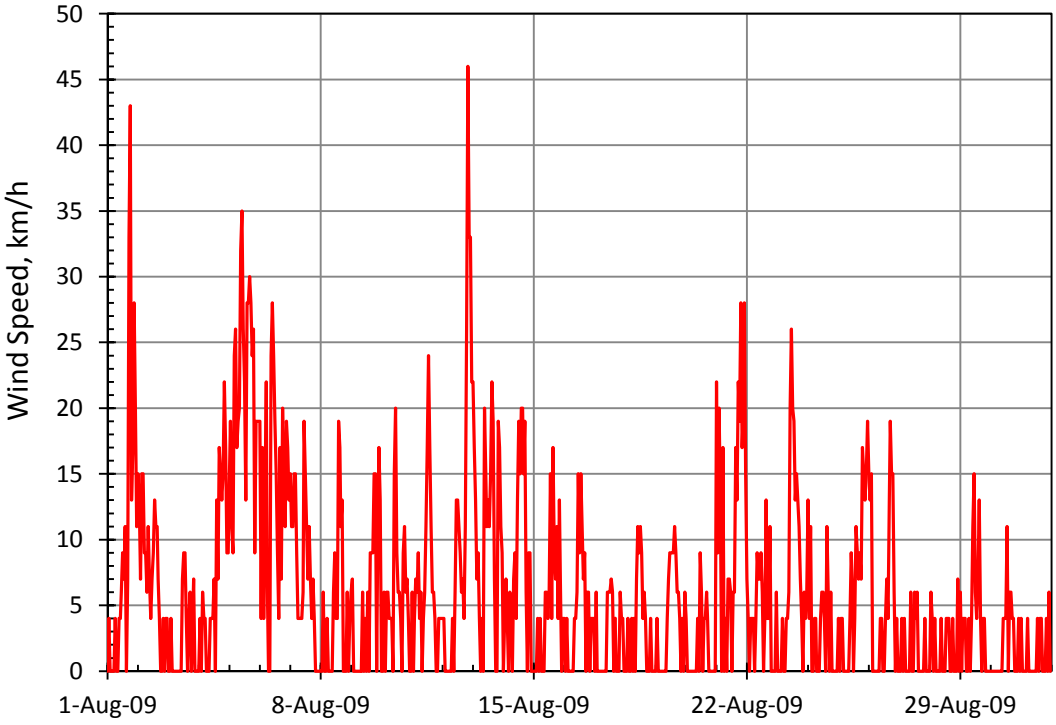

Figure 5.6c Wind speeds recorded at Revelstoke Airport meteorological station in August, 2009.

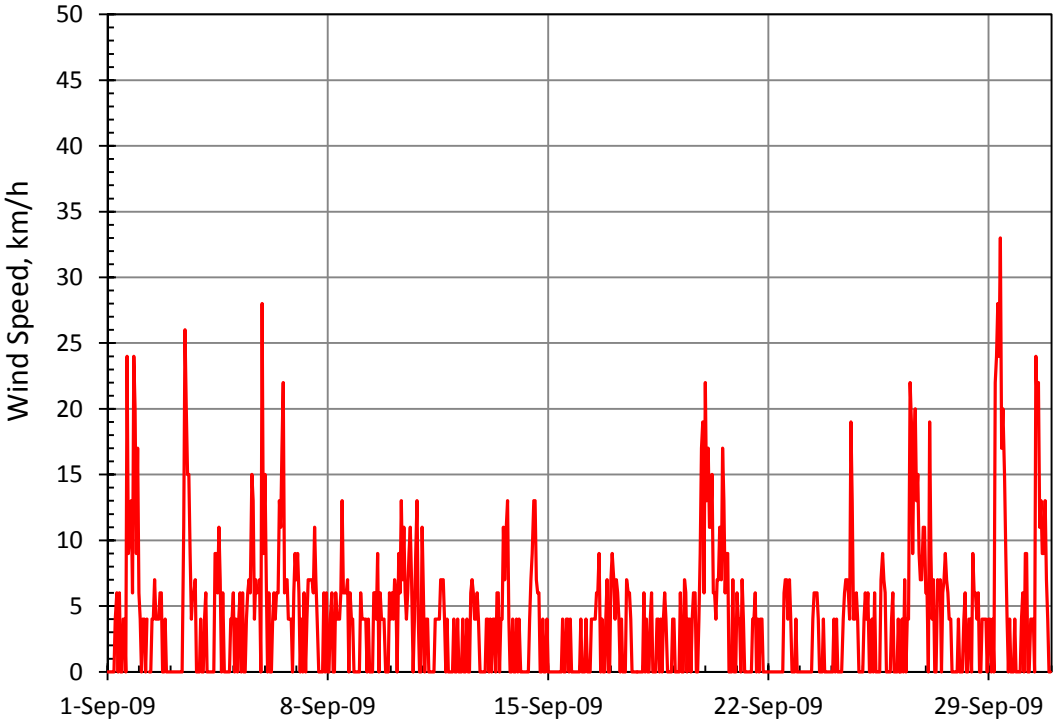

Figure 5.6d Wind speeds recorded at Revelstoke Airport meteorological station in September, 2009.

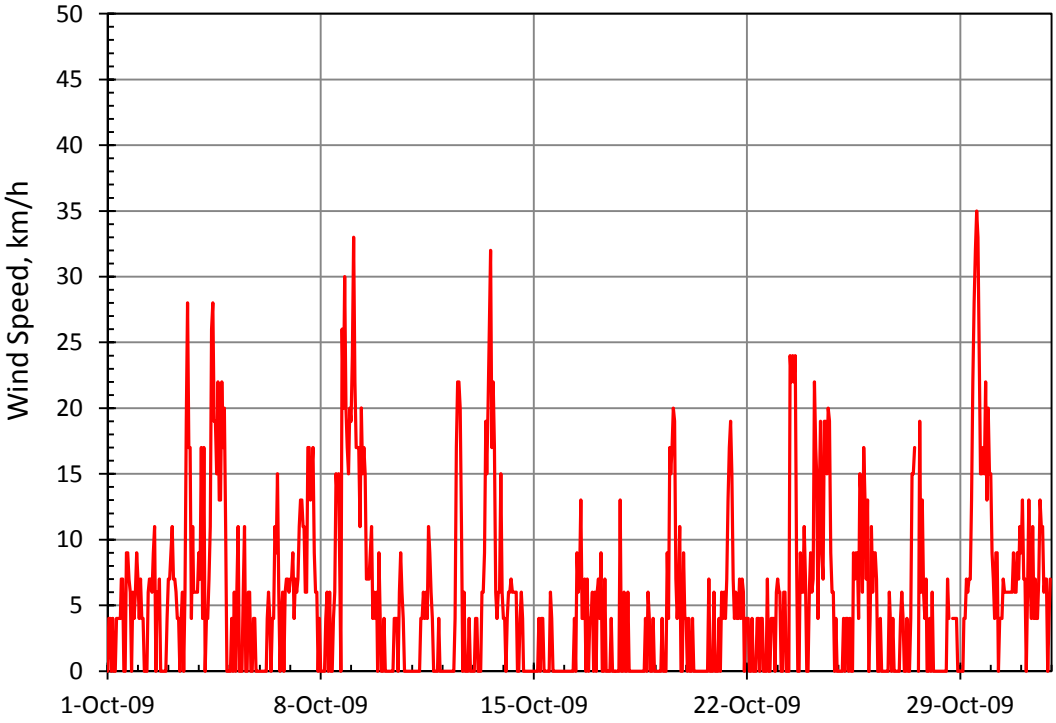

Figure 5.6e Wind speeds recorded at Revelstoke Airport meteorological station in October, 2009.

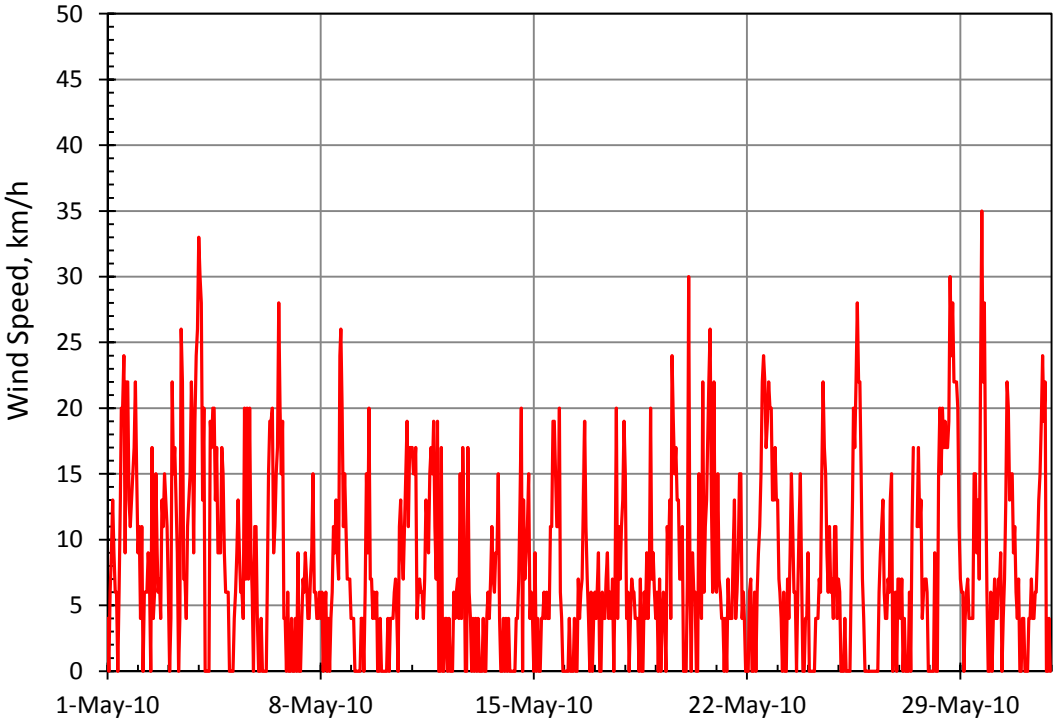

Figure 5.7a Wind speeds recorded at Revelstoke Airport meteorological station in May, 2010 .

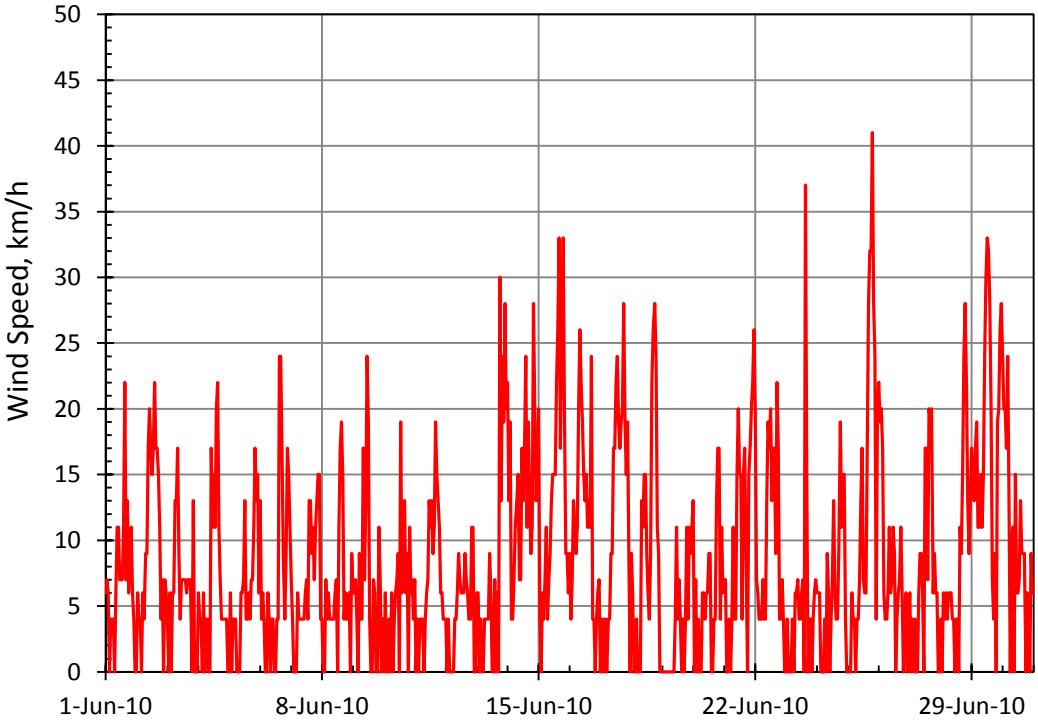

Figure 5.7b Wind speeds recorded at Revelstoke Airport meteorological station in June, 2010 .

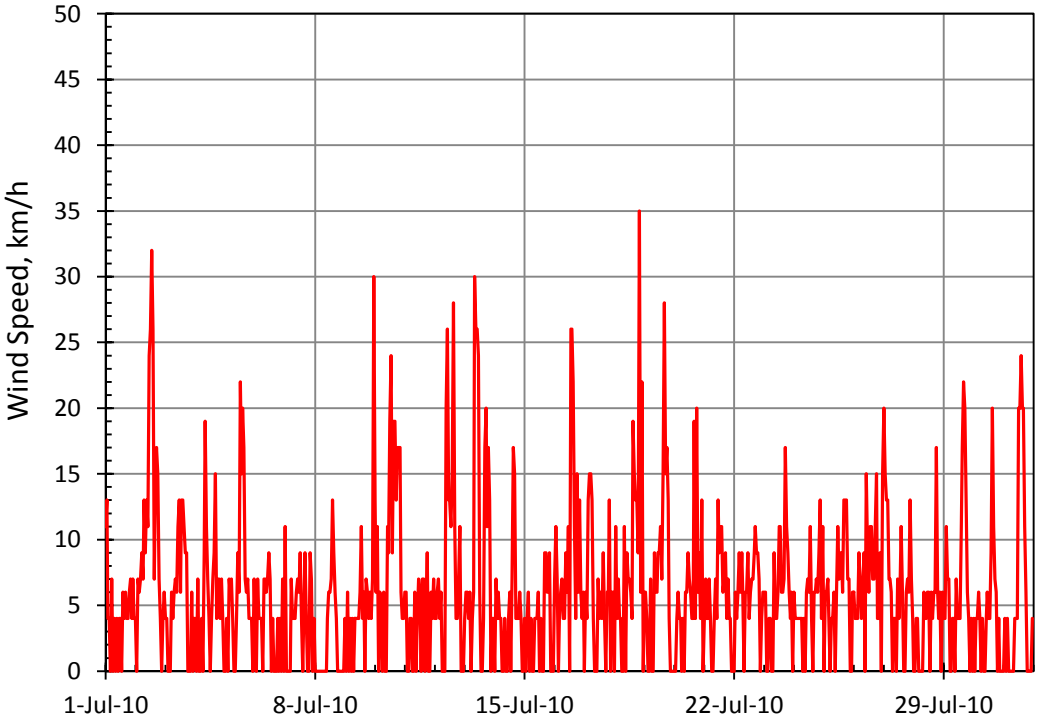

Figure 5.7c Wind speeds recorded at Revelstoke Airport meteorological station in July, 2010 .

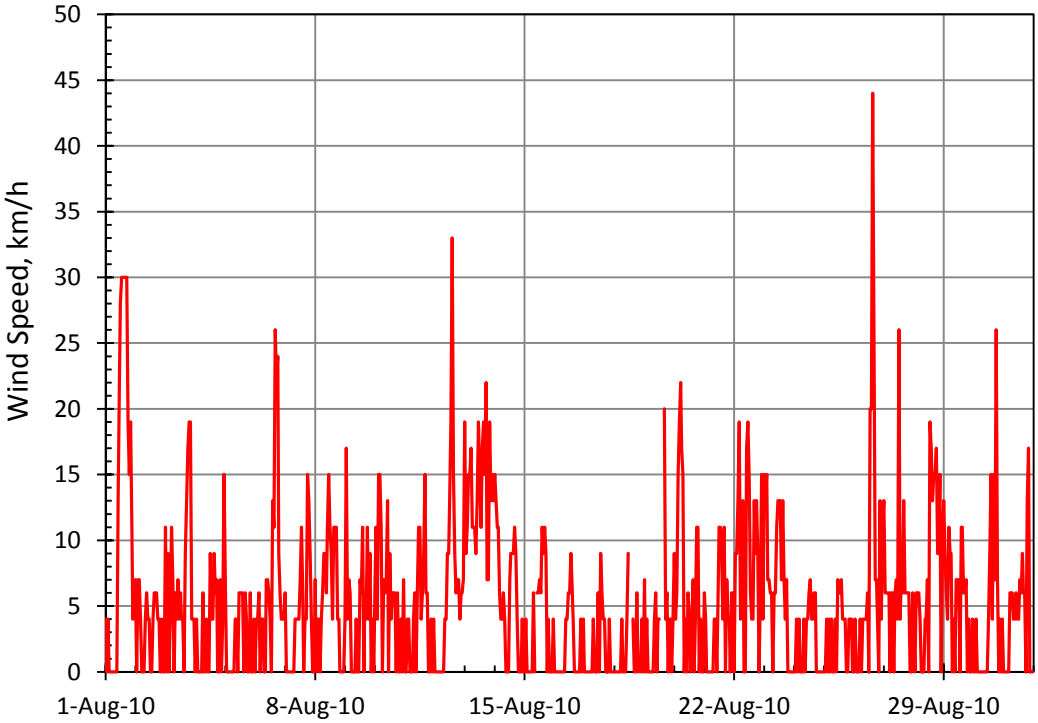

Figure 5.7d Wind speeds recorded at Revelstoke Airport meteorological station in August, 2010 .

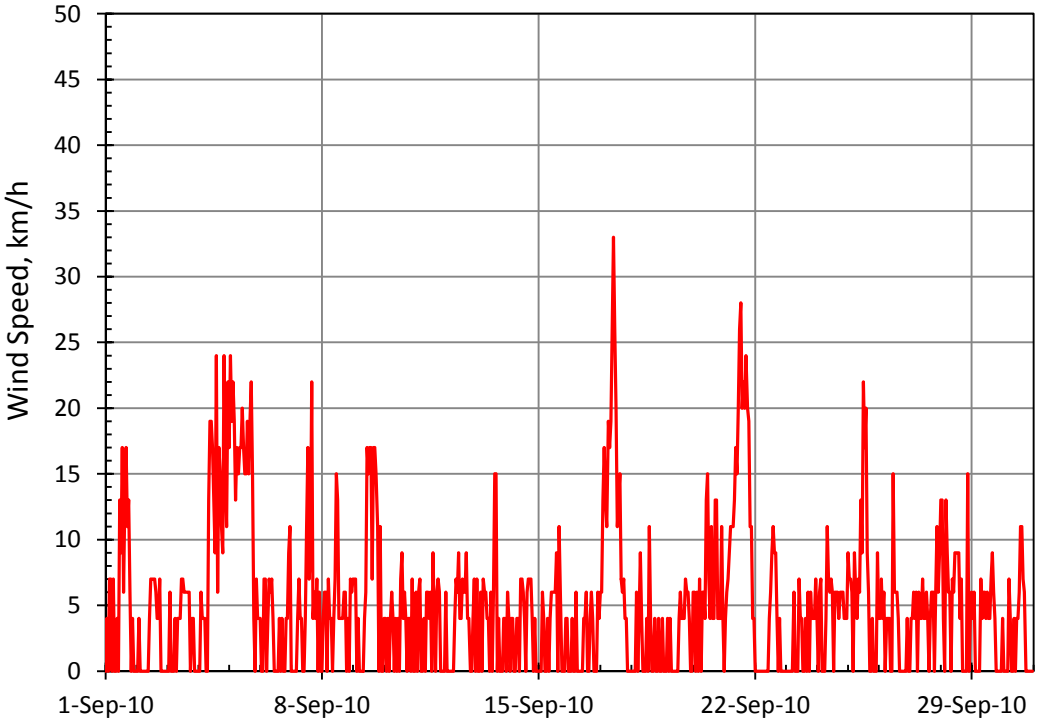

Figure 5.7e Wind speeds recorded at Revelstoke Airport meteorological station in September, 2010 .

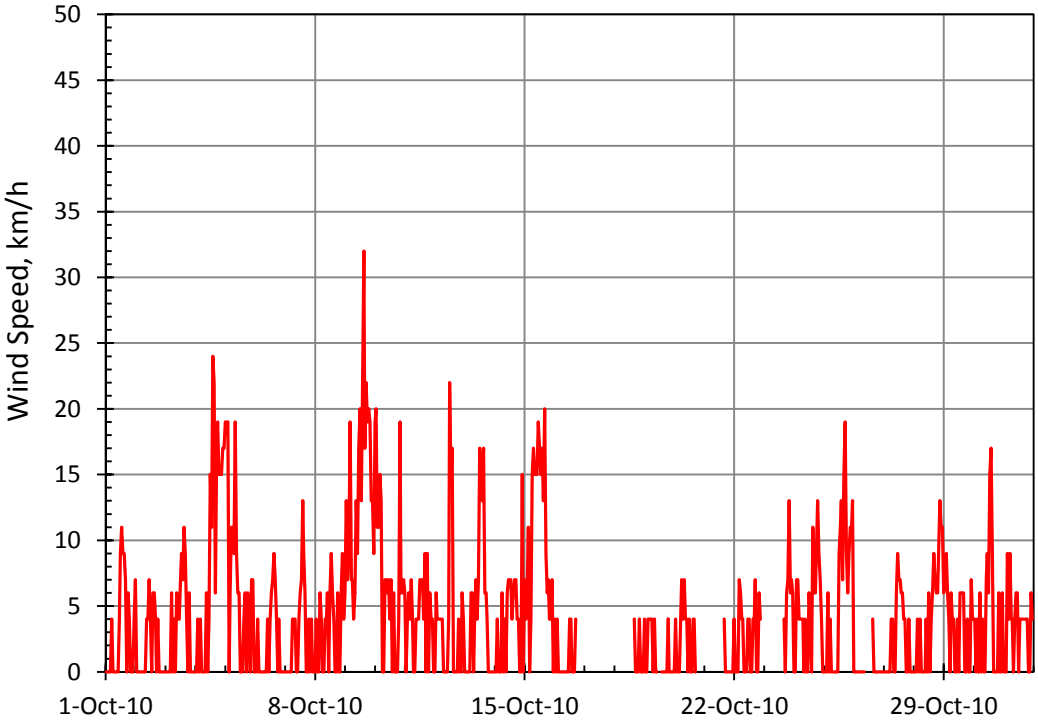

Figure 5.7f Wind speeds recorded at Revelstoke Airport meteorological station in October, 2010 .

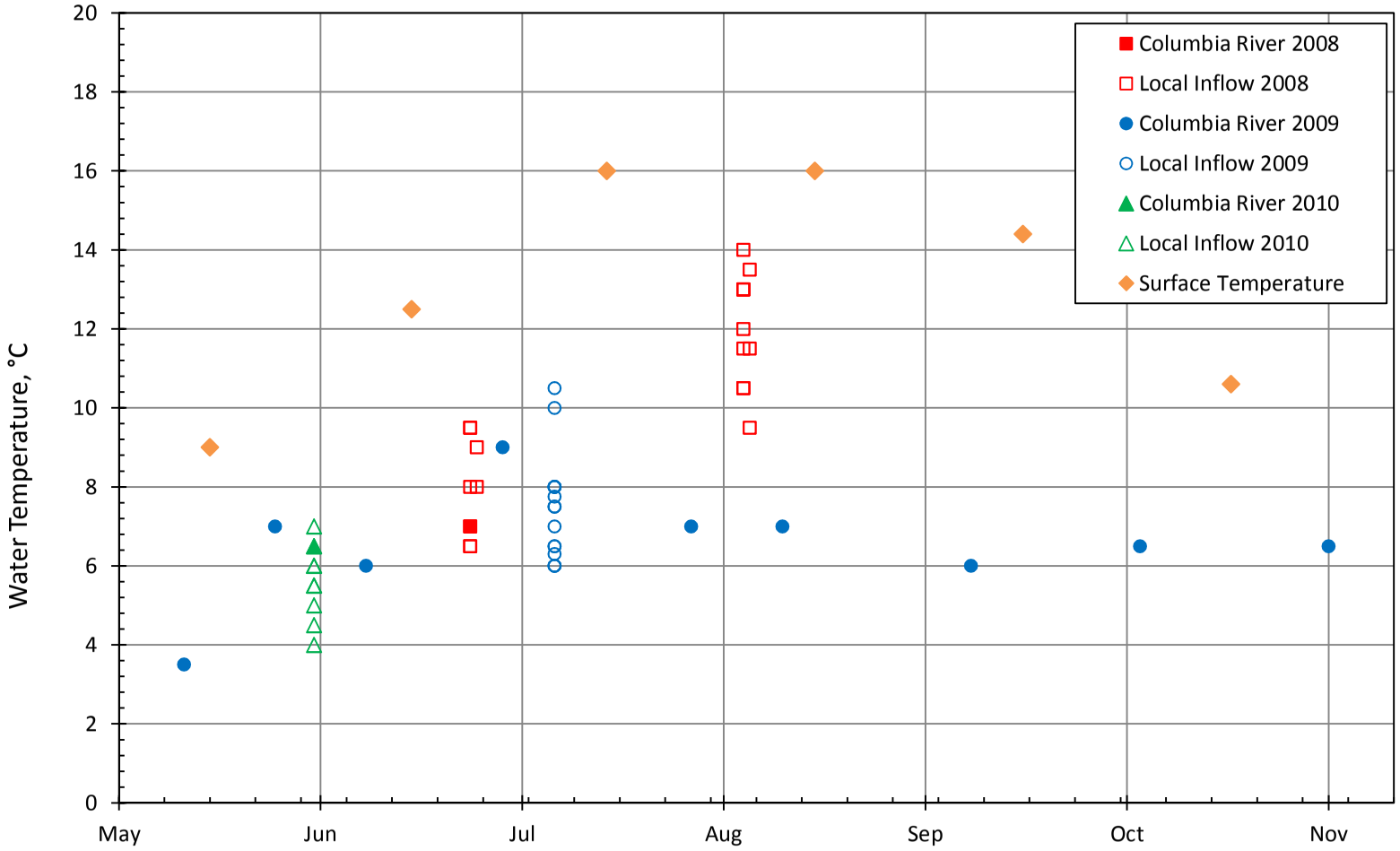

Figure 5.8 Columbia River inflow, local inflow and surface water temperatures for Revelstoke reservoir.

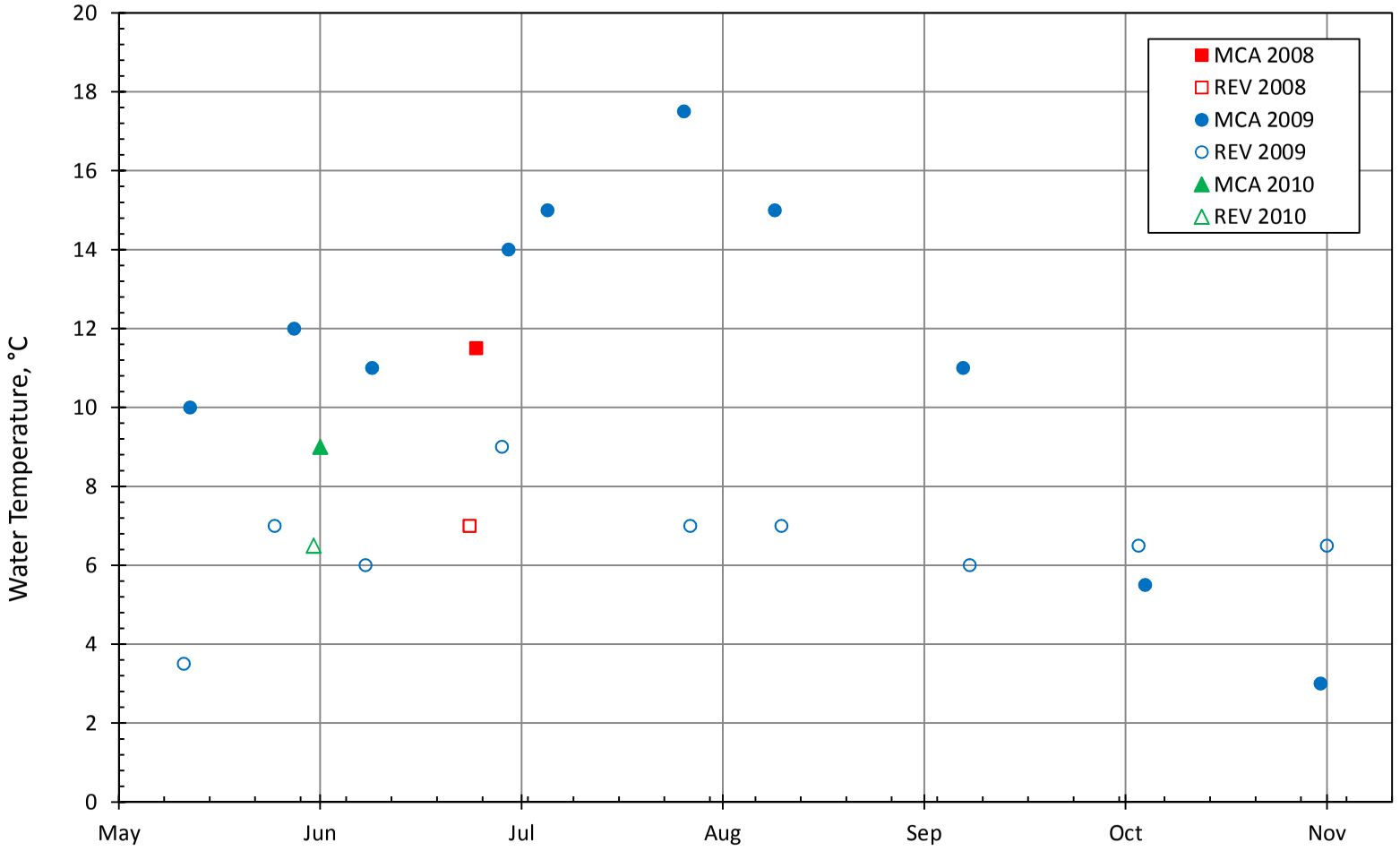

Figure 5.9 Columbia River inflow temperatures for Kinbasket (solid symbols) and Revelstoke (empty symbols) reservoirs.

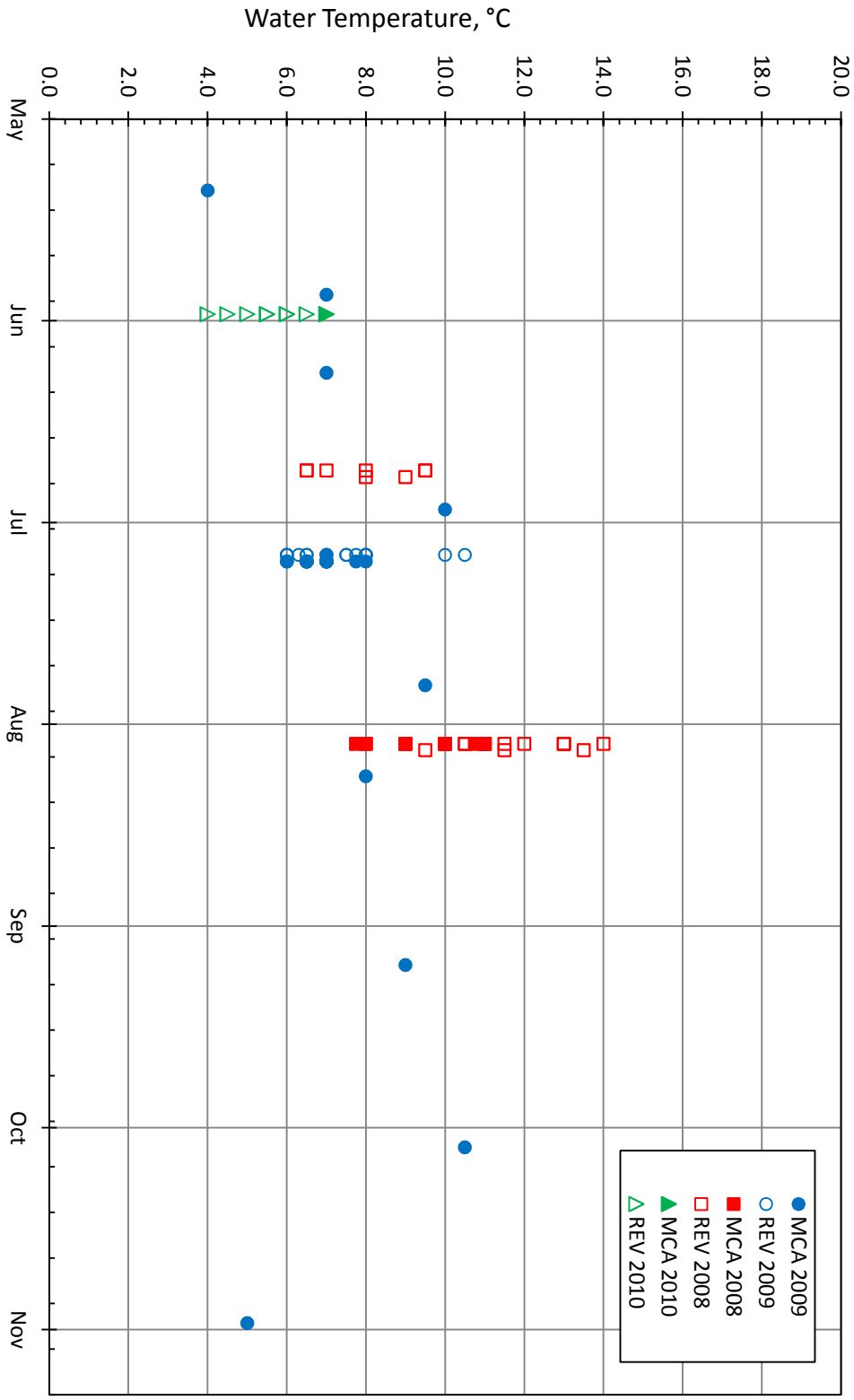

Figure 5.10 Local inflow temperatures for Kinbasket (solid symbols) and Revelstoke (empty symbols) reservoirs.

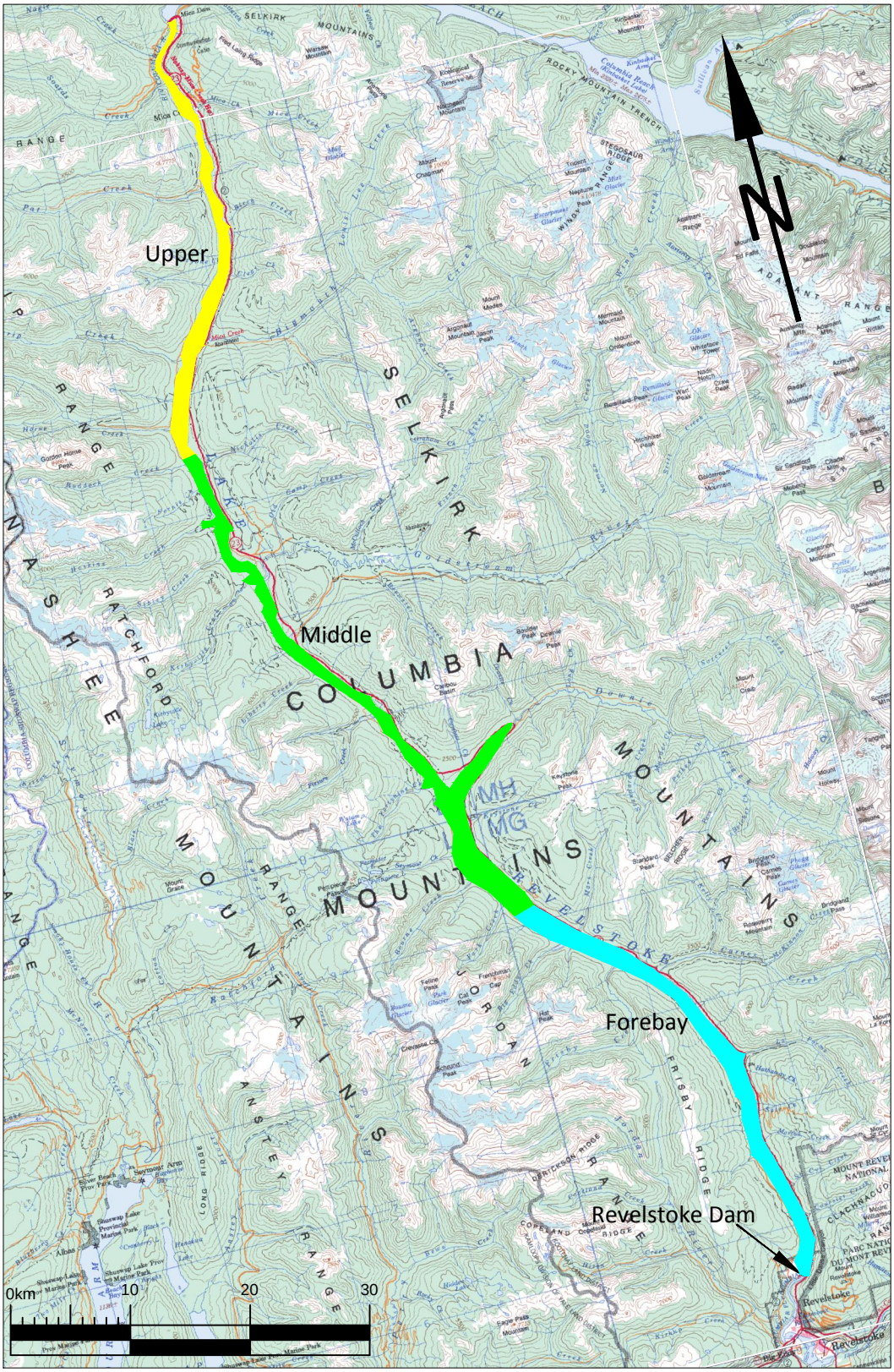

Figure 5.11 General locations of instantaneous temperature profiles at Revelstoke reservoir taken in 2008, 2009, and 2010.

Appendix A

Depth of Wind Mixing Equations

The depth of wind mixing can be calculated based on the net heat flux at the water surface and the wind shear stress. It is hydrologically intensive and requires numerous meteorological inputs to calculate the surface heat flux. The following equations were used to calculate this parameter using the energy budget method (Anderson, 1954):

$$H_N = (1-\alpha)H_s - H_L - H_E - H_H \quad [14]$$

where:

H_N = the total heat exchange at the water's surface;

α = the albedo of the water surface;

H_s = the net solar radiation (short wave);

H_L = the net long wave radiation;

H_E = the energy used for evaporation; and

H_H = the sensible heat flux.

Shortwave solar radiation (H_s) reaching the earth's outer atmosphere can be estimated using the effective radiation intensity. This parameter was given by the equations (Kaczmarek et al., 1996):

$$I_o = \frac{W_o \sin a}{r^2} \quad [15]$$

where:

I_o = the effective radiation intensity;

W_o = the solar constant/4;

r = the (actual earth – sun distance)/(mean earth – sun distance); and

a = the solar altitude.

The solar altitude was given by the equation:

$$\sin a = \sin\delta \sin\varphi + \cos\delta \cos\varphi \cos\tau \quad [16]$$

where:

δ = the declination of the sun;

φ = the local latitude; and

τ = the sun's hour angle.

The effective radiation intensity was determined on an hourly basis for the time period of the observed water temperature data, July 16 – August 19. The declination of the sun and hour angle were determined using the estimations given by Kaczmarek et al. (1996). The dam site was located at 49°20'36"N and 117°46'28"W in the Pacific Standard time zone.

Solar radiation reaching the earth's atmosphere does not equal the solar radiation reaching the earth's surface. The incoming extraterrestrial radiation gets reflected by the earth's albedo, absorbed by gases in the atmosphere, scattered by particulates in the air, and also scattered by clouds (Shuttleworth, 1993). Some estimates of the percentage of solar radiation reaching the earth's surface (net solar radiation, H_s) are 51% (Linsley et al., 1982), 47% (Gray, 1970), 55% (UNAS, 1975), and 49% (Datta, 2002). An average value of 50% was adopted as the value of solar radiation reaching the earth's surface. Therefore, the net solar radiation was calculated using the equation:

$$H_S = 0.50\, I_o \qquad [17]$$

When the net solar radiation finally reaches the earth's surface, part of it is reflected due to the albedo of the surface. This explains the (1 – α) term in the energy balance equation [13]. Albedo depends on transient features (i.e. solar beam direction) as well as the land cover class (Shuttleworth, 1993). The albedo used in this project for an open water surface was 0.08 (Shuttleworth, 1993).

This method of calculating the net solar radiation (H_s) had several drawbacks. The varying cloud cover was not taken into account. Instead, an average value of previous estimates was used (i.e. 50%). Also, the solar constant was taken as 1350 W/m^2 (Gray and Prowse, 1993). This number is an average value and changes depending on the sunspot number, which varies over the year.

The net long wave radiation term (H_L) is comprised of two parts. It consists of long wave radiation emitted from the water's surface, H_{LS}, and the amount that is reflected back down by the atmosphere, H_{LN} (Rasmusson et al., 1993). According to the black body theorem, any physical body that is at a temperature greater than 0 K will radiate heat (i.e. Planck's law). The amount of long wave radiation emitted can be estimated by the Stefan-Boltzman law:

$$H_{LS} = \varepsilon \sigma T^4 \quad [18]$$

where:

H_{LS} = the long wave radiation from water's surface;

ε = the emittance for non-perfect black bodies;

σ = the Stefan-Boltzman constant (5.67×10^{-8} W/m^2·K^4); and

T = the water temperature (K).

The emittance for non-perfect black bodies was taken as 0.97 for water (Anderson, 1954). The long wave radiation emitted from the water surface was much larger than the incoming solar radiation. However, when the long wave radiation was emitted upwards from the water's surface, a large portion of the energy was reflected back down by the atmosphere. This is known as the "greenhouse effect" and keeps the earth's surface at a habitable temperature (Rasmusson et al., 1993). Two estimates of this re-radiated portion are 84% (Datta, 2002) and 88% (Gray, 1970). However, for these calculations, the portion of reflected long wave radiation was estimated using Brunt's formula (Anderson, 1954):

$$H_{LA} = (A + B\sqrt{e_a})\sigma {T_a}^4 \quad [19]$$

where:

H_{LA} = the long wave radiation reflected back from atmosphere;

A, B = empirical constants;

e_a = the actual vapour pressure; and

T_a = the temperature of air near the ground (K).

The empirical constants were chosen based on various values published by Anderson (1954). There were nine different values published, which were based on the location of the lake/reservoir. Taking the extreme values of the coefficients resulted in a difference of about only 40 W/m^2. Since there was not a study for the constants at the dam site available, an average value for the coefficients were used (*i.e.* a = 0.56, b = 0.059) to obtain the reflected long wave radiation.

Finally, the net long wave radiation was given by:

$$H_L = H_{LS} - H_{LA} \quad [20]$$

The net long wave radiation term represented the energy leaving the water surface, since it was a negative term in the energy balance equation.

The major drawback for the calculation of net long wave radiation was estimating the empirical constants for Brunt's formula. So many factors play a role in the re-radiation of energy from the atmosphere, and they are all accounted for in these empirical constants. It is difficult to determine similarities between locations to evaluate which constant would be most representative of the dam site.

The amount of energy required to evaporate water (vapour heat flux) can be estimated by the equation:

$$H_E = EL_v \quad [21]$$

where:

E = the evaporation rate; and

L_v = the latent heat of vaporization (J/kg).

The vapour heat flux was the energy flowing out of the water's surface due to the evaporation. The amount of evaporation will be relatively large on an open body of water, meaning it will influence the energy flux at the water's surface significantly.

Various methods were available for estimation of the evaporation rate. Included in these was the energy balance method (Shuttleworth, 1993):

$$E_s = \frac{(1-\alpha)H_s}{L_v} \quad [22]$$

where:

E_s = the energy balance evaporation rate.

The latent heat of vaporization was given by:

$$L_v = 2.501 \times 10^6 - 2361T_s \quad [23]$$

where:

T_s = the temperature at the surface (°C).

The temperature at the surface was estimated as the air temperature.

Another method of estimating evaporation rate was the aerodynamic method (Shuttleworth, 1993):

$$E_a = \frac{0.622 k^{*2} \rho_a u_w}{P \rho_w (\ln(\frac{Z_{10}}{Z_o})^2)} (e_s - e_a) \quad [24]$$

where:

E_a = the aerodynamic evaporation rate;

k^* = the von Karman constant (0.4);

P = the atmospheric pressure (Pa);

ρ_w = the density of water (1000 kg/m^3);

Z_{10} = the height at which wind measurements are taken from (10m);

Z_o = the roughness height (0.0001m); and

e_s = the saturation vapour pressure.

Both the energy balance and the aerodynamic methods have aspects that were valid to the true evaporation rate. Therefore, an equation that incorporated both of these processes was developed by Penman (Shuttleworth, 1993) known as the combination method:

$$E_c = \frac{\Delta E_s + \gamma E_a}{\Delta + \gamma} \quad [25]$$

where:

E_c = the combined evaporation rate;

Δ = the saturation vapour pressure gradient; and

γ = the psychrometric constant (66.6 Pa/°C).

The saturation vapour pressure was given by:

$$\Delta = \frac{4098}{(237.3 + T_s)^2} e_s \quad [26]$$

Since the combination method was based on more physical parameters, it was used for determining the vapour heat flux for the energy budget equation [13].

Sensible heat flux was the portion of radiant energy that was not used for evaporation, but warming the atmosphere that was in contact with the ground. The sensible heat flux was related to the vapour heat flux. Bowen determined a proportional constant between them known as Bowen's ratio (Shuttleworth, 1993):

$$\beta = \gamma \frac{T_s - T_a}{e_s - e_a} \quad [27]$$

where:

β = Bowen's ratio.

It should be noted that in this equation the surface temperature, T_s, could not be estimated as the air temperature, otherwise β would always be zero. Therefore the water surface temperature was used for T_s. It may be somewhat counterproductive to use the values of the water temperature we are trying to predict, but the data was limited in this study.

The sensible heat flux was proportional to the vapour heat flux as follows (Shuttleworth, 1993):

$$H_H = \beta H_E \quad [28]$$

Equations [16], [19], [20], and [27] were used in equation [13] to determine the net surface heat flux, H_N. The depth of wind mixing was calculated using the following equations (Fischer et al., 1979):

$$D_t = \frac{u^{*3}}{g\alpha^* k \frac{H_N}{\rho_w C_p}} \quad [29]$$

where:

D_t = the approximate depth of wind mixing;

u^* = the shear velocity of the wind;

α^* = the volumetric coefficient of thermal expansion (1.8 x 10^{-4}/°C); and

C_p = the specific heat of water (4186 J/kg°C).

The shear velocity of wind was calculated using (Fischer et al., 1979):

$$u^* = \sqrt{\frac{\tau_o}{\rho_w}} \quad [30]$$